

A THREE-DIMENSIONAL PRINTED,
POLYCAPROLACTONE/HYDROGEL BASED, TISSUE ENGINEERED
MENISCUS

A THESIS SUBMITTED TO
THE GRADUATE SCHOOL OF NATURAL AND APPLIED SCIENCES
OF
MIDDLE EAST TECHNICAL UNIVERSITY

BY

GÖKHAN BAHÇECİOĞLU

IN PARTIAL FULFILLMENT OF THE REQUIREMENTS
FOR
THE DEGREE OF DOCTOR OF PHILOSOPHY
IN
BIOTECHNOLOGY

FEBRUARY 2018

Approval of the thesis:

**A THREE-DIMENSIONAL PRINTED,
POLYCAPROLACTONE/HYDROGEL BASED, TISSUE ENGINEERED
MENISCUS**

submitted by **GÖKHAN BAHÇECİOĞLU** in partial fulfillment of the requirements
for the degree of **Doctor of Philosophy in Biotechnology Department, Middle
East Technical University** by,

Prof. Dr. Gülbin Dural Ünver
Dean, Graduate School of **Natural and Applied Sciences**

Assoc. Prof. Dr. Can Özen
Head of Department, **Biotechnology, METU**

Prof. Dr. Vasif Hasırcı
Supervisor, **Dept. of Biological Sciences, METU**

Prof. Dr. Nesrin Hasırcı
Co-supervisor, **Dept. of Chemistry, METU**

Examining Committee Members:

Prof. Dr. Nuhan Puralı
Dept. of Biophysics, Hacettepe University

Prof. Dr. Vasif Hasırcı
Dept. of Biological Sciences, METU

Prof. Dr. Dilek Keskin Şendil
Dept. of Engineering Sciences, METU

Prof. Dr. Aykut Özkul
Dept. of Virology, Fac. of Veterinary Med., Ankara University

Assoc. Prof. Dr. Can Özen
Dept. of Biotechnology, METU

Date: 02.02.2018

I hereby declare that all information in this document has been obtained and presented in accordance with academic rules and ethical conduct. I also declare that, as required by these rules and conduct, I have fully cited and referenced all material and results that are not original to this work.

Name, Last Name: Gökhan Bahçeciöđlu

Signature :

ABSTRACT

A THREE-DIMENSIONAL PRINTED, POLYCAPROLACTONE/HYDROGEL BASED, TISSUE ENGINEERED MENISCUS

Bahçeciöđlu, Gökhan

Ph.D., Department of Biotechnology

Supervisor: Prof. Dr. Vasıf Hasırcı

Co-Supervisor: Prof. Dr. Nesrin Hasırcı

February 2018, 164 pages

Three dimensional (3D) printing has recently been in the spotlight of tissue engineering field, because it enables production of patient-specific tissue engineered scaffolds with desired shapes, porosities and pore sizes. In the current study, the aim was to develop a meniscal construct via tissue engineering that would serve as a functional replacement for the damaged tissues. The scaffold involves 3D printed polycaprolactone (PCL) structure embedded in different hydrogels; the hydrogel used at the inner region induces glycosaminoglycan (GAG) production similar to the cartilage-like tissues, and the hydrogel used at the outer region induces collagen production similar to fibrocartilage-like tissue. Various hydrogels such as agarose (Ag), methacrylated gelatin (GelMA), methacrylated hyaluronic acid (MeHA) and GelMA-MeHA were prepared and their effect on cell activities were studied by using two different cells, porcine fibrochondrocytes and human fibrochondrocytes.

Constructs were tested *in vitro* using porcine fibrochondrocytes in order to investigate their performance before any animal experimentation. Different hydrogels (Ag, GelMA, MeHA and GelMA-MeHA) were seeded with the cells and tested under static (no load) or dynamic (compression, 5-15% strain) culture

conditions. Ag (which promoted GAG production) and GelMA (which promoted collagen production) were selected to embed the 3D printed PCL scaffolds. After 56 days of culture, PCL scaffolds embedded in Ag resulted in 2-fold higher collagen and 3-fold higher GAG production, and the ones embedded in GelMA resulted in a 10-fold higher collagen production compared to untreated PCL. Mechanical properties of the PCL did not change after embedding in Ag or GelMA. PCL scaffolds with meniscus-shapes were 3D printed and embedded in Ag and GelMA at the inner and outer regions, respectively. The inner region of the constructs that was embedded in Ag produced high amounts of GAG, and the outer region that was embedded in GelMA produced high amounts of collagen after 56 days of incubation. Thus, the meniscus-shaped constructs mimicking the biochemical content of the meniscal tissue were produced.

In order to investigate the performance of the constructs *in vitro* before any clinical applications, human fibrochondrocytes were used to engineer the meniscus. To this end, square prism-shaped PCL scaffolds having different designs were printed with various interior (with or without shifting of the consecutive layers) and exterior (with or without circumferential strands) architectures, and studied for their suitability as human meniscus substitutes. Shifting of the strands led to lower mechanical properties while introduction of the circumferential strands enhanced mechanical properties in all combinations. The compressive modulus of the scaffolds when the scaffolds were produced in shifted architecture and with circumferential strands (~0.4 MPa) was close to that of the human meniscus (0.3-2 MPa), while the tensile modulus (18 MPa) was lower than that of the meniscus (70-130 MPa).

The 3D printed PCL scaffolds were produced in shifted architecture and with circumferential strands, embedded in the human fibrochondrocyte-carrying Ag, GelMA or GelMA-Ag, and incubated for 42 days under static culture conditions. The order of collagen deposition on the hydrogel-embedded scaffolds from the highest to the lowest was GelMA > GelMA-Ag > Ag. When the meniscus-shaped constructs with the circumferential strands were embedded in GelMA-Ag at the inner region instead of agarose alone, collagen deposition was increased. At the end, a zonal difference in the biochemical content of the constructs, high COL I at the outer

region and high COL II at the inner region, was created, mimicking the native meniscus. The structural organization of the meniscus was also mimicked with introducing circumferential strands to the engineered constructs.

Keywords: meniscus, tissue engineering, 3D printing, PCL, agarose, GelMA

ÖZ

ÜÇ BOYUTLU BASIM VE DOKU MÜHENDİSLİĞİ YÖNTEMLERİYLE ÜRETİLMİŞ POLİKAPROLAKTON/HİDROJEL TEMELLİ YAPAY MENİSKÜS

Bahçecioğlu, Gökhan

Doktora, Biyoteknoloji Bölümü

Tez Yöneticisi: Prof. Dr. Vasıf Hasırcı

Ortak Tez Yöneticisi: Prof. Dr. Nesrin Hasırcı

Şubat 2018, 164 sayfa

Üç boyutlu (3B) basım, hastaya özel, kontrol edilebilir şekil, gözeneklilik ve gözenek boyutuna sahip doku mühendisliği taşıyıcılarının üretimine olanak sağladığı için, son zamanlarda doku mühendisliği alanında çok revaçtadır. Bu çalışmada amaç doku mühendisliği yaklaşımıyla, zedelenmiş menisküs dokusunun yerine geçebilecek işlevsel bir taşıyıcı geliştirmektir. Taşıyıcı, 3B basım yöntemiyle menisküs şeklinde üretilen ve iç ve dış kısımlarda değişik hidrojellere emdirilmiş polikaprolakton (PCL) temelli bir yapıdır; yapının iç kısmı kıkırdak dokusundaki gibi glukozaminaglikan (GAG) üretimini uyaran bir hidrojele, dış kısmı da fibrokıkırdak dokusundaki gibi kollajen üretimini uyaran bir hidrojele emdirilmiştir. Bunun için agaroz (Ag), metakrile jelatin (GelMA), metakrile hiyalüronik asit (MeHA) ve GelMA-MeHA gibi birçok hidrojel hazırlanmış ve bunların domuz ve insan fibrokondrosit hücrelerinin aktivitelerine etkileri incelenmiştir.

Herhangi bir hayvan deneyinde kullanılmadan önce, yapıların performansları *in vitro* koşullarda domuz fibrokondrositleriyle test edilmiştir. Bunun için çeşitli hidrojellere (Ag, GelMA, MeHA ve GelMA-MeHA) hücre ekilip statik (yüksüz) ya da dinamik (basma, %5-15 gerilme ile) kültür ortamında denenmiştir. 3B basılmış PCL

taşıyıcılarını kaplamak üzere GAG üretimini artıran Ag ve kollajen üretimini artıran GelMA seçilmiştir. Elli altı günlük kültür sonunda Ag'a emdirilmiş PCL'nin hidrojel emdirilmemiş PCL'e göre 2 kat daha fazla kollajen ve 3 kat daha fazla GAG ürettiği, GelMA'ya emdirilmiş PCL'in ise 10 kat daha fazla kollajen ürettiği görülmüştür. PCL taşıyıcıların mekanik özellikleri hidrojellerin varlığında değişim göstermemiştir. Menisküs şeklindeki PCL taşıyıcılar 3B basımla elde edilmiş ve iç kısımda Ag'a, dış kısımda GelMA'ya emdirilmiştir. Elli altı günlük kültürün sonunda garoza emdirilmiş iç kısımda yüksek oranda GAG, GelMA'ya emdirilmiş iç kısımda yüksek oranda kollajen üretimi görülmüştür. Böylece menisküs dokusunun biyokimyasal içeriğine benzer taşıyıcılar elde edilmiştir.

Taşıyıcıların klinik deneylerden önce *in vitro* koşullarındaki performanslarını test etmek için, yapay dokular insan fibrokondrositleri kullanılarak üretilmiştir. Bu amaçla, değişik tasarımlarda ve çeşitli iç (katmanları kaydırmadan ya da kaydırarak) ve dış (çevresel fiberler içeren ya da içermeyen) mimarilere sahip, dikdörtgen prizma şeklinde PCL taşıyıcılar üretilmiş ve bu taşıyıcıların menisküs implantı olarak kullanıma uygunluğu araştırılmıştır. Katmanların kaydırılması mekanik özelliklerin düşmesine, çevresel fiberlerin eklenmesi ise mekanik özelliklerin artmasına neden olmuştur. Taşıyıcılar hem kaydırmalı katmanlar şeklinde hem de çevresel fiberlerin varlığında üretildiğinde, menisküs değerlerine (0.3-2 MPa) yakın basma modülü (~0.4 MPa) ve menisküsünkünden (70-130 MPa) daha düşük çekme modülü (18 MPa) değerleri göstermiştir.

Sonuçta, 3B basılmış PCL taşıyıcılar kaydırmalı katmanlar şeklinde ve çevresel fiberler eklenerek üretilmiş, insan hücresi taşıyan Ag, GelMA ya da GelMA-Ag hidrojellerine emdirilmiş ve statik kültür ortamında 42 gün inkübe edilmişlerdir. Hidrojellere emdirilmiş taşıyıcıların en yüksekten en düşüğe doğru kollajen üretimleri GelMA > GelMA-Ag > Ag sıralamasında olmuştur. Menisküs şeklinde üretilen ve çevresel fiberler içeren taşıyıcıların iç kısımları Ag yerine GelMA-Ag ile kaplandığında kollajen üretiminde bir artış gözlenmiştir. Sonuçta menisküs dokusuna benzer bir şekilde biyokimyasal açıdan bölgesel değişkenlik gösteren (dış kısımda yüksek COL I, dış kısımda da yüksek COL II) taşıyıcılar elde edilmiştir. Aynı

zamanda menisküs dokusunun yapısal organizasyonu da çevresel fiberler eklenerek taklit edilmiştir.

Anahtar kelimeler: menisküs doku mühendisliği, 3B basım, PCL, agaroz, GelMA

Dedicated to my family, Eda and Demir Ayaz...

ACKNOWLEDGEMENTS

I would like to express my deepest gratitude and respect to my thesis advisor, Prof. Dr. Vasif Hasırcı, who has been supervising me for 10 years now, including my undergraduate and graduate education. He has opened many paths in my life and has been more than an advisor to me.

I would like to express my special thanks to my co-advisor, Prof. Dr. Nesrin Hasırcı, who has taught me several things not only in my academic life, but also in my social life.

I would like to thank Assist. Prof. Bahar Bilgen for her contributions to my thesis and for providing me with all the sources she had in her Lab at Brown University. She has been not only a good mentor, but also a valuable friend to me.

I present my endless thanks to Prof. Dr. Dilek Keskin Şendil and Prof. Dr. Nuhan Puralı for their contributions to my studies as my thesis monitoring committee members, and for the time and efforts they had spent during my thesis work.

I would like to express my deepest love and compassion to my family. I would like to thank my loving wife, Eda Bahçecioğlu for her dignity, and the endless support, patience, and understanding she showed during my thesis work. She is all what I desire in my life, my best friend, my family, and my nearest and dearest. I would like to thank my lovely baby, Demir Ayaz Bahçecioğlu for just giving me the joy of having him. I would like to thank my parents Ahmet and Azize Bahçecioğlu for always being compassionate to me throughout my life. I would like to thank my sisters and brothers, Eylem, Can, Ozgur, Suphi and Ozlem for the nicest moments we have shared throughout my life.

I would like to thank my lab mates for their friendship and support in my professional and social lives. I would like to thank Aylin Kömez, Ezgi Antmen and Deniz Sezlev Bilecen for their sincere friendship and the joyous moments we shared

during this long journey. I would like to thank my roommates Cemile Bektař and Menekse Ermiř Ően for their friendship and support. I would like to thank Gzde Eke for her valuable friendship. I want to thank aęla Mirasyedioęlu for her friendship and the candid conversations we have had. I thank Tuęba Dursun, Esen Sayın, Arda Byksungur, Senem Byksungur, Selcen Alagz, Emre Ergene, Elbay Malikmamadov and Dilara Tamay for their friendship. I thank Deniz Atilla for her help in the mechanical testing. I also thank Zeynel Akın, Ramazan Kavak and Yksel Gneř for their help and effort throughout these years.

This study was supported by TBTAK through BDEB 2214-A Scholarship.

TABLE OF CONTENTS

ABSTRACT	v
ÖZ	ix
ACKNOWLEDGEMENTS	xiii
TABLE OF CONTENTS	xv
LIST OF TABLES	xix
LIST OF FIGURES	xxi
LIST OF ABBREVIATIONS	xxvii
CHAPTERS	
1. INTRODUCTION	1
1.1. Rationale	1
1.2. The Knee Meniscus.....	2
1.2.1. Anatomy of the Meniscus	2
1.2.2. Biology and Structure of the Meniscus	2
1.2.3. Blood Supply.....	4
1.2.4. Cell Types in the Meniscus	4
1.3. Meniscus Biomechanics.....	5
1.4. Meniscal Injury and Its Treatment	6
1.4.1. Meniscal Injury	6
1.4.2. Conventional Treatment Methods.....	6
1.4.2.1. Meniscal Repair	6
1.4.2.2. Meniscal Substitutes	7
1.4.3. Tissue Engineering of the Meniscus	9
1.4.3.1. Cells	9
1.4.3.2. Biochemical and Mechanical Stimuli.....	10
1.4.3.3. Scaffolds	11

1.5. Design of the Construct.....	20
1.6. Design of the Study.....	21
2. MATERIALS AND METHODS	25
2.1. Materials.....	25
2.2. Methods.....	26
2.2.1. Isolation of Meniscus Cells (Fibrochondrocytes)	26
2.2.2. Preparation of the Constructs	27
2.2.2.1. Three Dimensional Printing of the PCL Scaffolds	27
2.2.2.2. Preparation of the Hydrogel Constructs.....	28
2.2.2.3. Preparation of the 3D Printed PCL/Hydrogel Composite Constructs.....	32
2.2.3. Characterization of the Constructs	42
2.2.3.1. Characterization of GelMA and MeHA.....	42
2.2.3.2. Macroscopic Characterization	43
2.2.3.3. Microscopic Characterization	43
2.2.3.4. Mechanical Characterization	44
2.2.3.5. Cell Viability Analysis.....	45
2.2.3.6. Cell Metabolic Activity.....	46
2.2.3.7. Cell Morphology	46
2.2.3.8. Cell-Material Interactions	46
2.2.3.9. Biochemical Analysis	47
2.2.3.10. Histology and Immunohistochemistry	48
2.2.3.11. Immunofluorescence	49
2.2.4. Statistical Analysis	49
3. RESULTS AND DISCUSSION	51
3.1. Characterization of the Cells Isolated from Menisci	51
3.1.1. Flow Cytometry.....	51
3.1.2. Microscopy.....	51
3.2. Optimization of the 3D Printing Process Using PCL	52
3.3. Characterization of GelMA and MeHA Polymers.....	54
3.3.1. Optimization of Hydrogel Photocrosslinking Process	54

3.3.2. Proton NMR Spectroscopic Characterization	55
3.3.3. ATR-FTIR Characterization	55
3.4. Porcine Fibrochondrocyte-Based Studies	58
3.4.1. Hydrogel Constructs	58
3.4.1.1. Change in Physical Properties of the Constructs	58
3.4.1.2. Microarchitecture of the Constructs	63
3.4.1.3. Compressive Mechanical Properties of the Constructs	64
3.4.1.4. Cell Viability and Cell Metabolic Activity.....	66
3.4.1.5. Collagen Contents of the Constructs	70
3.4.1.6. Sulfated GAG Contents of the Constructs.....	74
3.4.1.7. Cell Morphology.....	76
3.4.1.8. Cell-Material Interactions	78
3.4.2. Square Prism-Shaped PCL/Hydrogel Composite Constructs	81
3.4.2.1. Microscopic Evaluation	81
3.4.2.2. Mechanical Properties.....	82
3.4.2.3. Cell Viability on Constructs	85
3.4.2.4. GAG Contents.....	88
3.4.2.5. Collagen Contents.....	90
3.4.2.6. Immunofluorescence.....	91
3.4.3. Meniscus-Shaped PCL/Hydrogel Composite Constructs	97
3.4.3.1. Microscopic Evaluation	97
3.4.3.2. Cell Viability.....	99
3.4.3.3. GAG Contents.....	101
3.4.3.4. Collagen Contents.....	103
3.4.3.5. Immunofluorescence.....	105
3.5. Human Fibrochondrocyte-Based Studies	110
3.5.1. Square Prism-Shaped Composite Constructs.....	110
3.5.1.1. Scaffold Microarchitecture	110
3.5.1.2. Mechanical Properties of the Scaffolds	111
3.5.1.3. Cell Morphology and Spreading Behavior	115
3.5.1.4. Cell Viability.....	116
3.5.1.5. Immunofluorescence.....	118

3.5.2. Meniscus-Shaped PCL/Hydrogel Composite Constructs	124
3.5.2.1. Macro- and Microarchitecture of the Scaffolds	124
3.5.2.2. Cell Morphology on PCL Scaffolds	125
3.5.2.3. Preparation of the Final 3D Composite Constructs	127
3.5.2.4. Cell Viability on the Final 3D Composite Constructs	127
3.5.2.5. Immunofluorescence	127
4. CONCLUSION.....	131
REFERENCES.....	135
APPENDICES.....	155
A: ALAMAR BLUE ASSAY	155
B: STANDARD CURVE FOR DNA QUANTIFICATION.....	157
C: STANDARD CURVE FOR sGAG QUANTIFICATION	159
D: STANDARD CURVE FOR COLLAGEN QUANTIFICATION.....	161
CURRICULUM VITAE	163

LIST OF TABLES

Table 3.1. Minimum time of UV exposure required for gelation of GelMA (porcine) and MeHA.....	54
Table 3.2. Porcine fibrochondrocyte viability on square prism-shaped, PCL-based constructs on Day 42 as determined with live/dead assay.....	89
Table 3.3. Human fibrochondrocyte viability on square prism-shaped constructs as determined with live-dead assay.....	120

LIST OF FIGURES

Figure 1.1. Schematic illustration of the meniscus	3
Figure 1.2. Collagen organization in the meniscus.....	4
Figure 1.3. Diagram showing the soft lithography technique	15
Figure 1.4. Three dimensional printing techniques.....	17
Figure 1.5. The design of the proposed 3D printed PCL scaffold	22
Figure 2.1. Isolation of fibrochondrocytes from the medial porcine meniscus	27
Figure 2.2. Schematic representation of the different settings of the 3D printing process.....	28
Figure 2.3. Methacrylation of gelatin and hyaluronic acid	29
Figure 2.4. Crosslinking of GelMA and MeHA by UV radiation	30
Figure 2.5. Scaffold preparation and culture conditions	33
Figure 2.6. Preparation of the 3D printed PCL-Hydrogel constructs	34
Figure 2.7. Preparation of the square prism shaped PCL/hydrogel constructs	35
Figure 2.8. PCL/hydrogel constructs were incubated under static or dynamic culture conditions	36
Figure 2.9. Design of the coliseum shaped structure that is cut into two halves to obtain the meniscus shaped constructs, and its preparation and culture	39
Figure 2.10. Designs of the compression head and the constructs, and depiction of the dynamic compression applied on the constructs.....	41

Figure 2.11. Representative graphs showing the calculations of the modulus values	45
Figure 3.1. Phase contrast micrograph of the fibrochondrocytes cultured on TCPS..	52
Figure 3.2. Optimization of the 3D printing of PCL 80.....	53
Figure 3.3. Proton NMR spectroscopy of gelatin, GelMA, and MeHA	56
Figure 3.4. ATR-FTIR absorbance intensity of the untreated and UV-treated polymers	57
Figure 3.5. The change in size of the cell-seeded and cell-free samples over 35 days of culture	59
Figure 3.6. Physical properties of the hydrogels on Day 35 relative to Day 1	61
Figure 3.7 Microarchitecture of the cell-free constructs after 35 days of incubation in culture media	63
Figure 3.8. Compressive mechanical properties of the constructs after 35 days of culture.....	65
Figure 3.9. DNA contents of the constructs.....	67
Figure 3.10. Cell metabolic activity in the constructs.....	68
Figure 3.11. Live/dead cell viability assay results of the constructs on Day 35	69
Figure 3.12. Collagen contents of the constructs and the native meniscus determined with orthohydroxyproline (OHP) assay	71
Fig 3.13. Immunohistochemistry of the hydrogels incubated for 35 days in culture..	73
Figure 3.14. Sulfated glycosaminoglycan (sGAG) contents of the constructs and the native meniscus	75
Figure 3.15. Histology showing sulfated GAG deposition on the constructs after 35 days of culture	76

Figure 3.16. Representative images showing the cell morphologies cell adhesion on the hydrogels	77
Figure 3.17. Summary of the results obtained with hydrogel-based studies.	80
Figure 3.18. Microscopy of the dry, cell-free constructs	82
Figure 3.19. Elastic modulus of the constructs under compressive and tensile load..	83
Figure 3.20. DNA contents and cell viability on the square prism shaped constructs... ..	86
Figure 3.21. The sulfated GAG and collagen contents of the square prism shaped constructs	89
Figure 3.22. Immunofluorescence of the PCL constructs.....	93
Figure 3.23. Immunofluorescence of the PCL-Ag constructs	94
Figure 3.24. Immunofluorescence of the PCL-GelMA constructs	96
Figure 3.25. The meniscus-shaped PCL scaffold and its microarchitecture.....	98
Figure 3.26. Cell viability on the constructs after 56 days of culture period.....	100
Figure 3.27. Sulfated GAG contents of the cell-seeded constructs after 56 days of culture period	102
Figure 3.28. Collagen contents of the PCL-based constructs after 56 days incubation in culture media.....	104
Figure 3.29. Immunofluorescence of the PCL-Ag constructs after 56 days of culture.. ..	107
Figure 3.30. Immunofluorescence of the PCL-Ag-GelMA constructs after 56 days of culture.....	108
Figure 3.31. The overall scheme showing the design and findings of the study	109
Figure 3.32. Macro- and micro-architecture of the PCL 50 scaffolds	111

Figure 3.33. Mechanical properties of the PCL 50 scaffolds.....	113
Figure 3.34. Morphology of the human fibrochondrocytes on the constructs after incubation for 7 days.....	115
Figure 3.35. Cell viability of the square prism-shaped constructs after 42 days of culture.....	117
Figure 3.36. Collagen deposition on the human fibrochondrocyte-seeded square prism-shaped PCL constructs.....	119
Figure 3.37. Collagen deposition on the human fibrochondrocyte-seeded square prism-shaped PCL-Ag constructs.....	120
Figure 3.38. Collagen deposition on the human fibrochondrocyte-seeded square prism-shaped PCL-GelMA constructs	121
Figure 3.39. Collagen deposition on the human fibrochondrocyte-seeded square prism-shaped PCL-(GelMA-Ag) constructs	122
Figure 3.40. Macro- and micro-architecture of the meniscus-shaped PCL scaffolds... ..	125
Figure 3.41. CLSM images of the human fibrochondrocyte-seeded PCL scaffolds after incubation for 14 days in culture media.....	126
Figure 3.42. Representative photographs of the final constructs and their comparison to the native menisci.....	128
Figure 3.43. Representative images showing cell viability on the final meniscus-shaped constructs as determined with the live/dead assay.....	129
Figure 3.44. Collagen deposition on the human fibrochondrocyte-seeded meniscus-shaped constructs.....	129
Figure B.1. A representative standard curve for the PicoGreen dsDNA quantification assay.. ..	157
Figure C.1. A representative standard curve for the DMMB assay	159

Figure D.1. A representative standard curve for the orthohydroxyproline assay ... 161

LIST OF ABBREVIATIONS

BSA	Bovine Serum Albumin
CLSM	Confocal Laser Scanning Microscopy
CO ₂	Carbon Dioxide
DAPI	4', 6-diamidino-2-phenylindole
DMEM	Dulbecco's Modified Eagle Medium
DMSO	Dimethyl Sulfoxide
ECM	Extracellular Matrix
EDTA	Ethylenediaminetetraacetic Acid
TGF- β	Transformal Growth Factor Beta
FAK	Focal Adhesion Kinase
FBS	Fetal Bovine Serum
FITC	Fluorescein Isothiocyanate
FTIR	Fourier Transform Infrared
MW	Molecular Weight
PBS	Phosphate Buffer Saline
PCL	Poly(ϵ -caprolactone)
PDMS	Poly(dimethylsiloxane)
Pen/Strep	Penicillin/Streptomycin
RGD	Arginine Glycine Aspartic Acid Sequence
SEM	Scanning Electron Microscopy
TCPS	Tissue Culture Polystyrene

CHAPTER 1

INTRODUCTION

1.1. Rationale

Meniscal tears, among the most commonly experienced knee injuries, are mostly encountered during harsh sports activities or due to ageing that results in tissue degeneration. Swelling, locking of the knee joint, and pain are some of the symptoms related to meniscal tears. In addition to health problems, they lead to considerable financial expenses, as well as labor and productivity. More than 800,000 people suffer from meniscal problems each year in Europe (MedTech Insight Web Page), and more than 1 million in the USA (American Academy of Orthopaedic Surgeons Web Page). Majority of the patients (more than 1.5 million per year) are going through meniscal surgery (Azellon Cell Therapeutics Web Page).

The meniscus has a low regenerative potential due to its limited vasculature, and needs to be treated surgically if injured seriously (Arnoczky and Warren, 1983). Repair of the meniscus using sutures, staples, and glues leads to fibrous scar, which in turn results in alteration of the knee biomechanics. Meniscectomy, the partial or total removal of the meniscus, has been applied to reduce pain, but results in osteoarthritis in the long term (Lohmander *et al.*, 2007). Therefore, a tissue substitute is required to prevent the degeneration of the hyaline cartilage underlying the meniscus. Transplantation is one approach to replace the meniscus, but there is a shortage of donor tissue, and the risks of rejection and disease transmission (Kuhn and Wojtys, 1996). In addition, transplants do not prevent osteoarthritis in the long term (Van den Straeten *et al.*, 2016). Prostheses, on the other hand, fail after some time and some may lead to osteophyte formation and synovitis (Messner, 1994). All these urge the necessity of an alternative treatment method that would be an efficient solution to serious meniscal tears.

1.2. The Knee Meniscus

Meniscus is a crescent-like fibrocartilage located between the femur and the tibia (Fig. 1.1A). The tissue has many roles including load bearing and transmission in the knee, shock absorption, and joint stability and lubrication (Fithian *et al.*, 1990).

1.2.1. Anatomy of the Meniscus

The meniscus resembles an amphitheater (or coliseum); it is semilunar when viewed from the top, and wedge-shaped at the cross section (Fig. 1.1). The top (superior) surface is concave enabling a fit with the femoral condyles, and the bottom (inferior) surface is relatively flat and sits on the tibial plateau. There are two menisci in a knee: lateral and medial, which are attached to the tibia through their horns (Fig. 1.1B). The peripheral portion of the tissue is attached to the joint capsule (Arnoczky, 1992).

1.2.2. Biology and Structure of the Meniscus

Seventy percent of the meniscus is water, and most of its dry weight is composed of collagen (85-95%), while the remaining contains proteoglycans (glycosaminoglycans (GAGs) that are bound by a protein core) and non-collagenous proteins like elastin (Fithian *et al.*, 1990; Eyre and Wu, 1983; McDevitt and Weber, 1990). The collagen in the meniscus is mainly type I (75%), and there are also type II, III, V, and VI collagens (Eyre and Wu, 1983; Herwig *et al.*, 1984). The tissue exhibits fibrous characteristics at the outer periphery and cartilaginous characteristics in the inner region, although there is no defined borders separating the two regions. The collagen in the outer region is mainly type I (COL I) (80%), while that in the inner region is mainly type II (COL II) (60% COL II, and 40% COL I) (Cheung, 1987). GAGs are also more abundant in the inner region of the meniscus (2-4%) than the outer region (1%) (Herwig *et al.*, 1984; Sanchez-Adams *et al.*, 2013).

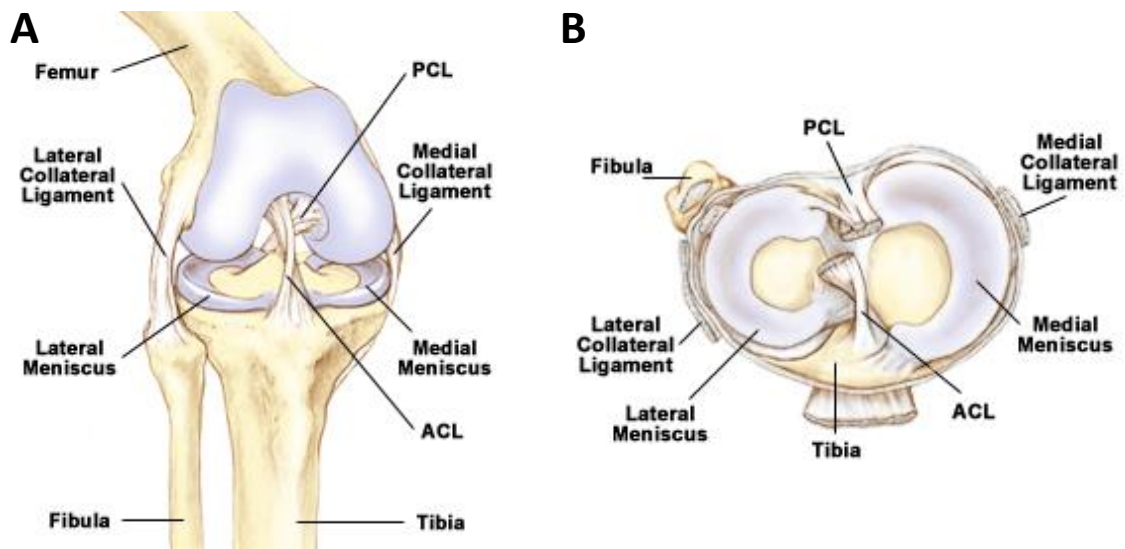


Figure 1.1. Schematic illustration of the meniscus. (A) Lateral, and (B) top view of the knee menisci (adapted from <http://www.leadingmd.com/patiented/meniscus/over view.asp>).

Aligned collagen (COL I and COL II) triple helices (diameter: 1.5 nm, length: 300 nm) organize into microfibrils (diameter: 20~500 nm), which also organize into fibrils (diameter <10 μm) (Birk *et al.*, 1991). The collagen fibrils are organized randomly at the surface, and aligned circumferentially at the center with few tie fibers binding these fibrils radially (Ghadially *et al.*, 1983; Petersen and Tillman, 1998) (Fig. 1.2). This organization of the collagen fibrils is what makes the tissue strong against tensile load (Fithian *et al.*, 1990).

Glycosaminoglycans (GAGs), the negatively charged polysaccharides, bind a considerable amount of water and help in building hydrostatic pressure against compressive load (Adams and Muir, 1981; Meyers *et al.*, 1988; Adams and Hukins, 1992). The main types of GAGs present in the human meniscus are chondroitin sulfate, dermatan sulfate, and keratan sulfate (Herwig *et al.*, 1984).

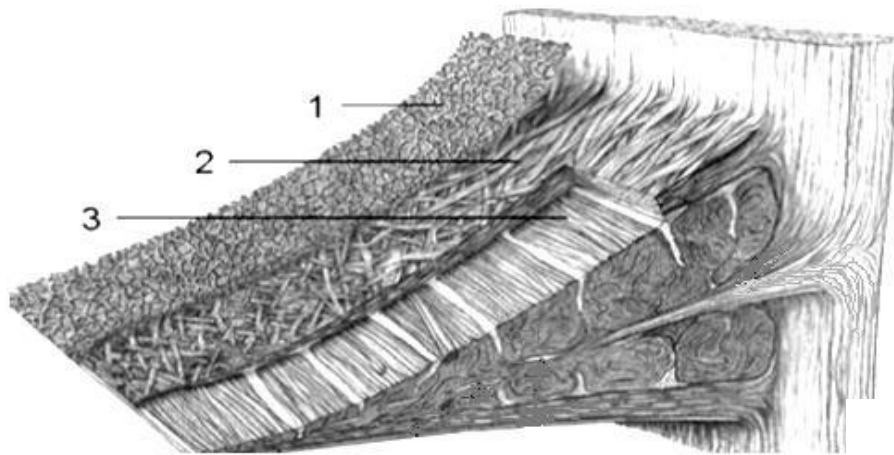


Figure 1.2. Collagen organization in the meniscus. (1) Superficial layer: with randomly oriented collagen fibers, (2) lamellar layer: with randomly and radially oriented thick collagen bundles, and (3) deep layer: with circumferentially oriented collagen fibrils. (Adapted from Petersen and Tillman, 1998).

1.2.3. Blood Supply

The meniscus is divided into three zones in terms of presence of blood vessels, although these regions do not have defined borders and the blood supply changes gradually from the outer to the inner region. The outer region (10-30% of the tissue at the periphery) is called the red-red zone and contains blood vessels (Drengk *et al.*, 2008). The inner region is called the white-white zone and lacks blood supply. The middle region is called red-white zone and has some blood vessels, but in limited abundance (Drengk *et al.*, 2008).

1.2.4. Cell Types in the Meniscus

Three cell types have been reported in the meniscus, each residing in different parts of the tissue (Ghadially *et al.*, 1978). Whether they are cells of the same origin assuming different morphologies depending on the region they reside in or they are cells of different origins is not known.

One cell type is the round-shaped or polygonal cell which is present in the inner region and expresses chondrocytic phenotype (Hellio Le Graverand *et al.*, 2001).

Another cell type is the branched cell with long processes and expresses fibroblastic phenotype, and is located in the outer region of the tissue. The last cell type is the spindle-like cell which resides in the superficial layer and expresses fibroblastic behavior (Hellio Le Graverand *et al.*, 2001). These cells are suggested to be progenitor cells, which could aid in regeneration of the meniscus (Van der Bracht *et al.*, 2007). In fact, they have been shown to exhibit potency; they can be differentiated towards adipogenic, chondrogenic and osteogenic lineages (Mauck *et al.*, 2007). These cells are called fibrochondrocytes due to their fibrocytic and chondrocytic phenotypes.

1.3. Meniscus Biomechanics

A load up to 5 times the body weight is exerted on the knee joint at physiological conditions (Paul, 1976), and the meniscus can carry up to 75% of this load (Shrive *et al.*, 1978). The tissue can withstand various stresses including shear, tension and compression owing to its biochemical composition and structural organization (Makris *et al.*, 2011). In fact, during the early developmental stages, the meniscus is exposed to mechanical load, leading to maturation of the tissue (Setton *et al.*, 1999).

The main component of the meniscal tissue is the collagen, which is aligned to form the circumferential fibers and thus increases the tensile properties of the tissue (Fithian *et al.*, 1990). On the other hand, GAGs bind considerable amounts of water, and presence of this bound water in the tissue contributes to the viscoelastic properties (compressive and equilibrium modulus) of the tissue (McDermott *et al.*, 2008).

The composition and organization of the meniscus are very important in providing resistance against the stresses exerted on it, and thus play critical role in its functionality. The human meniscus has an aggregate (or equilibrium) modulus of 40-220 kPa (Joshi *et al.* 1995; Sweigart *et al.* 2004; Chia and Hull, 2008), a compressive modulus of 0.3-1 MPa (Chia and Hull, 2008), and a tensile modulus of 4-20 MPa in radial direction and 70-130 MPa in circumferential direction (Tissakht and Ahmed, 1995).

1.4. Meniscal Injury and Its Treatment

1.4.1. Meniscal Injury

Meniscal tears generally occur as a result of ageing and degeneration of the tissue, and also during intense physical activity and traumatic injuries (Greis *et al.* 2002). Torn meniscus leads to high medical expenses and loss of labor, in addition to severe pain, restricted flexion and extension of the knee, stiffness and swelling, and difficulty in movement (American Academy of Orthopaedic Surgeons Web Page).

Meniscal tears in the outer periphery can heal due to presence of blood vessels that confer the tissue a regenerative capacity, while tears in the inner region cannot heal without medical intervention (Arnoczky and Warren, 1983).

1.4.2. Conventional Treatment Methods

There are many treatment methods to reduce the symptoms of mild meniscal injury, including ice treatment, compression, and elevation of the knee (American Academy of Orthopaedic Surgeons Web Page). However, these are only useful when the symptoms are mild, and do not work in the treatment of severe meniscal injuries.

When the meniscus is severely injured and a complex meniscal tear occurs, it should be treated surgically. Tears could be repaired or replaced with prostheses, transplants or implants.

1.4.2.1. Meniscal Repair

Surgical interventions performed to facilitate meniscal repair include the use of hydrogel materials such as gelatin (Szomor *et al.*, 2008), fibrin glue and suture (Arnoczky *et al.*, 1988; Noyes *et al.*, 2002) to seal the torn meniscus, and rasping (Uchio *et al.*, 2003) to facilitate the access of blood to the site of injury. These methods are easy to apply, require short time, and have reduced risks and high success rate (Baker *et al.*, 2011; Makris *et al.*, 2011). However, these methods may lead to fibrous scar formation or disruption of the extracellular matrix (ECM) organization, and eventually to limited movement due to disrupted biomechanics of

the knee (Newman *et al.*, 1989). These methods are used successfully in treatment of simple tears, but when it comes to complex tears they are not as useful.

1.4.2.2. Meniscal Substitutes

In some cases when the tears are complex, the repair methods cannot be used. Instead, the torn portion of the meniscus (partial meniscectomy) or the whole tissue (total meniscectomy) is removed. Meniscectomy may lead to degeneration of the underlying cartilage and eventually to osteoarthritis (OA) in the long term (Lohmander *et al.*, 2007). In order to prevent the degeneration of the underlying cartilage, tissue substitutes can be used after meniscectomy.

Transplantation is a common method used to replace the meniscectomized tissue with autografts and allografts (Gao *et al.*, 1998; Rath *et al.*, 2001; Dienst *et al.*, 2007). However, this method bears the risks of disease transmission and tissue rejection, and the drawbacks of donor tissue shortage (Kuhn and Wojtys, 1996; Gao *et al.*, 1998; Becker and Jakse, 2007). Besides, transplants may not be an efficient method to prevent OA in the long term (Gao *et al.*, 1998; Van der Straeten *et al.*, 2016).

Another approach to replace the resected meniscus is the decellularized tissue substitutes. Decellularization is the removal of the cell components in the tissue by exposing it to various detergents and enzymes, in order to reduce the antigen content and the risk of immune reaction, and increase the shelf life of the tissue (Farr *et al.*, 2011; Demange and Gomoll, 2012). Many decellularized tissues can be used to replace the meniscus, including the meniscus itself, small intestinal submucosa (SIS), tendon, and periosteal or perichondral tissues (Bruns *et al.*, 1998; Stone *et al.*, 1998; Walsh *et al.*, 1999; Cook *et al.*, 1999; Maier *et al.*, 2007; Stapleton *et al.*, 2008; Stabile *et al.*, 2010; Stapleton *et al.*, 2011; Gao *et al.*, 2016). The main disadvantages of the decellularized tissues are their low mechanical properties and the problem of calcification post implantation (Kohn *et al.*, 1992; Bruns *et al.*, 2000). In addition, the decellularized tissue substitutes limit the infiltration of the surrounding tissue and thus the regeneration of the meniscus, due to their limited porosity (Johnson and Feagin, 2000).

One other method to replace the resected meniscus is the use of prostheses. Prostheses are designed to stay for a long time in the body and replace the function of the meniscus. Many materials, including natural and synthetic polymers, can be processed into a meniscal shape and implanted in the knee as prostheses.

The only natural polymer used to produce prostheses is collagen. One of the most promising prosthetic device is the Collagen Meniscus Implant (CMI, Regen Menaflex®), a commercial implant made of collagen and GAGs. Although CMI has good clinical outcomes for the chronic meniscus injuries (Stone *et al.*, 1990; 1992; 1997; Steadman and Rodkey, 2005; Rodkey *et al.*, 2008), it is not as successful in treatment of the acute injuries (Rodkey *et al.*, 2008). Another problem is the deterioration of the implant and significant reduction of its size after implantation (Mueller *et al.*, 1999; Zaffagnini *et al.*, 2011; Efe *et al.*, 2012).

The synthetic polymers used to produce prostheses are polycaprolactone (PCL) and polylactic acid (PLA) (Chiari *et al.*, 2006; Kon *et al.*, 2008; 2012), polyvinyl alcohol (PVA) (Kobayashi *et al.*, 2003; 2005; Kelly *et al.*, 2007; Holloway *et al.*, 2010), PCL and polyurethane (PU) (Actifit®) (de Groot, 2010; Tienen *et al.*, 2006; Welsing *et al.*, 2008; Maher *et al.*, 2010; Brophy *et al.*, 2010; Verdonk *et al.*, 2012), Teflon (poly(tetrafluoroethylene), PTFE), and Dacron (poly(ethylene terephthalate), PET)) (Veth *et al.*, 1986; Stone *et al.*, 1990; Sommerlath *et al.*, 1992; Messner and Gillquist, 1993; Messner, 1994), polycarbonate urethane (PCU) (Vrancken *et al.*, 2015), polyethylene (PE) and PCU (NUsurface®) (Elsner *et al.*, 2010; Linder-Ganz *et al.*, 2010; Zur *et al.*, 2011), and poly (desaminotyrosyl-tyrosine dodecyl ester dodecanoate) (pDTDDD) (Patel *et al.*, 2016). All these prostheses show good results when implanted; however, they also have some drawbacks including extrusion or dislocation of the implants due to poor fixation (Kon *et al.*, 2012), degeneration of the underlying cartilage (Kelly *et al.*, 2007; Vrancken *et al.*, 2015), having no advantages over the untreated control group (Zur *et al.*, 2011), and low mechanical properties (Verdonk *et al.*, 2012).

Transplantation remains to be the best treatment option after meniscectomy, despite its risks. This indicates that an efficient treatment method alternative to all these methods is essential.

1.4.3. Tissue Engineering of the Meniscus

Tissue engineering is a viable alternative to the conventional treatment methods for serious meniscal injuries (Harston *et al.*, 2012). Tissue engineering is a regenerative approach aiming to repair, augment, and replace the functions of a damaged tissue (Langer and Vacanti, 1993). The tissue engineered construct replaces the tissue or a part of it that has lost its functions, and restores the functionality of that tissue. Tissue engineering consists of three elements: (1) the cells that produce the tissue, (2) the biochemical and mechanical stimuli that induce cell proliferation, differentiation and ECM production, and (3) the biodegradable scaffolds that guide the cells by presenting mechanical cues and provide the mechanical support until the tissue is regenerated.

1.4.3.1. Cells

The cell is the main component of tissue engineering; they build the tissue by depositing ECM. The cell types used to engineer the meniscus are fibrochondrocytes (Vanderploeg *et al.*, 2004; Mandal *et al.*, 2011a; Ballyns and Bonassar, 2011; Ndreu-Halili *et al.*, 2014; Bahcecioglu *et al.*, 2014; Puetzer *et al.*, 2015; McCorry *et al.*, 2016; Bahcecioglu *et al.*, 2018) mesenchymal stem cells (MSCs) (Mandal *et al.*, 2011b; Lee *et al.*, 2014; McCorry *et al.*, 2016; Zhang *et al.*, 2017), fibroblasts (Gunja and Athnasiou, 2009; Mandal *et al.*, 2011a; Bahcecioglu *et al.*, 2018), and chondrocytes (Marsano *et al.*, 2006a; Kon *et al.*, 2008; Kalpakci *et al.*, 2011; Mandal *et al.*, 2011a). Chondrocytes are hard to culture and expand (Ho *et al.*, 2009), and fibroblasts do not produce fibrocartilaginous tissue, preventing these cells to be the preferred cell types. MSCs are good candidates for use in meniscal tissue engineering applications because they have a great differentiation potential and can be harvested easily, but they require a proper differentiation step, which otherwise can lead to cell lineages other than fibrochondrocytes. Meniscal fibrochondrocytes, on the other

hand, are already mature, adult cells which can be isolated easily from the damaged tissue, and thus are preferred in the current study.

1.4.3.2. Biochemical and Mechanical Stimuli

The biochemical and mechanical signals guide the cells to produce the proper ECM components. The biochemical signals include the growth factors, and the mechanical signals include static or dynamic compression, tension, and shear.

1.4.3.2.1. Growth Factors

Growth factors are commonly used to direct cell behavior. Basic fibroblast growth factor (FGFb), platelet-derived growth factor AB (PDGF-AB), bone morphogenetic protein 2 (BMP-2), and hepatocyte growth factor (HGF) have been used to enhance cell proliferation, insulin-like growth factor 1 (IGF-1), epidermal growth factor (EGF), BMP-2, PDGF-AB, and HGF to promote cell migration, and connective tissue growth factor (CTGF), transforming growth factor- β 1 (TGF- β 1) and TGF- β 3 to enhance ECM production (Webber *et al.*, 1985; Bhargava *et al.*, 1999; Collier and Ghosh, 1995; Tanaka *et al.*, 1999; Gunja *et al.*, 2009; Ballyns and Bonassar, 2011; Kalpakci *et al.*, 2011; Lee *et al.*, 2014; McCorry *et al.*, 2016). In order to induce meniscal ECM production, TGF- β 1 is applied in the current study.

1.4.3.2.2. Mechanical Stimuli

During the early developmental stages, the meniscus is exposed to mechanical load, leading to maturation of the tissue (Setton *et al.*, 1999). To this end, dynamic compression and tension have been applied *in vitro* in tissue engineering applications in order to mechanically stimulate the cells to produce cartilaginous and fibrocartilaginous tissues (Imler, 2005; Mauck *et al.*, 2007; Baker *et al.*, 2011; Ballyns and Bonassar, 2011; Puetzer *et al.*, 2015). Dynamic compression has been shown to enhance GAG and collagen production (Kisiday *et al.*, 2004; Aufderheide and Athanasiou, 2006; Kisiday *et al.*, 2009; Ballyns and Bonassar, 2011; Puetzer *et al.*, 2012), while dynamic tension to enhance collagen production (Baker *et al.*, 2011; Puetzer *et al.*, 2015).

Most of the studies employing dynamic compression involve the application of compressive strain in the range of 3-20%, at frequency ranges of 0.3-3 Hz, and duration of 30-120 minutes a day (Kisiday *et al.*, 2004; Aufderheide and Athanasiou, 2006; Waldmann *et al.*, 2007; Mauck *et al.*, 2007; Kisiday *et al.*, 2009; Babalola and Bonassar, 2009; Bian *et al.*, 2010; Ballyns and Bonassar, 2011; Huey and Athanasiou, 2011; Puetzer *et al.*, 2012; Petri *et al.*, 2012).

Dynamic compression on meniscal explants induces ECM production when applied at 10% strain, while results in breakdown of the ECM components when at 20% (Zielinska *et al.*, 2011). The meniscus is subject to average strain of 12% (ranging between 5-15%) under physiologically relevant loading environment (Freutel *et al.*, 2014). Therefore, in the current study a dynamic compression at 15% strain and 1 Hz is applied on the constructs for 1 h a day.

1.4.3.3. Scaffolds

The scaffolds are the substrates on which the cells attach, proliferate, and produce the new tissue. Scaffolds are biocompatible materials that guide the cells to produce the new tissue in the desired shape and structure. Thus, they should provide a space for the cells to migrate and produce the new tissue, and for the nutrients, oxygen, and waste products to be transported (Kim and Mooney, 1998). Therefore, they should be porous and biodegradable to allow for the new tissue to be deposited. In addition to that, scaffolds should provide the necessary mechanical strength to carry the loads exerted on the tissue until the new tissue forms and they are degraded in the body (Hutmacher, 2000).

The choice of the scaffold material is very important in determining the fate of the tissue that is to be engineered. The material is selected depending on the application; material properties should match those of the target tissue. Scaffold materials can be of natural or synthetic origin. Natural polymers that have been used for engineering of fibrocartilaginous tissues include agarose, alginate, cellulose, chitosan, collagen, fibrin gels, gelatin, hyaluronic acid, and silk (Aufderheide and Athanasiou, 2005; Martinek *et al.*, 2006; Mauck *et al.*, 2007; Angele *et al.*, 2008; Gruber *et al.*, 2008; Gunja *et al.*, 2009; Wilson *et al.*, 2009; Chung *et al.*, 2009; Ballyns and Bonassar,

2011; Mandal *et al.*, 2011; Petri *et al.*, 2012; Puetzer *et al.*, 2012; Sarem *et al.*, 2013; Grogan *et al.*, 2013; Ndreu-Halili *et al.*, 2014; Bahcecioglu *et al.*, 2014; Puetzer *et al.*, 2015; McCorry *et al.*, 2016; Pfeifer *et al.*, 2016; Donnelly *et al.*, 2017; Bahcecioglu *et al.*, 2018).

Gelatin and collagen are of particular importance in tissue engineering applications because they present biologic recognition sites, including arginine-glycine-aspartic acid (RGD) sequences that could induce cell adhesion (Liu *et al.*, 2010), and target sequences for matrix metalloproteinases (MMPs) that allow for ECM remodeling (Van den Steen *et al.*, 2002). However, these materials have poor mechanical strength (Lynn *et al.*, 2004), and may invoke inflammatory or immune reactions (Furhtmayr, 1976). The disadvantage of gelatin over collagen is its poorer mechanical strength due to loss of its tertiary structure, and the advantages are its high solubility and lower antigenicity (Maurer, 1954; Gorgieva and Kokol, 2011). Methacrylated gelatin (GelMA), a photoactive polymer, has recently been used in engineering of the cartilaginous tissues (Grogan *et al.*, 2013; Puetzer *et al.*, 2015; Levett *et al.*, 2014a; Levett *et al.*, 2014b; Visser *et al.*, 2015; Daly *et al.*, 2016). Less than 5% of the amino acids in these photoactive hydrogels are occupied due to modification with methacrylic anhydride (MA), which means that most of the bioactive motifs remain intact after modification (Van den Bulcke *et al.*, 2000; Yue *et al.*, 2015).

Synthetic polymers are also used to produce tissue engineering scaffolds. The advantage of these polymers are reproducibility and high mechanical properties (Buma, 2004; Atala, 2009), and the disadvantage is the inflammatory reaction against their degradation products (Bostman, 1991). Synthetic polymers that have been used in cartilaginous tissue engineering include PCL, PLA, poly(glycolic acid) (PGA), poly(lactide-co-glycolide) (PLGA), PU, polyesters, PVA, and combinations of these (Heijkants *et al.*, 2004; Gunja and Athanasiou, 2009; Holloway *et al.*, 2010; Nerurkar *et al.*, 2011; Baker *et al.*, 2011, Bahcecioglu *et al.*, 2014; Lee *et al.*, 2014; Baek *et al.*, 2015; Brunger *et al.*, 2014; Hayes *et al.*, 2016; Cengiz *et al.*, 2016; Daly *et al.*, 2016; Stocco *et al.*, 2017; Moradi *et al.*, 2017; Murakami *et al.*, 2017; Zhang *et al.*, 2017; Bahcecioglu *et al.*, 2018).

All these materials have their advantages and disadvantages. The choice of the materials should be done depending on the properties of the tissue to be engineered, the application, and the processing techniques appropriate for production of the construct.

1.4.3.3.1. Scaffold Processing Techniques

The processing technique used to produce a scaffold is as important as the material itself. The choice of the processing technique is dictated by the material used and the target application. For example, some techniques require heat, which is not appropriate for most of the natural polymers, while some others enable the use of soft materials only.

The processing techniques include freeze drying, solvent casting/particulate leaching, gas foaming, electrospinning, wet spinning, lithography, and three dimensional (3D) printing (additive manufacturing).

1.4.3.3.1.1. Freeze Drying (Lyophilization)

Freeze drying or lyophilization is based on freezing of a polymer solution to create a phase separation between the solvent and the polymer, and sublimation of the solvent under low temperature and high vacuum (Hasirci *et al.*, 2016). At the end, a porous foam or sponge is formed. Almost all the polymeric materials can be processed using this technique. Freeze drying has commonly been used in meniscus tissue engineering applications (Heijkants *et al.*, 2004; Mandal *et al.*, 2011a; Mandal *et al.*, 2011b; Ndreu-Halili *et al.*, 2014; Bahcecioglu *et al.*, 2014; Heo *et al.*, 2016; Bahcecioglu *et al.*, 2018).

1.4.3.3.1.2. Solvent Casting/Particulate Leaching

Solvent casting and particulate leaching are used together to form tissue engineering scaffolds. This technique is based on casting a polymer solution in a mold full of particulates (salt or porogen), solidifying the polymer, and removal of the particulates using a liquid that dissolves the particulate but not the polymer. After removal of the particulates a porous scaffold is obtained (Lee SB *et al.*, 2005). This technique was used to produce scaffolds for meniscus tissue engineering applications

(de Groot *et al.*, 1990; Mandal *et al.*, 2011a; Mandal *et al.*, 2011b; Yan *et al.*, 2012; Moradi *et al.*, 2017).

1.4.3.3.1.3. Gas Foaming

Gas foaming is similar to particulate leaching method, yet uses gas bubbles as a porogen (Nam *et al.*, 2000). The gas is usually carbon dioxide, and is formed by a chemical reaction of an acid with sodium carbonate during the polymerization of the scaffold polymer (Hasirci *et al.*, 2016). Gas foaming has been used in combination with other techniques for meniscus tissue engineering applications (Spaans *et al.*, 2000; Lee YH *et al.*, 2005; Joshi *et al.*, 2015).

1.4.3.3.1.4. Electrospinning

In electrospinning, an electric field is generated between the needle of a syringe full of a polymer solution and a grounded collector placed at a certain distance from the syringe (Ndreu, 2007). With the help of the electric field, a polymer jet is formed and ejected from the needle tip towards the collector, on which the polymer filaments are collected (Viswanathan *et al.*, 2006). During this process, the solvent is evaporated with the help of the high voltage applied before it reaches the collector, and a polymer mat builds up at the collector side. This technique has recently been used in meniscus applications (Lee YH *et al.*, 2005; Baker *et al.*, 2011; Ndreu-Halili *et al.*, 2014; Gao *et al.*, 2017).

1.4.3.3.1.5. Wet Spinning

Wet spinning is based on extrusion of a polymer solution through a spinneret into a non-solvent that is miscible with the solvent of the polymer, resulting in extraction of the solvent and precipitation of the polymer a continuous filament (Ucar *et al.*, 2013). The spinneret is moved during spinning process to produce a 3D scaffold. This technique has not been used in meniscus applications.

1.4.3.3.1.6. Lithography

Lithography is the production of scaffolds in the desired shape with the help of a mold or a mask (Hasirci *et al.*, 2016) (Fig. 1.3). In soft lithography, molds of

polydimethylsiloxane (PDMS) and poly(methyl methacrylate) (PMMA) are used (Hasturk *et al.*, 2016; Ermis *et al.*, 2016), due to their hydrophobic surface that allows for easy removal of the scaffolds (Selimovic *et al.*, 2012). In photolithography, light is used to photopolymerize the scaffold material, and a patterned mask is used to allow light to penetrate at some regions on the scaffold while preventing light from access to other regions (Komez *et al.*, 2016). Thus, some regions on the scaffold are crosslinked, while others are not. After washing of the uncrosslinked regions a pattern is formed on the surface of the scaffold. Lithography has been widely used to create molds into which meniscus tissue engineering scaffolds are cast (Kon *et al.*, 2008; Kon *et al.*, 2012; Wataya *et al.*, 2012).

1.4.3.3.1.7. Three Dimensional (3D) Printing

Three dimensional printing or additive manufacturing is based on the construction of complex structures by layer-by-layer deposition of a material through a nozzle with computer controlled devices (Chan *et al.*, 2010). It allows for rapid production of spatially controlled, patient-specific 3D scaffolds using the computer aided design (CAD) data that can be modeled or generated using the magnetic resonance imaging (MRI) or computed tomography (CT) scans (Hasirci *et al.*, 2016).

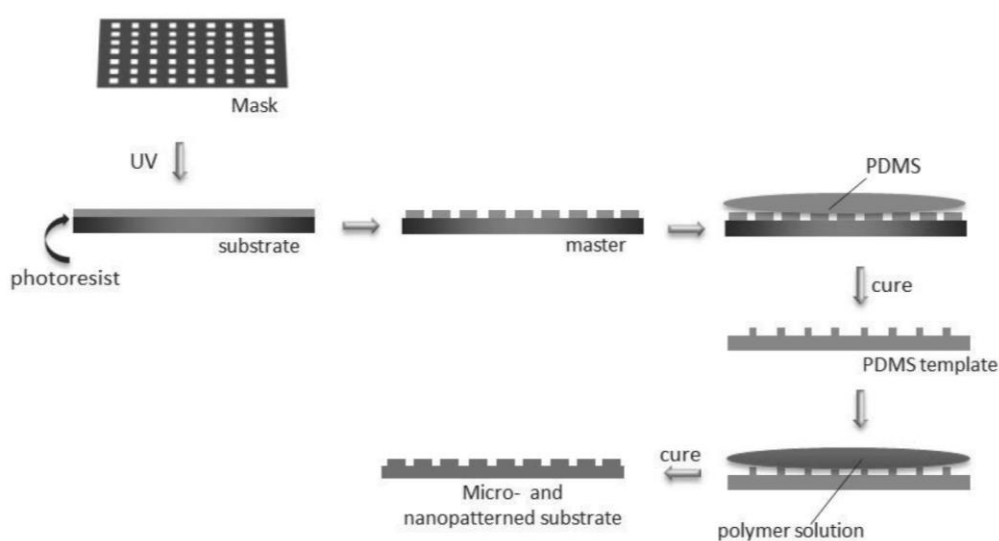


Figure 1.3. Diagram showing the soft lithography technique (adapted from Hasirci *et al.*, 2016).

There are various different 3D printing approaches, including stereolithography (SLA), two photon polymerization (2PP), inkjet 3D printing (I3P), selective laser sintering (SLS), particle binding (PB), direct ink writing (DIW), melt electrospinning writing (MEW), and fused deposition modeling (FDM) (Fig. 1.4) (Guvendiren *et al.*, 2016).

1.4.3.3.1.7.1. Stereolithography (SLA) and Two Photon Polymerization (2PP)

Stereolithography (SLA) is based on exposure of a reservoir of photoactive polymer to ultraviolet (UV), infrared (IR) or visible light at a specific focal plane to form a cured polymer layer (Hasirci *et al.*, 2016; Jang *et al.*, 2018) (Fig. 1.4A). Successive layers are built up on the first layer, by repeating this process after lowering the reservoir stage. Despite its high resolution (below 25 μm), SLA requires extensive postprocessing and washing steps, and the use of this technique is limited to photoactive polymers (Guvendiren *et al.*, 2016). SLA has been used in production of scaffolds for meniscus regeneration, but with poor mechanical properties (Grogan *et al.*, 2013; Van Bochove *et al.*, 2016).

Two photon polymerization (2PP) follows the same principle as SLA, but uses two photons of infrared light instead of UV, which are directed on one focal point instead of a focal plane, to excite and polymerize the polymer (Hasirci *et al.*, 2016).

1.4.3.3.1.7.2. Inkjet 3D Printing (I3P)

In inkjet systems, pressure pulses are applied through an orifice, by the use of a gas bubble or a piezoelectric actuator, to force a very small sample of the polymer solution (less than 100 pL) out of a the nozzle (Tasoglu and Demirci, 2013) (Fig. 1.4B). This technique is used to dispense droplets of cell-laden polymer solutions, and has a very high accuracy (10 μm) and high speed (Sears, *et al.*, 2016; Guvendiren *et al.*, 2016). This technique has been used to produce tissue engineering constructs for cartilage applications, but with poor mechanical properties (Xu *et al.*, 2013).

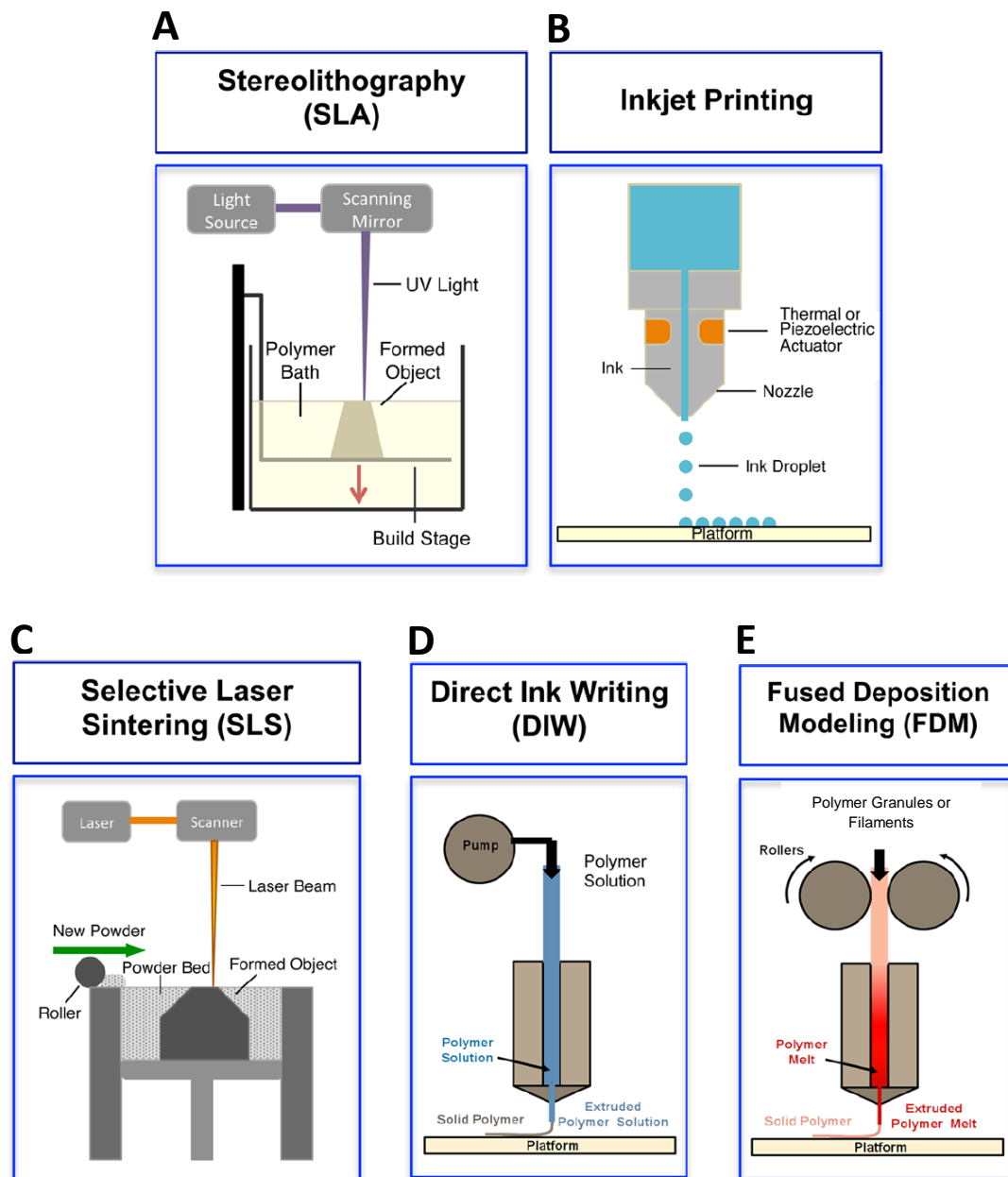


Figure 1.4. Three dimensional printing techniques. (A) Stereolithography, (B) inkjet printing, (C) selective laser sintering, (D) direct ink writing, and (E) fused deposition modeling (adapted from Guvendiren *et al.*, 2016).

1.4.3.3.1.7.3. Selective Laser Sintering (SLS), Selective Laser Melting (SLM), and Particle Binding (PB)

Selective laser sintering (SLS) and melting (SLM) are based on application of laser beam on a powdered material to raise its surface temperature above its melting point, enabling fusion of the adjacent particles (Yang *et al.*, 2002) (Fig. 1.4C). As in SLA, the laser beam is controlled by a computerized system to produce consecutive layers on top of each other (Guvendiren *et al.*, 2016). SLS is used for sintering metal or ceramic particles, and is not suitable for use in meniscal applications. SLM, on the other hand, is used with polymers, but has not found use in cartilaginous tissue engineering applications. Particle binding (PB) works with the same principle as SLM, but uses a binder solution to fuse the polymer particles, instead of laser beam.

1.4.3.3.1.7.4. Direct Ink Writing (DIW)

Direct ink writing (DIW) is based on application of air or mechanical pressure to extrude the polymer solution as dots or lines through a nozzle (Chang *et al.*, 2011) (Fig. 1.4D). The pressure is controlled with computer-driven actuators and the nozzle moves at x, y, and z directions. The advantage of this technique is that it allows for bioprinting (extrusion of cell- or bioactive molecule-laden polymer solutions) if used with aqueous polymer solutions (Annabi *et al.*, 2014).

This technique has been used to produce meniscal tissue engineering scaffolds, but with poor mechanical properties (Cohen *et al.*, 2006; Ballyns *et al.*, 2010; Rhee *et al.*, 2016; Yang *et al.*, 2017).

1.4.3.3.1.7.5. Melt Electrospinning Writing (MEW) or Electrohydrodynamic (EHD) Jet Printing

Melt electrospinning writing (MEW) or electrohydrodynamic jet printing is the electrospinning of the polymer melts instead of polymer solutions. The advantage of MEW is that it does not require using of toxic solvents, while the disadvantage is the thermal instability of the polymers (Hutmacher and Dalton, 2011; Brown *et al.*, 2016). The absence of solvents in MEW allows for printing straight lines, because of the very low conductivity of the polymer melts which prevents whipping (Brown *et*

al., 2016). This technology has recently started to be applied in the tissue engineering field, and has only one application in meniscal regeneration (Li, 2014).

1.4.3.3.1.7.6. Fused Deposition Modeling (FDM)

Fused deposition modeling (FDM) involves melting of a thermoplastic polymer in a cartridge and extrusion of this polymer melt through a nozzle to form scaffolds with predefined shapes (Sears *et al.*, 2016) (Fig. 1.4E). The nozzle follows a computer controlled path as the extrusion process continues, resulting in layer-by-layer buildup of the 3D scaffold (Guvendiren *et al.*, 2016). FDM is the most widely used 3D printing technique because it is a simple method and it results in formation of scaffolds of high mechanical strength (Turner *et al.*, 2014). PCL is widely used in FDM-based 3D printing, due to its biocompatibility, low melting temperature (60°C), and good viscoelastic properties (Lee *et al.*, 2014; Boere *et al.*, 2014).

FDM has been commonly used for printing of meniscus tissue engineering scaffolds (Moroni *et al.*, 2007; Lee *et al.*, 2014; Daly *et al.*, 2016; Cengiz *et al.*, 2016; Szojka *et al.*, 2017; Zhang *et al.*, 2017) or molds to cast the scaffold materials on (Ballyns and Bonassar, 2011; Wataya *et al.*, 2012; Puetzer *et al.*, 2012; Puetzer *et al.*, 2015).

Cengiz *et al.*, produced PCL-based, anatomically shaped meniscal constructs with 0-45⁰-90⁰ and 0-90⁰ strand orientations (2016). They demonstrated higher mechanical properties with the scaffolds having 0-90⁰ orientation (Cengiz *et al.*, 2016).

Moroni *et al.* produced poly(ethylene oxide-terephthalate)-co-poly(butylene terephthalate) (PEOT/PBT)-based, anatomically shaped meniscal constructs with hollow strands in order to obtain compressive modulus closer to that of the native meniscus (2007). However, the strands had traditional 0-45⁰-90⁰ orientation, which did not fully mimic the collagen fiber orientation in the meniscus, and the interaction of cells with these scaffolds was not tested.

Szojka *et al.* produced PCL-based, anatomically shaped meniscal constructs with circumferentially oriented strands that mimic the collagen organization in the meniscus and suture tabs (extensions at the horns) that allow for fixation of the constructs to tibia (2017). They also showed that they could control the compressive

properties of the scaffolds by changing the distance between the strands and introducing strand shifts (offsets) at each layer that builds on the previous. However, they obtained very high compressive modulus values, and they did not test their constructs in presence of cells *in vitro* or *in vivo* (Szojka *et al.*, 2017).

Zhang *et al.* produced PCL-based meniscal constructs with circumferential strands, and implanted them to New Zealand white rabbits (2017). They tested the performance of the MSC-seeded and cell-free constructs 12 and 24 month after implantation. They showed higher proteoglycan, COL I, COL II, and COL III deposition on the cell-seeded constructs (Zhang *et al.*, 2017).

Daly *et al.*, produced PCL-hydrogel based, rectangular prism-shaped constructs and seeded them with bone marrow-MSCs (2016). They used many hydrogels to test their effects on ECM production, and showed that alginate and agarose led to higher production of COL II and GAGs, while polyethylene glycol methacrylate (PEGMA) and GelMA led to a higher production of COL I. They suggested these scaffolds for use in cartilage and fibrocartilage regeneration, but they had not produced these scaffolds in meniscus shapes (Daly *et al.*, 2016).

The only study that mimicked the structural organization and biochemical content of the meniscus was done by Lee *et al.* (2014). They produced PCL-based, anatomically shaped meniscal constructs with circumferential strands, and seeded them with MSCs. They used microspheres containing CTGF in the outer region of the scaffolds and TGF β 3 in the inner region, in order to direct the MSCs to fibrogenic and chondrogenic differentiation, respectively. This study achieved to fully mimic the structure of the native meniscus; however, the scaffold resulted in degeneration of the underlying cartilage (Lee *et al.*, 2014). Moreover, the use of growth factors in the body may pose possible risks (Witsch *et al.*, 2010).

1.5. Design of the Construct

The aim of the current study is to design a novel scaffold for meniscus tissue engineering which would mimic the structural organization of the native tissue and thus have appropriate mechanical (both compressive and tensile) properties. To this end, production of a PCL-based scaffold with circumferential strands is proposed,

which would be embedded in hydrogels inducing chondrogenic behavior in the inner region and fibrous behavior in the outer region.

PCL is printed using the FDM technique to produce a porous scaffold with high mechanical properties matching those of the native meniscus. Conventionally, FDM-printed scaffolds have 0-45° or 0-90° strand orientation (Fig. 1.5A). In this study, circumferential strands are introduced in order to mimic the collagen fiber organization in the native tissue (Fig. 1.5B). The construct is printed in an amphitheater shape (like the coliseum) (Fig. 1.5C), and seeded with the fibrochondrocytes and incubated for some time to allow for cells to attach and proliferate. Then, the scaffolds are embedded in cell-laden agarose at the inner region to induce chondrogenic phenotype, and in cell-laden GelMA at the outer region to induce fibrous phenotype. The purpose of this is to mimic the biochemical and histological content of the native meniscus, which is cartilage-like in the inner region and fibrous in the outer region. Moreover presence of hydrogels is expected to reduce the friction between the PCL scaffold and the hyaline cartilage after implantation into the knee. After incubation for a predetermined duration, the scaffold is cut into two halves to obtain the final meniscus shaped constructs (Fig. 1.5D).

With this design, we aim to fully mimic the structure of the native meniscus, without using any growth factors that may have possible risks and supposedly with reduced friction due to presence of the hydrogels. We account for the zonal difference by simply using different hydrogels in different regions of the constructs.

1.6. Design of the Study

This study is conducted using two fibrochondrocyte sources: porcine and human cells. Porcine fibrochondrocytes are used to evaluate *in vitro* meniscal regeneration before these constructs are tested *in vivo* in a porcine model, and a high molecular weight PCL (80 kDa) is used to match the scaffold mechanical properties to the high mechanical properties of the porcine meniscus (equilibrium modulus around 100-120 kPa (Abdegaied *et al.*, 2015), compressive modulus ranging between 1-5 MPa

(Yasura *et al.*, 2007), and tensile modulus around 100-150 MPa) (Abdelgaied *et al.*, 2015).

Human fibrochondrocytes are used to evaluate *in vitro* meniscal regeneration on the constructs before use in clinical trials, and a lower molecular weight (50 kPa) PCL (PCL 50) is used to match the mechanical properties of the constructs with those of the human meniscus (equilibrium modulus 40-80 kPa (Sweigart *et al.*, 2004; Chia and Hull, 2008), compressive modulus 0.3-2 MPa (Chia and Hull, 2008; Fischenich *et al.*, 2017), and tensile modulus 70-130 MPa (Tissakht and Ahmed, 1995).

The studies are divided into three parts. In the first part, the effect of hydrogel materials on the degradation, mechanical properties, cell viability and *in vitro* ECM production is evaluated and the hydrogels that support meniscal regeneration are selected. In the second and third parts, square prism- and meniscus-shaped PCL/hydrogel composite constructs are produced and evaluated for scaffold integrity, cell viability, and *in vitro* meniscal regeneration.

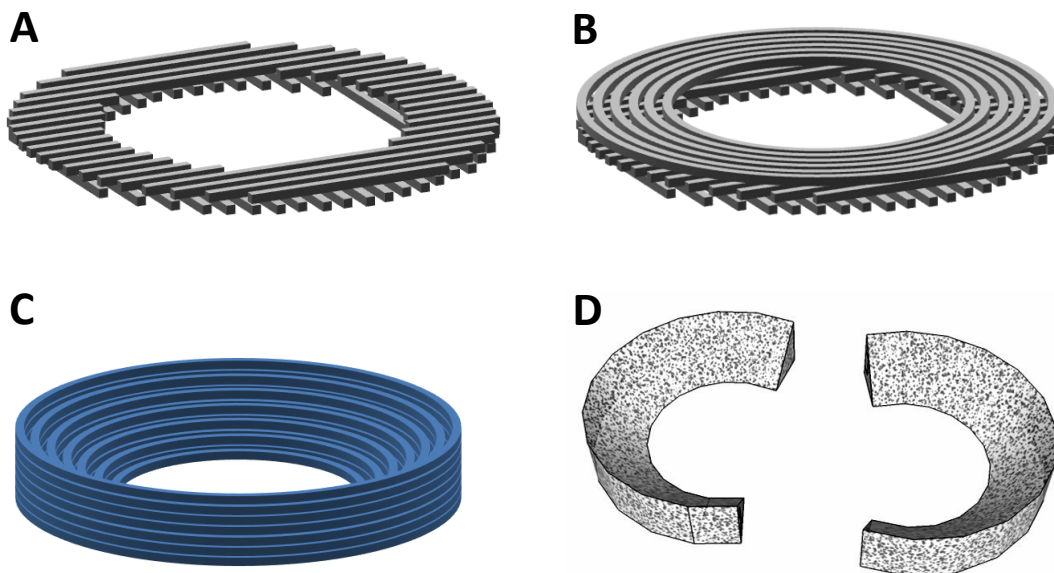


Figure 1.5. The design of the proposed 3D printed PCL scaffold. Strand are printed in (A) 0-90⁰, and (B) 0-90⁰-circumferential orientation. (C) The coliseum-shaped, and (D) the final meniscus-shaped scaffolds.

This study is unique in exploiting the potential of agarose and GelMA hydrogels to induce chondrogenic and fibrous ECM production, for use in the inner and outer regions of 3D printed PCL-based meniscal constructs, respectively. The zonal difference in the inner (cartilaginous) and outer (fibrous) regions of the meniscus is mimicked for the first time using two different hydrogels. This study is significant for its potential to produce biologically and mechanically functional meniscus tissue engineering constructs, which have the potential to go into animal and clinical trials for partial or total meniscal replacements.

CHAPTER 2

MATERIALS AND METHODS

2.1. Materials

Poly(ϵ -caprolactone) (PCL) (M_n : 80 kDa), agarose (type VII, low gelling temperature), porcine gelatin (from porcine skin, 300 Bloom) and bovine gelatin (from bovine skin, 225 Bloom), methacrylic anhydride, hyaluronic acid (HA, from *streptococcus equi*, M_w : 0.6-1.1 MDa), Irgacure 2959, Trypsin-EDTA (0.25%), amphotericin-B ($0.25 \mu\text{g}\cdot\text{mL}^{-1}$), pen/strep (100 units/mL/100 $\mu\text{g}\cdot\text{mL}^{-1}$), bovine serum albumin (BSA), papain, Triton-X 100, type II collagenase (from *C. histolyticum*), glutaraldehyde, paraformaldehyde, sodium cacodylate trihydrate, FITC-labeled phalloidin, 4',6-diamidino-2-phenylindole dihydrochloride (DAPI), hyaluronidase, mouse primary antibody against COL I, Safranin-O, Fast Green, mouse primary antibody against paxillin, chondroitin sulfate (from bovine trachea), and CC/Mount® mounting solution were purchased from Sigma-Aldrich (USA and Germany).

Dulbecco's Modified Eagle Medium (DMEM):Ham's F12 (1:1) mixture (DMEM/F12), DMEM-F12 colorless, fetal bovine serum (FBS), ITS+ Premix, trypsin-EDTA (0.25 %), SnakeSkin pleated dialysis tubing, AlamarBlue® cell viability assay kit, LIVE/DEAD™ cell viability/cytotoxicity kit for mammalian cells, Quant-iT™ PicoGreen™ dsDNA quantification assay kit, pepsin, mouse primary antibodies against COL II, Alexafluor 532-labelled phalloidin, and Alexafluor 488-labelled goat anti-mouse IgG secondary antibody were purchased from Thermo Fischer Scientific (USA).

PCL (M_w : 50 kDa) was bought from Polysciences Inc. (USA), and biotinylated horse anti-mouse IgG and horse radish peroxidase kits from Vector Laboratories (USA). Alexafluor 488-labelled donkey anti-mouse secondary antibody was from

Abcam (USA), DRAQ5, mouse antibody against COL I and rabbit antibody against COL II, Alexafluor 488-labelled goat anti-rabbit IgG and Alexafluor 532-labelled goat anti-mouse IgG, and TO-PRO™-3 Iodide was from Cell Signaling Technology (USA). Sodium phosphate monobasic and dibasic, ethanol, acetic acid (HAc), and sodium chloride were purchased from Merck Millipore (Germany). Sprague-Dawley rat tails were kindly provided by GATA Animal Experiments Laboratory (Turkey).

2.2. Methods

2.2.1. Isolation of Meniscus Cells (Fibrochondrocytes)

Meniscus cells (fibrochondrocytes) from two different sources, human and porcine, were isolated. The isolation procedure was performed according to a modification of a previously described procedure (Weber *et al.*, 1985).

For porcine fibrochondrocyte isolation, medial menisci of two postmortem Yorkshire pigs (female, 2 months old) were harvested according to the Lifespan Institutional Animal Care and Use Committee (IACUC) Policy for the Responsible Conduct of Animal Research and Use of Central Research Facilities (USA), which requires no review. Menisci were sliced and digested overnight at 37 °C in type II collagenase (0.15%, w/v) (Fig. 2.1). Digests were incubated in growth media (DMEM-F12 (1:1) supplemented with 10% FBS, pen/strep (100 units/mL/100 µg/mL) and 1 µg/mL amphotericin B) containing 1% ITS+ Premix at 37 °C for cell expansion.

For human fibrochondrocyte isolation, a biopsy sample of the medial meniscus of a 56 year old patient was harvested at the Department of Orthopedics at Hacettepe University (Turkey) with her written consent (Ndreu-Halili *et al.*, 2014; Bahcecioglu *et al.*, 2014). Briefly, the meniscus sample was sliced and incubated in type II collagenase solution (0.3%, w/v) at 37 °C for 24 h. After washing with 10% FBS, the cells were suspended in DMEM/F12 (1:1) medium supplemented with 10% FBS and pen/strep (100 units/mL/100 µg/mL), and incubated in a humidified CO₂ incubator (Heal Force, China) for expansion.

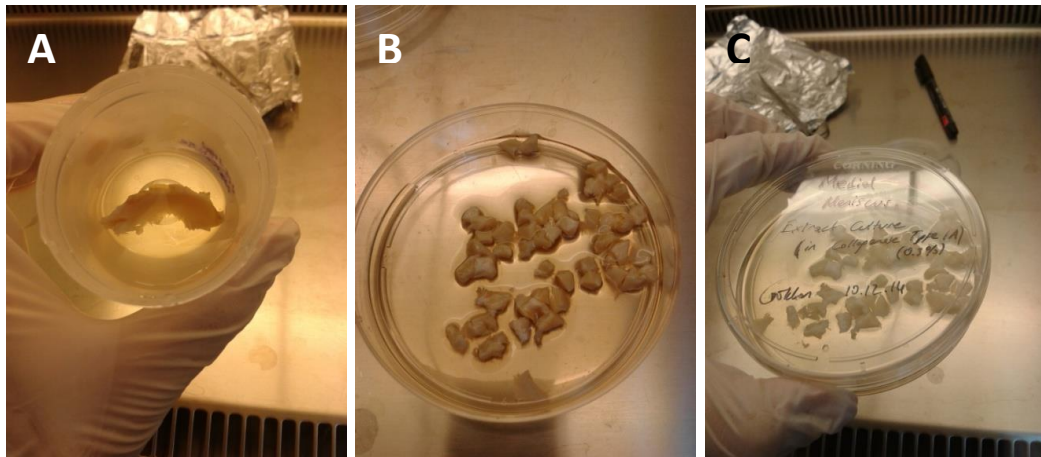


Figure 2.1. Isolation of fibrochondrocytes from the medial porcine meniscus. The meniscus tissue was (A) harvested from medial menisci, (B) sliced into small pieces, and (C) incubated overnight in collagenase and in growth media for cell expansion.

2.2.2. Preparation of the Constructs

2.2.2.1. Three Dimensional Printing of the PCL Scaffolds

Poly(ϵ -caprolactone) (PCL) with two different molecular weights were used for 3D printing: PCL 80 (M_n : 80 kDa, M_w : ~150 kDa) and PCL 50 (M_w : 50 kDa). PCL 80 was used in experiments conducted with porcine fibrochondrocytes and PCL 50 was used in experiments conducted with human fibrochondrocytes.

For 3D printing, first, the 3D models of the scaffolds were designed using the 3D modeling software SketchUp (Google Inc, USA) and loaded to the computer-aided manufacturing (CAM) software (Prim-CAM, Einsiedeln, Switzerland) of the 3D printer (Bioscaffolder, SYS-ENG, Salzgitter-Bad, Germany). Then, the polymer melted in the cartridge of the 3D printer was extruded at 1 mm strand distance, 0.14 mm layer thickness, and in 0-90° strand orientation. Scaffolds were produced with or without shifting of the strands at the consecutive layers (shifting distance: 0.5 mm), and with or without contour (0.1 mm from the outer border) (Fig. 2.2).

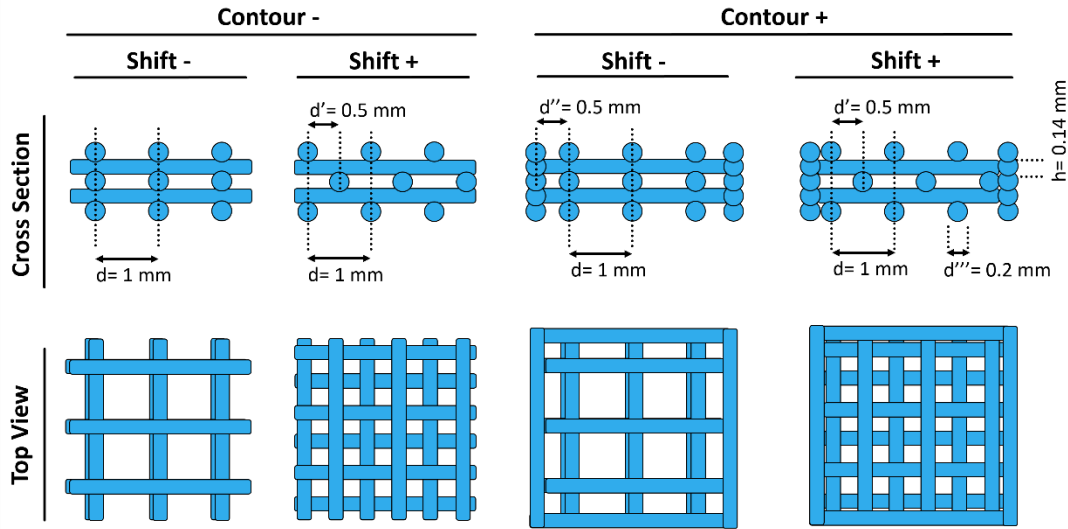


Figure 2.2. Schematic representation of the different settings of the 3D printing process. PCL was extruded at strand distance 1 mm and layer thickness 0.14 mm. Strands were produced with or without shifting at consecutive layers (shift distance: 0.5 mm), and with or without contours.

2.2.2.1.1. Optimization of the 3D Printing Process

In order to optimize the 3D printing process, two parameters were changed and PCL was dispensed: temperature (T) of the cartridge, and the movement speed of the nozzle at x-y direction (F_{xy}). The optimal conditions were those under which PCL strands were straight, and the pores and the scaffold edges were in the desired shape. PCL with no shifting or contour settings were used in the following experiments unless stated otherwise.

2.2.2.2. Preparation of the Hydrogel Constructs

2.2.2.2.1. Methacrylation of Gelatin and Hyaluronic acid

Two different gelatin sources were used: porcine gelatin (300 Bloom) and bovine gelatin (225 Bloom). Porcine gelatin was used when human fibrochondrocytes were employed, and bovine gelatin was used when porcine fibrochondrocytes were employed.

In order to prepare GelMA, porcine and bovine gelatin solutions (10% w/v, in PBS, pH 7.2) were mixed with methacrylic anhydride (MA) (Sigma-Aldrich, USA) at volume ratios of 4:1 and 7:1 (Gelatin solution:MA), respectively. Solutions were incubated at 50 °C for 1.5 h to synthesize GelMA (Nichol *et al.*, 2010) (Fig. 2.3A).

Hyaluronic acid (HA) solution (0.5% w/v, in distilled water:dimethylformamide (3:2, v/v)) and MA were mixed at a volume ratio of 99:1 (HA:MA) and incubated overnight at 4 °C to synthesize MeHA (Hachet *et al.*, 2012) (Fig. 2.3B).

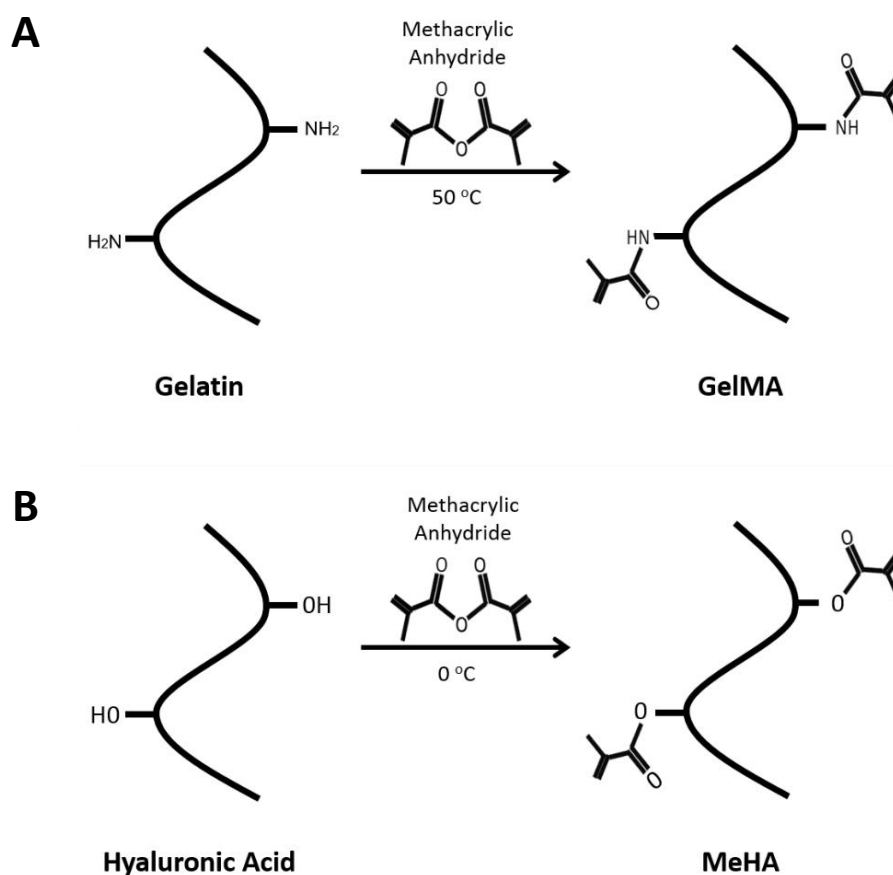


Figure 2.3. Methacrylation of gelatin and hyaluronic acid. Synthesis of (A) GelMA and (B) MeHA.

The resulting polymer solutions were placed in dialysis tubing and dialyzed against phosphate buffer (pH 7.2) for 3 days, with refreshing the buffer two times a day to remove the photoinitiators and crosslinkers that remained in the solution. Finally, the solution was frozen at -80 °C and lyophilized to obtain the polymer pellets. The resulting polymers were sterilized with ethylene oxide and stored at -20 °C until use.

2.2.2.2.2. Preparation of the Hydrogels

2.2.2.2.2.1. Optimization of the Crosslinking Process of the Methacrylated Polymers

The methacrylated polymers are crosslinked by applying UV in the presence of a photoinitiator, Irgacure2959 (Fig. 2.4). Crosslinking of the methacrylated polymers was optimized by changing the polymer and photoinitiator concentrations, and UV exposure time. For this purpose, porcine GelMA (5 and 8%, w/v) and MeHA (0.5 and 1%, w/v) solutions were prepared in PBS. The photoinitiator was added at two concentrations, 1 and 2% (w/v), and the solutions were exposed to UV (λ : 365 nm) for 1-30 min at 0.120 J/mm. The minimum time required for gelation of the solutions was determined.

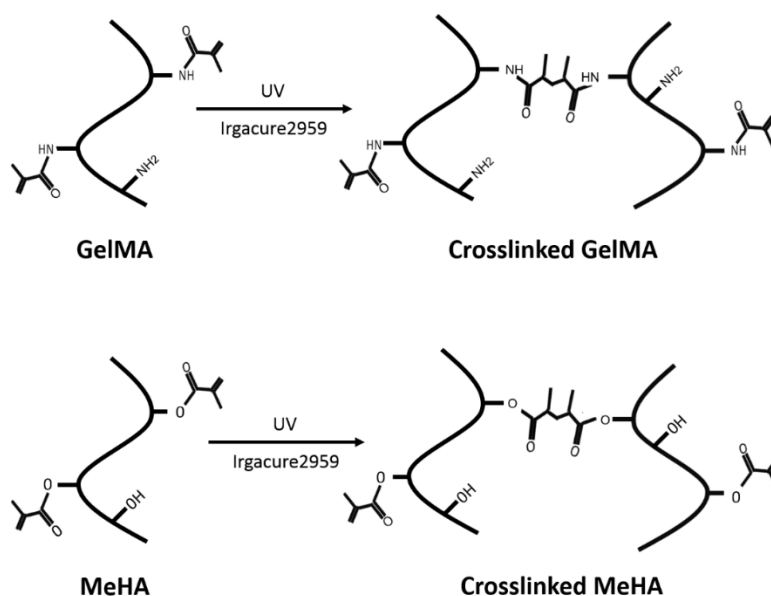


Figure 2.4. Crosslinking of GelMA and MeHA by UV radiation. Photoinitiator: Irgacure 2959.

2.2.2.2.2. Preparation of the Cell-Hydrogel Constructs

2.2.2.2.2.1. Preparation of Porcine Fibrochondrocyte-Hydrogel Constructs

Porcine fibrochondrocytes were suspended at a cell density of $6-7 \times 10^6$ cells/mL in ethylene oxide-sterilized GelMA (bovine, 6.4%, w/v) or MeHA (0.8%, w/v) or blend of GelMA (3.2%, w/v) and MeHA (0.4%, w/v) (GelMA-MeHA) solutions in growth media containing the photoinitiator Irgacure2959 (1%, w/v). The cell suspensions were cast between two parallel glass plates 1.5 mm apart to obtain gels of uniform thickness (Fig. 2.5A). The system was exposed to UV for 5 min to crosslink the polymers. The glass plates were removed and gel disks of 5 mm diameter were obtained using tissue punches.

Cell-agarose constructs were prepared similarly. Porcine fibrochondrocytes were suspended in heat-sterilized agarose (Ag) solution (2% in DMEM-F12 media) maintained at 43 °C. Cell-agarose mixture was immediately cast between the glass plates and left to cool down below 35 °C to solidify (Fig. 2.5A). When gelation was complete, the glass plates were removed and disks of gels (5 mm diameter) were obtained using tissue punches.

Ethanol sterilized PCL was used as a control. Cells were seeded on PCL scaffolds at a cell density of 1.5×10^5 cells/scaffold (Fig. 2.5A). Cell-free hydrogel and PCL constructs were used as controls.

The constructs were cultured for a week in growth media containing ITS+ Premix at 37 °C with changes of media every 2 days (Fig. 2.5), followed by four weeks in fibrochondrogenic media (growth media containing 1% ITS+ Premix, 40 mM L-proline, 1 mM nonessential amino acids NEAA, 50 µg/mL L-ascorbic acid 2-phosphate). Dexamethasone (100 nM) and TGF-β1 (10 ng/mL) were freshly prepared and added at media changes between Days 7-28. Constructs were incubated under static or dynamic culture conditions. Dynamic compression was applied at 10% strain (starting from a 5% basal strain to a 15% peak strain), 1 Hz frequency, for four weeks, 1 h/day, 5 days/week, in a home-made bioreactor with a polysulfone-based platen that fits in 24-well culture plates (Fig. 2.5C) (Bilgen *et al.*, 2013).

Constructs were removed from culture media on Days 1 and 35 and prepared for analysis (Section 2.2.3).

2.2.2.2.2.2. Preparation of Human Fibrochondrocyte-Hydrogel Constructs

After optimization, filter sterilized GelMA solution (5%, w/v in culture medium) was prepared, and Irgacure2959 was added at a 1% (w/v) concentration. Agarose (Ag) solution (2%, w/v in DMEM-F12 medium) was prepared by heating in microwave for 2 min with stirring. GelMA-Ag solutions were prepared by mixing the GelMA and Ag solutions (1:1 volume ratio or 5:2 weight ratio).

Human fibrochondrocytes were suspended in GelMA (5%), Ag (2%), and GelMA-Ag (5:2 w/w GelMA:Ag) (3.5% w/v) solutions at a cell density of 3×10^4 cells/construct. The suspensions were placed in cylinder-shaped molds ($d = 7 \text{ mm}$, $h = 2 \text{ mm}$) and crosslinked. Agarose-cell suspension was left to cool. GelMA-containing cell suspensions were exposed to UV for 3 min to obtain the hydrogels. Cells were seeded on the 3D printed PCL 50 (as a control) at a cell density of 3×10^4 cells/scaffold. The cell seeded constructs were then incubated in the growth media for 7 days with change of media every 2 days. Cell attachment and spreading on the scaffolds were analyzed to evaluate the behavior of cells on the constructs.

2.2.2.3. Preparation of the 3D Printed PCL/Hydrogel Composite Constructs

2.2.2.3.1. Preparation of the Square Prism Shaped PCL/Hydrogel Constructs

2.2.2.3.1.1. Preparation of Porcine Fibrochondrocyte-Based Constructs

PCL 80 was printed in square prism shapes of $20 \text{ mm} \times 20 \text{ mm} \times 3 \text{ mm}$, with no shifting of the strands and with no contour as described in Section 2.2.2.1 (Fig. 2.2). Samples were cut using a scalpel into smaller square prisms of $5 \text{ mm} \times 5 \text{ mm} \times 3 \text{ mm}$ for use in the cell culture experiments and compressive mechanical testing, and into rectangular prisms of $20 \text{ mm} \times 10 \text{ mm} \times 3 \text{ mm}$ for use in tensile testing.

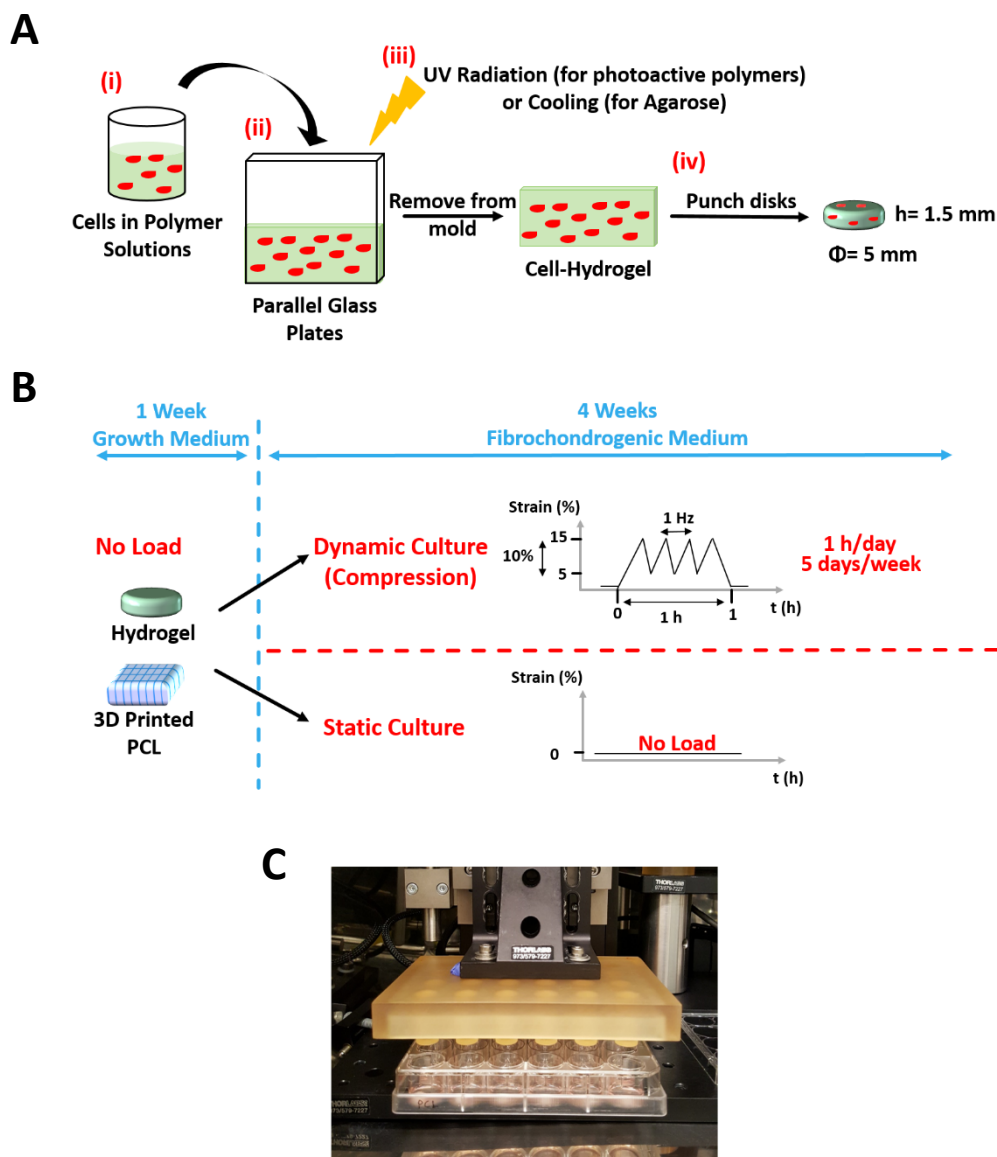


Figure 2.5. Scaffold preparation and culture conditions. (A) Preparation of the gels. (i) Cell suspensions were prepared in agarose, GelMA, MeHA, and GelMA-MeHA solutions. (ii) Cell-polymer suspensions were cast between two parallel plates. (iii) Agarose was cooled and other polymers were UV radiated for gelation to take place. (iv) Disks of gels were obtained using a tissue punch. (B) Culture conditions. Constructs were cultured for a week in growth media, and four weeks in fibrochondrogenic media under static or dynamic conditions. Dynamic compression (oscillating between strain levels of 5-15%) was applied after Day 7, for 4 weeks, 1 h/day, 5 days/week at 1 Hz frequency in a (C) custom-made bioreactor.

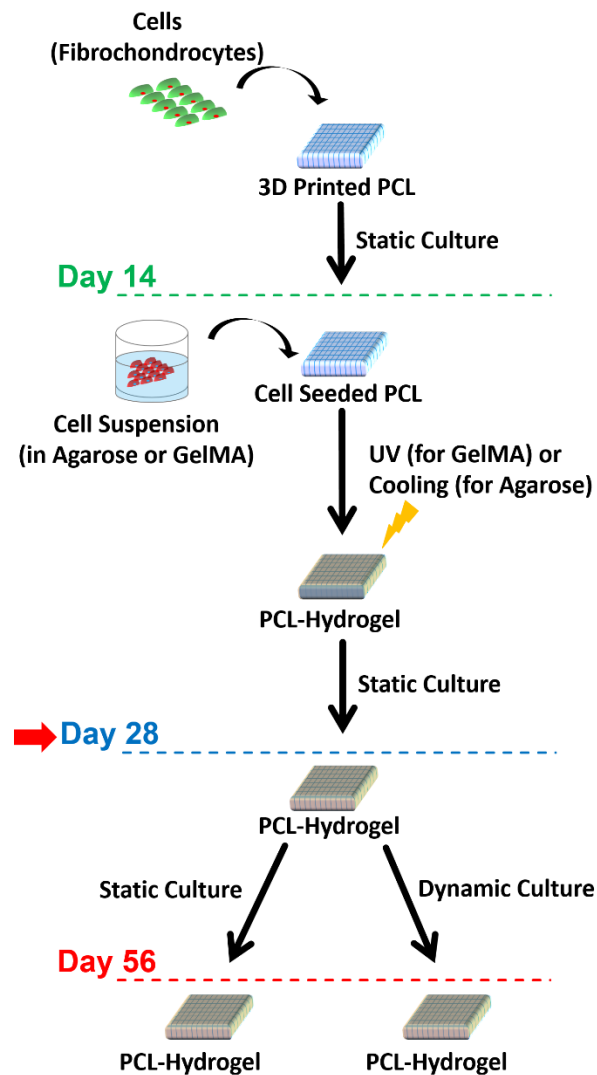


Figure 2.6. Preparation of the 3D printed PCL-Hydrogel constructs. The 3D PCL was seeded with porcine fibrochondrocytes and incubated for 14 days in growth media. On Day 14, the pre-seeded PCL was embedded in cell-laden agarose or GelMA, which were crosslinked (cooled for PCL-Ag, and UV irradiated for PCL-GelMA). Constructs were incubated until Day 28, when dynamic compression was applied. Constructs were incubated under static or dynamic conditions until Day 56. Arrowhead: start of dynamic culture.

Porcine fibrochondrocytes (passage 3) were expanded, trypsinized, suspended in growth media, and seeded onto sterile PCL 80 scaffolds at a cell density of 1.3×10^5 cells/scaffold. The constructs were cultured for 2 weeks in growth media containing ITS+ Premix at 37 °C in a CO₂ incubator with changes of media every 2 days (Fig. 2.6). On Day 14, porcine cells were suspended in agarose (2% w/v in DMEM-F12 media, at 43 °C) or GelMA (6.4% w/v in DMEM containing 1% (v/v) photoinitiator) solutions and the pre-seeded PCL (final cell density in the hydrogels was 2×10^5 cells/scaffold) was embedded in these suspensions (Fig. 2.7). PCL-Ag was left to cool for gelation to take place, and PCL-GelMA was exposed to UV for 5 min. PCL alone was used as control. Three different constructs were produced after Day 14: PCL, PCL-Ag, and PCL-GelMA (Fig. 2.7).

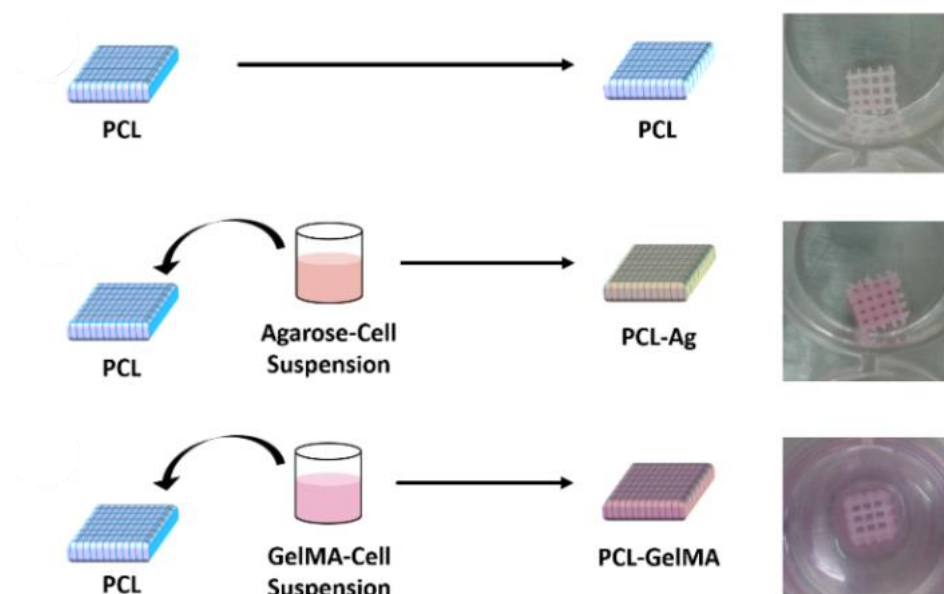


Figure 2.7. Preparation of the square prism shaped PCL/hydrogel constructs. PCL-Ag, and PCL-GelMA were produced on Day 14, and PCL scaffold was used as control.

After Day 14, the constructs were transferred into fibrochondrogenic media. TGF- β 1 (10 ng/mL) was added for 4 weeks between Days 14 and 42 (Fig. 2.8A). Starting at Day 28, constructs were exposed to dynamic compression (at 10% strain, oscillating between a 5% basal strain and a 15% peak strain) at 1 Hz, for 1 h/day, 5 days/week, for 4 weeks between Days 28 and 56 (Figs. 2.6 and 2.8, arrowheads), in a bioreactor that allows the use of 24-well plates (Fig. 2.8B). Constructs were removed from culture media on Days 1, 14, 28, 42, and 56 and analyzed (Section 2.2.3).

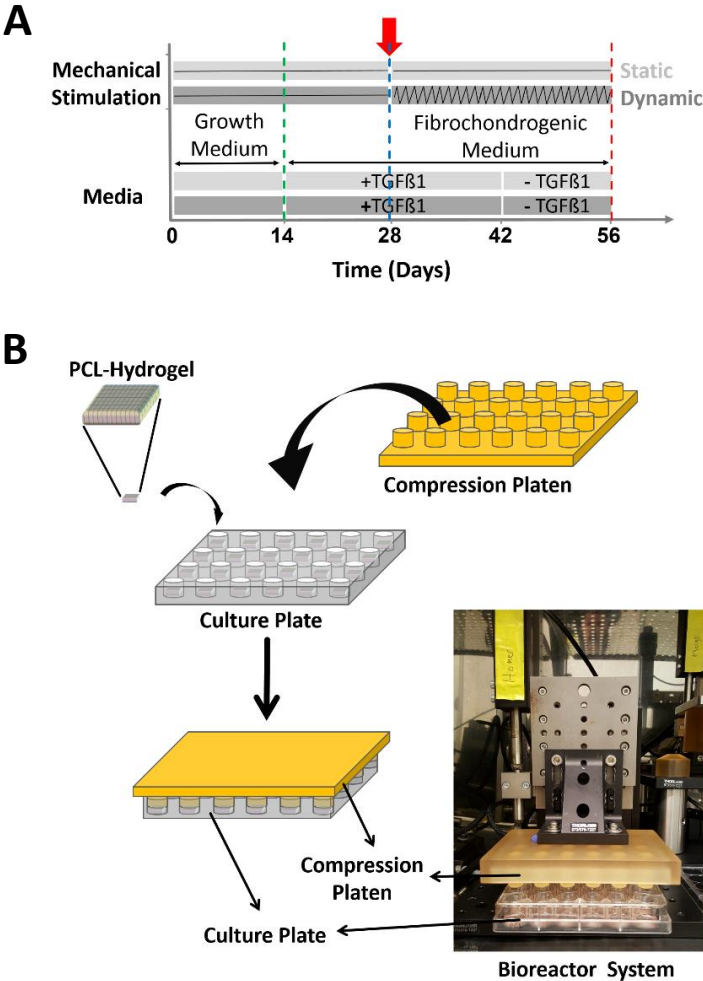


Figure 2.8. PCL/hydrogel constructs were incubated under static or dynamic culture conditions. (A) Culture conditions. (B) Dynamic compression was applied starting at Day 28 in the bioreactor system. Arrowhead: start of dynamic compression. TGF β 1: transforming growth factor β 1.

2.2.2.3.1.2. Preparation of Human Fibrochondrocyte-Based Constructs

PCL 50 was printed in square prism shapes (10 mm x 10 mm x 3 mm) for use in cell culture experiments and compressive mechanical testing, and in rectangular prism shapes (30 mm x 10 mm x 3 mm) for use in tensile testing. Scaffolds were printed with or without shifting (shift distance: 0.5 mm), and with or without contour as described in Section 2.2.2.1 (Fig. 2.2).

Human fibrochondrocytes (passage 3) were expanded, trypsinized, suspended in growth media, and seeded onto sterile PCL 50 scaffolds at a cell density of 3×10^4 cells/scaffolds. The constructs were cultured for 2 weeks in growth media. On Day 14, human cells were suspended in agarose (2% w/v in DMEM at 43 °C) or GelMA (porcine, 5% w/v in DMEM containing 1% (v/v) photoinitiator) or GelMA-Ag (1:1, v/v of the GelMA and agarose) solutions (final cell densities were 3×10^4 cells/scaffold). The pre-seeded PCL was embedded in these cell suspensions (Fig. 2.7). Unembedded PCL was kept as a control. After gelation, the constructs were incubated in growth media for additional 28 days until Day 42 with no addition of growth factors. Constructs were removed from culture media on Days 14 and 42 and analyzed.

2.2.2.3.2. Preparation of the Meniscus Shaped PCL/Hydrogel Constructs

2.2.2.3.2.1. Preparation of Porcine Fibrochondrocyte-Based Constructs

PCL 80 was printed in coliseum shapes (Fig. 2.9A), with no shifting of the strands and with no contour as described in Section 2.2.2.1 (Fig. 2.2). The coliseum-like structure had an outer diameter of 30 mm, inner diameter of 10 mm, and a height of 5 mm at the outer edge.

Porcine fibrochondrocytes were expanded (passage 3, P3), trypsinized, and suspended to a final cell density of 1×10^7 cells/mL. Cells were seeded onto coliseum shaped PCL scaffolds at a cell density of 2.5×10^6 cells/scaffolds and cultured at 37 °C for 2 weeks in growth media containing ITS+ Premix in Petri dishes, with changes of media every 2 days (Fig. 2.9B).

On Day 14, porcine fibrochondrocytes were suspended in agarose (2% w/v in DMEM-F12 media, 43 °C) or GelMA (6.4% w/v in DMEM containing 1% (v/v) photoinitiator) solutions. The in the inner portion of the constructs was embedded in agarose-cell suspension (final cell density in agarose: 2×10^6 cells/scaffold), and the outer portion was embedded in GelMA-cell suspension (final cell density in GelMA: 4×10^6 cells/scaffold) (Fig. 2.9B). As a control, a set of the constructs was embedded in agarose on the inner portion and the outer portion was left unembedded. Agarose was left to cool for gelation to take place, and GelMA was exposed to UV for 5 min. At the end of Day 14, two types of constructs were obtained: PCL-Ag, and PCL-Ag-GelMA.

After Day 14, the constructs were incubated 6 weeks in fibrochondrogenic media with addition of TGF- β 1 (10 ng/mL) between Days 14 and 42 as described in Section 2.2.2.3.1 (Fig. 2.8A). Starting from day 28, constructs were subjected to dynamic compression for 4 weeks. After 56 days of culture, samples were removed from the culture and cut into two halves to obtain the meniscus shaped constructs (Fig. 2.9B).

A compression head that would fit on the upper surface of the coliseum-like constructs was designed (Fig. 2.10A), so that the dynamic compression applied was uniform throughout the scaffold surface. When compression was to be applied, constructs were removed from incubators where they were under static conditions (at position (0)) (Fig. 2.10B), the compression head was placed on the samples, and the system was fit under the platen of the bioreactor (Fig. 2.10A). Samples were subjected to dynamic compression starting from a basal load at position (1) (constructs were compressed 50 μ m) to a peak load at position (2) (constructs were compressed 150 μ m) (Fig. 2.10B). The corresponding strain levels were between 5% and 15% on the innermost portion of the construct where construct height was 1 mm, and between 1% and 3% on the outer portion where height was 5 mm (Fig. 2.10B). The dynamic compression was applied at 1 Hz, for 1 h/day, and 5 days/week.

Constructs were removed from culture media on Day 56 and analyzed (Section 2.2.3).

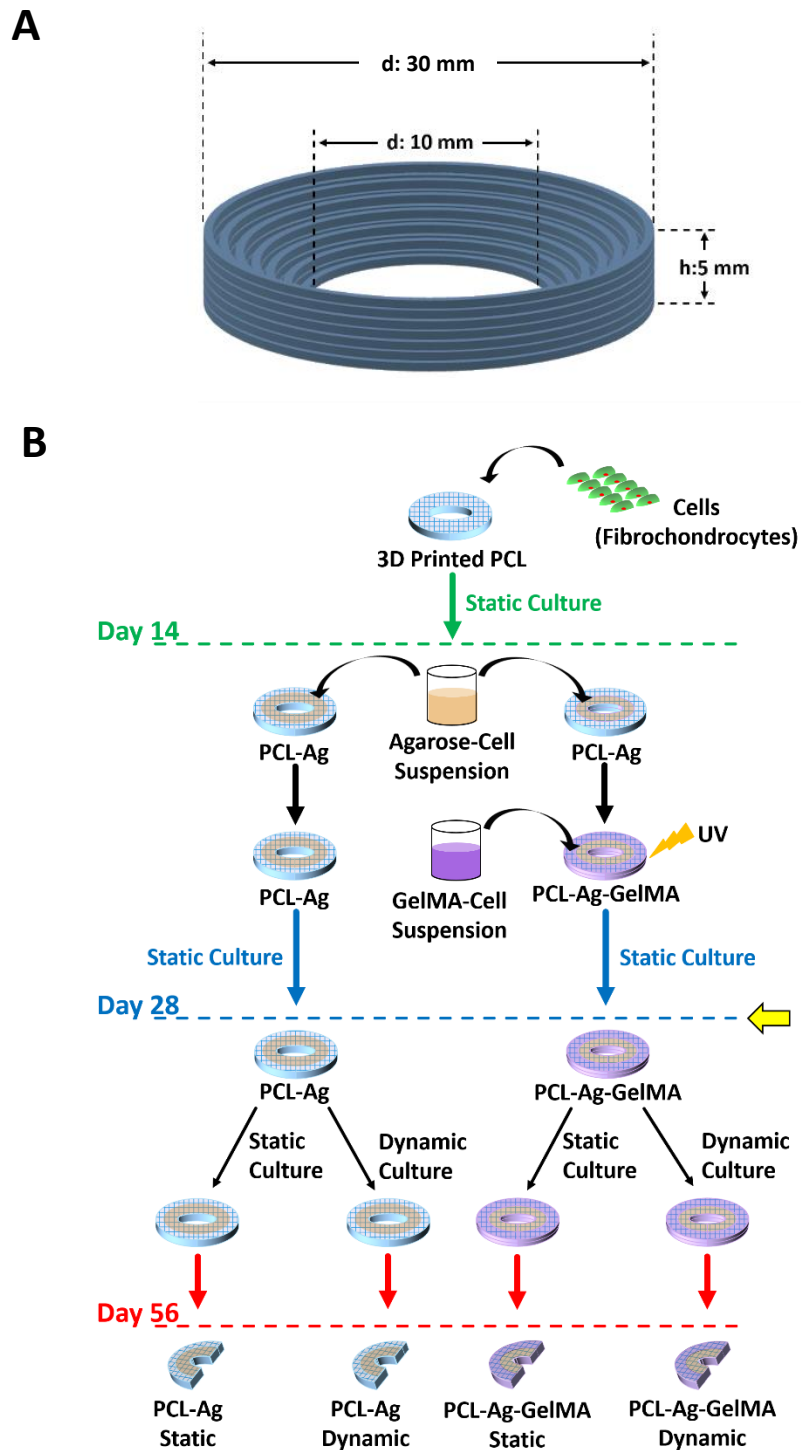


Figure 2.9. Design of the coliseum shaped structure that is cut into two halves to obtain the meniscus shaped constructs, and its preparation and culture. (A) Design of the coliseum shaped construct.

Figure 2.9. (Continued). (B) Preparation and culture of the constructs. PCL constructs were seeded with porcine fibrochondrocytes and incubated for 14 days in growth media. On Day 14, the inner and outer portions of the pre-seeded PCL were embedded in cell-laden agarose or GelMA, respectively, and crosslinked (cooled for PCL-Ag, and UV irradiated for PCL-GelMA). As a control, the outer portions of a group of constructs were not unembedded in a hydrogel. Constructs were incubated in fibrochondrogenic media until Day 28, when dynamic compression was started. Constructs were incubated under static or dynamic conditions until Day 56. Arrowhead: start of dynamic culture.

2.2.2.3.2.2. Preparation of Human Fibrochondrocyte-Based Constructs

PCL 50 was printed in coliseum shape, with and without shifting of the strands (shift distance: 0.5 mm), and with contour as described in Section 2.2.2.1 (Fig. 2.2) to mimic the circumferential fibers in the native meniscus. The coliseum-like structure had an outer diameter of 24 mm, inner diameter of 12 mm, and a height of 4.5 mm at the outer edge.

Human fibrochondrocytes (passage 3) were expanded, trypsinized, suspended in growth media, and seeded onto sterile PCL 50 scaffolds at a cell density of 1×10^5 cells/scaffolds. The constructs were cultured for 2 weeks in growth media. On Day 14, human cells were suspended in GelMA (porcine, 5% w/v in DMEM containing 1% (v/v) photoinitiator) or GelMA-Ag (1:1, v/v of the GelMA and agarose (2%, w/v) at 43 °C) solutions (final cell densities were 6×10^4 cells/scaffold). The pre-seeded PCL scaffolds were embedded in these cell suspensions. After gelation (with cooling for agarose and 5 min UV irradiation for GelMA), the constructs were incubated in growth media until Day 42 with no addition of growth factors. Constructs were removed from culture media on Day 42, cut into two meniscus shaped constructs, and prepared for analyses.

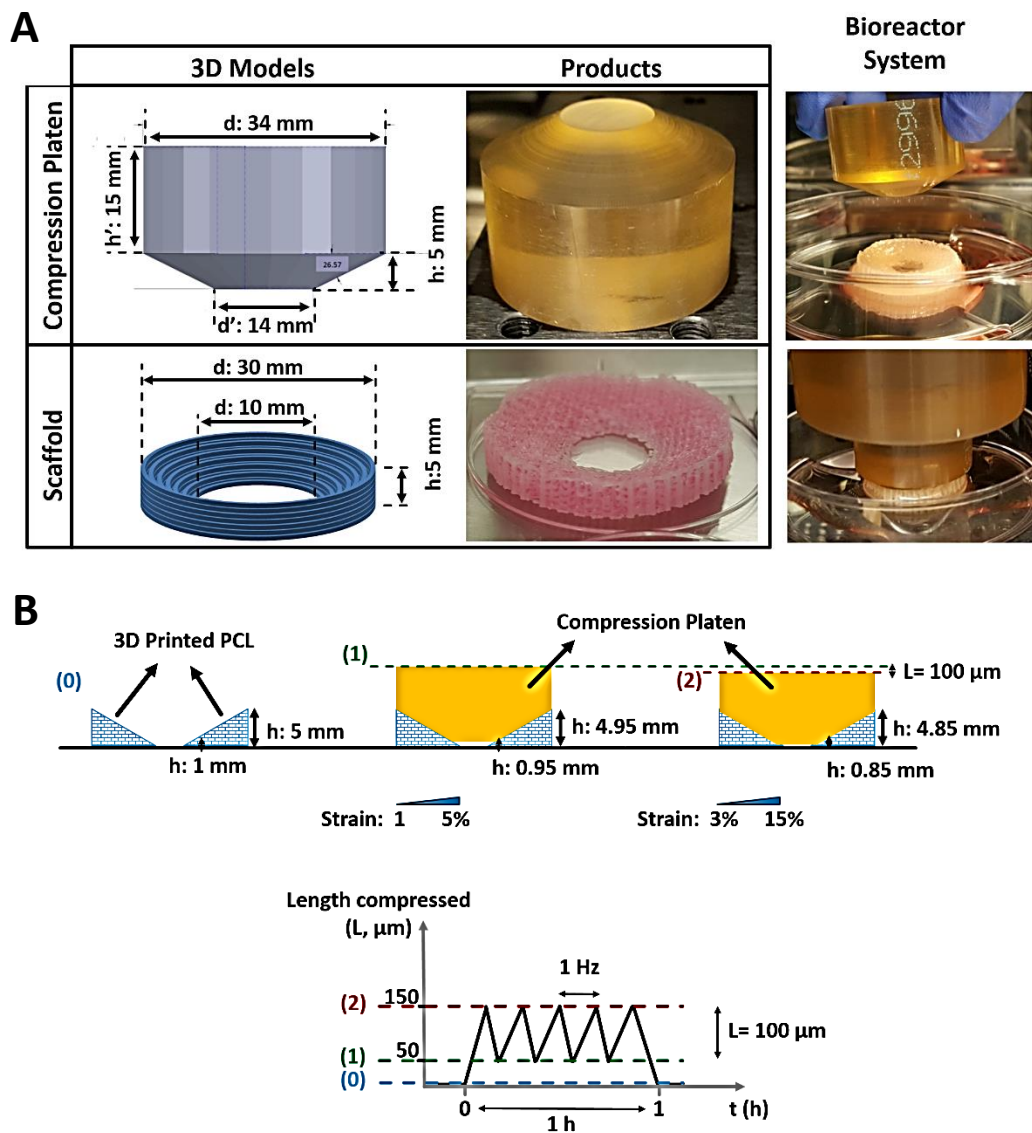


Figure 2.10. Designs of the compression head and the constructs, and depiction of the dynamic compression applied on the constructs. (A) A compression head was modelled and produced. The compression head was designed such that it would fit on the construct to enable application of dynamic compression. (B) The compression head was placed on the constructs and the system placed in a bioreactor. The sample was normally at position (0) under static culture. Dynamic compression was applied such that compression head cycles from position (1) (basal compression: 50 μm from position (0)) to position (2) (peak compression: 150 μm from position (0)) at 1 Hz frequency, 1 h/day, 5 days/week.

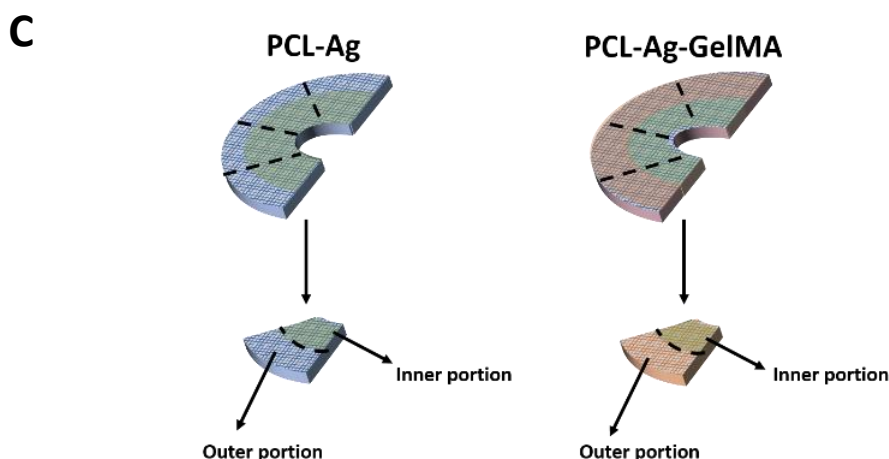


Figure 2.10. (Continued). (C) Sample preparation for analysis. Samples were cut radially into four pieces, and each piece was cut circumferentially at the gel boundaries.

In order to prepare samples for analyses, the meniscus shaped constructs were cut radially into four samples, and then each sample was cut circumferentially to obtain an inner and an outer portion of the samples (Fig. 2.10C).

2.2.3. Characterization of the Constructs

2.2.3.1. Characterization of GelMA and MeHA

2.2.3.1.1. FTIR Characterization

GelMA and MeHA were analyzed with Attenuated Total Reflectance (ATR) unit of the Fourier Transform Infrared (FTIR) spectrophotometry before or after UV crosslinking, and the absorbance values at wavenumbers ranging from 4000 to 400 cm^{-1} were determined.

2.2.3.1.2. Proton NMR Spectroscopic Characterization

Gelatin and GelMA polymers (50 mg/mL) from two different sources (bovine and porcine), and MeHA (1 mg/mL) were dissolved in deuterium oxide at 35 °C and the solutions were characterized with Proton (^1H) NMR spectrometer (Bruker DPX 400) operating at a ^1H resonance frequency of 400 MHz.

Degree of methacrylation (DM) was calculated for each polymer. For GelMA, DM is defined as the ratio of the methacrylated groups on GelMA to lysyl amine groups (Hoch *et al.*, 2012). Thus, DM was calculated from the peak integration (area) of the protons of the lysyl methylene groups (peak at 2.90 ppm) in GelMA relative to that in unmodified gelatin, using the NMR spectrum analysis software (MestreNova, Spain). The peak integrations were normalized to the phenylalanine (the aromatic group which does not show a shift in NMR spectrum) (peak at 7.2 ppm) to eliminate the change in signal intensities arising from concentration differences. DM was calculated according to the equation:

$$DM (\%) = \left(1 - \left(\frac{\text{Peak integration of lysyl methylene in GelMA}}{\text{Peak integration of lysyl methylene in gelatin}} \right) \right) * 100$$

The DM for MeHA is defined as the ratio of methacrylate groups on one disaccharide repeat unit of MeHA to hydroxyl groups (Bencherif *et al.*, 2008). Thus, DM was calculated from the ratio of the relative peak integrations of the protons of the methacrylate groups in MeHA (peak at 1.85 ppm) to methyl protons (peak at 1.9 ppm). DM was calculated according to the equation:

$$DM (\%) = \frac{\text{Peak integration of methacrylate protons}}{\text{Total peak integrations of methacrylate and methyl protons}} * 100$$

2.2.3.2. Macroscopic Characterization

Hydrogel samples were examined macroscopically every week during the culture period. The thickness and diameter of the samples were measured on Days 1 and 35 using a micrometer (with a sensitivity of 1 μm), and the volume was calculated. Samples were weighed (wet weight, WW), frozen at -20 $^{\circ}\text{C}$, lyophilized for 24 h, and weighed again (dry weight, DW).

2.2.3.3. Microscopic Characterization

2.2.3.3.1. Stereomicroscopic Characterization

The constructs were examined under a stereomicroscope (Nikon SMZ 1500, USA) to examine the surface topography.

2.2.3.3.2. SEM Characterization

For examination of scaffold microarchitecture, cell-free samples were washed with cacodylate buffer, incubated in glutaraldehyde (2.5%) for 2 h, frozen at -80 °C, and lyophilized for 3 h. The samples were sputter-coated with gold-palladium, and examined under a scanning electron microscope (SEM) (FEI, Quanta 400 F, USA) under high vacuum.

2.2.3.4. Mechanical Characterization

The PCL and hydrogels (n=6) were subjected to stress-relaxation test under unconfined compression using Instron (ElectroPuls E1000, USA) equipped with 10 N-load cell. Stress-relaxation test was performed by applying compression to samples and keeping them under constant strain (10%) for 30 min (relaxation) until equilibrium is reached (Fig. 2.11A). Equilibrium (or aggregate) modulus (H_A) was calculated from the stress at equilibrium and the strain applied.

Cell-free, square prism-shaped PCL/Hydrogel constructs (n=5) were incubated in phosphate buffered saline (PBS) for 24 h and then subjected to compression and tensile testing using CellScale (Univert, Canada) equipped with 10 N-load cell. Compression tests were performed on square prism shaped samples at a displacement rate of $1 \text{ mm}\cdot\text{min}^{-1}$, and the compressive modulus (E^*) of the constructs was calculated from the stress-strain curve (Harley *et al.*, 2007) (Fig. 2.11B).

Uniaxial tensile tests were performed on rectangular prism shaped samples at a displacement rate of $1 \text{ mm}\cdot\text{min}^{-1}$ and with a gauge length of 10 mm according to ASTM D882-00, and Young's modulus (E) was calculated from the stress-strain curve (Fig. 2.11C).

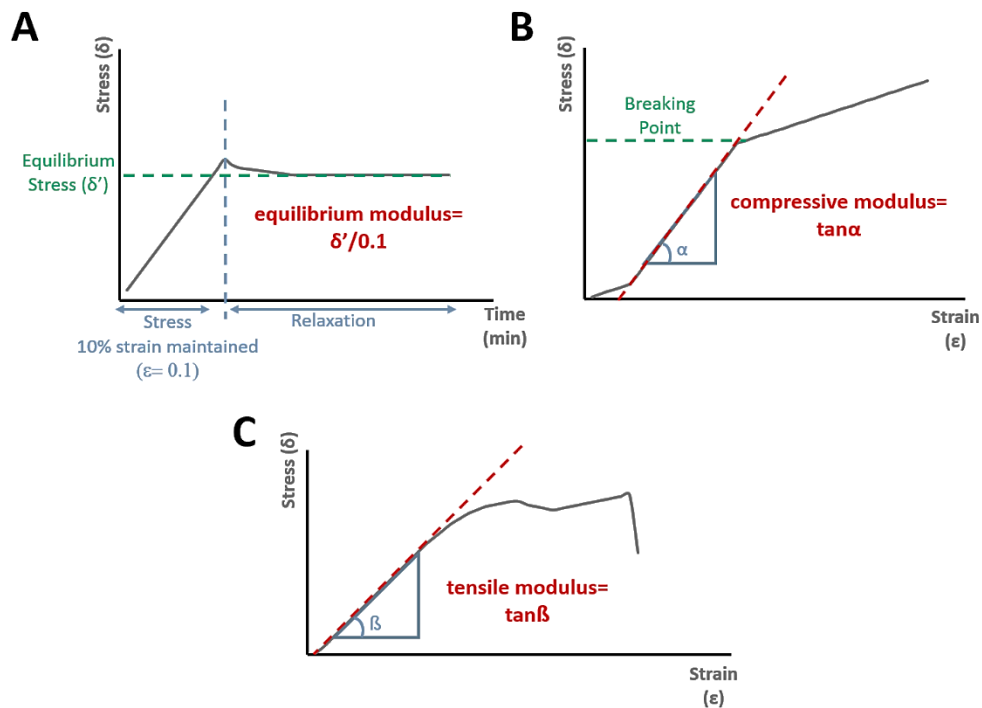


Figure 2.11. Representative graphs showing the calculations of the modulus values. (A) Equilibrium (or aggregate) modulus (H_A) at 10% strain, (B) compressive modulus (E^*), and (C) tensile modulus (E).

2.2.3.5. Cell Viability Analysis

Viability of cells in the constructs was assessed using the live/dead cell viability/cytotoxicity assay. Samples were incubated in a solution of Calcein-AM (2 μ M in PBS) (for live cells, green) and ethidium homodimer (EthD)-1 (4 μ M) (for dead cells, red) for 30 min., and visualized using confocal laser scanning microscope (CLSM) (Nikon Eclipse TE2000E, Japan). CLSM images ($n \geq 2$) were analyzed using ImageJ software (National Institutes of Health, USA) to assess cell viability. First, images were split into channels (converted to 8-bit images) and the number of cells in each channel was estimated using the software. The following formula was used to calculate cell viability.

$$\text{Cell viability (\%)} = \frac{\text{Number of live cells (green)}}{\text{Number of total cells (green and red)}} * 100$$

2.2.3.6. Cell Metabolic Activity

Cell numbers were determined by AlamarBlue® cell viability assay. Cell-seeded constructs ($n \geq 10$) were removed from culture media on Days 1, 7, 14, 21, 28, and 35 washed with colorless DMEM-F12 medium, and incubated at 37 °C in AlamarBlue® solution (10%, v/v in growth media). After 1 h incubation, the supernatants were transferred into 96-well plates, and absorbances at 570 and 595 nm were determined. Cell metabolic activity was calculated as percent reduction of the Alamar Blue dye, as described by the manufacturer (Appendix A). All experiments were performed in triplicates for each sample.

2.2.3.7. Cell Morphology

Cell morphology was examined by SEM. Samples were removed from culture media, washed with 0.1 M cacodylate buffer (pH 7.2), fixed in glutaraldehyde (2.5% in cacodylate buffer), frozen at -80 °C and lyophilized for 3 h. The samples were sputter-coated with gold-palladium and visualized using SEM (FEI, Quanta 400 F, USA) under high vacuum.

Cell-seeded constructs were washed with PBS, fixed with 4% paraformaldehyde for 15 min at room temperature, and incubated in Triton X-100 (0.1% v/v in 10 mM Tris-HCl buffer) for 5 min at room temperature, and in BSA (1% w/v in PBS) at 37 °C for 30 min to block nonspecific binding. Samples were then incubated in Alexafluor 488-Phalloidin at 37 °C for 1 h to stain actin, and in DRAQ5 at room temperature for 10 min to stain the nuclei. After washing with PBS, the constructs were examined under a CLSM (Leica DM 2500, Germany).

2.2.3.8. Cell-Material Interactions

For evaluation of cell-material interactions, hydrogels were stained for paxillin. Cell-seeded hydrogels were incubated in 0.1% Triton X-100 for 5 min and in 1% BSA for 30 min to block nonspecific binding. Samples were then incubated in mouse primary antibody against paxillin (dilution 1:100) for 1 h followed by Alexafluor 488-labelled goat anti-mouse IgG secondary antibody (dilution 1:400) for 1 h at 37 °C. In order to stain the actin and nuclei, samples were incubated in Alexafluor 532-labelled

phalloidin (dilution 1:400) for 1 h and in DRAQ5 (dilution 1:200) at 37 °C for 30 min. Cover slips were used as controls. Samples were visualized using CLSM (Leica DM 2500, Germany).

2.2.3.9. Biochemical Analysis

Samples were removed from culture media, lyophilized for 16 h, and digested overnight at 60 °C in papain solution (125 U/mL). The DNA, sulfated glycosaminoglycan (sGAG), and collagen contents of the samples were determined.

2.2.3.9.1. DNA Contents

DNA contents were measured using the Quant-iT™ PicoGreen® dsDNA quantification assay. Aliquots (100 µL) of the DNA standards and papain-digested samples were placed in 96-well dark-bottom plates and PicoGreen dye (100 µL, dilution 1:100) was added. The fluorescence measurements were done ($\lambda_{\text{excitation}}$: 480 nm and $\lambda_{\text{emission}}$: 520 nm) using a spectrophotometer (Molecular Devices, USA), and the DNA contents were calculated according to a standard curve constructed using the DNA standards (Appendix B, Fig. B.1).

2.2.3.9.2. Sulfated GAG Contents

Sulfated GAG contents were determined using the dimethylmethylene blue (DMMB) assay. Aliquots (20 µL) of the chondroitin sulfate standards and the papain-digested samples were placed in 96-well plates, and 200 µL of the DMMB dye (46 µm 1,9-dimethylmethylene blue, 40 mM NaCl, and 40 mM glycine) (pH 3) was added. The absorbance measurements were done at 535 nm immediately after addition of the dye. The sGAG contents were calculated according to a standard curve constructed using the chondroitin sulfate standards (Appendix C, Fig. C.1).

2.2.3.9.3. Collagen Contents

Collagen contents were determined using the orthohydroxyproline (OHP) assay. Papain-digested samples were digested in concentrated hydrochloric acid solution (overnight at 110 °C) and heat dried (overnight at 60°C). The samples were dissolved in OHP assay buffer (25 mM citric acid, 85 mM sodium hydroxide and 0.12% (v/v)

acetic acid) (pH 6), and transferred into 96 well plates. Chloramine T solution was added on to the samples and the plates were incubated in dark for 20 min, and then, p-dimethylaminobenzaldehyde (pDAB) solution was added. The plates were incubated at 60°C in dark for 15 min, and the absorbance was determined at 540 nm. OHP contents were calculated according to a standard curve constructed using OHP standards (Appendix D, Fig. D.1), and OHP contents were converted to collagen contents by applying a conversion factor, 7.64, which is the collagen to OHP weight ratio (Hollander *et al.*, 1994).

2.2.3.10. Histology and Immunohistochemistry

Samples were removed from culture media, fixed in acetone/methanol (1:1, v/v), embedded in paraffin, sectioned (6 µm thick) and fixed on slides. For histology, sections were deparaffinized, stained with Safranin-O to visualize the GAGs, and counterstained with Fast Green to visualize the other components including cells and proteins.

Immunohistochemistry was carried out using Vectastain ABC kit. First, sections were deparaffinized, treated with pepsin for 30 min to retrieve antigens, with hydrogen peroxide to eliminate the endogenous peroxidases, and with blocking solution to prevent nonspecific binding. Sections were then incubated overnight at 4 °C in mouse primary antibodies against type I (dilution 1:100) or type II (dilution 1:100) collagen, and then in biotin-labelled horse anti-mouse IgG at room temperature for 1 h. The sections were then incubated in avidin-biotin complex for 30 min, and in 3,3-diaminobenzidine (DAB) chromogen which forms a brown color. Sections were counterstained with hematoxylin and imaged using a bright-field microscope.

Semi-quantitative image analysis ($n \geq 2$ images per sample) was performed to assess the intensity of staining (ImageJ). Briefly, micrographs were converted to 8-bit images, and the integrated density calculated after background subtraction. For each construct, 2-9 images per sample were used.

2.2.3.11. Immunofluorescence

Samples were removed from culture media, washed with PBS, fixed in paraformaldehyde (4%), treated with Triton X-100 (0.1%) to permeabilize the cell membrane, and incubated in serum solution to block nonspecific binding.

For immunostaining of the porcine fibrochondrocyte-seeded constructs, samples were incubated for 1 h in rhodamine-labelled phalloidin, for 10 min in DAPI, and overnight at 4 °C in mouse primary antibodies against type I (dilution 1:100) or type II (dilution 1:100) collagen. Samples were then incubated in Alexafluor 488-labelled donkey anti-mouse secondary antibody (dilution 1:400) for 1 h at room temperature, and visualized under CLSM (Nikon Eclipse TE2000E, Japan).

For double immunostaining of the human fibrochondrocyte-seeded constructs, samples were incubated for 1 h in mouse primary antibody against type I collagen (dilution 1:1000), and for another 1 h in rabbit primary antibody against collagen type II (dilution 1:1000). Samples were then incubated in a mixture of Alexafluor 488-labelled anti-rabbit IgG and Alexafluor 532-labelled anti-mouse IgG (dilutions: 1:1000) for 1 h at room temperature. Finally, samples were incubated in TO-PRO dye (dilution 1:1000) for 30 min at room temperature and visualized under CLSM (Leica DM 2500, Germany).

2.2.4. Statistical Analysis

Statistical analyses were performed using SPSS 23 (IBM, USA). One-way ANOVA was performed, followed by Tukey-Kramer (equal variance) or Dunnett's T3 (unequal variance) post-hoc tests depending on whether samples had equal variance. Data are presented as the mean \pm standard deviation. Significance level was $\alpha < 0.05$.

CHAPTER 3

RESULTS AND DISCUSSION

3.1. Characterization of the Cells Isolated from Menisci

3.1.1. Flow Cytometry

Cells isolated from human donors were characterized previously using flow cytometry (Ndreu-Halili *et al.*, 2014). Cells were reported to have 97% viability after isolation, and they were positive for CD44 (99%) and CD105 (93%), and negative for CD14 (0.37%), CD15 (1.33%), CD31 (0.72%), CD34 (0.93%), CD45 (0.59%) (Ndreu-Halili *et al.*, 2014). These results are similar to those reported by others stating that human fibrochondrocytes were positive for CD44 and CD105, and negative for many other differentiation markers (Verdonk *et al.*, 2005). Thus, it was concluded that majority of the cells isolated in this study were fibrochondrocytes with high cell viability. As there are blood vessels and nerves in the meniscus, it is quite expected that some of the cells extracted from the tissue also express smooth muscle cell, endothelial cell and nerve cell markers.

3.1.2. Microscopy

Phase contrast micrographs of the human and porcine cells used in this study revealed presence of three types of cells when cultured on TCPS: chondrocyte-like cells (round or polygonal in shape), fibroblast-like cells (with long cell processes), and spindle-shaped cells for both human and porcine cells (Fig. 3. 1). These results are in parallel with other reports stating that cells obtained from human meniscus consisted of these three types of cells (Webber *et al.*, 1985).

3.2. Optimization of the 3D Printing Process Using PCL

For optimization of 3D printing process, a square prism shaped 3D model (20 mm x 20 mm x 3 mm) was used, with PCL 80 being the polymer to be dispensed. Temperature (T) of the cartridge, and speed of the nozzle movement in x-y direction (F_{xy}) were the parameters changed. The temperatures used were 150, 160, and 170 °C, and the movement speeds were 200, 400, 600, and 700 mm/min.

It was observed that PCL strands became smoother, thinner, and straighter as the temperature was lowered or the nozzle movement speed was increased (Fig. 3.2). At lower speeds, the PCL strands became thicker and wavy, and even fused with each other, leading to products with smaller pores. At 200 mm/min and 170 °C, no pores remained. The polymer tended to get darker at high temperature levels (170 °C), indicating oxidation. The optimal parameter settings for PCL 80 were established as 150 °C and 700 mm/min.

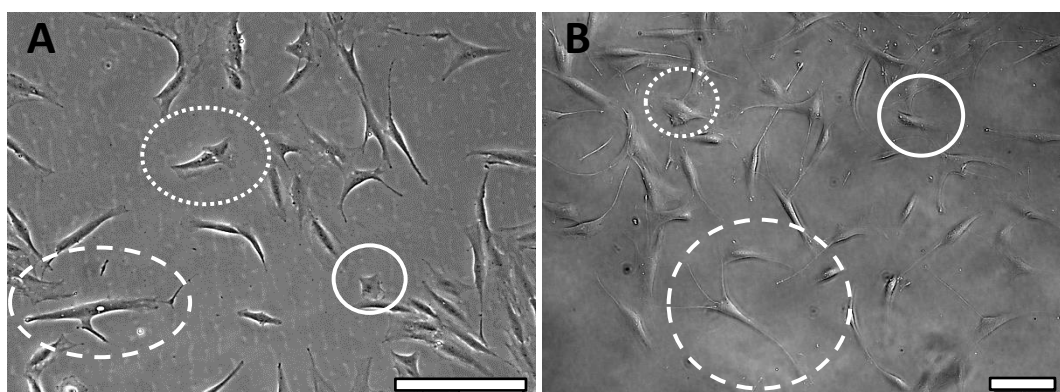


Figure 3.1. Phase contrast micrograph of the fibrochondrocytes cultured on TCPS. (A) Human fibrochondrocytes, and (B) porcine fibrochondrocytes. Circles: spindle-shaped cells, dotted circles: chondrocyte-like cells, and dashed circles: fibroblast-like cells. Scale bars: 100 μ m.

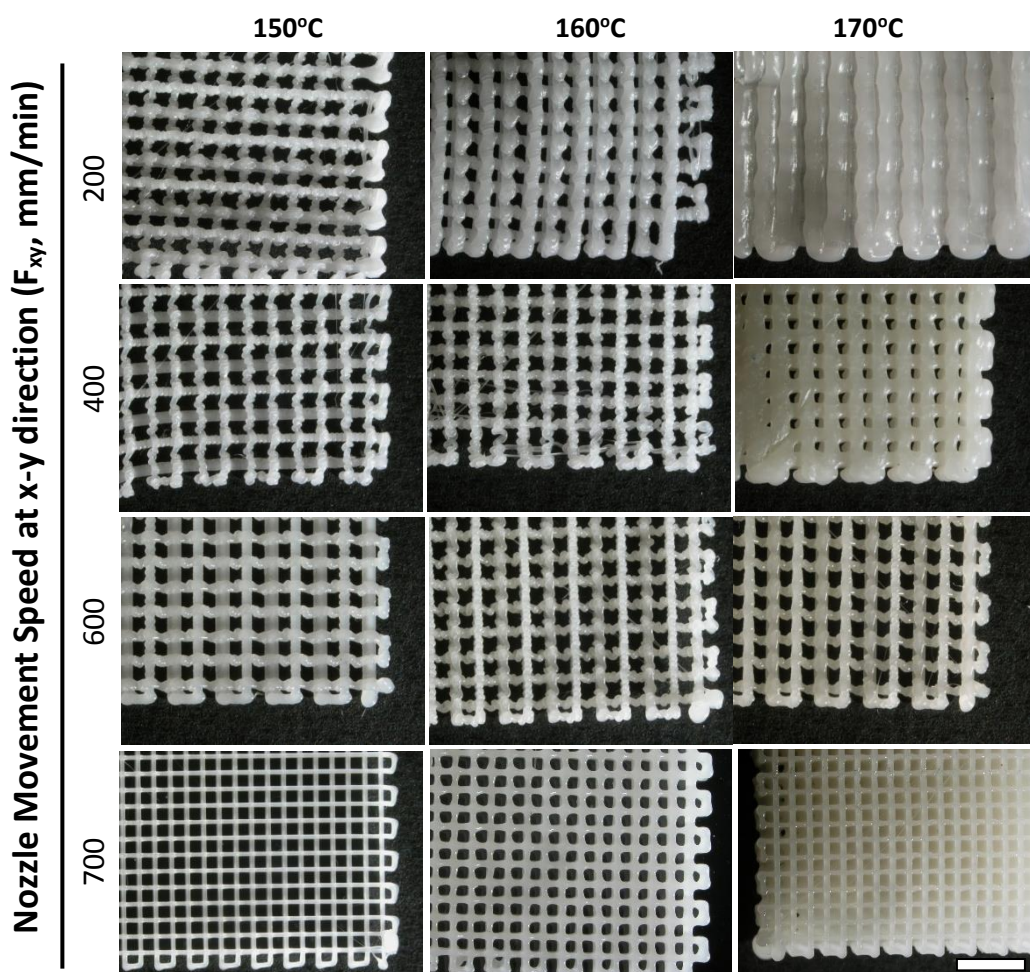


Figure 3.2. Optimization of the 3D printing of PCL 80. Two parameters were changed. Temperature: left panel, 150 °C; middle panel, 160 °C; and right panel, 170 °C. Movement speed of the nozzle ranged from 200 (top) to 700 mm/min (bottom). Scale bar: 4 mm.

Similar characterization was conducted with PCL 50, a lower molecular weight polymer. Optimal printing parameters were determined as 120 °C and 500 mm/min.

In the following experiments, PCL 80 was printed at 150 °C and 700 mm/min, and PCL 50 was printed at 120 °C and 500 mm/min.

3.3. Characterization of GelMA and MeHA Polymers

3.3.1. Optimization of Hydrogel Photocrosslinking Process

For optimization of the hydrogel photocrosslinking, first, GelMA (from porcine gelatin) (5 and 8%, w/v) and MeHA (0.5 and 1%, w/v) solutions were prepared and the photoinitiator, Irgacure 2959, (1 and 2%, w/v) was added. The solutions were exposed to UV light for up to 2 min, and the minimum time required for the gelation was determined.

Gelation time generally decreased as the polymer and photoinitiator concentrations increased (Table 3.1). Since gelation time did not vary much with the photoinitiator concentration, and the photoinitiator is known to be cytotoxic, a low concentration (1%) was chosen for use during crosslinking process. The minimum times required for gelation of GelMA and MeHA were 45 and 30 s, respectively.

For GelMA, 5% (w/v) was chosen, since stable GelMA gels were produced at this polymer concentration. For MeHA, 1% (w/v) was chosen, because it resulted in stable hydrogels.

Table 3.1. Minimum time of UV exposure required for gelation of GelMA (porcine) and MeHA.

		Polymer Concentration (%)	Photoinitiator Concentration (%)	Minimum Time Required (s)
Gel-MA	*	5	1	90
		5	2	60
		8	1	60
		8	2	45
MeHA		0.5	1	60
		0.5	2	60
	*	1	1	45
		1	2	30

*Rows indicate the optimal conditions for each polymer.

3.3.2. Proton NMR Spectroscopic Characterization

In order to calculate the degrees of methacrylation of GelMA and MeHA, the unmethacrylated (native) and methacrylated forms of gelatin and hyaluronic acid were analyzed with proton NMR spectroscopy. The results are shown in Figure 3.3. The degree of methacrylation (DM) of GelMA was calculated from the decrease in the intensity of the peak corresponding to lysyl amine group (highlighted as orange) upon methacrylation of gelatin, after the intensity of the aromatic phenylalanine groups (asterisk) of gelatin and GelMA were normalized (Fig. 3.3A). The DM of MeHA was calculated from the peak integration of the methacrylate protons (highlighted as blue) relative to that of methyl protons after methacrylation of hyaluronic acid (HA) (Fig. 3.3B).

The DMs of porcine and bovine GelMA were around 64 and 52%, respectively. This difference was the result of the methacrylic anhydride (MA) concentration used during the synthesis of each. The MA concentrations used for porcine and bovine GelMA were 20 and 12.5% (v/v), respectively. The DM of MeHA was around 25%, again due to the low concentration of MA used during the synthesis of MeHA. These are similar to the results reported previously in our group (60-65% for porcine GelMA and 25% for MeHA) (Eke *et al.*, 2017; Kilic-Bektas and Hasirci, 2017).

3.3.3. ATR-FTIR Characterization

Solutions of GelMA and MeHA were prepared according to Table 3.1 in Section 3.3.1 and ATR-FTIR spectrophotometry was performed before and after crosslinking as a result of UV exposure (Fig. 3.4).

Results showed that UV treatment decreased the absorbance of the polymers at 1640 cm^{-1} (Fig. 3.4). This peak corresponds to carbon-carbon double bonds (C=C). These bonds belong to the methacrylate groups in GelMA and MeHA, and are used up during crosslinking as a result of UV exposure (Section 2.2.2.2.3.1, Fig. 2.4). This explains the decrease in absorbance intensity of the bands corresponding to C=C.

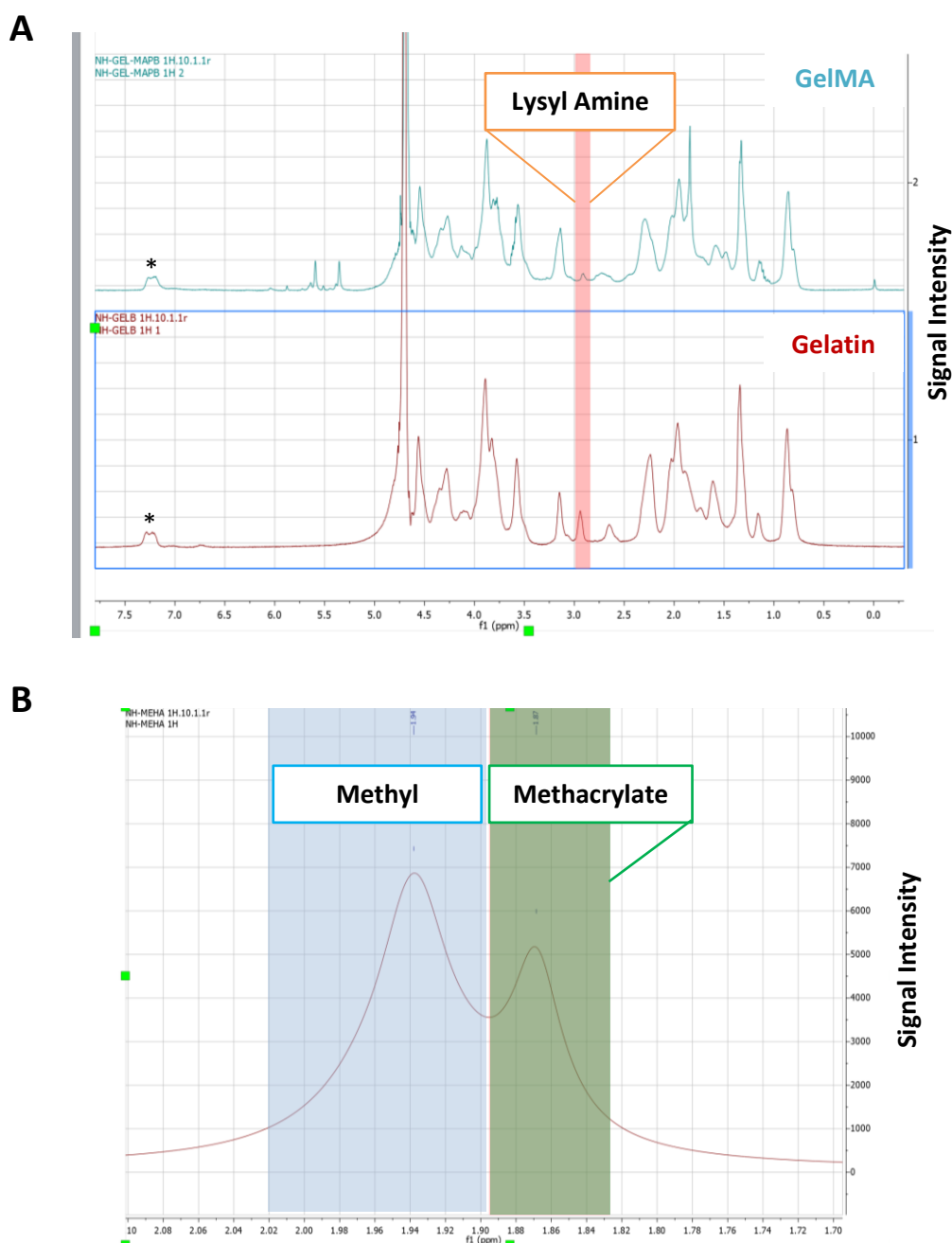


Figure 3.3. Proton NMR spectroscopy of gelatin, GelMA, and MeHA. (A) Representative spectra of porcine gelatin, and GelMA. Peak integration of the lysyl amine (highlighted in orange) was normalized to that of phenylalanine (asterisk), and the degree of integration (DM) was calculated from the decrease in the intensity of lysyl amine group. (B) NMR Spectra of MeHA. DM was calculated by the ratio of the integration of methyl protons (highlighted as blue) to that of methacrylate protons (highlighted as green).

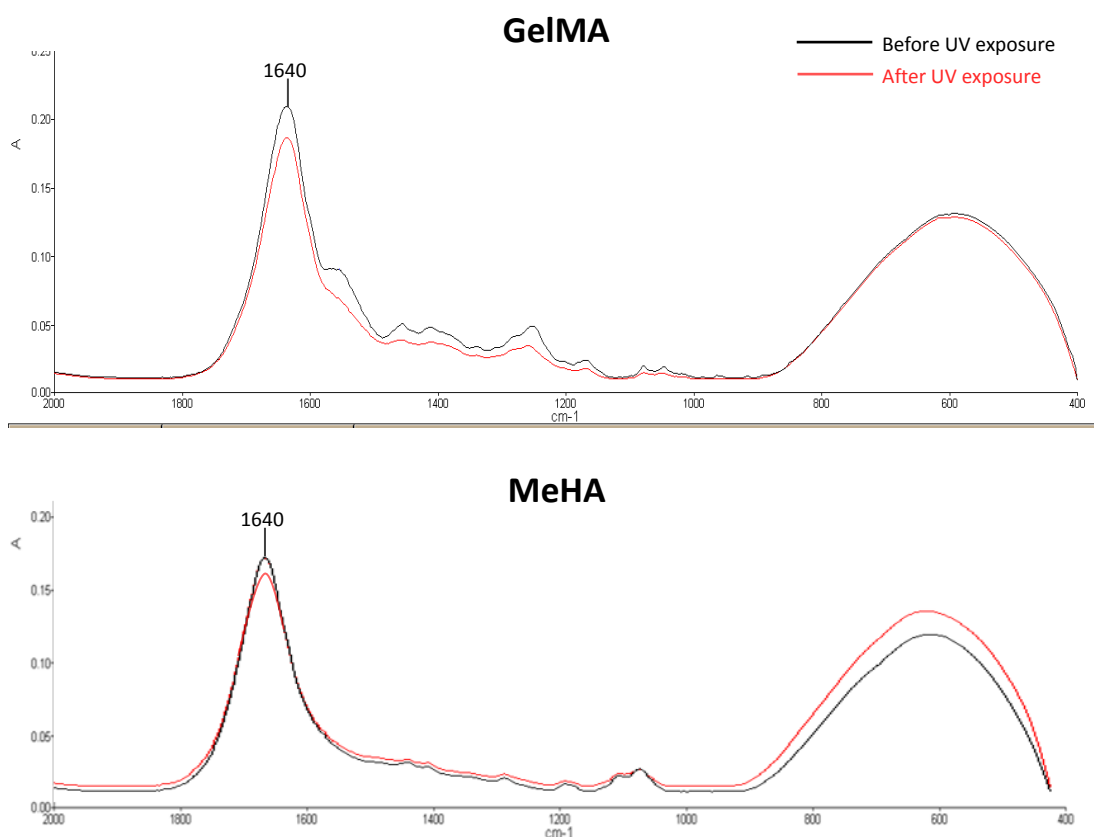


Figure 3.4. ATR-FTIR absorbance intensity of the untreated and UV-treated polymers. The peak at 1640 cm^{-1} corresponds to carbon-carbon double bonds (C=C).

Similar observation was reported in another study showing a decrease in the intensity of the peaks at 1640 cm^{-1} with the increasing duration of UV exposure (Shin *et al.*, 2012). The decrease in absorbance intensity of the C=C bonds indicated that crosslinking of the methacrylated polymers was achieved, and thus hydrogel formation was successful.

3.4. Porcine Fibrochondrocyte-Based Studies

The current thesis was divided into two parts: porcine fibrochondrocyte-based studies and human fibrochondrocyte-based studies. Here, the porcine cell-based studies are presented.

3.4.1. Hydrogel Constructs

Disk-shaped hydrogels were investigated for their potential to induce meniscal regeneration. The gels were seeded with porcine fibrochondrocytes and incubated for 35 days. The samples were tested for weight loss, contraction, microarchitecture, mechanical properties, cell viability, cell morphology, and GAG and collagen (type I and II) production. The square prism-shaped 3D printed PCL 80 was used as the control group.

3.4.1.1. Change in Physical Properties of the Constructs

The photographs of the hydrogels and the 3D printed PCL were taken every week until Day 35, in order to follow the changes in size of the constructs (Fig. 3.5). Gross examination revealed that the size of the cell-free constructs generally remained unchanged throughout the 35-day culture period. The size of the cell-seeded constructs also did not change, except for GelMA-MeHA which significantly decreased in size. The size of the cell-seeded agarose did not change much over time, and those of GelMA and MeHA decreased to some extent. The size of PCL, on the other hand, remained the same throughout the culture period, regardless of cell presence.

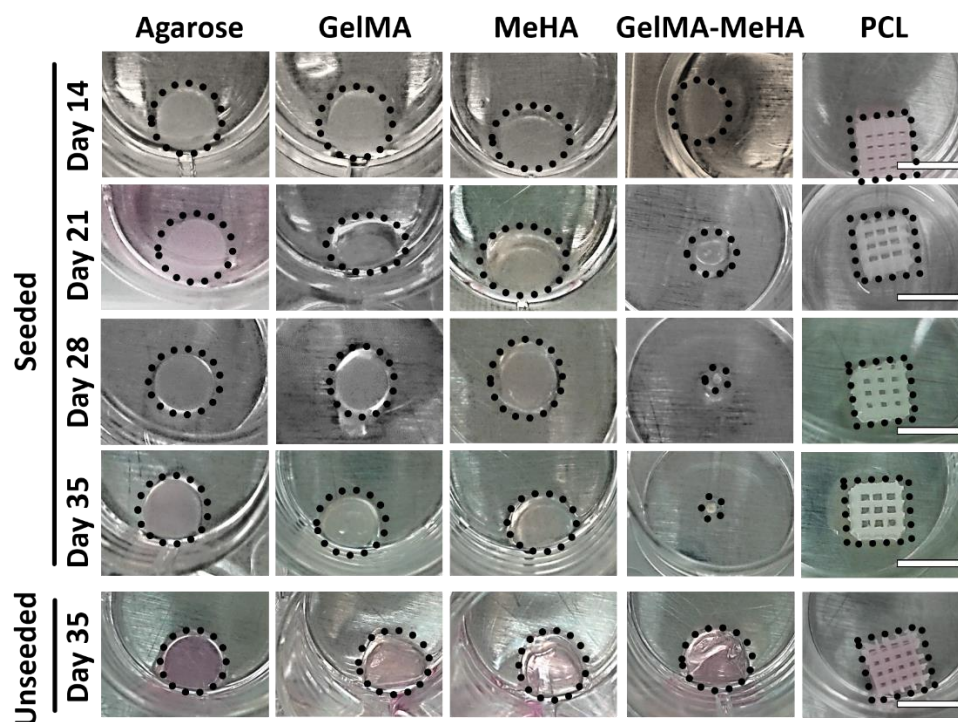


Figure 3.5. The change in size of the cell-seeded and cell-free samples over 35 days of culture. Dotted lines encircle the constructs. Scale bars: 5 mm.

The thickness and diameter of the hydrogels were measured using a micrometer (with a sensitivity of 1 μm), and the volumes were calculated. In general, when the gels were unseeded, the thickness, diameter, and volume of the gels remained unchanged, while dry weight (DW) decreased especially for GelMA-containing gels (Fig. 3.6, left). When cells were present, thickness, diameter, and DW of the gels generally decreased, with a few exceptions (Fig. 3.6, right). Thickness of the cell-seeded agarose and GelMA, and DW of agarose increased compared to the gels on Day 1 and also compared to the unseeded gels on Day 35. On the other hand, DW of GelMA increased after introduction of cells.

Dynamic compression did not result in a significant change in the physical properties of the gels, except it decreased the DW of the cell-seeded GelMA ($p < 0.05$).

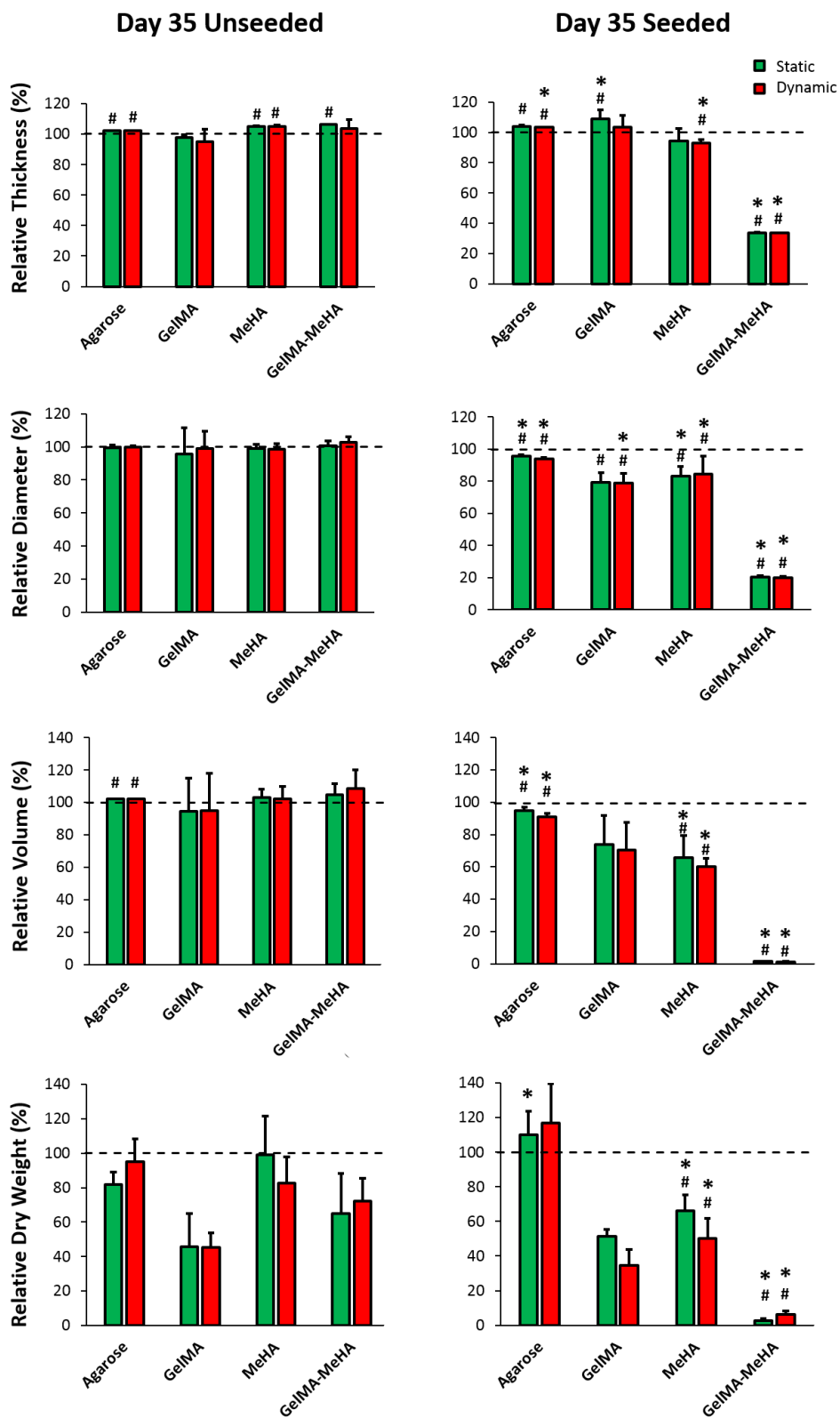


Figure 3.6. (Continued).

Figure 3.6. (Continued). Physical properties of the hydrogels on Day 35 relative to Day 1. Relative thickness, diameter, volume, and dry weights (DWs) of the constructs, showing the change in physical properties of the hydrogels over time. Thickness and diameter were measured with a micrometer, and DW was weighed using an analytical balance. Dashed lines show Day 1 results. Data are presented as the mean \pm SD. #Significant difference between results compared to Day 1 results of the same material incubated under the same condition. *Significant difference between the unseeded and seeded groups of the same material incubated under the same condition.

Possible reasons for an increase in hydrogel volume are the swelling of the gels over the 35 days of incubation in the culture media due to hydration, or thickening due to ECM production. Possible reasons for a decrease in the volumes could be cell-mediated gel contraction as a result of the traction forces exerted by cells on the material (Ghassemi *et al.*, 2012), or due to degradation because of the matrix metalloproteinase (MMP) activity in the cells (Naqvi *et al.*, 2005). A decrease in DW could be due to gel degradation, and an increase could be due to ECM deposition.

In the current study, cells reduced the diameter and increased the thickness of agarose and GelMA, which indicates that these gels went through cell-mediated contraction. The increase in DW of the hydrogels, indicated that ECM was produced by the cells. Diameter, thickness, volume, and DW of MeHA and GelMA-MeHA were reduced in the presence of cells ($p < 0.05$), which indicated that cells facilitated degradation of these gels and this process was dominant over ECM production.

Agarose resisted cell-mediated contraction because it is highly hydrophilic, which prevented cells from attaching, spreading, and forming stress fibers (and thus traction forces). It also resisted degradation because it lacks target sequences for MMPs. GelMA lost most of its weight over the culture period in the presence or absence of cells, which showed that it went through both hydrolytic and enzymatic degradation.

Gelatin and hyaluronic acid have target sequences for MMPs (Van den Steen *et al.*, 2002), and thus are prone to enzymatic degradation, which explains the rapid weight

loss in GelMA and MeHA in the presence of cells. GelMA-MeHA gel lost a significantly higher amount of its weight than GelMA or MeHA alone, probably because the integration of GelMA MeHA was not sufficiently strong. This was probably due to the highly hydrophilic nature of MeHA (Necas *et al.*, 2008), which absorbs a considerable amount of water that prevented proper interactions with GelMA. Thus, the level of crosslinking between GelMA and MeHA polymers could be so low that the two materials could not crosslink with each other to form a stable gel. When cells were present, the weak bonds between GelMA and MeHA could break easily due to contraction or MMP activity.

Similar observations have been reported. Scaffold-free constructs containing chondrocytes and fibrochondrocytes in 1:1 ratio were reported to shrink or contract after stimulation with TGF- β 1 (Huey and Athanasiou, 2011). Fibrochondrocyte-seeded agarose gels were also shown to contract in diameter and lose weight when in the presence of TGF- β 1 or FBS (Kalpakci *et al.*, 2011). In contrast, no contraction and weight loss were reported in the chondrocyte-seeded constructs (Kalpakci *et al.*, 2011). This shows that fibrochondrocytes have a relatively high MMP activity compared to chondrocytes. This is in parallel with our results which showed contraction in the TGF- β 1-treated agarose gels. However, we found an increase in dry weight of agarose over time, which may be a result of the contribution of ECM production. This shows that agarose gels did not degrade in the presence of cells, but rather went through cell-mediated gel contraction.

Degradation and cell-mediated gel contraction in gelatin and collagen gels were also reported in the literature. Sarem *et al.* (2013) showed that gelatin gels lost most of their weight after 75 days of incubation in PBS in the absence of cells. Chemically crosslinked collagen gels were reported to contract and lose significant amount of their weight after seeding with fibrochondrocytes (Puetzer *et al.*, 2015). Similarly, the uncrosslinked collagen gels were reported to lose weight and contract by over than 40% in diameter in 4 h, while crosslinked gels contracted by 10% in 66h (Heo *et al.*, 2016). All these studies showed that gelatin and/or collagen are prone to hydrolytic and enzymatic degradation.

3.4.1.2. Microarchitecture of the Constructs

The microarchitecture of the cell-free constructs incubated 35 days in culture media was examined using SEM. Agarose and MeHA were both nonporous, while GelMA-containing gels were porous (Fig. 3.7). Pore sizes of GelMA and GelMA-MeHA were around 50 and 30 μm , respectively. These observations were made under SEM at dry conditions after freeze drying of the gels, and do not reflect the porosity and pore size of the gels in the aqueous environment. However, they still give information about the density of polymer struts in the gel solutions prior to freeze drying. The strand distance in PCL was already designed to be 800 μm , and this was the case in our constructs (Fig. 3.7).

Our results are in parallel with the other reports. Pure agarose was reported to have smaller pores than collagen, and trace amounts of agarose in collagen-agarose gels was shown to reduce the pore size compared to pure collagen gels (Ulrich *et al.*, 2010; Lake and Barokas, 2011; Branco da Cunha, 2014).

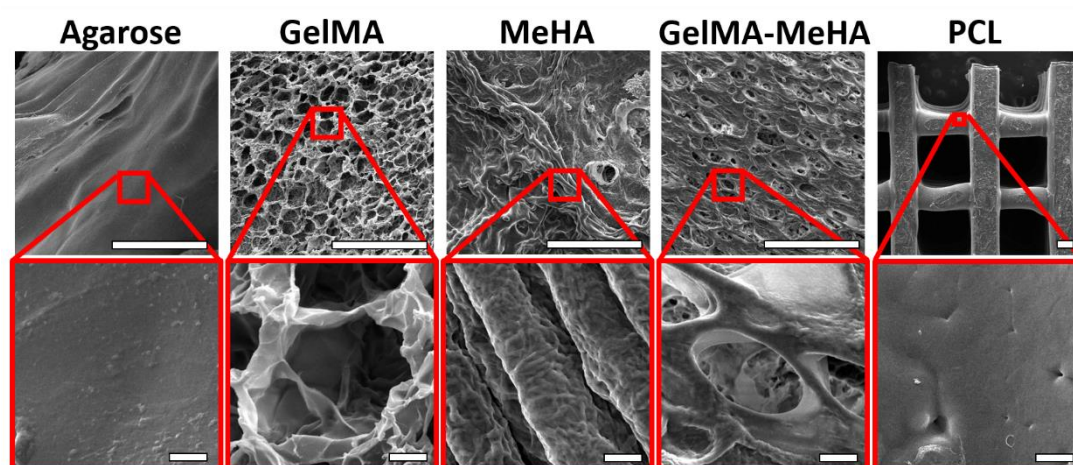


Figure 3.7 Microarchitecture of the cell-free constructs after 35 days of incubation in culture media. SEM of the constructs at low (upper panel, scale bars: 200 μm) and high (lower panel, scale bars: 10 μm) magnifications.

3.4.1.3. Compressive Mechanical Properties of the Constructs

After 35 days of incubation in culture media, constructs were subjected to stress-relaxation tests under compression and the equilibrium moduli were determined. The results are presented in Figure 3.8. For the unseeded hydrogels, equilibrium modulus of agarose (ca. 16 kPa) was the highest of all ($p < 0.01$) (Fig. 3.8A). Modulus of unseeded GelMA (ca. 7 kPa) was the lowest; significantly lower than MeHA and GelMA-MeHA (both around 11 kPa) ($p < 0.05$). The equilibrium modulus of the cell-free 3D printed PCL (ca. 2.3 MPa) was much higher than those of the hydrogels.

For the cell-seeded samples, the highest equilibrium modulus was obtained with agarose (ca. 13 kPa) ($p < 0.05$), the second was GelMA (ca. 9 kPa), and the lowest was MeHA (ca. 3 kPa) ($p < 0.01$) (Fig. 3.8B). Modulus of GelMA-MeHA could not be tested due to its extremely small size upon incubation in the culture media. Presence of cells significantly decreased the modulus of agarose ($p < 0.05$) and MeHA ($p < 0.001$), and slightly increased that of GelMA ($p > 0.05$). Finally, dynamic compression did not have any effect on the equilibrium modulus of the gels.

Higher equilibrium moduli were obtained with the cell-free agarose (2%, w/v) and MeHA (0.8 %, w/v) than GelMA (5%, w/v), although the concentration of GelMA was higher than the former two. The reason for this could be that agarose and MeHA are high molecular weight polymers and exhibit a nonporous structure under SEM, while GelMA is a relatively lower molecular weight polymer and exhibits a porous structure (pore size around 50 μm) (Section 3.4.1.2, Figure 3.7). Equilibrium modulus of GelMA increased upon addition of cells (from 7 kPa to 9), probably due to the high level of ECM produced on this gel. The decrease in the modulus of MeHA (from 12 to 3 kPa) could be a result of low level of ECM production on, and rapid degradation of, these gels (Section 3.4.1.1, Figure 3.6). Modulus of agarose also decreased upon introduction of cells although its DW increased, probably due to dissolution of agarose in the presence of cells. Other researchers have also reported a decrease in the modulus of agarose and HA gels upon cell seeding (Buckley *et al.*, 2009; Levett *et al.*, 2014).

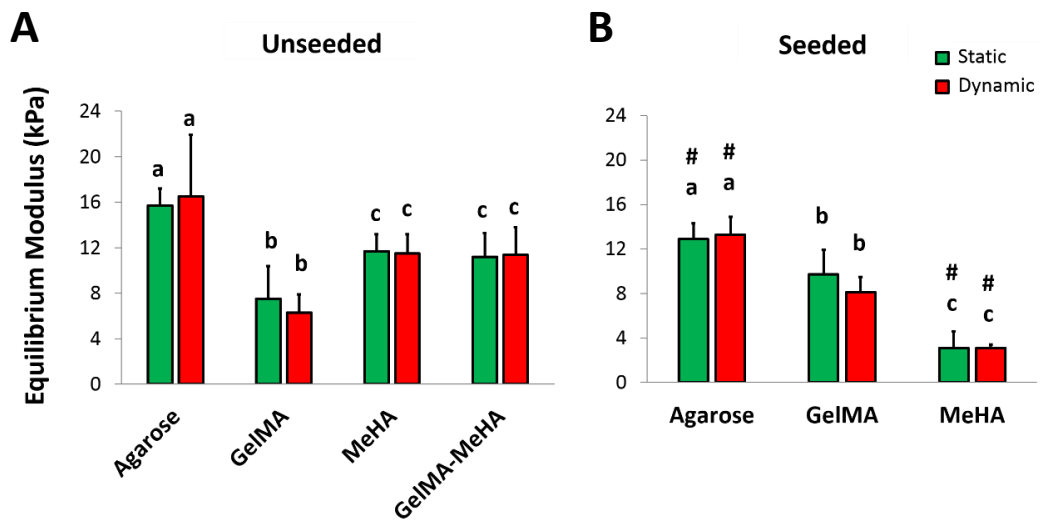


Figure 3.8. Compressive mechanical properties of the constructs after 35 days of culture. Equilibrium modulus of the (A) cell-free (unseeded), and (B) cell-seeded hydrogels. Data are presented as the mean \pm SD. For statistical significance: $p < 0.05$. Significant difference between hydrogels in the same graph when no letters in common. #Significant difference between unseeded and seeded groups of the same material.

The modulus values obtained in this study are consistent with those reported in other studies. An equilibrium modulus of 10-12 kPa were reported for 2% agarose (Buckley *et al.*, 2009), a modulus of 12-14 kPa for 15% GelMA (Grogan *et al.*, 2013), and a modulus of 5-16 kPa for 2.5% hyaluronic acid (Donnelly *et al.*, 2017). These values are an order of magnitude lower than equilibrium modulus of the native porcine meniscus (100-120 kPa) (Abdelgaied *et al.*, 2015).

The compressive properties of hydrogels used in this study could be increased by changing the polymer or photoinitiator concentrations, and time of UV exposure for photoactive gels to improve the degree of crosslinking. However, doing so could also harm the cells and lead to poor cell-material interactions due to reduction of functional groups on the polymer chains. PCL has good mechanical properties compared to hydrogels. Therefore, reinforcement of the hydrogels with PCL is important in order to produce a meniscal construct with good mechanical properties.

3.4.1.4. Cell Viability and Cell Metabolic Activity

Cell viability was evaluated by determining the DNA contents on Days 1 and 35. The initial DNA contents of the hydrogels measured on Day 1 ranged between 0.85-1.29 μg DNA/sample (Fig 3.9A, left). The highest initial DNA contents were on GelMA and PCL (around 1.2 μg DNA/sample), which were significantly higher than that of the MeHA-containing gels (around 0.9 μg DNA/sample) ($p < 0.05$). The DNA content of agarose was 1 μg DNA/sample.

On Day 35, the highest DNA content was again on PCL (around 1.3 μg DNA/sample), significantly higher than the DNA contents of the hydrogels (Fig. 3.9A, right). Among the hydrogels, the highest DNA content was on GelMA (0.8 μg DNA/sample). The DNA contents were GelMA > agarose > MeHA > GelMA-MeHA in a descending order.

The only sample that responded to dynamic compression was GelMA, which exhibited a significant decrease in DNA content (ca. 30%) ($p < 0.05$).

Relative DNA content results showed that DNA contents of the hydrogels incubated under static conditions decreased by 40% for agarose, 20% for GelMA, 60% for MeHA, and 90% for GelMA-MeHA over 35 days of culture, while that of PCL increased by 5% (Fig. 3.9B). The highest relative DNA content was obtained with PCL and the static samples of GelMA.

Dynamic compression did not have a significant effect on DNA contents, except for GelMA, which decreased significantly ($p < 0.05$). This could be due to the increased thickness of the cell-seeded GelMA over 35 days of incubation in culture media (Section 3.4.1.1, Fig. 3.6). Similar observation was reported with agarose and collagen gels incubated under dynamic compression at 15% strain (Ballyns and Bonassar, 2011; Puetzer *et al.*, 2012).

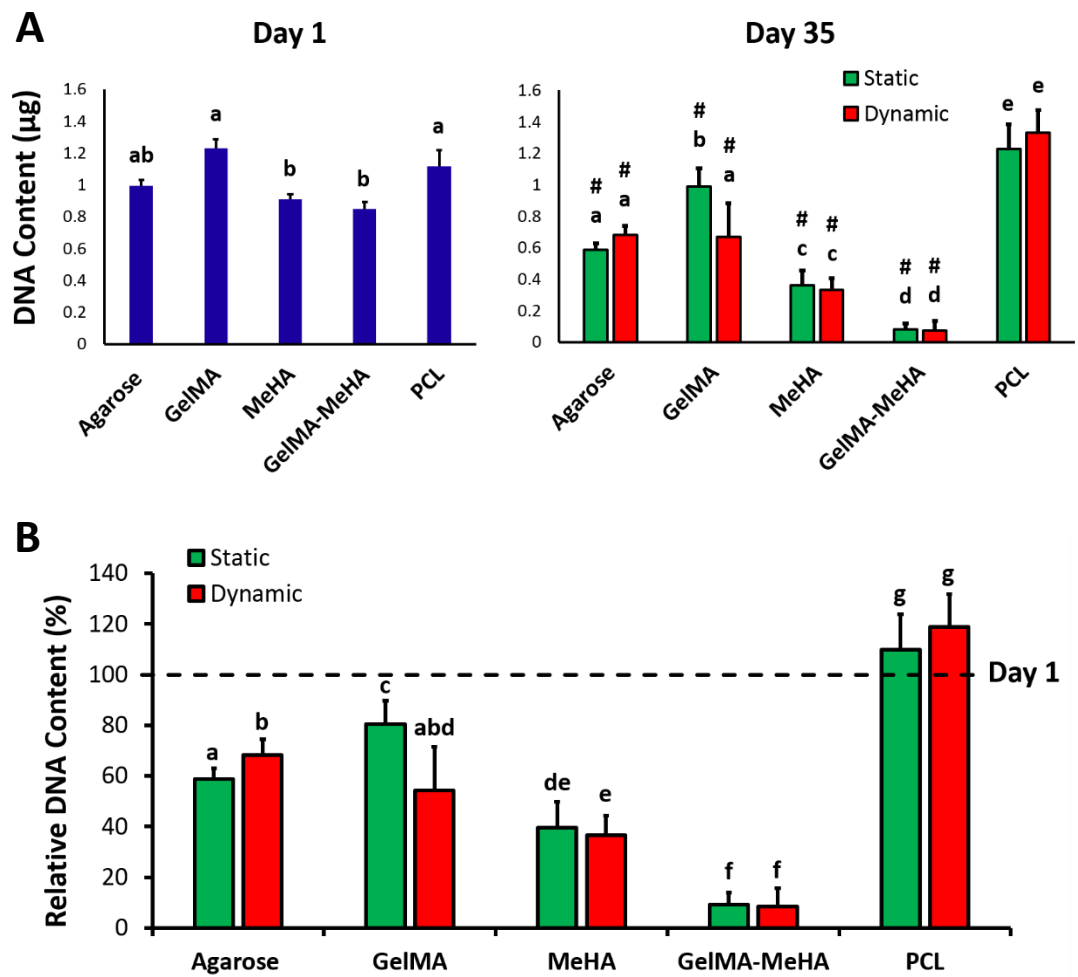


Figure 3.9. DNA contents of the constructs. (A) DNA contents of the constructs on Day 1 (left) and Day 35 (right). (B) Relative DNA contents (%) of the constructs (DNA content on Day 35 (n= 3-6) relative to that on Day 1 (n= 3)). Results are presented as the mean \pm SD. For statistical significance $p < 0.05$. Significant difference between constructs in the same graph when no letters in common. #Significant difference between Day 1 and Day 35 results.

In order to assess cell proliferation using a method based on cell metabolic activity, AlamarBlue cell viability assay was performed. Cell metabolic activity increased until Day 14, and then decreased in most of the constructs (Fig. 3.10). Cell metabolic activity could reflect the proliferation of cells, because it is generally accepted that metabolic activity cell number are proportional. This indicated that cell proliferation decreased after Day 14, probably because the cells tended to produce ECM instead of

proliferating, and/or because some of the hydrogels started to degrade leading to loss of material and cells.

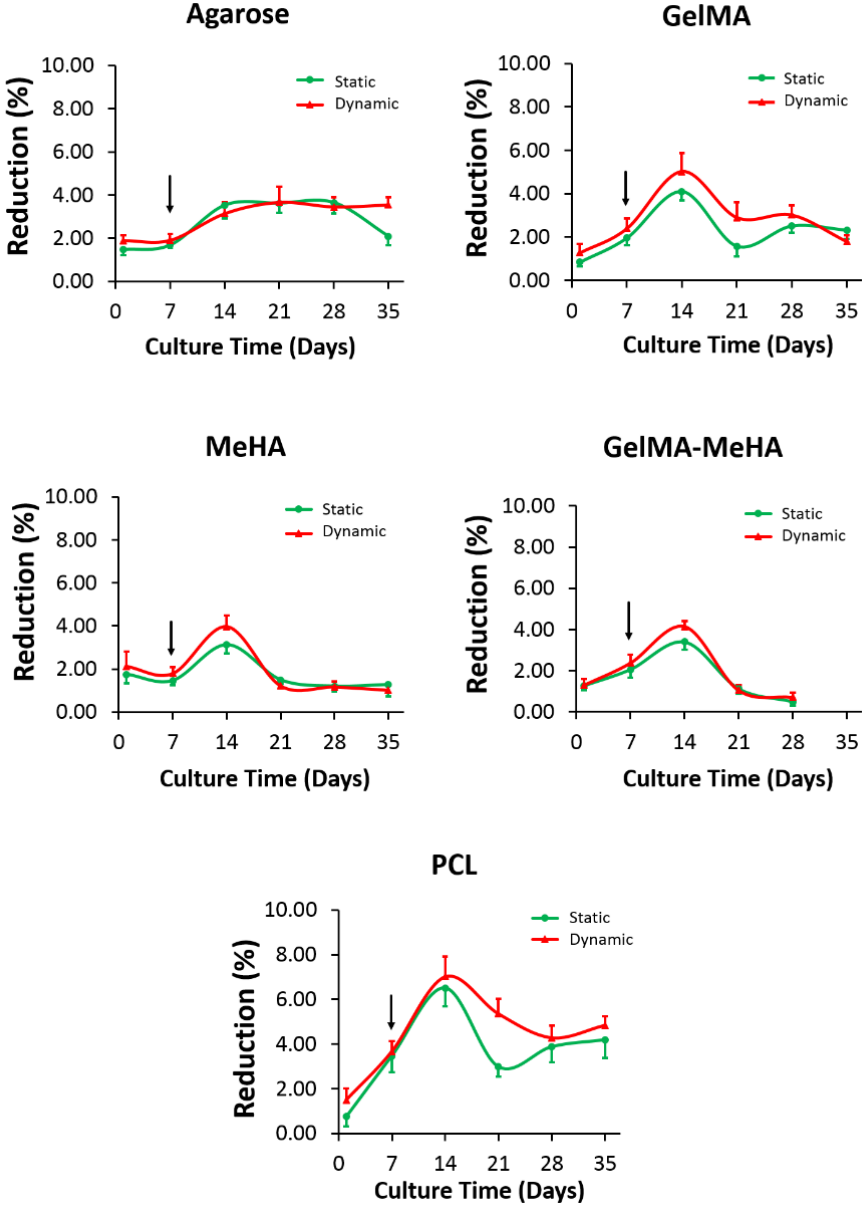


Figure 3.10. Cell metabolic activity in the constructs. Percent reduction of the alamarBlue dye. Results are presented as the mean \pm SD. Arrows indicate the start of dynamic compression (Day 7). $n \geq 10$.

Live/dead cell viability assay results of the constructs on Day 35 also indicated that cell viability (green cells) was high on GelMA and PCL, and low on MeHA-containing gels (Fig. 3.11). ImageJ analysis of the images showed around 80% cell viability in agarose, GelMA, and PCL, and around 60% viability in MeHA and GelMA-MeHA. Cell viability did not change upon dynamic compression.

The reasons for the decrease in cell viability and metabolic activity in the constructs could be the formation of a cell layer on the surface of the constructs that limited the transport of oxygen and nutrients to the core of the gels (Murphy *et al.*, 2010), the degradation of the constructs which led to loss of material and cells (Section 3.4.1.1, Fig. 3.6), and the tendency of cells to produce ECM rather than proliferate after Day 14 (Zorlutuna *et al.*, 2009; Ballyns and Bonassar, 2011; Bahcecioglu *et al.*, 2014). The high cell viability and metabolic activity on PCL, on the other hand, was probably due to the 2D microenvironment on the PCL surface which allowed for spreading of the cells, the high stiffness of PCL which could increase the proliferation rate (Section 3.4.1.3), and the large pores (Section 3.4.1.2, Figure 3.7) that allow for easy transport of oxygen and nutrients and larger space for the cells.

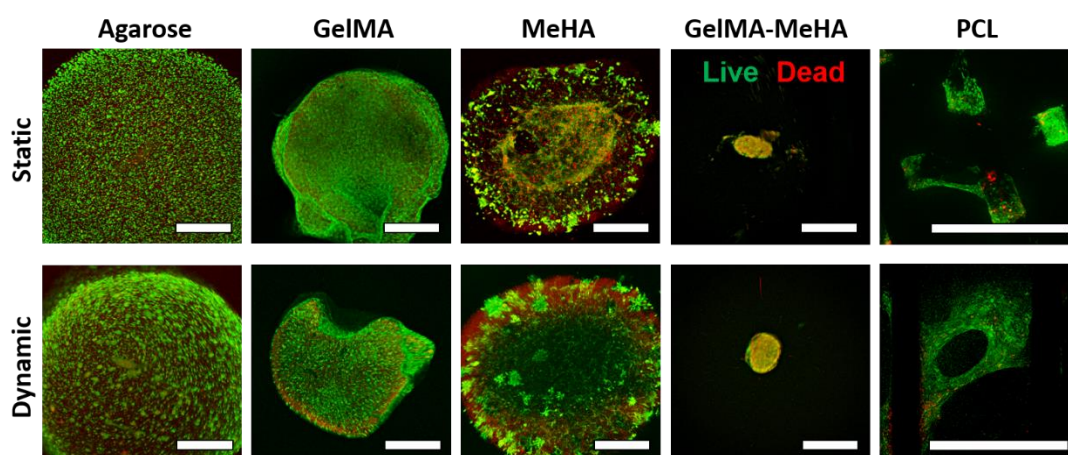


Figure 3.11. Live/dead cell viability assay results of the constructs on Day 35. CLSM images of the samples cultured under static (top) and dynamic (bottom) conditions. Green: calcein-AM (live cells); red: ethidium homodimer-1 (dead cells). Scale bars: 1 mm.

Since GelMA-MeHA constructs were too small to handle, they could not be analyzed further, and excluded from the following sections.

3.4.1.5. Collagen Contents of the Constructs

Collagen contents of the cell seeded constructs were calculated from the hydroxyproline amounts in the constructs (assuming a collagen:hydroxyproline ratio of 7.64), which were assessed using the orthohydroxyproline (OHP) assay (Hollander *et al.*, 1994). In order to eliminate the size differences in the samples and also the effects of degradation, the results were normalized to dry weights (Fig. 3.12A). In order to eliminate the background signal resulting from the scaffold materials (especially gelatin) and compare the constructs, the results were presented as the change in collagen contents between Days 1 and 35 (Fig. 3.12B).

The highest collagen content was observed on GelMA (Figs. 3.12A and 3.12B). Collagen content of GelMA increased significantly over time ($p < 0.05$) (Fig. 3.12A), and the net increase in collagen content of GelMA was 14-18% of the sample DW (Fig. 3.12B). On the other hand, collagen contents of agarose, MeHA, and PCL did not change significantly over the culture period. Collagen contents of the inner and outer regions of the native meniscus were 85 and 96% of their DWs, respectively (Fig. 3.12C).

When cultured under dynamic compression, the net collagen production in GelMA was around 18% of its DW (235 μg collagen/ μg DNA), about 20-25% of the collagen present in the native meniscus. The high collagen production in GelMA could be a result of the biologic recognition sites on gelatin, such as RGD sequences (Liu and Chan-Park, 2010), which enhances cell adhesion, proliferation and ECM production. In some other studies, 2 μg collagen/ μg DNA (McCorry *et al.*, 2016), or 10-20% of the native meniscus (Puetzer *et al.*, 2015) were reported in fibrochondrocyte-seeded collagen gels, both of which were lower than our results. The collagen content of the meniscus obtained in this study (85% of its DW in the inner region and 96% in the outer region) (Fig. 3.12C) was in accordance with the results reported in the literature (82% of its DW in the inner region and 90% in the outer region) (Sanchez-Adams *et al.*, 2011).

Agarose, MeHA, and PCL all exhibited low amounts of collagen in our study. Similar results were reported by others for fibrochondrocyte-seeded agarose (Wilson *et al.*, 2009) and PCL (Lee *et al.*, 2014).

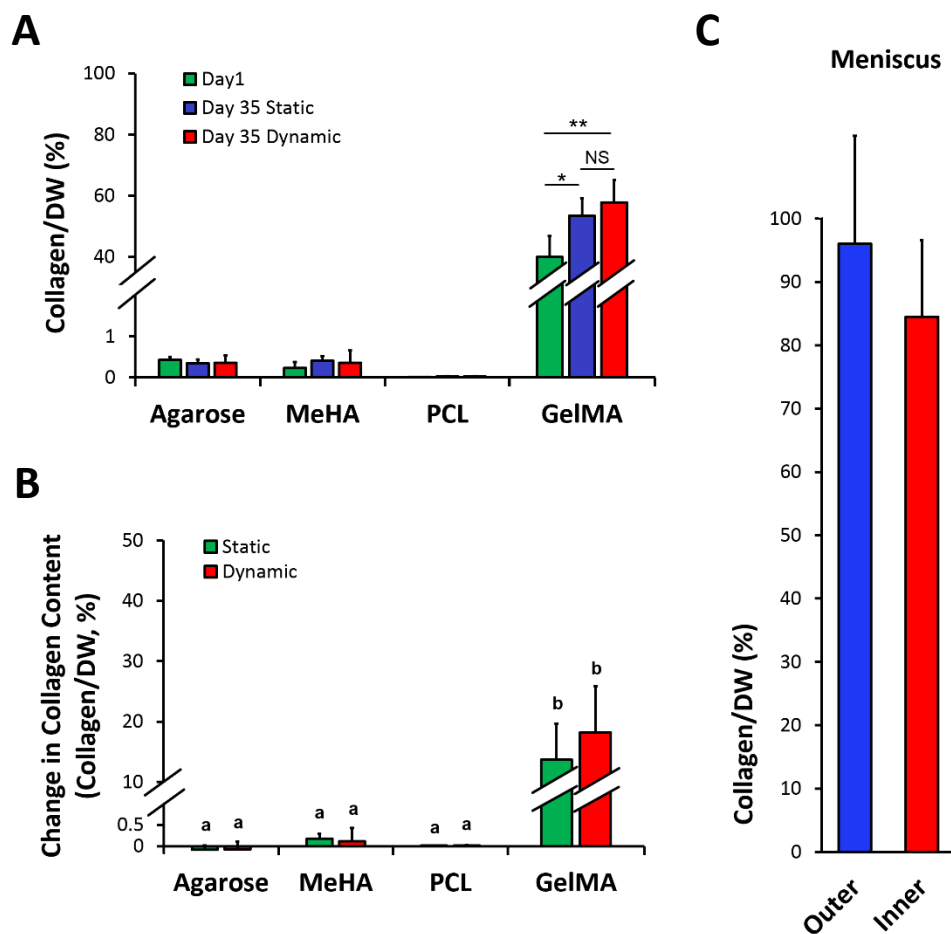


Figure 3.12. Collagen contents of the constructs and the native meniscus determined with orthohydroxyproline (OHP) assay. (A) Collagen content normalized to DWs (%) of the constructs. (B) Net change in collagen contents of the constructs between Days 1 ($n=3$) and 35 ($n\geq 5$). (C) Collagen content of the native meniscus ($n=6$). Data are presented as the mean \pm SD. NS: not significant. Statistical significance: $*p<0.05$, $**p<0.01$. Significant difference when no letters in common.

Biochemical assay does not distinguish between the types of collagen deposited on the constructs. In order to assess type I (COL I) and type II (COL II) collagen production on the constructs, immunohistochemistry was performed.

Immunohistochemistry supported the biochemical assay results (Fig 3.13A). The highest level of COL I and COL II production was observed on GelMA. Images of the cross and horizontal sections revealed that collagen was intensely stained throughout the gels. Collagen staining on agarose and MeHA was weak, indicating low collagen production on these gels. Intense staining of COL I and COL II was observed in the meniscus, which was the positive control.

One observation was that the collagen deposited on agarose and MeHA was globular in shape, and that deposited on GelMA was dendritic and continuous especially on the surface (Fig. 3.13A).

ImageJ analysis revealed that COL I ($p<0.001$) and COL II ($p<0.05$) staining were the highest on GelMA (Fig 3.13B). The unseeded constructs exhibited background staining of COL I and COL II. Thus, the net COL I and COL II intensities corrected for the background were 18 and 7 A.U, respectively, which were lower ($p<0.05$) than the native meniscus results (around 40 A.U for COL I and COL II in the inner region of the meniscus, and 55 A.U for COL I and 35 A.U for COL II in the outer region). In parallel with the biochemical assay results (Fig. 3.12), agarose and MeHA exhibited low COL I and COL II production. Similar to the results obtained in the current study, Daly and colleagues reported higher COL I staining than COL II on GelMA, and higher COL II staining than COL I on agarose (2016). However, unlike the results in the current study, they reported higher deposition of COL II on agarose than on GelMA.

In agarose and MeHA, COL I and COL II were produced at the same levels, a result similar to that in the inner region of the native meniscus (Fig. 3.13B). However, in GelMA, the intensity of COL I was 2-fold higher than COL II, similar to the result in the outer region of the meniscus. In fact, COL I was reported to constitute 90% of the outer region of the native meniscus and 40% of the inner region, while COL II was reported to constitute 60% of the inner region (Cheung, 1987).

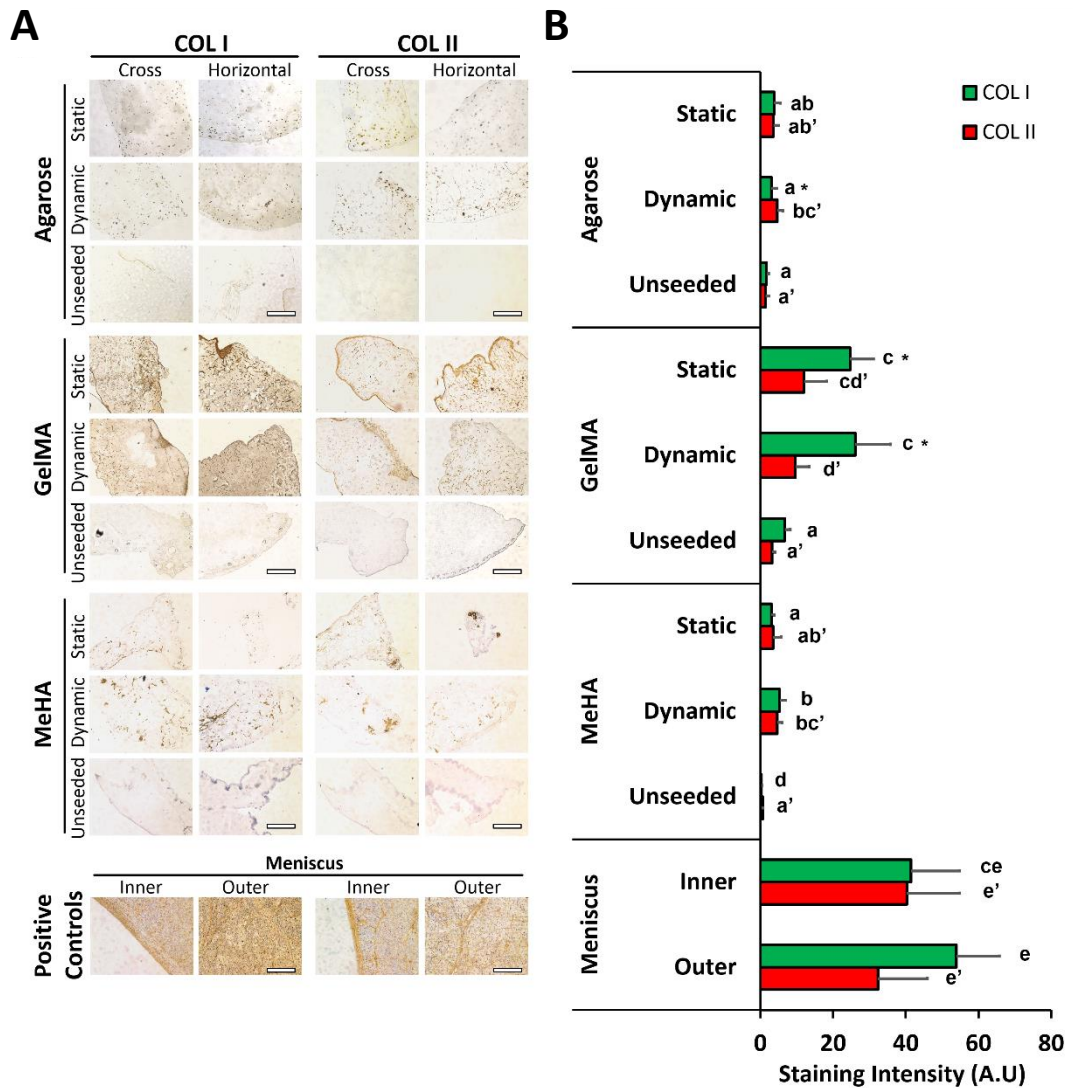


Fig 3.13. Immunohistochemistry of the hydrogels incubated for 35 days in culture. (A) Representative images showing COL I and COL II immunostaining of the cross and horizontal sections of the gels. For the native meniscus, left: inner region, and right: outer region. Chromogen: DAB (brown), and counterstain: hematoxylin (dark blue). Scale bars: 500 μ m. (B) Intensity of collagen staining on gels (n=3) measured with ImageJ software (n=2-9 images/sample). A.U: arbitrary units. Significant difference between hydrogels when no letters in common. Comparison between samples stained for ^{a, b, c, d}COL I and ^{a', b', c', d'}COL II. *significant difference between COL I and COL II results of the same material at a particular loading regimen.

3.4.1.6. Sulfated GAG Contents of the Constructs

Sulfated GAG contents were calculated using the DMMB assay. In order to eliminate the size differences in the samples and also the effect of degradation, the results were normalized to dry weights (Fig. 3.14A). In order to eliminate the background signal resulting from the scaffold materials (especially gelatin) and compare the constructs, the results were presented as the change in collagen contents between Days 1 and 35 (Fig. 3.14B).

The results showed that sGAG content of agarose increased significantly after 35 days of culture ($p < 0.001$), and dynamic compression further increased the sGAG content ($p < 0.05$ compared to static group) (Fig. 3.14A). Similarly, sGAG contents of GelMA ($p < 0.01$) and MeHA ($p > 0.05$) increased over time. The sGAG content of PCL, however, did not change over time and was very low compared to hydrogels (Fig. 3.14B).

The net sGAG production in agarose after 35 days of incubation was significantly higher than that on the other constructs ($p < 0.05$) (Fig. 3.14B), and lower than ($p < 0.05$) but comparable to the results for the meniscus (Fig. 3.14C).

The GAG results obtained in agarose in this study (0.7% DW or 0.07% WW or 12 $\mu\text{g GAG}/\mu\text{g DNA}$) were higher than those reported in another study when fibrochondrocyte-seeded agarose was used (8 $\mu\text{g GAG}/\mu\text{g DNA}$), but lower when chondrocytes were used (Wilson *et al.*, 2009). Daly *et al.* also reported higher GAG content results with bone marrow MSC-laden agarose gels (0.8% of WW) (2016).

GAG content of GelMA gels obtained in this study (0.25% of DW or 0.025% of WW or 3.2 $\mu\text{g GAG}/\mu\text{g DNA}$) were similar to that reported by Visser *et al.* (0.02% WW) (2015), and by Krouwels *et al.* (2-5 $\mu\text{g GAG}/\mu\text{g DNA}$) (2017).

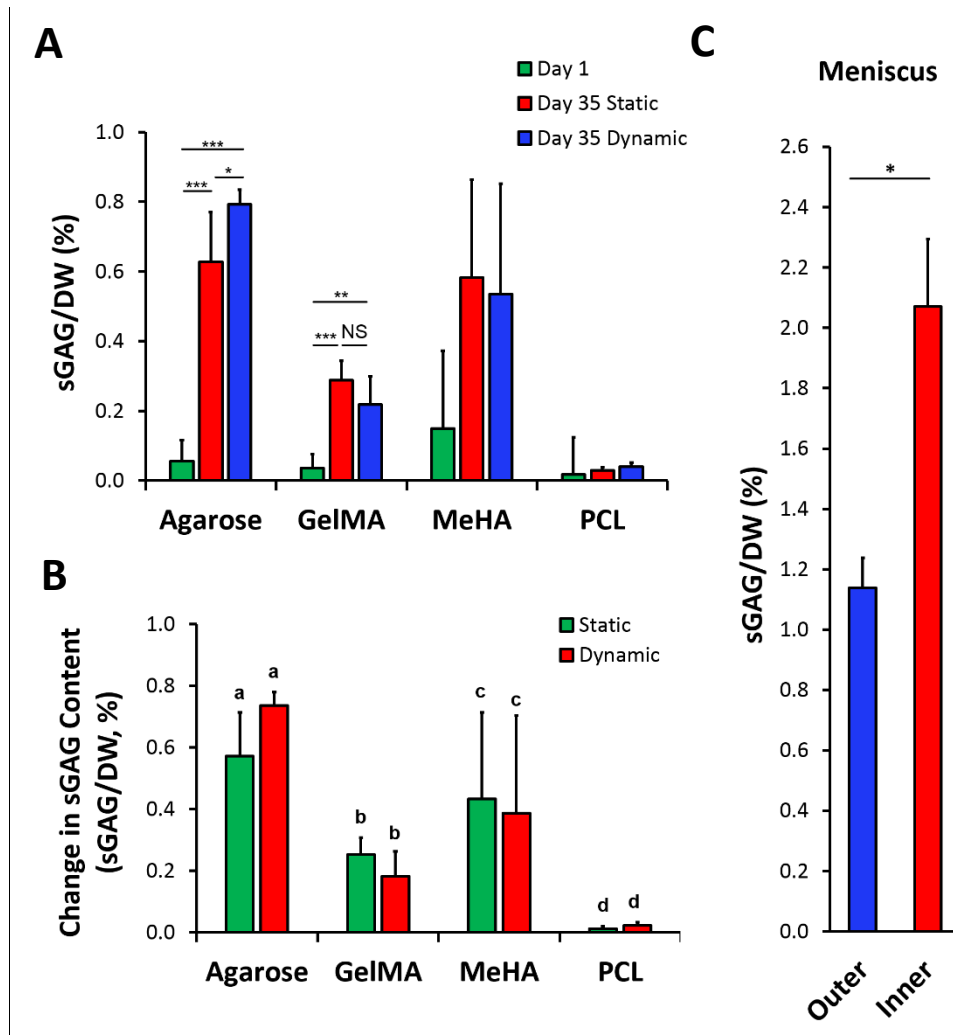


Figure 3.14. Sulfated glycosaminoglycan (sGAG) contents of the constructs and the native meniscus. (A) Dry weight-normalized sGAG contents on Days 1 ($n=3$) and 35 ($n=6$). (B) Net change in sGAG contents of the constructs between Days 1 and 35. (C) sGAG content of the native meniscus ($n=6$). Data are presented as the mean \pm SD. NS: not significant. Statistical significance: $*p<0.05$, $**p<0.01$, $***p<0.001$. ^{a,b,c,d}Significant difference when no letters in common.

For the unseeded constructs, histology revealed no or little background Safranin-O (Saf-O) staining on agarose and GelMA, but intense staining on MeHA gels (Fig. 3.15). This is probably due to the hyaluronic acid backbone of the gel material.

Upon cell seeding agarose and GelMA exhibited weak Saf-O staining, but still more intense than the unseeded controls. On the other hand, the intensity of the staining on MeHA decreased upon addition of cells. The reason for the decrease in the staining of MeHA could be the degradation of this gel in the presence of cells. Therefore, it was concluded that cells deposited GAG on agarose and GelMA, however the deposition on MeHA could not be detected.

GAG staining was low on the inner region of the native meniscus and high on the hyaline cartilage (Fig. 3.15). Considering that the GAG staining on the inner portion of the meniscus was low compared to the hyaline cartilage, the low staining on the constructs was quite expected, because porcine fibrochondrocytes do not produce GAGs as much as chondrocytes do.

3.4.1.7. Cell Morphology

The morphology of the fibrochondrocytes are shown in Figure 3.16. Histology sections revealed that the morphology of the cells differed from each other depending on the gel type (Fig. 3.16A). Cells were mainly round in agarose, MeHA, and at the center (C) of GelMA, while spread and dendritic on the surface (S) of GelMA. Cells at the inner region of the native meniscus were mainly round, while those at the outer region were mainly dendritic and/or elongated (Fig. 3.16A).

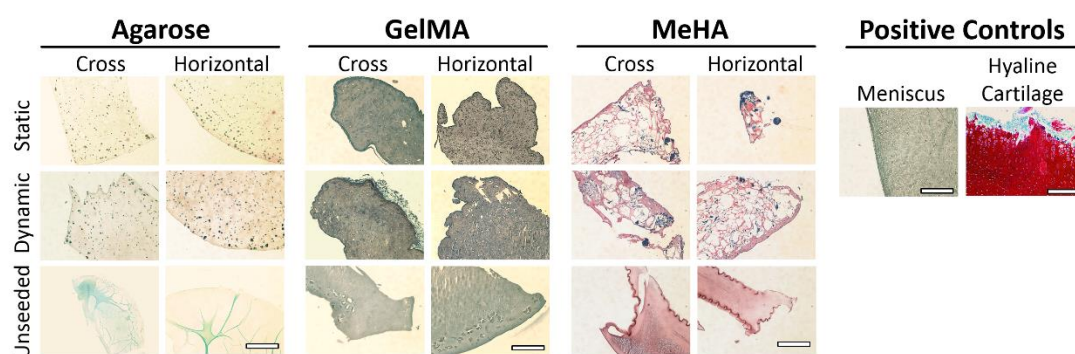


Figure 3.15. Histology showing sulfated GAG deposition on the constructs after 35 days of culture. Cross and horizontal sections were stained for GAGs. Stain: Safranin-O (red) and counterstain: Fast Green (green). Positive controls: the inner portion of the native meniscus, and the hyaline cartilage. Scale bars: 500 μ m.

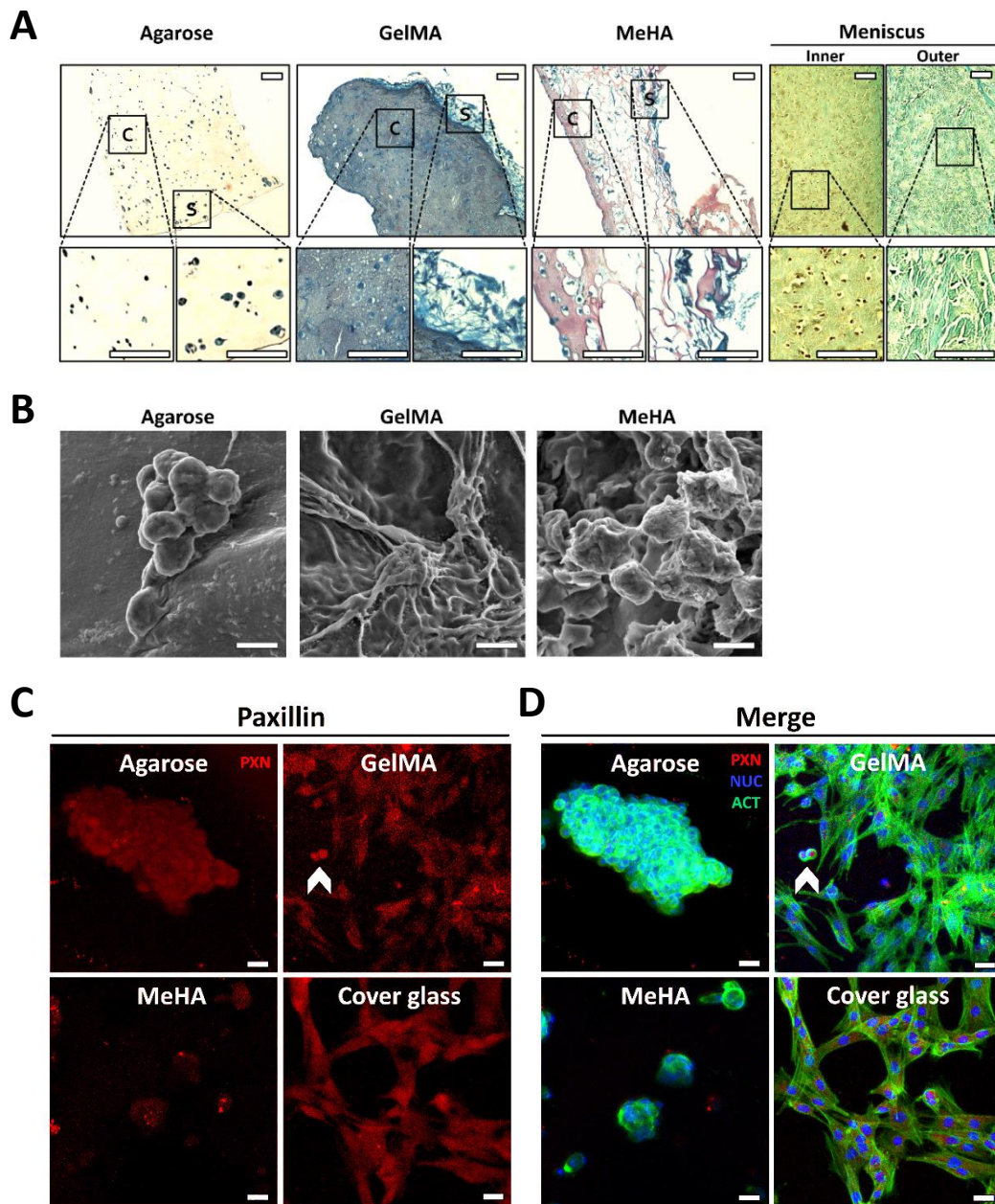


Figure 3.16. Representative images showing the cell morphologies cell adhesion on the hydrogels. (A) Bright field microscopy images of the cells in the gels (Day 35). Staining: Safranin-O (red), counterstaining: Fast Green (green). Insets: high magnifications. C: center; S: surface. Scale bars: 200 μm . (B) SEM images of cells on the surface of hydrogels (Day 21). Scale bars: 20 μm . (C, D) Cell adhesion on hydrogels after 21 days of culture. CLSM images of the gels stained for paxillin (PAXN, red), nuclei (NUC, blue), and actin (ACT, green). (C) Paxillin, and (D) merge images. Scale bars: 25 μm . Arrowheads: round cells.

SEM examination also confirmed that cells on the surface of agarose and MeHA were round and aggregated, while on the surface of GelMA they were mainly dendritic (Fig. 3.16B).

3.4.1.8. Cell-Material Interactions

Different morphologies of the cells on different gels could be a result of cell-material interactions or due to encapsulating of the cells in the gels which restricted their spreading behavior. In order to investigate the cell-material interactions on the hydrogels, constructs were stained for paxillin, a factor involved in cell adhesion signaling pathway. Paxillin staining was strong on GelMA both with the round (arrows) and with the spread cells (Fig. 3.16C), indicating strong cell adhesion on this gel. Paxillin staining on agarose and MeHA was weak, indicating weak cell adhesion on these gels. Strong paxillin was observed on the cover glass which was used as a control.

Cells on GelMA were spread with clear actin fibers, the same with the cells on the cover glass (Fig. 3.16D). On the other hand, cells on agarose and MeHA were round with no actin fibers.

Weak cell adhesion on the gels could lead to round cell morphology, whereas strong binding could lead to spread cell morphology (Ahearne, 2014). Gelatin presents biologic recognition sites and allows for cell adhesion through RGD sequences (Lui and Chan-Park, 2010), whereas agarose and MeHA (Necas *et al.*, 2008) are highly hydrophilic and lack such binding sites, which limit cell adhesion. Nevertheless, cells on agarose and MeHA were stained positive with paxillin probably due to the pericellular matrix produced by the cells, which could serve as a substrate for the cells to bind on (Steward *et al.*, 2013).

When cells are encapsulated in the hydrogels they tend to be round (Steward *et al.*, 2013). Cells in the center of agarose, MeHA, and GelMA were mainly round because their mobility and spreading was probably limited due to the stiff polymer mesh surrounding them (Lake and Barocas, 2011; Ulrich *et al.*, 2010).

The morphology of chondrocytes was shown to remain round in agarose gels even after modification of agarose with RGD or arginine-glycine-glutamic acid (RGE) sequences (Schuh *et al.*, 2012). When chondrocytes were encapsulated in soft agarose gels, they spread significantly more than the cells encapsulated in rigid gels (Karim and Hall, 2016). This shows that the rigid mesh structure of the gels restrict cell spreading. This also explains the round cell morphology in the center of GelMA in the current study, despite strong cell adhesion on this gel.

Cell morphology could influence the ECM production on the scaffolds. More GAGs were produced in agarose and MeHA, where cells were round, and more collagen was produced on the surface of GelMA where the cells were mainly spread and dendritic. This is similar to the round fibrochondrocytes in the inner region of the meniscus where the tissue is more abundant in GAGs and COL II, and the spread and dendritic cells in the outer region where COL I is more abundant (Sanchez-Adams *et al.*, 2011). When chondrocytes were forced to get a round morphology in collagen gels, the level of aggrecan, GAGs and COL II production was reported to increase (McCorry *et al.*, 2016). Nucleus pulposus cells treated with focal adhesion kinase inhibitors (FAKi) were shown to assume a round cell morphology in GelMA gels and produce more GAGs than the untreated gels (Krouwels *et al.*, 2017). These findings indicate that cell morphology could influence the level and nature of the ECM produced.

Finally, soft substrates have been reported to induce chondrogenic gene expression (Glennon-Alty *et al.*, 2013); however, this was not the case in the current study. GAG production was higher on agarose and MeHA, which were stiff, than GelMA, which was soft.

The findings in this part of the study are summarized in Figure 3.17. Hydrogels present a 3D microenvironment to the cells that induces ECM production by cells, while PCL provides a 2D microenvironment that induces cell proliferation but not ECM production. Agarose and MeHA are nonporous (or slightly porous), stiff, and non-bioactive, which result in round cell morphology and promotes the production of GAGs, while GelMA is porous, soft, and bioactive, which result in spread and

dendritic cells morphology and promotes collagen production. PCL is very stiff and results in elongated cell morphology.

In conclusion, although it is difficult to compare the DW-normalized collagen contents of the constructs due to different densities of the materials, it could be concluded that hydrogels induce meniscal ECM production more than PCL does. Among the various hydrogels tested, agarose and GelMA were chosen to be used in the following studies. Since agarose induced production of GAGs (the cartilaginous ECM component in the meniscus), it could be used to produce the inner portion of the meniscal constructs. GelMA, on the other hand, could be used in the outer region, because it induced production of collagen, the fibrous ECM component. Therefore, in the next section, the 3D printed PCL scaffolds were embedded in cell-laden agarose and GelMA to test the integrity and meniscal regeneration capacity of these composite constructs.

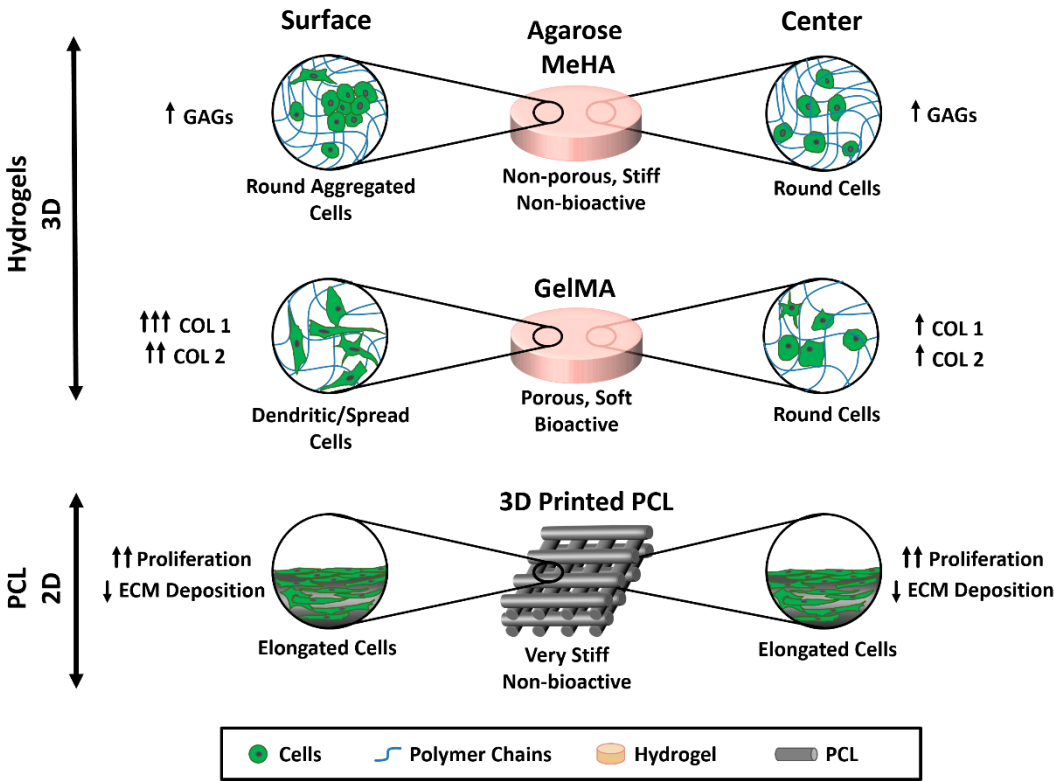


Figure 3.17. Summary of the results obtained with hydrogel-based studies.

3.4.2. Square Prism-Shaped PCL/Hydrogel Composite Constructs

After selection of the hydrogels that induce production of meniscal ECM, the 3D printed, square prism-shaped PCL scaffolds were embedded in these hydrogels (agarose and GelMA), and tested for structural integrity, mechanical properties, cell viability, and meniscal ECM production capacity.

3.4.2.1. Microscopic Evaluation

The microarchitecture of the constructs, they were studied microscopically (Fig. 3.18). Stereomicroscopy revealed that PCL was printed in well-defined shapes, with straight strands, and uniform strand thickness and pore size (top view) (Fig. 3.18A). Cross sections showed that the pores were interconnected not only in depth (at z-direction) but also laterally (at xy direction). The distance between strands was smaller at z-direction (around 150 μm) than that at xy-direction (800 μm).

Similar observations were made for PCL-Ag and PCL-GelMA (Fig. 3.18A). PCL strands were straight and the thickness was uniform. The pores were also well-defined. Agarose and GelMA filled the pores of PCL, leaving no or little space between the strands. In PCL-Ag, all the space between the strands was occupied (filled in) by agarose, while in PCL-GelMA there were some unfilled pores. The reason for this may be the low viscosity of GelMA at 37 °C, which resulted in leakage of the polymer solution through the pores of PCL before it was UV crosslinked. More GelMA polymer could be seen at the bottom of the scaffolds (cross sections) than on the top (Fig. 3.18A). Agarose, on the other hand, solidified rapidly below 40 °C after being poured on the colder PCL scaffolds, and thus filled all the pores on PCL.

SEM analysis showed that PCL was successfully embedded in agarose, with no phase separation at the boundaries (Fig. 3.18B). GelMA, on the other hand, did not stick well on the surface of PCL, which resulted in phase separation at the boundaries (cross sections).

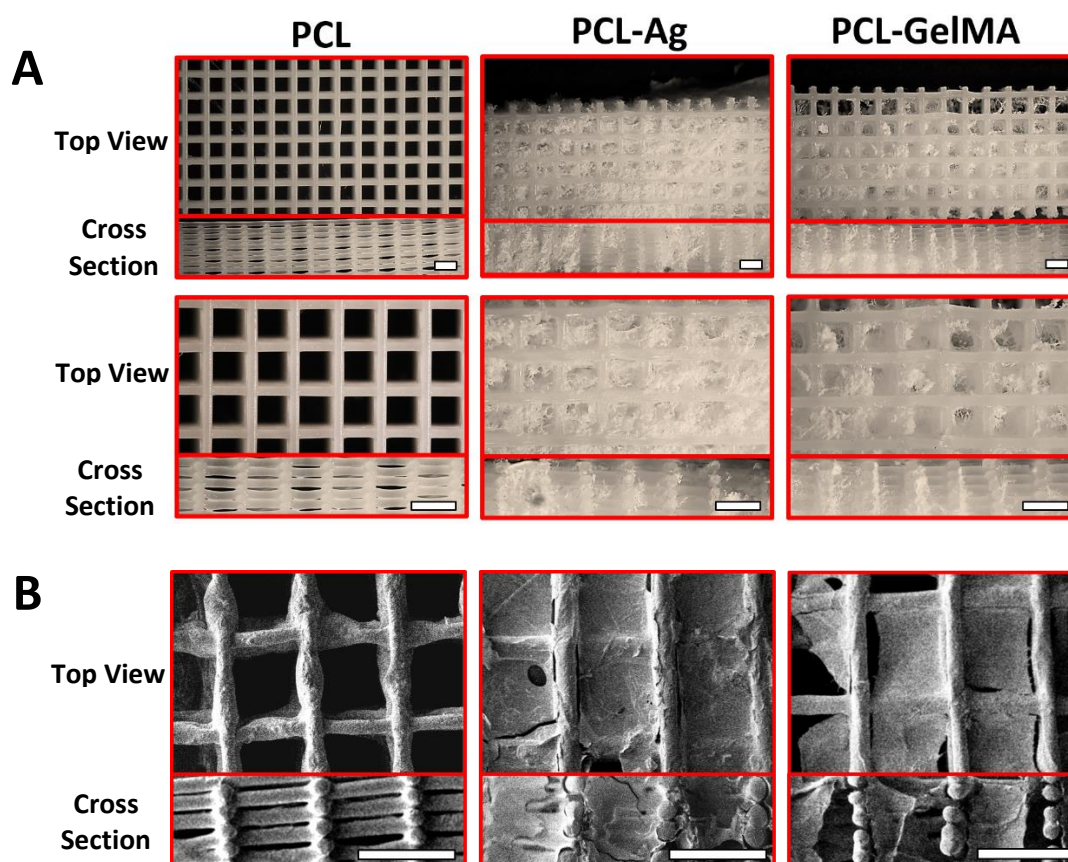


Figure 3.18. Microscopy of the dry, cell-free constructs. (A) Stereomicroscopy and (B) SEM images of the constructs viewed from the top and at the cross sections. Scale bars: 1 mm.

3.4.2.2. Mechanical Properties

Cell-free constructs were incubated in PBS for 24 h, and then exposed to compression and tension tests. Compressive moduli of all the constructs were around 10 MPa, and tensile moduli were around 30 MPa (Fig. 3.19). PCL exhibited a similar modulus to those of PCL-Ag and PCL-GelMA, which indicated that hydrogel incorporation did not contribute to the mechanical properties of the constructs. Compressive moduli of our constructs were higher than that of porcine meniscus (1-5 MPa) (Yasura *et al.*, 2007). This shows that these constructs could support the knee against the load exerted during walking and running activities. However, one

problem with the rigid scaffolds could be wear, which could result in degeneration of the underlying cartilage when the constructs are implanted in the knee.

On the other hand, tensile moduli of the constructs were lower than that of the porcine meniscus (110-140 MPa) (Abdelgaied *et al.*, 2015). The cell-free constructs proposed in the current study exhibited mechanical properties similar to or higher than most of the PCL-based constructs produced using techniques other than 3D printing. Brunger *et al.* reported an equilibrium modulus of 240 kPa with the woven PCL scaffolds after 28 days of culture (2014), which was lower than that of constructs obtained in this study. MSC-seeded electrospun PCL was reported to have a compressive modulus of 12.5 kPa and a tensile modulus of 35 MPa after 120 days of incubation (Nerurkar *et al.*, 2011), very similar tensile properties with the constructs produced in the current study, but with lower compressive properties. Han *et al.* reported an increase in the tensile modulus (from 10 MPa to 25 MPa) after seeding their electrospun PCL constructs with MCSs (2016), which were slightly lower than results the current study. Similarly, a tensile modulus as high as 35 MPa was reported in a study employing electrospun PCL, after application of cyclic tensile loading for 10 weeks (Baker *et al.*, 2011), which was similar to the unseeded constructs in this study.

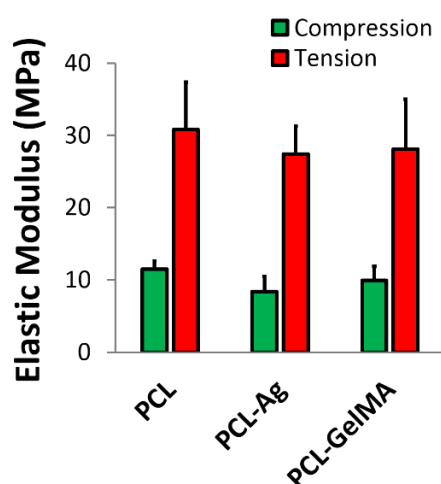


Figure 3.19. Elastic modulus of the constructs under compressive and tensile load. Data are presented as the mean \pm SD.

On the other hand, the results obtained in this study were comparable to the mechanical properties reported by other researchers using 3D printed PCL. An MSC-seeded 3D printed PCL was reported to have a compressive modulus of 2 MPa, and a tensile modulus of around 80 MPa after implantation in a sheep model for 12 weeks (Lee *et al.*, 2014). Their results were lower under compressive load than the current study, but higher under tensile load. They reported degeneration of the cartilage after implantation to the sheep model. In another study, a 3D printed PCL with two strand orientations (0-90° and 0-45-90°) were reported to have compressive modulus of 54 and 30 MPa, respectively (Cengiz *et al.*, 2016). This value is even larger than that obtained in our study, and could lead to extensive degeneration of the cartilage after implantation in the knee. A 3D printed meniscus with circumferential strand orientation was reported to have an aggregate modulus of 30 kPa, and a tensile modulus of 40 MPa after implantation into a rabbit model (Zhang *et al.*, 2017), which are much higher than our results and could lead to degeneration of the cartilage. Another construct was shown to have an equilibrium modulus of 10-30 MPa at 10% strain depending on the design of the scaffold (Szojka *et al.*, 2017), similar to the modulus of the constructs obtained in this study. Equilibrium moduli obtained in these studies were very high compared to equilibrium modulus of the porcine (100-120 kPa) (Abdelgaied *et al.*, 2015) and human menisci (100-220 kPa) (Joshi *et al.*, 1995; Sweigart *et al.*, 2004). Compressive modulus results were also much higher than the native human meniscus (0.3-2 MPa) (Chia and Hull, 2008; Fischenich *et al.*, 2017).

In the current study, mechanical properties of the cell-free constructs were reported. Tensile properties could increase considerably upon cell seeding and/or implantation in an animal model (Baker *et al.*, 2011; Han *et al.*, 2016; Zhang *et al.*, 2017). The tensile properties of the 3D printed constructs obtained in the current study could be increased by reducing the distance between the strands and/or increasing the diameter of the nozzle orifice.

3.4.2.3. Cell Viability on Constructs

PicoGreen assay was performed to monitor the change in DNA contents (and thus cell numbers) of the constructs over time. DNA content of PCL was very low on Day 1, but increased 10-folds by the end of Day 14 (Fig. 3.20A). DNA content of PCL-GelMA was significantly lower than the unembedded PCL and PCL-Ag on Day 14, but it increased significantly until the end of Day 56. Nevertheless, DNA content of PCL-GelMA was significantly lower than the other constructs at the end of 56-day culture period ($p < 0.01$). Dynamic compression led to a decrease in the DNA content of unembedded PCL ($p < 0.05$) and an increase in that of PCL-Ag ($p < 0.01$).

The low DNA content of PCL-GelMA on Day 14 could be explained with leaking of GelMA solution through the pores of PCL before the crosslinking process. This resulted in cell and material loss. However, this does not explain the lower DNA content of PCL-GelMA than the unembedded PCL constructs, since the cell-laden GelMA should have introduced more cells to the constructs. DNA contents on Day 14 were assessed immediately after gelation of GelMA and agarose. Therefore, all the cells in the constructs, whether dead or alive, contributed to the DNA content results because they were entrapped in the hydrogels. Hence, the reason for the lower DNA content of PCL-GelMA group on Day 14 compared to PCL group could not be the toxicity of GelMA. Instead, DNA on PCL strands of the PCL-GelMA constructs was probably low before it was embedded in GelMA. The variations in DNA contents of PCL in different construct groups could be the low seeding efficiency on PCL (10%) because of the large pores that lead to loss of cells during seeding process. Another reason for the low DNA content on GelMA-embedded PCL could be the lower cell viability after application of UV. Extended exposure of cell-laden hydrogels to UV (from 1 min to 5 min) was shown to reduce cell viability in collagen gels (Heo *et al.*, 2016).

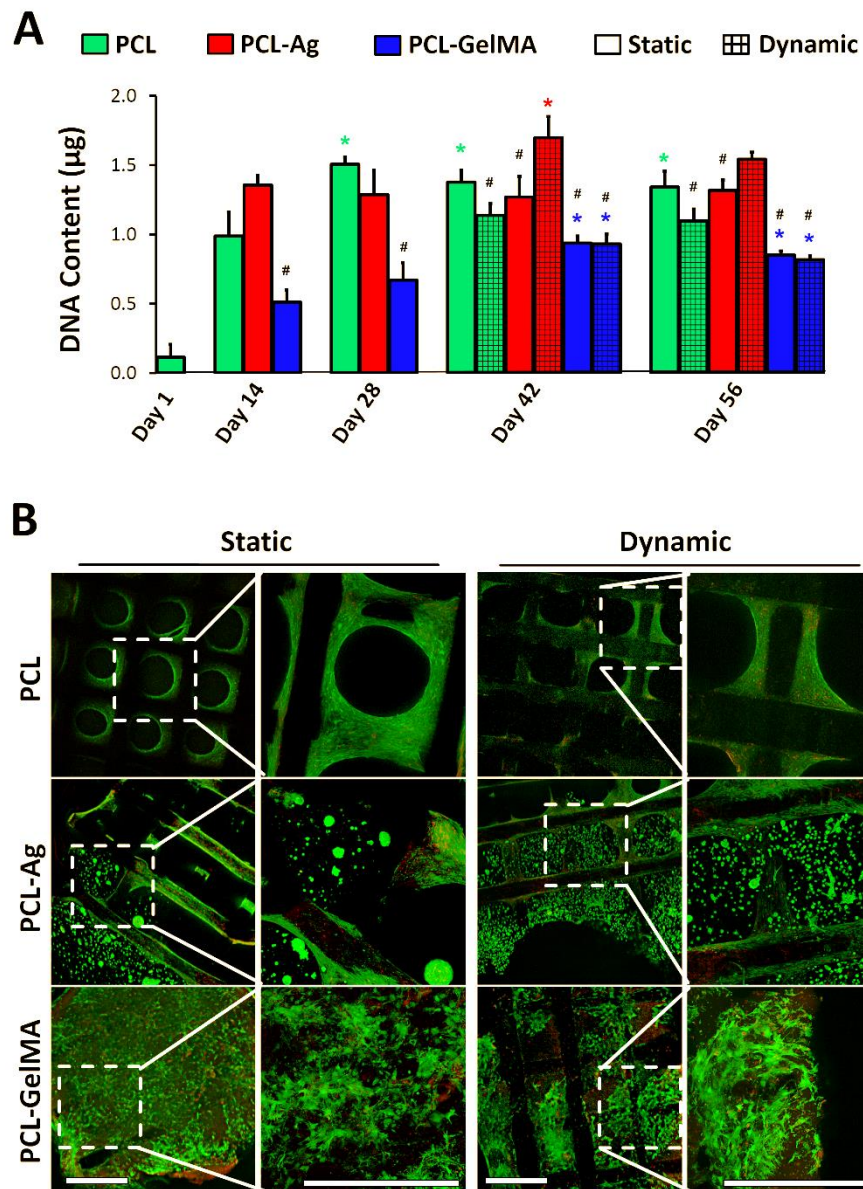


Figure 3.20. DNA contents and cell viability on the square prism shaped constructs. (A) DNA contents. Data are presented as the mean \pm SD. *Significant difference compared to Day 14 results of a particular construct. #Significant difference compared to static samples of PCL at a particular time point. (B) CLSM images of the constructs on Day 42 showing the live/dead assay results. Green: calcein-AM (live cells); red: ethidium homodimer-1 (EthD-1) (dead cells). Insets magnified further. Scale bars: 1 mm.

In order to test the viability of the cells on the constructs, live/dead assay was performed. Live/dead assay revealed high cell viability in the constructs after 42 days of culture (Fig. 3.20B). ImageJ analysis of the CLSM images revealed similar cell viability on all construct types (75-80%) (Table 3.2).

Dynamic compression slightly reduced cell viability on PCL-Ag constructs, but this difference was not significant ($p > 0.05$). One observation was that cells were elongated on PCL, round on agarose, and dendritic on GelMA (Fig. 3.20B). There was a low number of cells (and a high proportion of the cells were dead) on the strands of the PCL-GelMA constructs, supporting the DNA content results on Day 14 (Fig. 3.20B).

Others also reported around 80% cell viability on FDM printed (Daly *et al.*, 2016) or melt electrospun PCL (Visser *et al.*, 2015), which are in parallel with the results obtained in the current study.

Dynamic compression was also reported to decrease cell viability or DNA content, when a strain of 10% (Huey and Athanasiou, 2011) or 15% (Ballyns and Bonassar, 2011) was applied.

Table 3.2. Porcine fibrochondrocyte viability on square prism-shaped, PCL-based constructs on Day 42 as determined with live/dead assay.

<i>Constructs</i>	<i>Viability (%)</i>	
	Static	Dynamic
PCL	78 ± 7	78 ± 5
PCL-Ag	82 ± 3	75 ± 7
PCL-GelMA	75 ± 2	74 ± 2

3.4.2.4. GAG Contents

One of the most important components of meniscus are the GAGs, which are found abundantly in the inner cartilaginous portion (2-4% of the dry weight in the inner region compared to 0.9% in the outer region) (Sanchez-Adams *et al.*, 2011). It is essential that the engineered tissue contain a considerable amount of GAGs.

DMMB assay results are presented in Figure 3.21A. Sulfated GAG content of PCL was very low on Day 1, and it increased significantly in 14 days ($p < 0.05$). After Day 14, however, PCL constructs did not exhibit a significant increase in GAG content (Fig. 3.21A).

PCL-Ag exhibited the highest GAG content throughout the culture period (Fig. 3.21). GAG content of PCL-Ag increased significantly over time (about 3-fold increase in 4 weeks, $p < 0.01$), but decreased slightly after Day 42.

GAG content of PCL-GelMA on Day 14 was significantly lower than the other constructs (Fig. 3.21), probably due to the low cell number on these constructs (Section 3.4.2.3, Fig. 3.20). However, it increased significantly over time (4-fold) and exceeded the GAG content of PCL by Day 56 (Fig. 3.21).

Dynamic compression led to a reduced GAG contents of the constructs in the first two weeks of application (Days 28 to 42), but then GAG contents increased to the same level with the constructs incubated under static conditions by Day 56. The reason for this could be that when dynamic compression was applied, the GAGs in the constructs were pumped out or released to the culture media. The GAGs in the constructs, therefore, was lower than the static samples which did not lose its GAGs. In fact, it was reported that GAGs were lost to the culture media after 4 weeks of dynamic compression (Ballyns and Bonassar, 2011).

In brief, the highest GAG content was obtained with PCL-Ag and dynamic compression had no effect on the GAG contents after 4 weeks of application. These findings were consistent with the previous results in which the highest GAG production was observed on Agarose gels (Section 3.4.1.6, Fig. 3.14).

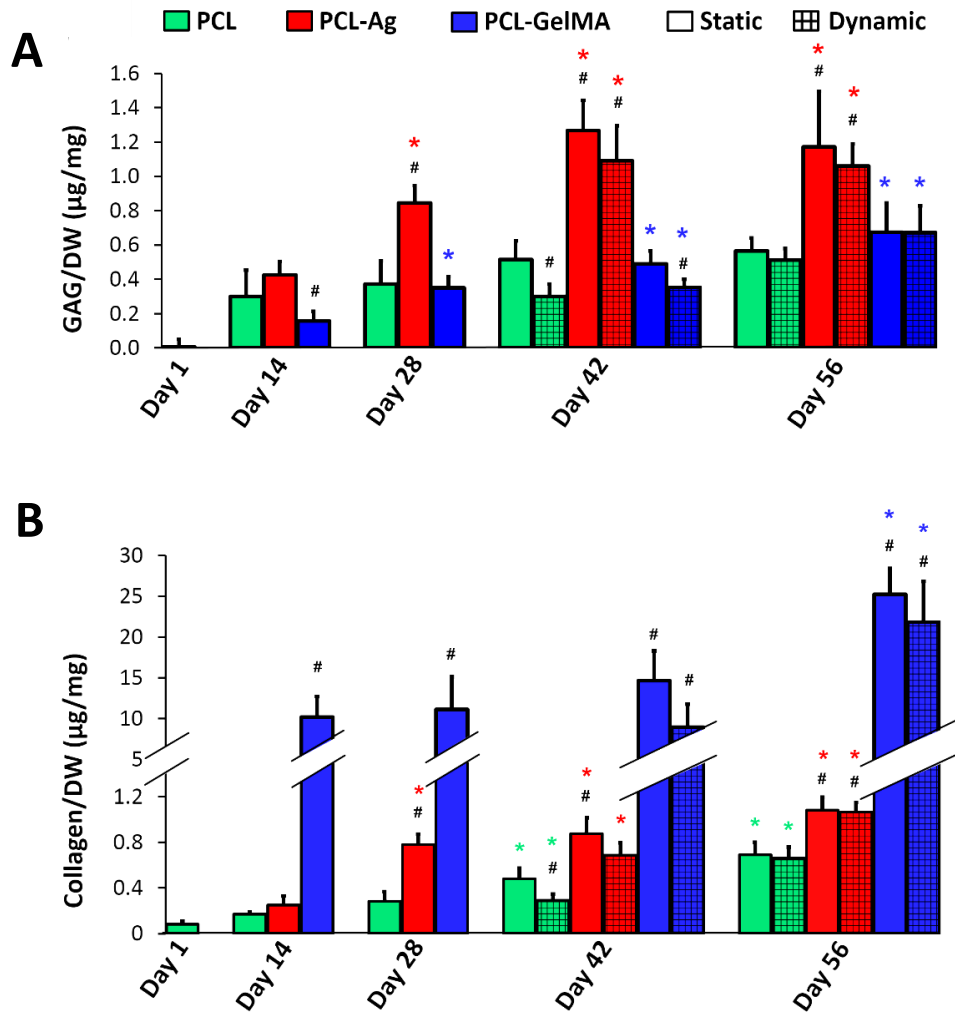


Figure 3.21. The sulfated GAG and collagen contents of the square prism shaped constructs. Dry weight-normalized (A) sGAG contents and (B) collagen contents of the constructs. *Significant difference compared to Day 14 results of a particular construct. #Significant difference compared to static samples of PCL at a particular time point.

These results are in parallel with the results reported in previous sections (Section 3.4.1.6, Fig. 14), and with the results reported by Daly and colleagues who obtained higher production of GAGs in agarose gels than GelMA (2016). Visser *et al.* reported a similar GAG content in chondrocyte-seeded PCL-GelMA (2015) with those obtained in PCL-GelMA constructs in this study, but lower than the results obtained with the PCL-Ag constructs. The results obtained in the current study were

similar to those reported by Lee *et al.* who used MSC-seeded, 3D printed PCL treated with CTGF followed by TGF- β 3 (2014, suppl.), but lower than the results of Baker *et al.* who used electrospun PCL (2011). Baker *et al.*, reported a decrease when the culture time was extended to 10 weeks (2011).

3.4.2.5. Collagen Contents

Orthohydroxyproline (OHP) assay revealed that collagen contents of all construct types increased significantly over time, and the net increase was the highest on PCL-GelMA (Fig. 3.21B).

Dynamic compression had no effect on the collagen contents of the constructs at the end of 56 days of culture period.

Collagen content of PCL was very low on Day 1, but increased gradually over time (Fig. 3.21 B). Collagen contents on Days 42 (0.3 μ g collagen/mg DW) and 56 (0.6 μ g collagen/mg DW) were significantly higher than that on Day 14 (0.1 μ g collagen/mg DW). The same trend was observed for PCL-Ag constructs, but with higher collagen production than PCL (0.2 and 1.1 μ g collagen/mg DW on Days 14 and 56, respectively).

Collagen content of PCL-GelMA was very high on Day 14 (10 μ g collagen/mg DW), due to gelatin (Fig. 3.21 B). Therefore, although there was an increase in the collagen content between Days 14 and 42, this increase could not be observed clearly. However, collagen content increased steeply after Day 42, reaching to significantly higher level on Day 56 (26 μ g collagen/mg DW) than on the earlier time points ($p < 0.05$).

Dynamic load seemed to have a negative effect on collagen production during the first 2 weeks of application (Day 42) (Fig. 3.21 B). After 4 weeks of dynamic culture, however, collagen contents increased significantly, reaching to levels equal to those in static constructs. These results showed that the constructs were stable under mechanical loading, but dynamic compression did not improve the ECM production by cells. Load-applied samples produced lower amounts of collagen on

Day 42, probably due to loss of the newly produced collagen to the culture media as a result of the dynamic load applied.

Similar to the previous sections (Section 3.4.1.5, Figs. 3.12 and 3.13), the net collagen production in PCL-GelMA over 56 days of incubation (1.6% of DW or 0.5% of WW or 300 μg collagen/ μg DNA) was significantly higher than those of unembedded PCL (around 0.05% of DW) ($p < 0.01$) and PCL-Ag (around 0.08% of DW) ($p < 0.01$), which all were lower than collagen content of the native meniscus (80-90%) (Sanchez-Adams *et al.*, 2013). The high collagen production in GelMA was probably resulted from the biologic recognition sites on gelatin (Liu and Chan-Park, 2010), which enhanced cell adhesion and probably ECM production. Higher collagen production in GelMA compared to agarose was also reported by Daly *et al.* (2016). Others also reported high collagen production on GelMA gels (Visser *et al.*, 2015), and low production on agarose (Wilson *et al.*, 2009).

In brief, the highest collagen content was obtained with PCL-GelMA constructs, and dynamic compression at 5-15% strain did not have a significant effect on collagen production.

The PCL-GelMA constructs proposed in the current study (300 μg collagen/ μg DNA) exhibited an order of magnitude higher collagen production than the results reported by Lee *et al.* after treatment of MSCs with CTGF followed by TGF- β 3 (20 μg collagen/ μg DNA) (2014, suppl.), and also two times higher than results reported by Baker *et al.* on electrospun PCL after 10 weeks of incubation in dynamic culture (120 μg collagen/ μg DNA) (2011).

3.4.2.6. Immunofluorescence

The biochemical assays were unable to distinguish type I collagen (COL I) from type II (COL II). In order to assess COL I and COL II production, immunofluorescence was performed (Figs. 3.22-3.24).

On the PCL constructs a considerable amount of COL I was deposited both on Day 42 (Fig. 3.22A) and Day 56 (Fig. 3.22B). COL I was deposited as long, continuous and aligned fibers on the PCL strands (high magnification images). On the other

hand, COL II staining was weaker than COL I, and was not deposited as long and continuous fibers. Dynamic compression seemed not to have any effect on collagen deposition.

Collagen staining of PCL-Ag was similar to that of PCL, with additional collagen staining in agarose portion (Fig. 3.23). On Day 42, COL I staining was intense especially on the PCL portion of the constructs (Fig. 3.23A). COL II staining was nearly as intense as COL I, which indicated the contribution of agarose on production of the cartilaginous ECM components. COL II deposition seemed to increase with the dynamic compression.

On Day 56, both COL I and COL II deposition on the agarose portion of the constructs seemed to increase, and dynamic compression further enhanced collagen staining (Fig. 3.23B). Long and continuous collagen fibers (both COL I and COL II) were deposited on the PCL portion of the constructs, while globular and discontinuous collagen was on the agarose portion.

The reason for the different forms of the collagen produced on different parts of the constructs could be the cell morphology on the materials, which defined the pericellular matrix produced by the cells. Cells were elongated and aligned on PCL, whereas round in agarose (Fig. 3.20B), and therefore, they produced aligned collagen fibers on the PCL portion and globules of collagen in the agarose.

High deposition of collagen was observed on PCL-GelMA (Fig. 3.24). On Day 42, intense COL I and COL II staining was detected on the constructs, but the intensity of staining was higher on the dynamic samples than on the static samples (Fig. 3.24A). Dynamic compression seemed to enhance the expression of especially COL II. Collagen staining on Day 42, was similar to that of the PCL-Ag. The collagen deposited on the GelMA portion was globular, probably because cells were still round within the gels.

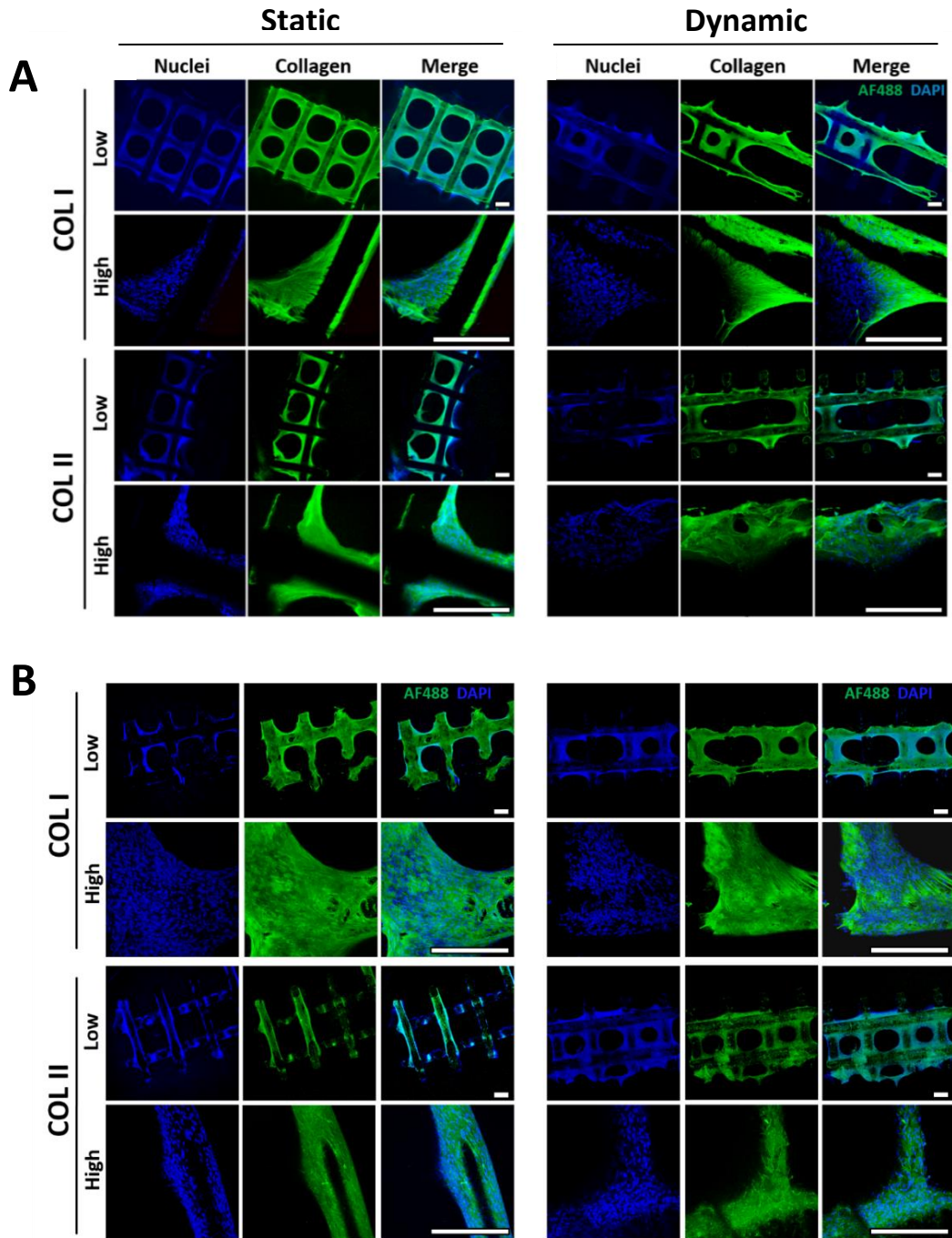


Figure 3.22. Immunofluorescence of the PCL constructs. Incubation time: (A) 42 and (B) 56 days. CLSM images of the samples incubated under static (left), and dynamic (right) conditions. Samples were stained for type I (COL I) and type II collagen (COL II) and visualized at low and high magnifications. Blue: DAPI (for nuclei), Green: Alexa fluor 488 (for collagen). Scale bars: 200 μ m.

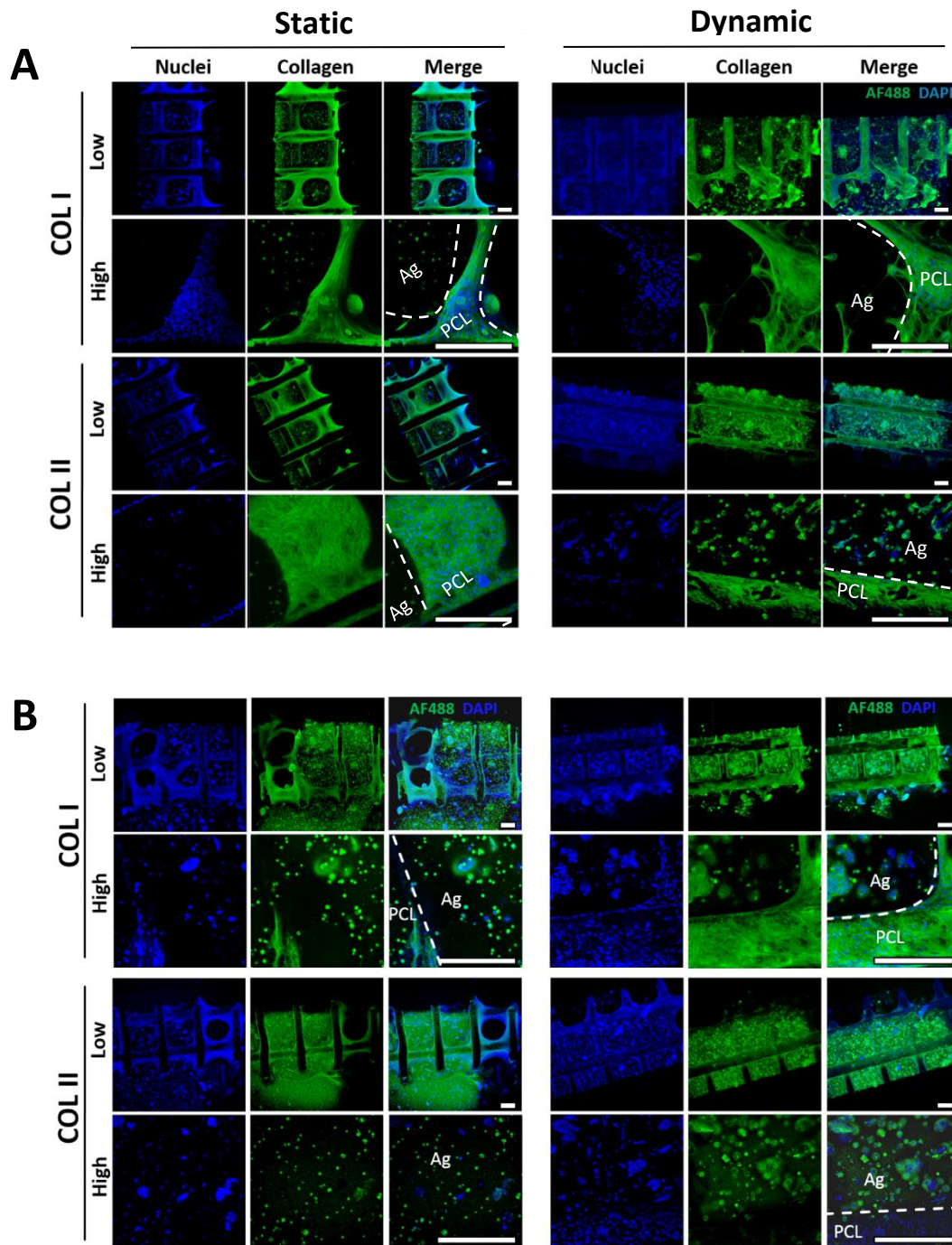


Figure 3.23. Immunofluorescence of the PCL-Ag constructs. Incubation time: (A) 42 and (B) 56 days. CLSM images of the samples incubated under static (left), and dynamic (right) conditions. Samples were stained for type I (COL I) and type II collagen (COL II) and visualized at low and high magnifications. Blue: DAPI (for nuclei), Green: Alexa fluor 488 (for collagen). Scale bars: 200 μm .

On the other hand, collagen staining of PCL-GelMA was very intense on Day 56 (Fig. 3.24B). Collagen seemed to diffuse throughout the gels, unlike the individual globules on Day 42. COL I seemed to dangle from the edges of the constructs, probably because of the high production of collagen especially on the surface of the constructs (low magnification images). COL I fibers seemed to form a network (high magnification images), which would probably increase the mechanical properties of the constructs. This network of collagen was probably resulted from the dendritic morphology of the cells (Fig. 3.20B). COL II was also highly deposited on PCL-GelMA constructs, but to a lesser extent than COL I.

In summary, although the hydrogels increased collagen production, PCL was crucial for the alignment of the collagen bundles. Collagen was globular on agarose, and fibrous on PCL and GelMA. Dynamic compression enhanced COL II production in hydrogel-embedded constructs.

The results presented in the current study are similar to the previous results reported by others. Daly *et al.* reported higher deposition COL I than COL II on GelMA gels, while higher deposition of COL II than COL I on agarose gels (2016). However, they reported higher COL I and lower COL II on GelMA than agarose. Lee *et al.* reported low deposition of COL I and II on the 3D printed PCL scaffolds, and COL I deposition was increased by treatment of the constructs with CTGF, while COL II deposition was increased by treatment with TGF- β (2014). Baek *et al.* reported high deposition of COL I on the electrospun PCL, and showed that GAG deposition increased with the addition of alginate (a non-bioactive gel resembling agarose) (2015). Similarly, high COL I deposition was reported on fibrochondrocyte-seeded domains of the electrospun PCL, and high COL II on the MSC-seeded domains (Han *et al.*, 2016). In contrary to these results Zhang *et al.* reported higher COL II deposition than COL I on the 3D printed PCL scaffolds implanted in a rabbit model (2017). All these results show that the PCL/hydrogels constructs suggested in this study were stable and have potential for meniscal regeneration. Agarose could be useful in stimulating the regeneration of the cartilaginous inner portion of the meniscus, and GelMA in stimulating the fibrous outer portion.

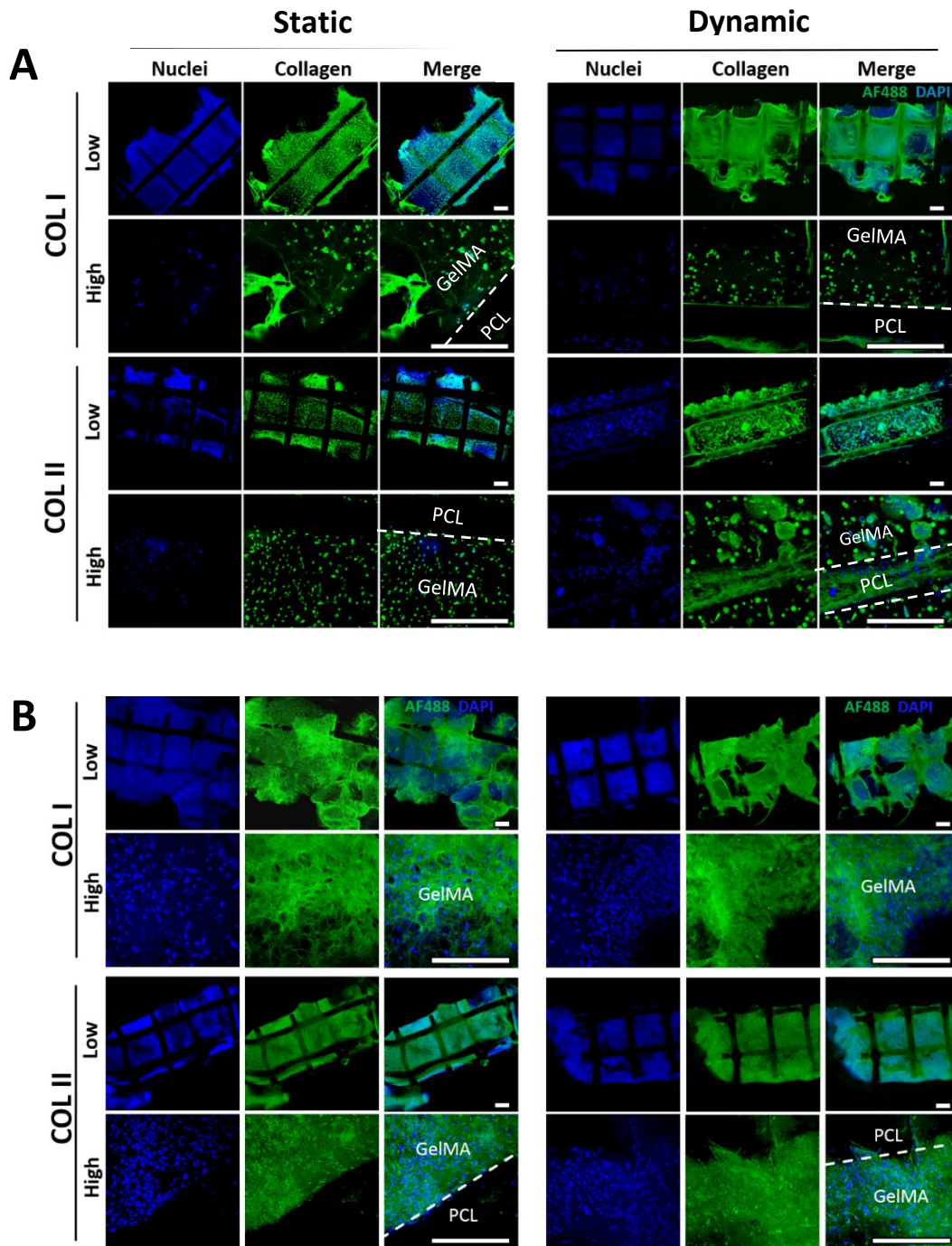


Figure 3.24. Immunofluorescence of the PCL-GelMA constructs. Incubation time: (A) 42 and (B) 56 days. CLSM images of the samples incubated under static (left), and dynamic (right) conditions. Samples were stained for type I (COL I) and type II collagen (COL II) and visualized at low and high magnifications. Blue: DAPI (for nuclei), Green: Alexafluor 488 (for collagen). Scale bars: 200 μm .

3.4.3. Meniscus-Shaped PCL/Hydrogel Composite Constructs

The composite constructs were produced by embedding the meniscus shaped PCL scaffolds in agarose and GelMA. Agarose was shown, in the previous sections, to induce the cartilaginous ECM component GAG, and GelMA was shown to induce the fibrous ECM components COL I and COL II. Therefore, in this section, the inner portion of the PCL scaffolds were embedded in agarose, and the outer portion in GelMA, to mimic the organization of the native meniscus (PCL-Ag-GelMA constructs). A set of the constructs were not embedded in a hydrogel at the outer portion (PCL-Ag constructs). At the end of 56-day culture period, the constructs were sectioned circumferentially to separate the inner and outer portions, which were then analyzed separately.

3.4.3.1. Microscopic Evaluation

PCL was printed in coliseum shapes at 0-90° strand orientation (upper panel), and cut into two halves to obtain the final meniscus-shaped scaffold (lower panel) (Fig. 3.25A). The scaffolds were printed as planned, with almost no apparent defects. The edges of the scaffolds were smooth with defined borders.

SEM examination revealed straight and smooth PCL strands (bottom and cross sectional views), with a regular pore structure (Fig. 3.25B). The pore dimensions were around 800 μm at xy-direction (dashed squares), and around 150 μm at z-direction. The pores on the top of the scaffolds seemed irregular, but this was due to the top surface which was inclined (arrows) (Fig. 3.25).

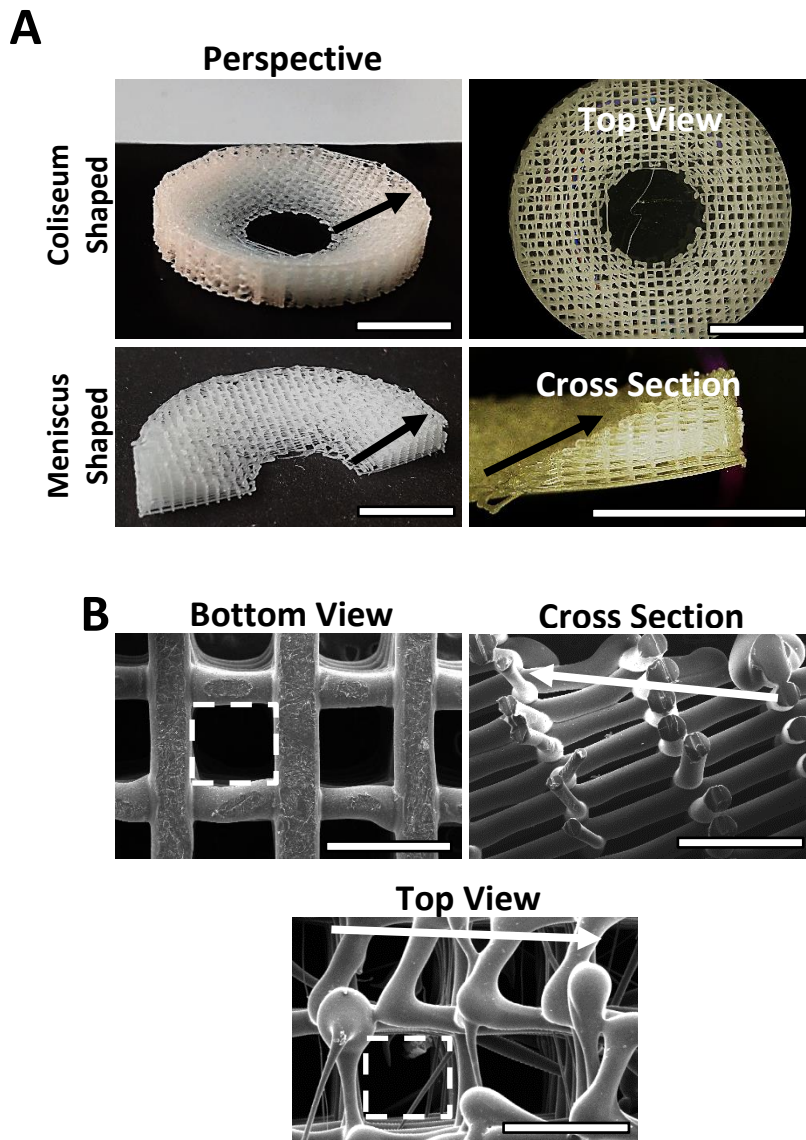


Figure 3.25. The meniscus-shaped PCL scaffold and its microarchitecture. (A) PCL was printed in coliseum shapes (upper panel), and then cut into two halves to produce the final meniscus-shaped scaffold (lower panel). Scale bars: 10 mm. (B) SEM images. Arrows show the inclined top surface (from inner region of the construct to outer-top region). Dashed squares show the pores. Scale bars: 1 mm.

3.4.3.2. Cell Viability

DNA contents of the PCL-based constructs on Day 56 are presented in Figure 3.26A. The inner regions of both constructs were embedded in agarose, while the outer regions were unembedded (PCL-Ag) or embedded in GelMA (PCL-Ag-GelMA). PCL-Ag exhibited a higher DNA content than PCL-Ag-GelMA both in the inner ($p<0.05$) and in the outer regions ($p<0.05$).

The reason for the higher DNA content on PCL-Ag could be the higher cell proliferation rate on the unembedded PCL than on the GelMA-embedded scaffold. Cell proliferation rate was very high on PCL, probably due to its high stiffness and large pores that allow oxygen and nutrient transport. Hydrogels on the other hand, limit cell proliferation because they entrap the cells and obscure the transport of oxygen and nutrients to the center of the constructs. When hydrogels were present, transport of oxygen and nutrients to cells was limited. Another reason for the low DNA content in PCL-Ag-GelMA could be the incomplete crosslinking of GelMA because of the irregular structure of the constructs (Section 3.4.3.1, Fig. 3.25, top view), which restricted the penetration of the UV light into the scaffold center. Still, other reasons could be the harmful effects of UV, the photoinitiator, and the crosslinker in GelMA on cells. DNA content was higher in the outer regions than in the inner regions ($p<0.01$), simply because larger samples were taken from the outer regions than those from the inner regions (Section 2.2.2.3.2.2, Fig. 2.10A).

Dynamic compression lowered the DNA contents in the inner regions of the constructs ($p<0.05$ for PCL-Ag) (Fig. 3.26A). This may be because of the decreased height of the constructs towards the inner region, which resulted in a higher compressive load (up to 15% strain in the inner region compared to 3% in the outer region). Besides, the compressive load was calculated based on the initial thickness of the PCL scaffolds, and thickness probably increased after embedding the constructs in the hydrogels. Thus, the actual strain was probably higher than 15% in the inner regions of the constructs. Dynamic compression at higher than 15% strain could be detrimental to cells especially in GelMA hydrogels and PCL, as shown in the previous sections (Section 3.4.1.4, Fig. 3.9; and Section 3.4.2.3, Fig. 3.20A).

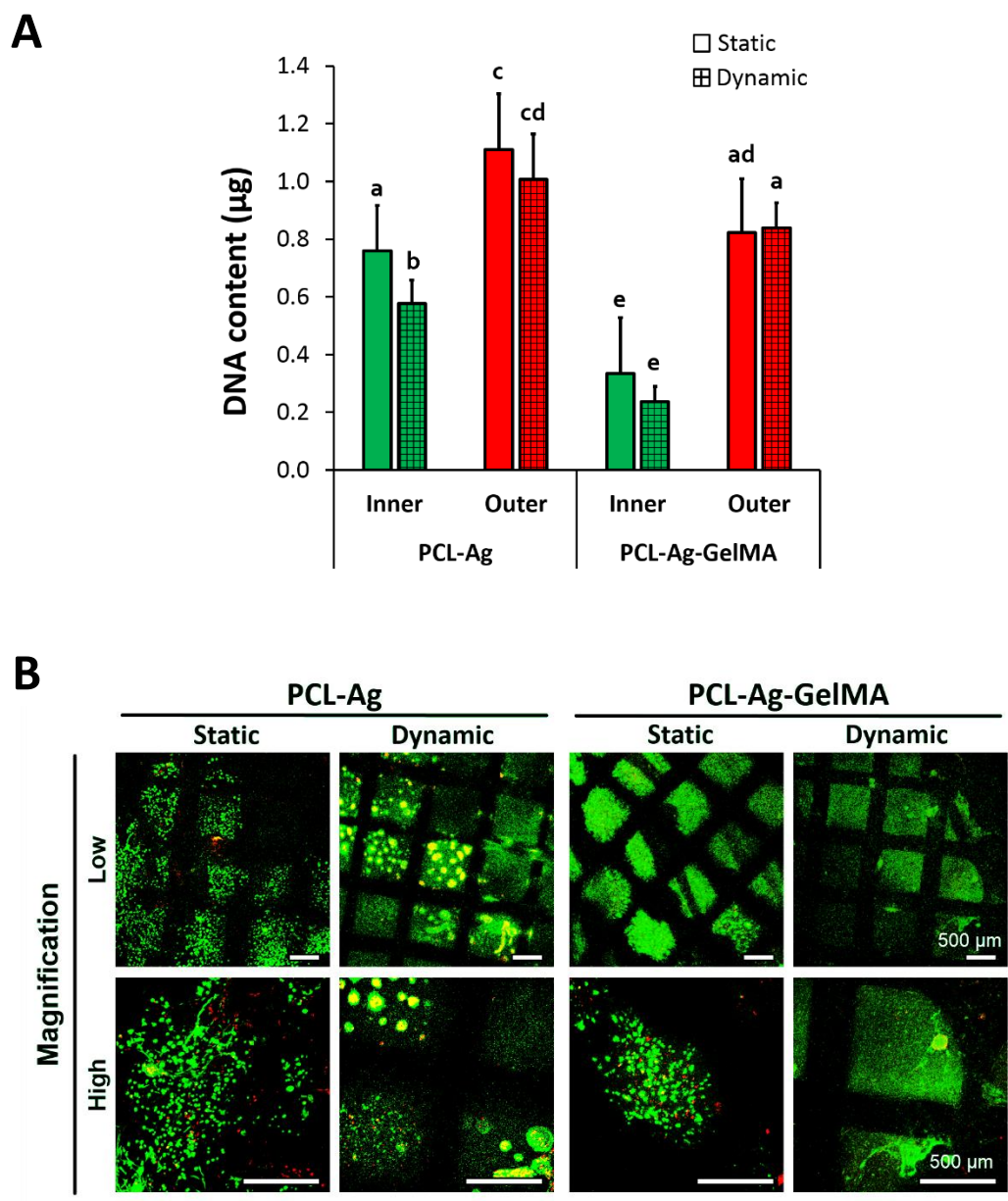


Figure 3.26. Cell viability on the constructs after 56 days of culture period. (A) DNA contents as determined with PicoGreen assay. Data are presented as the mean \pm SD. Significant difference between the results when no letter in common. (B) Live/dead assay results. Green: calcein-AM (live cells), red: ethidium homodimer-1 (EthD-1) (dead cells). Scale bars: 500 μ m.

Live-dead assay revealed high cell viability in the constructs (Fig. 3.26B). ImageJ analysis showed that cell viability was around 70% in both construct types. Dynamic compression slightly decreased cell viability in GelMA (from 73% to 66%), but this decrease was not significant. The slightly lower cell viability on PCL-Ag-GelMA constructs could be because cells proliferated rapidly on GelMA and covered the surface, limiting the access of oxygen and nutrients for the cells in the center of the scaffolds. Exposure of these constructs to UV could also result in cell death on GelMA-containing constructs.

Others also reported cell viability in the range of 70-90% after bioprinting of hydrogels (Hölzl *et al.*, 2016; Daly *et al.*, 2016; Rhee *et al.*, 2016), and around 80% on FDM printed (Daly *et al.*, 2016) or melt electrospun PCL (Visser *et al.*, 2015). Cell viability was shown to decrease after introduction of PCL to agarose (from 90% to 80%) and to GelMA (from 82% to 78%) (Daly *et al.*, 2016). Dynamic compression was also reported to decrease cell viability or DNA content, when a strain of 10% (Huey and Athanasiou, 2011) or 15% (Ballyns and Bonassar, 2011) was applied. These results support the findings of the current study.

3.4.3.3. GAG Contents

Sulfated GAG contents of the constructs as determined with the DMMB assay are presented in Figure 3.27. In the absence of the cells, GAG contents were negligible, indicating no background signal from the materials. The total GAG content of PCL-Ag (GAG amount in the inner and outer regions) was higher than that of PCL-Ag-GelMA. The highest level of GAGs was obtained at the inner region of PCL-Ag (1.1 μg GAG/mg DW or 0.11% of the DW). The lowest GAG content was observed in the dynamic samples of the outer region of PCL-Ag (0.1 μg GAG/mg DW or 0.01% of DW), where PCL was not embedded in a hydrogel. GAG content in the inner region of PCL-Ag-GelMA was lower than that in the inner region of PCL-Ag, although they were both embedded in agarose. The reason for this difference could be the significantly lower cell number (DNA) in the inner region of PCL-Ag-GelMA compared to PCL-Ag, probably due to the harmful effect of UV light applied during preparation of GelMA gels on cells. Presence of GelMA in the outer portion of PCL-

Ag-GelMA could also have a negative effect on the DMMB reading, since GelMA could lower the signal obtained from DMMB dye (Zheng and Levenston, 2015).

Dynamic compression significantly lowered the GAG content of PCL-Ag ($p < 0.01$) both in the inner region and in the outer periphery, while it slightly lowered GAG content of PCL-Ag-GelMA constructs (Fig. 3.27). The reason for the negative effect of dynamic compression on GAG contents may be the increased construct thickness after embedding in gels, which resulted in a higher actual load (higher than 15% target strain) applied on the PCL-Ag. This, in turn, could induce catabolic genes (MMPs) and result in degradation of the constructs. Dynamic compression on meniscal explants was reported to induce ECM production when applied at 10% strain, while it resulted in breakdown of the ECM components when applied at 20% (Zielinska *et al.*, 2011). However, this was not true for PCL-Ag-GelMA; the difference between GAG contents of the static and dynamic groups was not significant.

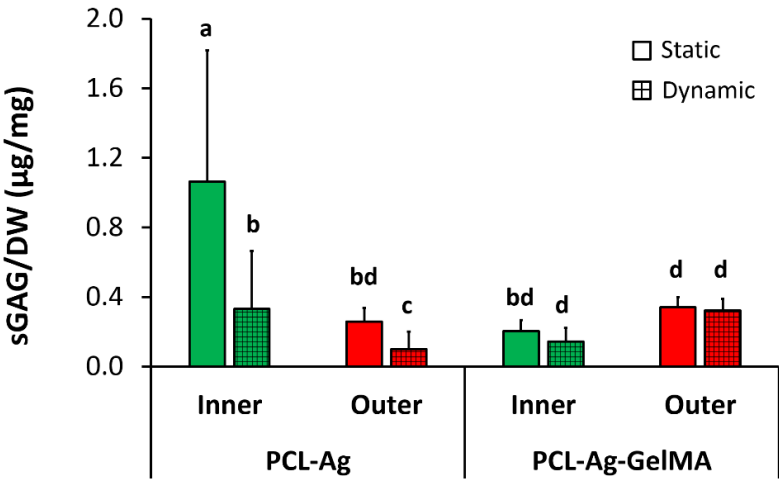


Figure 3.27. Sulfated GAG contents of the cell-seeded constructs after 56 days of culture period. Data are presented as the mean \pm SD. Significant difference between the results when no letters in common.

These results are in consistence with the results presented in the previous sections in that cells produced higher GAG in agarose than GelMA (Sections 3.4.1.6 and 3.4.2.4, Figs. 3.14 and 3.21). Similar results were reported by others (Daly *et al.*, 2016).

The inner portion of the static samples of PCL-Ag constructs proposed in the current study exhibited GAG results (55 $\mu\text{g GAG}/\mu\text{g DNA}$) higher than the results reported by Lee *et al.* (13 $\mu\text{g GAG}/\mu\text{g DNA}$) after treatment of MSCs with CTGF followed by TGF- β 3 (2014, suppl.), and comparable with the results of Baker *et al.* who reported a GAG content of 60 $\mu\text{g GAG}/\mu\text{g DNA}$ on electrospun PCL after 6 weeks of incubation (2011). Baker *et al.*, reported a decrease when the culture time was extended to 10 weeks (2011), which explains the slightly lower results obtained on constructs in the current study, which were incubated for 8 weeks.

3.4.3.4. Collagen Contents

Collagen contents of PCL-Ag and PCL-Ag-GelMA as determined with the OHP assay are presented in Fig. 3.28. Collagen content of PCL-Ag constructs in the agarose-embedded inner region was significantly higher than that in the unembedded outer region ($p < 0.01$), regardless of whether dynamic load was applied (Fig. 3.28A). This result shows that embedding PCL in agarose enhances collagen production. The collagen contents of the seeded constructs were higher than the unseeded controls both in the inner and outer regions ($p < 0.01$). Dynamic compression (applied at 5-15% strain) slightly reduced the collagen content of the constructs in the inner regions, but this decrease was not significant.

Collagen production in the outer regions of PCL-Ag-GelMA constructs was significantly higher than that produced in the inner regions ($p < 0.05$) (Fig. 3.28B). Constructs incubated under dynamic conditions exhibited higher levels of collagen than those incubated under static conditions ($p > 0.05$) or the unseeded samples ($p < 0.05$) (Fig. 3.28B). The total collagen contents of the constructs incubated under dynamic and static conditions were around 8.1 and 5.3 $\mu\text{g collagen}/\text{mg DW}$, respectively. The total collagen content in the unseeded controls was 4.7 $\mu\text{g collagen}/\text{mg DW}$.

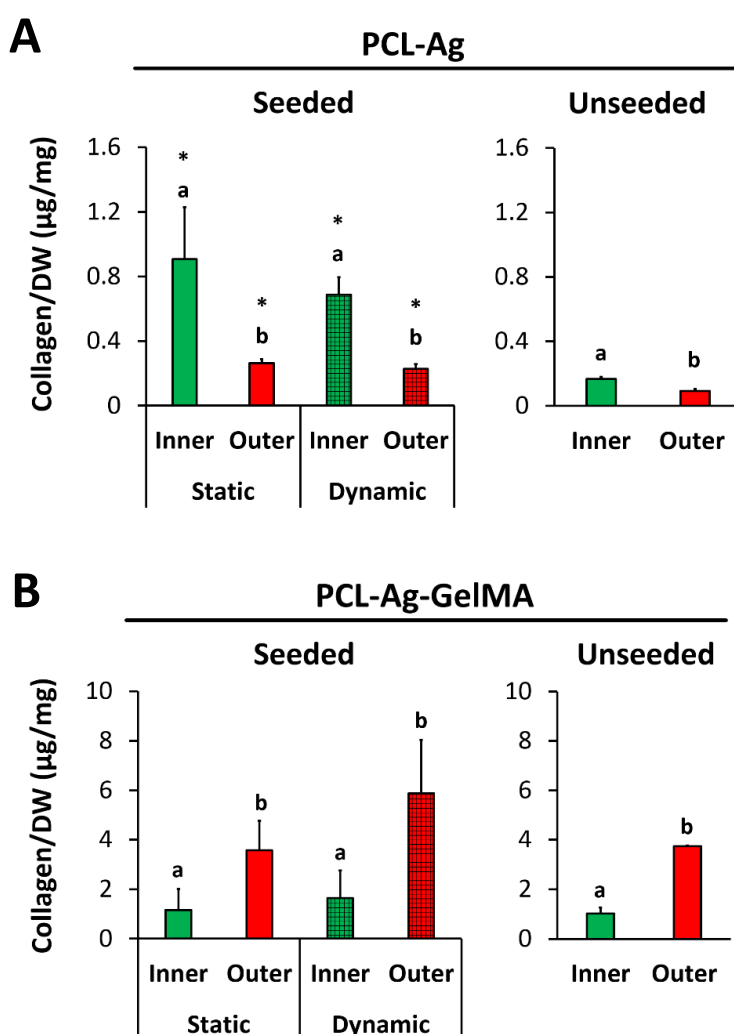


Figure 3.28. Collagen contents of the PCL-based constructs after 56 days incubation in culture media. Collagen contents of (A) PCL-Ag, and (B) PCL-Ag-GelMA. Left: seeded, right: unseeded samples. Data are presented as the mean \pm SD. Significant difference between the results when no letters in common. *Significant difference between seeded and unseeded samples.

Similar to the previous sections (Sections 3.4.1.5 and 3.4.2.5, Figs. 3.12, 3.13, and 3.21B), PCL-Ag-GelMA exhibited higher collagen production than PCL-Ag ($p < 0.01$), which exhibited higher production than the unembedded PCL ($p < 0.01$). These results showed that the presence of agarose and GelMA resulted in increased

collagen production on PCL scaffolds. Dynamic compression decreased the collagen production especially in the inner region of PCL-Ag ($p>0.05$), while it increased the production especially in the outer region of PCL-Ag-GelMA ($p>0.05$).

The outer portion of the PCL-Ag-GelMA constructs proposed in the current study ($3.4 \mu\text{g collagen/mg DW}$, which corresponded to around $400 \mu\text{g collagen}/\mu\text{g DNA}$) exhibited an order of magnitude higher collagen production than the highest results reported by Lee *et al.* after treatment of MSCs with CTGF followed by TGF- β 3 ($20 \mu\text{g collagen}/\mu\text{g DNA}$) (2014, suppl.), and also than Baker *et al.* who reported $120 \mu\text{g collagen}/\mu\text{g DNA}$ on electrospun PCL after 10 weeks of incubation in dynamic culture (2011).

3.4.3.5. Immunofluorescence

Immunofluorescence results of PCL-Ag constructs are presented in Figure 3.29. Both cross sectional and bottom view of the constructs revealed that gels were uniform, and cells were present throughout the constructs especially in the agarose-embedded side (Ag), showing that the constructs were stable and did not dissolved away or degraded. Staining of the cross sections revealed slightly more intense collagen staining on the Ag-embedded side of the constructs than the unembedded side (U). COL I staining was more intense than COL II on the constructs incubated under static conditions (Fig. 3.29A), whereas similar intensities of COL I and COL II staining were observed on the constructs incubated under dynamic conditions (Fig. 29B).

Closer examination of the constructs revealed higher deposition of collagen (arrowheads) on the static group than on the dynamic group; collagen (green) surrounded the cells (red, actin), indicating production of a pericellular matrix (Fig. 3.29B). The reason for this might be the high compressive load (15% strain) applied on the dynamic samples, which could be catabolic for collagen production and even kill the cells. Indeed, cell number in the inner regions of the constructs decreased upon dynamic compression (Section 3.4.3.2, Fig. 3.26).

High deposition of collagen was observed on PCL-Ag-GelMA constructs (Fig. 3.30). Collagen staining intensity was slightly lower on the static group (Fig. 3.30A) than

the dynamic (Fig. 3.30B). Collagen staining on the GelMA-embedded (G) side of the constructs was more intense than the Ag-embedded (Ag) or unembedded (U) sides. In fact, collagen staining on PCL-Ag-GelMA (Fig. 3.30) was more intense than on PCL-Ag (Fig. 3.29). This is in parallel with the results presented in the previous sections (Sections 3.4.1.5 and 3.4.2.5, Figs. 3.12, 3.13, 3.22, 3.23, and 3.24).

Cross sectional view of the constructs revealed that agarose was uniformly distributed within the inner regions of the scaffolds, whereas GelMA was not uniformly distributed in the outer region; GelMA gel was discontinuous with multiple patches at the bottom (B) and top (T) surfaces of the scaffolds (Fig. 3.30). The reason for this could be that UV could not penetrate deep into the inner portions of the scaffolds due to their irregular (coliseum-like) shapes (Section 3.4.3.1, Fig. 3.25), and the GelMA-cell suspension in the center of the scaffolds could not be crosslinked. This, in turn, resulted in cell and material loss in these constructs.

In brief, more collagen deposition was observed on PCL-Ag-GelMA constructs than on PCL-Ag, especially on the GelMA-embedded regions.

The results presented in the current study are similar to the previous reports. On agarose gels, higher COL II was reported than COL I, whereas on GelMA, higher COL I than COL II (Daly *et al.*, 2016). However, unlike the current study, they reported higher COL I deposition on GelMA than agarose, and higher COL II deposition on agarose than GelMA. Lee *et al.* reported low COL I and II deposition on the 3D printed PCL scaffolds, and they enhanced COL I deposition by treatment of the constructs with CTGF, and COL II by treatment with TGF- β (2014). Baek *et al.* reported high deposition of COL I on the electrospun PCL, and showed that GAG deposition increased with the addition of alginate (a non-bioactive gel resembling agarose) (2015). Similarly, high COL I deposition was reported on fibrochondrocyte-seeded domains of the electrospun PCL, and high COL II on the MSC-seeded domains (Han *et al.*, 2016). Zhang *et al.* (2017) reported higher COL II deposition on the 3D printed PCL scaffolds implanted in a rabbit model, which was not in accordance with our results.

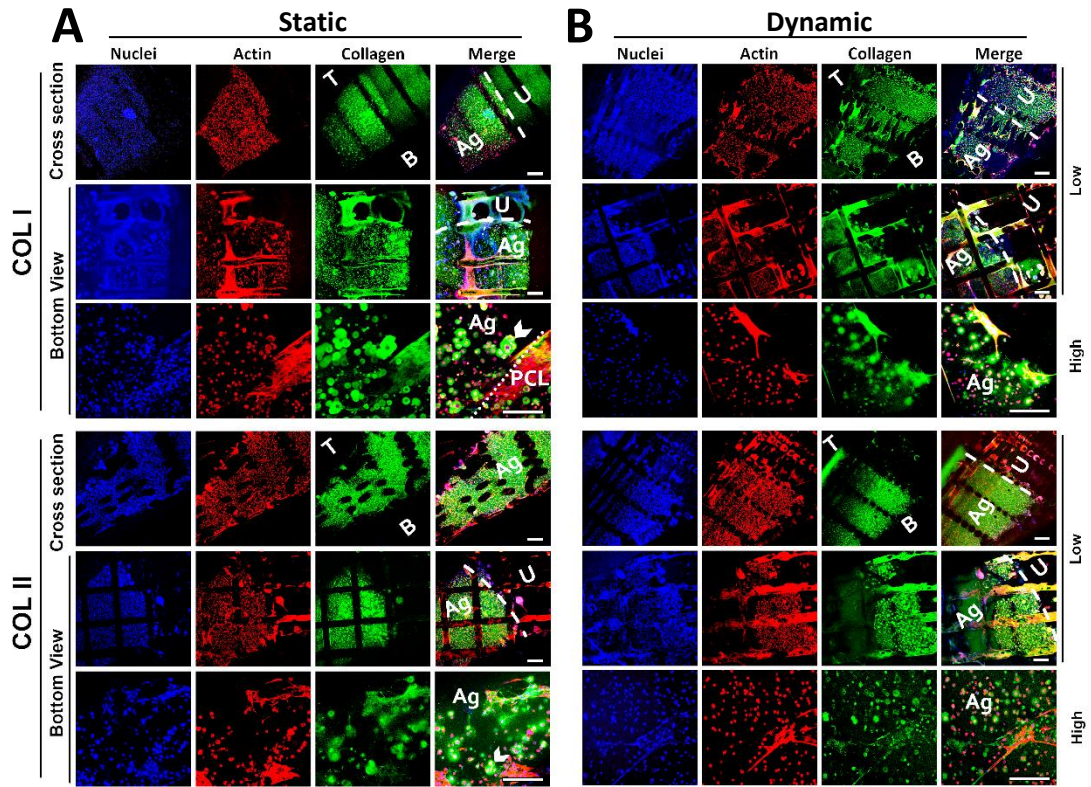


Figure 3.29. Immunofluorescence of the PCL-Ag constructs after 56 days of culture. Constructs incubated under (A) static, and (B) dynamic culture conditions. CLSM images at low and high magnifications. T: top, B: bottom surface of the constructs. Dashed lines: border between agarose-embedded (Ag) and unembedded parts (U). Dotted line: border between the agarose gel and PCL strands. Arrowheads point to the collagen produced in agarose surrounding the cells. Nuclei were stained with DAPI (blue), actin with rhodamine-labelled phalloidin (red), and collagen with Alexafluor 488-labelled antibodies (green). Scale bars: 500 μm .

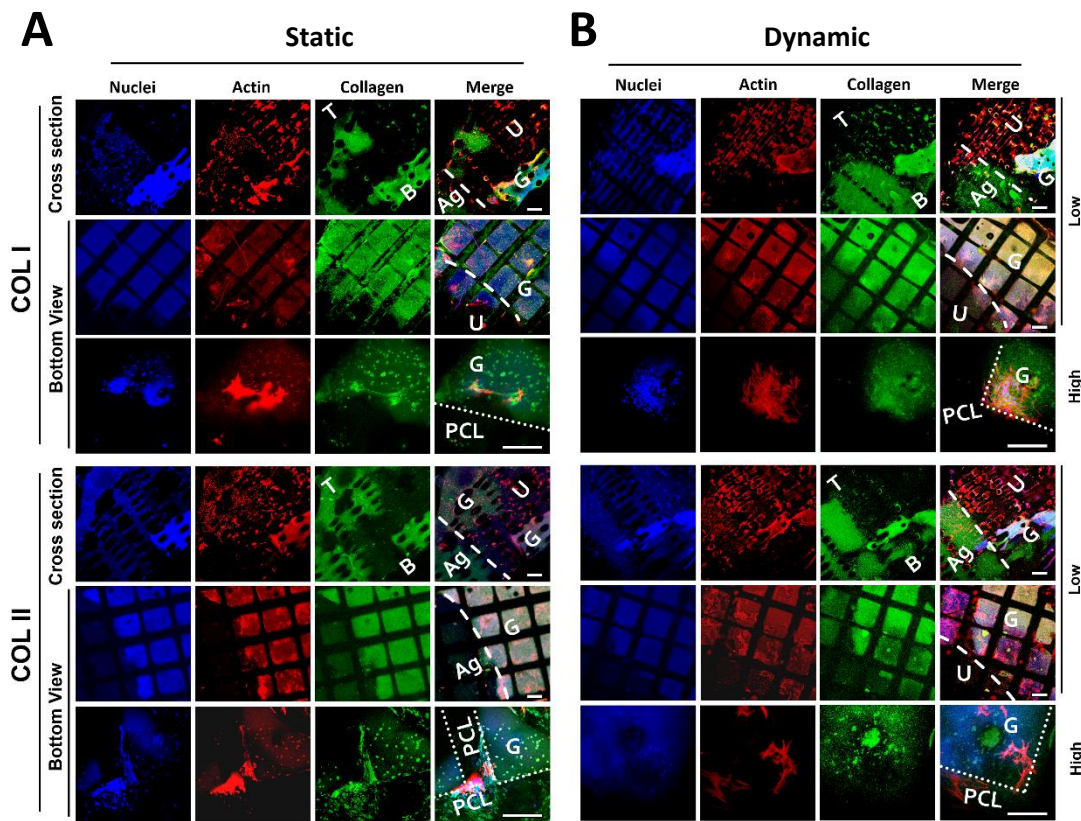


Figure 3.30. Immunofluorescence of the PCL-Ag-GelMA constructs after 56 days of culture. Constructs incubated under (A) static and (B) dynamic culture conditions. CLSM images at low and high magnifications. T: top, B: bottom surface of the constructs. Dashed lines: border between agarose-embedded (Ag) and GelMA-embedded (G) parts. Some parts in the outer region were unembedded (U). Dotted lines: borders between the GelMA gels and PCL strands. Nuclei were stained with DAPI (blue), actin with rhodamine-labelled phalloidin (red), and collagen with Alexafluor 488-labelled antibodies (green). Scale bars: 500 μm .

The zonal difference in the inner and outer regions of the constructs was achieved by Lee *et al.* (2014), who used different growth factors on the different zones of their 3D printed PCL constructs, and by Han *et al.* (2016), who used different cells in different domains of their electrospun PCL constructs and reported that heterogeneity induced fibrocartilage formation. In the current study we achieved to mimic the

different zones of the meniscus by using different hydrogels, which is a quite simple, safe and novel approach.

The summary of the results obtained in Section 3.4.3 are presented in Figure 3.31. In this part of the study, the coliseum shaped scaffolds were seeded with fibrochondrocytes, incubated for 14 days in the culture media, and embedded in agarose at the inner portion and in GelMA at the outer portion (PCL-Ag-GelMA). A set of constructs were embedded in agarose only at the inner region and left unembedded at the outer portion (PCL-Ag). After incubation for additional 42 days, PCL-Ag constructs exhibited high content of GAGs, and PCL-Ag-GelMA constructs exhibited high contents of COL I and COL II.

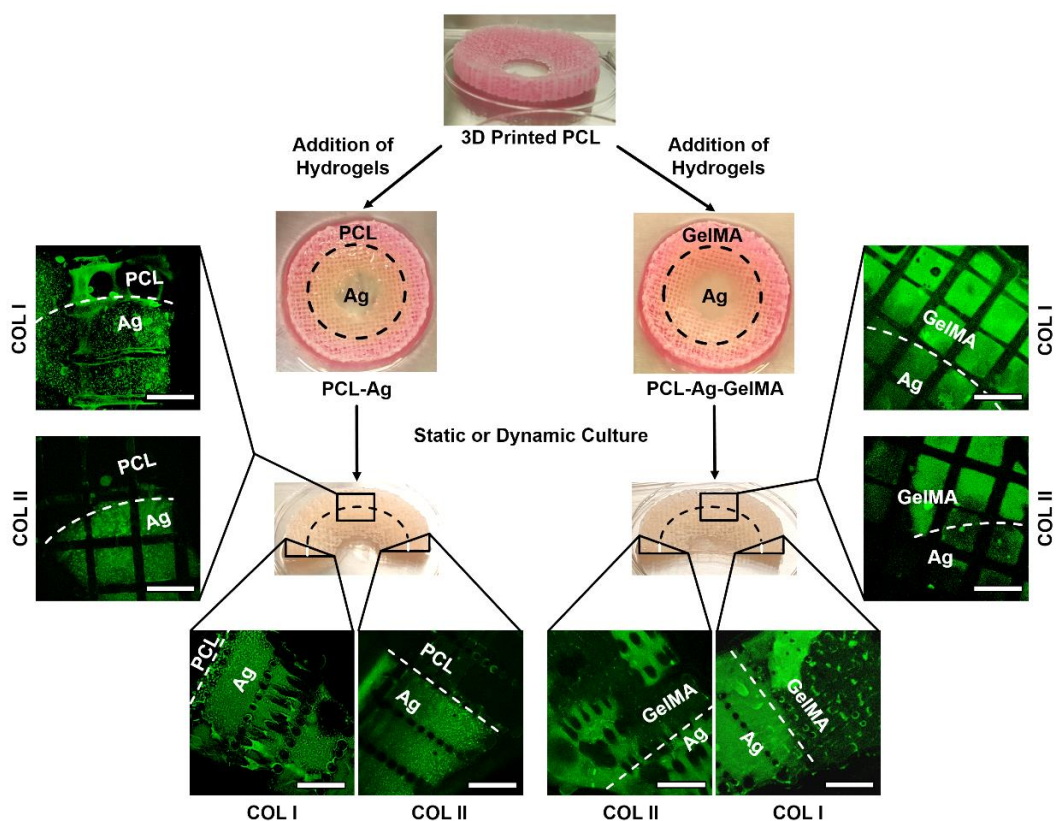


Figure 3.31. The overall scheme showing the design and findings of the study. The PCL-Ag and PCL-Ag-GelMA constructs were immunostained for type I (COL I) and type II (COL II) collagens. Scale bars: 1 mm.

3.5. Human Fibrochondrocyte-Based Studies

The compressive modulus of PCL 80 was very high in comparison to the native meniscus and could lead to degeneration of the underlying cartilage after implantation to the knees of the patients. Therefore, human fibrochondrocyte-based studies were conducted using a lower molecular weight (50 kDa) PCL, PCL 50. The polymer was printed with or without shifting of the consecutive layers, and with or without contour (or circumferential strands) at the outer borders. In this section, the source of gelatin was also changed. Porcine gelatin was used instead of bovine, because it results in formation of higher strength-gels and was the preferred source. Thus, all the studies conducted in the previous sections were replicated using human fibrochondrocytes and porcine gelatin, and with PCL 50 (with various designs). Finally, PCL scaffolds were embedded in GelMA-Ag blends, and the effect of GelMA-Ag blend on the ECM production capacity of human fibrochondrocytes was tested.

3.5.1. Square Prism-Shaped Composite Constructs

3.5.1.1. Scaffold Microarchitecture

The square prism-shaped PCL 50 scaffolds were printed with various designs of the interior (shifting of strands) and exterior (presence of circumferential strands) structures. Photographs of the scaffolds are shown in Figure 3.32A. The scaffolds were had more defined shapes when there were circumferential strands (contours), probably because the strands forming the interior structure fused with these circumferential strands at the exterior and formed a stronger structure. When the circumferential strands were missing, however, the edges of the scaffolds at the sides were distorted (inclined), leading to a narrower width at the top compared to the base of the scaffolds.

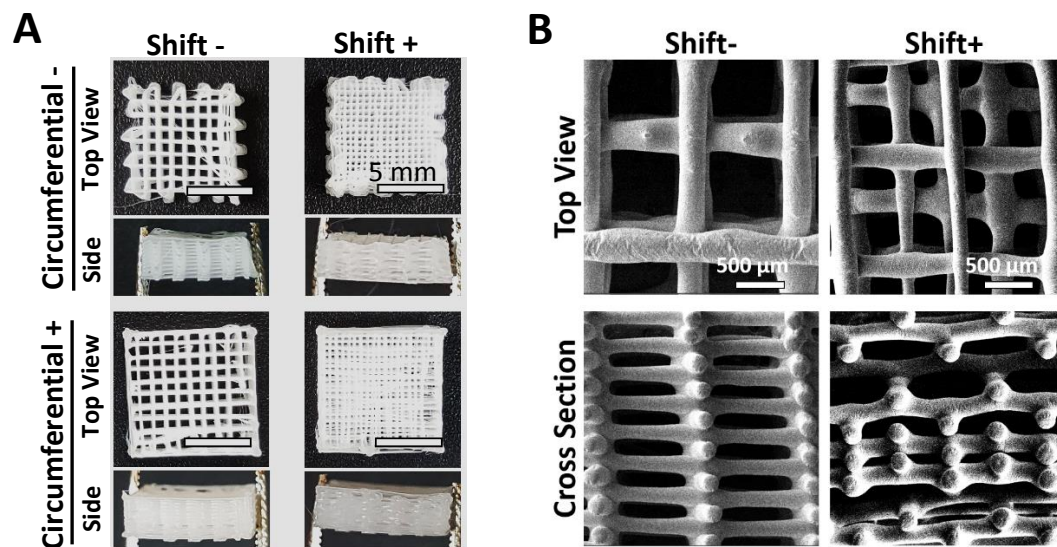


Figure 3.32. Macro- and micro-architecture of the PCL 50 scaffolds. (A) Photographs showing the macroarchitecture of the scaffolds. Scale bars: 5 mm. (B) SEM micrographs showing the microarchitecture of the scaffolds. Scale bars: 500 μm.

SEM examination show the interior structures of the shifted and non-shifted scaffolds (Fig. 3.32B). The scaffolds with no-shifts exhibited well-defined pores (width: 800 μm, height: 150 μm). The scaffolds with shifted strands seemed to have smaller pores and porosity. In fact, strand shifting was reported to decrease the porosity of the 3D printed PCL scaffolds (Buyuksungur *et al.*, 2017). The shifted structure increased the tortuosity of the scaffolds, which could allow cells in a pore to communicate with cells from many different pores. In contrast, pores in the non-shifted scaffolds produced tube-like spaces that extend along the height of the scaffolds.

3.5.1.2. Mechanical Properties of the Scaffolds

In order to investigate the effects of different scaffold designs on the mechanical properties of the scaffolds, compressive (Fig. 3.33A) and tensile (Fig. 3.33B) moduli were determined. Circumferential strands increased the compressive modulus, especially for the scaffolds with shifted strands ($p < 0.01$) (Fig. 3.33A). Interestingly,

shifting of the strands decreased the compressive modulus in the absence of circumferential strands ($p < 0.01$), but increased the modulus in the presence of them ($p > 0.05$). The non-shifted strands acted like buttresses of a building, supporting the structure against the compressive load and leading to high compressive modulus (Section 3.5.1.1, Fig. 3.32). The shifted strands, however, did not provide such a support, and exhibited low compressive modulus when no circumferential strands were present. Similar observations were reported in other studies, showing lower compressive properties when strands were shifted (Park *et al.*, 2011; Buyuksungur *et al.*, 2017).

ImageJ analysis of the photographs taken when the scaffolds were under 20% compressive strain revealed that the scaffolds with no shifts or circumferential strands were tilted the most at the edges, which could result in sliding of the strands during compressive load (Fig. 3.33C). On the other hand, shifted scaffolds that had the circumferential strands were not bent at the edges. When circumferential strands are present, the scaffolds are confined, which prevents bending and sliding of the strands (Fig. 3.33C). Thus, circumferential strands supported the scaffolds against the compressive load applied. This is similar to the stirrups in arches in a building supporting the concrete; the circumferential stirrup-confined concrete has higher compressive strength (Li *et al.*, 2016). The circumferential strands fused with the adjacent strands at the interior part of the scaffolds, which were present only in the shifted scaffolds (Section 2.2.2.1, Fig. 2.2), forming an even more rigid structure. This explains the significant increase (3-fold increase) in the modulus of the shifted scaffolds upon addition of the circumferential strands, but not in the non-shifted ones.

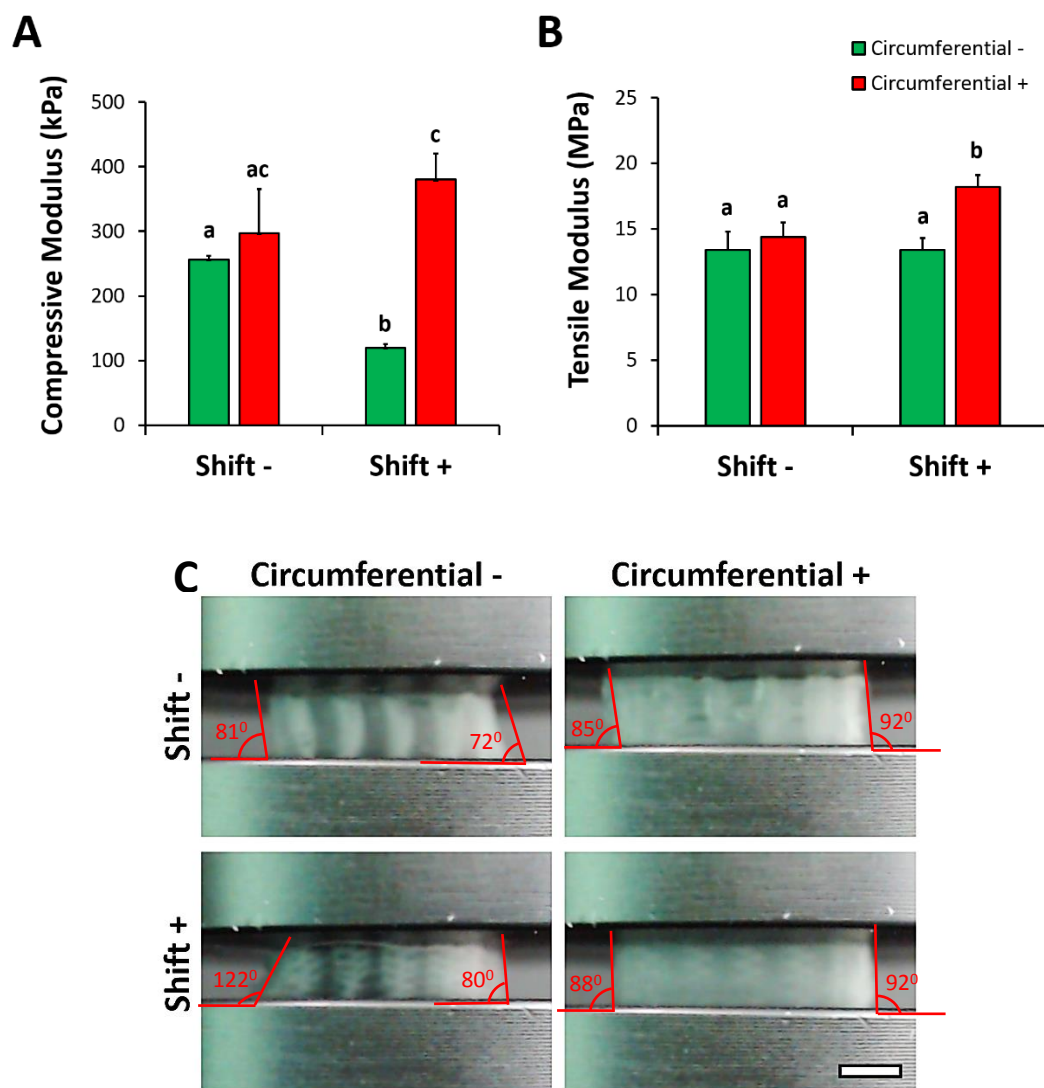


Figure 3.33. Mechanical properties of the PCL 50 scaffolds. (A) Compressive modulus, and (B) tensile modulus. (C) Representative images showing the scaffolds between the compression platens maintained at 20% compressive strain. Scale bar: 2.5 mm.

The highest compressive modulus was obtained when both shifted and circumferentially oriented strands were present (around 380 kPa) (Fig. 3.33A), which is in the range of compressive modulus reported for the native human meniscus (0.3-2 MPa) (Chia and Hull, 2008; Fischenich *et al.*, 2017). These results are lower than most of the FDM printed PCL scaffolds (10-55 MPa) (Cengiz *et al.*, 2016; Szojka *et al.*, 2017; Zhang *et al.*, 2017), which were much higher than the modulus of the

native meniscus. The only other study reporting a compressive modulus in the upper limit of the meniscus was that done by Lee *et al.* (2 MPa) (2014). The constructs proposed in the current study would probably perform better than the other studies reported in the literature when implanted in the knee, because their compressive modulus is closer to that of the native meniscus and thus would probably not lead to degeneration of the cartilage.

The highest tensile modulus was also obtained when the scaffolds were produced with shifting and circumferential strands (around 18 MPa), significantly higher than the other scaffolds (around 13 MPa) ($p < 0.05$) (Fig. 3.33B). Shifting of the strands or introduction of circumferential strands alone did not have an effect on the tensile properties of the scaffolds. However, tensile properties increased significantly when shifting and the circumferential strands were present together. As mentioned earlier, this could be caused by fusion of the circumferential strands with the adjacent strands at the interior part of the scaffolds, leading to formation of thicker and stronger strands at the edges. This, in turn, could result in scaffolds with high mechanical properties.

Tensile modulus of the constructs obtained here were comparable to that of the human menisci at radial direction (4-20 MPa) but not at circumferential (70-130 MPa) (Tissakht and Ahmed, 1995). The constructs also had tensile modulus similar to those of the electrospun (20-35 MPa) (Nerurkar *et al.*, 2011; Baker *et al.*, 2011; Han *et al.*, 2016) and 3D printed (40-80 MPa) (Lee *et al.*, 2014; Zhang *et al.*, 2017) PCL constructs.

Tensile moduli of the proposed constructs are expected to increase after seeding with cells and incubated in the culture media or after implantation.

3.5.1.3. Cell Morphology and Spreading Behavior

In order to assess the morphology of human fibrochondrocytes on the hydrogels and on the square prism shaped PCL 50, cell-seeded constructs were incubated for 7 days in culture media and stained for actin (green) and the nuclei (red) (Fig. 3.34). Cells were spread on GelMA, GelMA-Ag, and PCL, but remained mainly round on agarose gel, similar to the finding in the previous sections (Section 3.4.1.7, Fig. 3.16). Cells on GelMA were the most spread of all, indicating high cell-material interactions and strong adhesion on this hydrogel. Similarly, cells on PCL were spindle-shaped; they spread to some extent and elongated especially at the strand intersections. On agarose, cells were mainly round, indicating low cell-material interactions. Cells on GelMA-Ag were slightly spread or branched, with presence of round cells. These results are in parallel with the previous results (Section 3.4.1.8, Fig. 3.16).

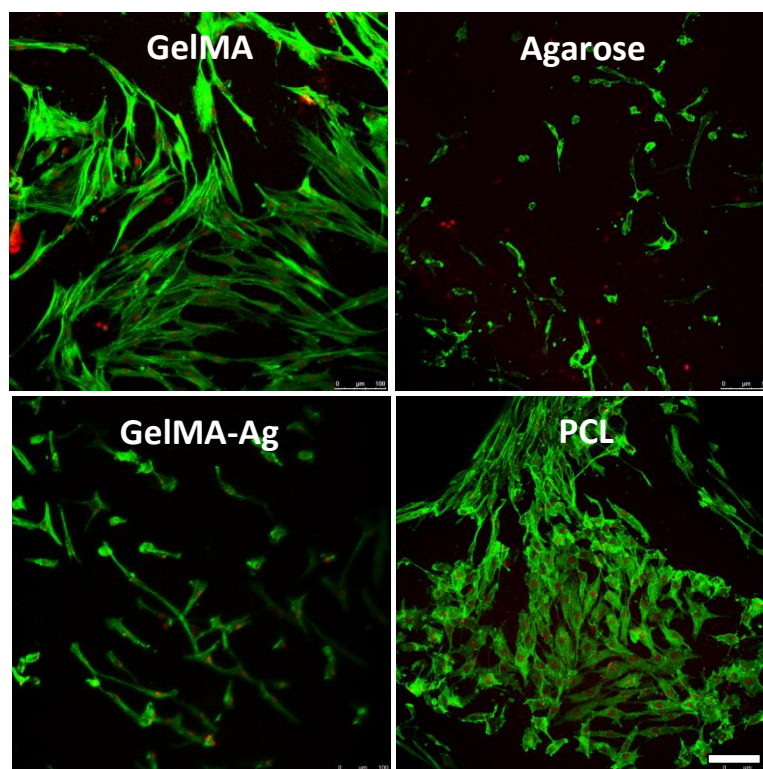


Figure 3.34. Morphology of the human fibrochondrocytes on the constructs after incubation for 7 days. Green: Alexa fluor 532-labelled phalloidin (for actin), and red: DRAQ5 (for nuclei). Scale bar: 100 μm .

The round cell morphology on agarose could be a result of weak cell adhesion on this gel, whereas the spread cell morphology on GelMA and PCL could be a result of strong cell adhesion (Ahearne, 2014). Gelatin presents biologic recognition sites and allows for cell adhesion through RGD sequences (Lui and Chan-Park, 2010), whereas agarose is highly hydrophilic and lack such binding sites, which limit cell adhesion. Similarly, it was reported that increasing proportion of agarose in collagen gels resulted in more round morphology (Ulrich *et al.*, 2010). The reason for the spindle-shaped morphology on PCL could be its rigid surface, which provides a 2D environment for the cells to spread, unlike the hydrogels which entrap the cells in a 3D microenvironment. In a previous study, we reported that spreading and elongation of fibrochondrocytes increased with the increase in stiffness (Bahcecioglu *et al.*, 2018).

3.5.1.4. Cell Viability

Live/dead assay results of the PCL-based constructs are presented in Figure 3.35. High cell viability was observed in all the constructs, whether they were produced without (Fig. 3.35A) or with shifts (Fig. 3.35B), and regardless of the hydrogels in which PCL scaffold was embedded. ImageJ analysis revealed the highest viability on PCL (over 90%) and the lowest on PCL-GelMA constructs (around 80%) (Table 3.3); however, this difference was not statistically significant ($p > 0.05$). The slightly reduced cell viability upon introduction of hydrogels could be due to restricted oxygen and nutrient transport to the center of the constructs or the hydrogels bulk. In fact, more dead cells were observed on the PCL strands of the hydrogel-embedded composite constructs, indicating that cells died because of limited sources (Fig. 3.35). Moreover, cross sectional view of the constructs revealed higher viability and cell density on the surface of PCL/hydrogel constructs than in the center (Fig. 3.35).

The square prism-shaped PCL 50 constructs seeded with human fibrochondrocytes exhibited similar cell viability with the PCL 80 constructs seeded with porcine fibrochondrocytes (around 75% cell viability) (Section 3.4.2.3, Table 3.2), but with slightly higher viability. This decrease in cell viability could be due to the shorter incubation of the human fibrochondrocytes (42 days) than the porcine cells (56

days). In fact, DNA contents of the porcine cell-seeded PCL 80 constructs decreased after Day 42 (Section 3.4.2.3, Fig. 3.20A).

Others also reported cell viability in the range of 70-90% after bioprinting of hydrogels (Hözl *et al.*, 2016; Daly *et al.*, 2016; Rhee *et al.*, 2016), and around 80% on FDM printed (Daly *et al.*, 2016) or melt electrospun printed PCL (Visser *et al.*, 2015). Cell viability was shown to decrease after introduction of PCL to agarose (from 90% to 80%) and to GelMA (from 82% to 78%) (Daly *et al.*, 2016).

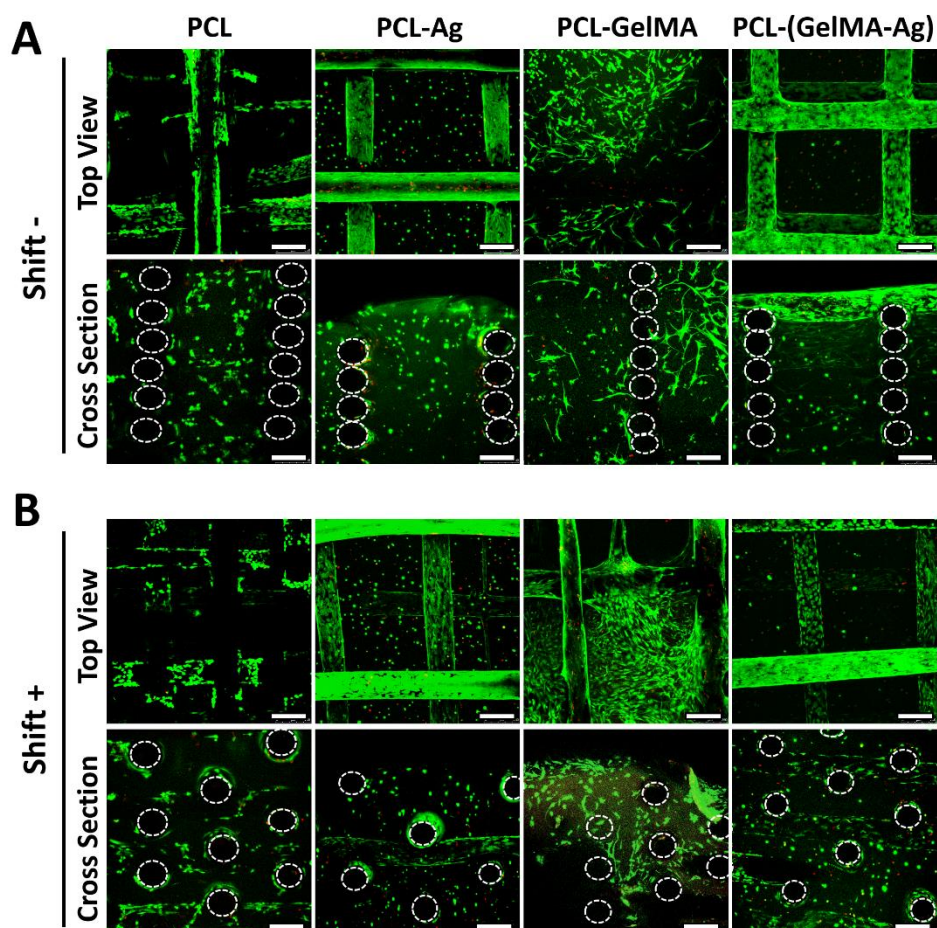


Figure 3.35. Cell viability of the square prism-shaped constructs after 42 days of culture. Constructs (A) without and (B) with strand shifting. Circles show PCL strands that are orthogonal to the view plane. Scale bars: 250 μm .

Table 3.3. Human fibrochondrocyte viability on square prism-shaped constructs as determined with live-dead assay.

<i>Constructs</i>	<i>Viability (%)</i>	
	Shift -	Shift +
PCL	90 ± 1	93 ± 1
PCL-Ag	85 ± 8	87 ± 2
PCL-GelMA	85 ± 2	82 ± 8
PCL-(GelMA-Ag)	87 ± 4	85 ± 3

3.5.1.5. Immunofluorescence

Immunofluorescence revealed deposition of low levels of COL I and II on the PCL constructs (Fig. 3.36). No difference was observed between collagen staining on the no-shift (Fig. 3.36A) and shifted (Fig. 3.36B) scaffolds. PCL scaffolds exhibited no or little collagen staining on Day 1, while some staining was observed on Day 42, indicating production of COL I and II. On the other hand, COL I deposition was higher (more intense red color) than COL II staining (green color) (Figs. 3.36A and 3.36B, merge images).

One observation was that when cells increased in number and formed aggregates on the PCL (dashed square), more intense collagen staining was observed (Fig. 3.36B, low magnification images), indicating higher collagen deposition when cells interacted with each other than when interacted with the PCL scaffold.

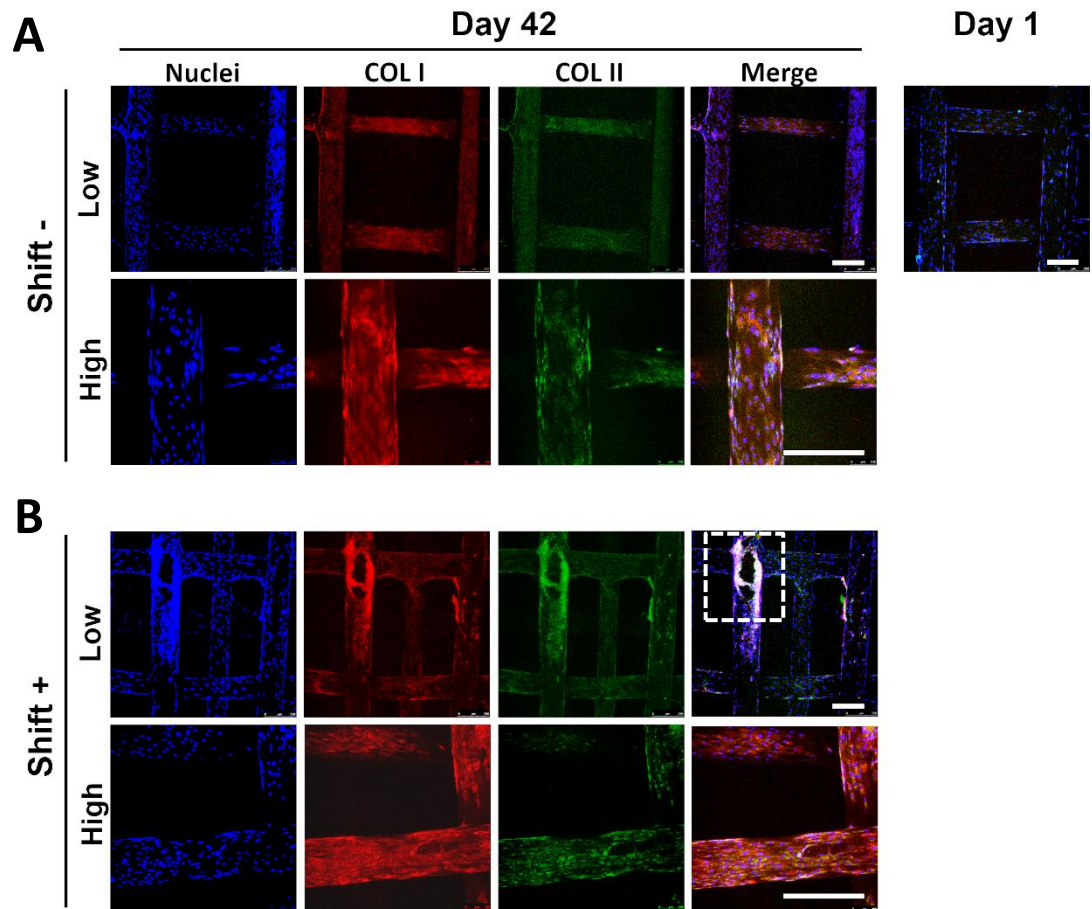


Figure 3.36. Collagen deposition on the human fibrochondrocyte-seeded square prism-shaped PCL constructs. Constructs (A) without, and (B) with shifting of the strands. The control was the cell-seeded PCL incubated for 1 day in culture media. Images were pseudocolored. Blue: TO-PRO (nuclei), red: Alexafluor 532 (COL I), and green: Alexafluor 488 (COL II). Dashed square: cell aggregates. Scale bars: 250 μm .

Collagen deposition was detected on PCL-Ag constructs, but at low levels (Fig. 3.37). No difference was observed between collagen deposition on the no-shift (Fig. 3.37A) and shifted (Fig. 3.37B) constructs. COL I and II stainings were equally intense.

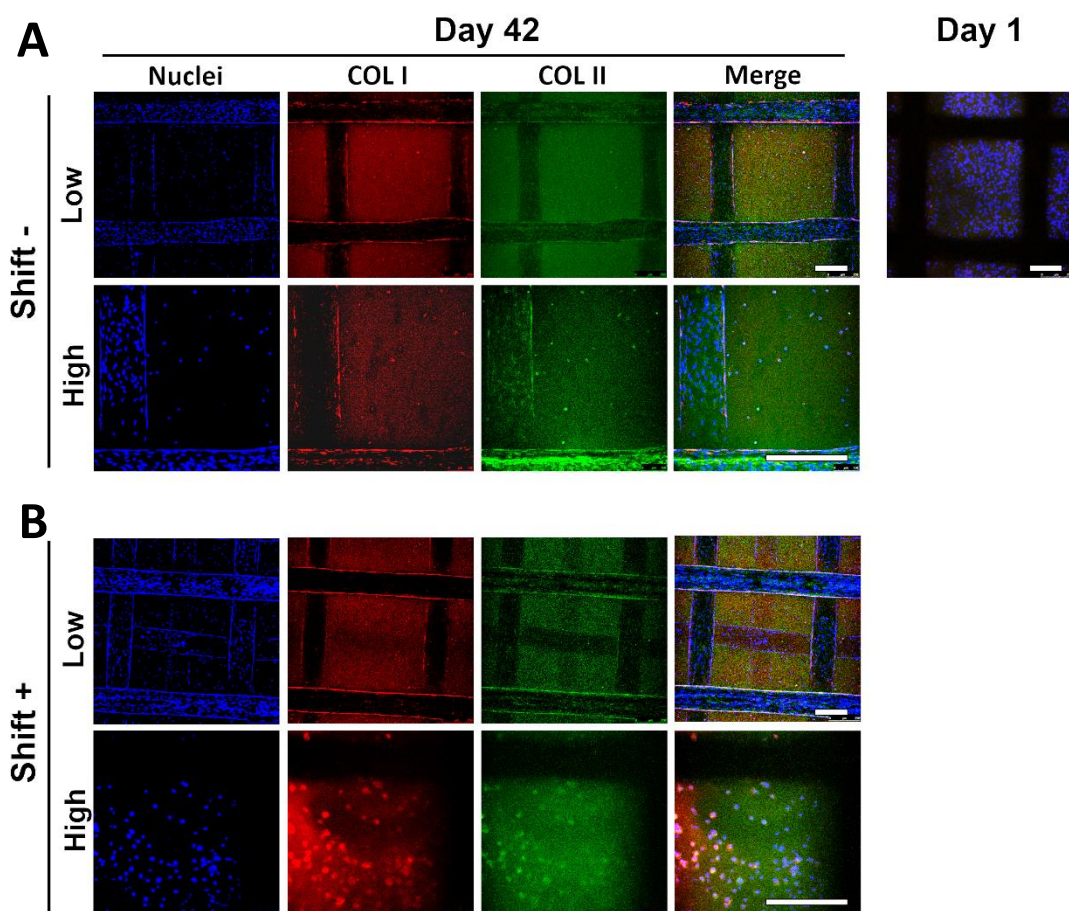


Figure 3.37. Collagen deposition on the human fibrochondrocyte-seeded square prism-shaped PCL-Ag constructs. Constructs (A) without, and (B) with shifting of the strands. The control was the cell-seeded PCL-Ag incubated for 1 day in culture media. Images were pseudocolored. Blue: TO-PRO (nuclei), red: Alexafluor 532 (COL I), and green: Alexafluor 488 (COL II). Scale bars: 250 μm .

Collagen deposition on the PCL-GelMA constructs was very high (high collagen deposition on Day 42 compared to Day 1), with higher COL I deposition than COL II (Fig. 3.38). Similar to other constructs, no difference was observed between collagen deposition on the non-shifted (Fig. 3.38A) and shifted (Fig. 3.38B) constructs. However, higher deposition of COL I was detected than COL II.

Some parts on the PCL scaffolds could not be embedded in GelMA, and almost no collagen deposition (very low COL I deposition) was observed on these unembedded

(U) PCL parts (dashed lines showing the border between the GelMA-embedded and unembedded parts) (Fig. 3.38). Finally, the collagen deposition on the surface (S) of GelMA was higher than that in the center (C) of the gel.

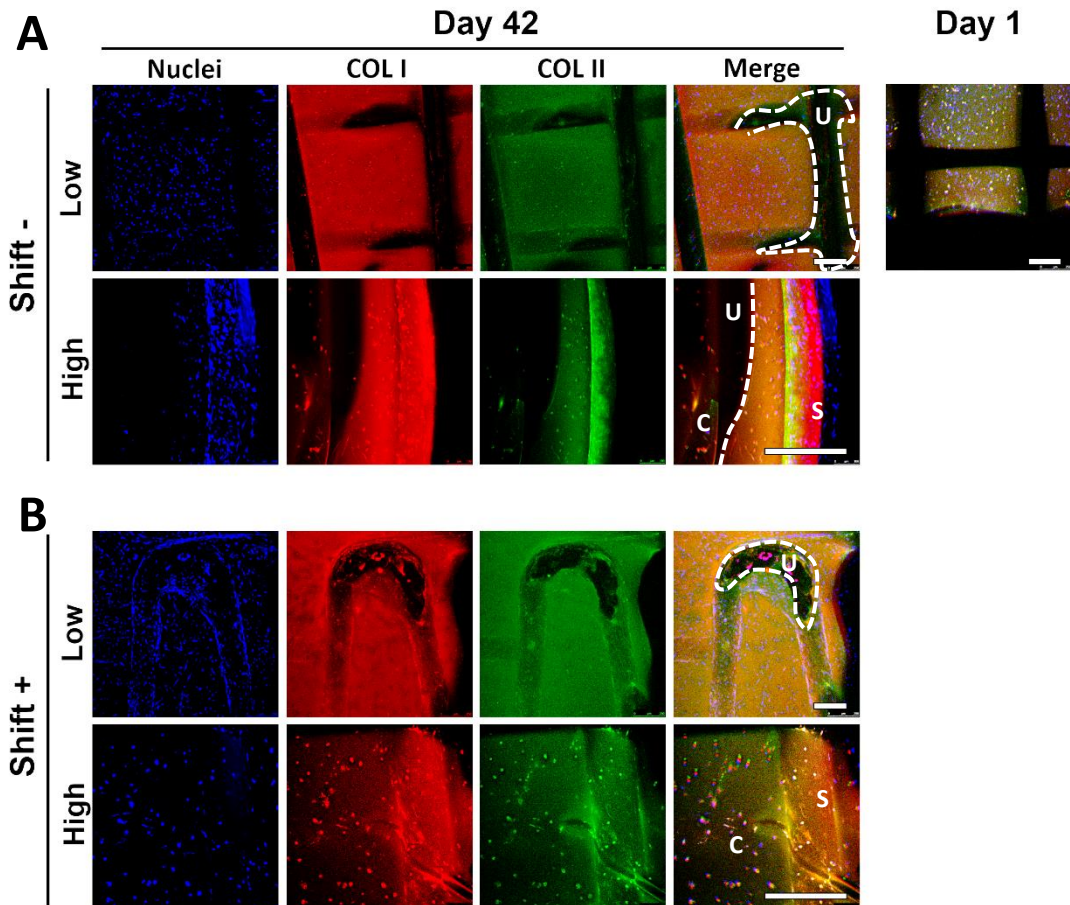


Figure 3.38. Collagen deposition on the human fibrochondrocyte-seeded square prism-shaped PCL-GelMA constructs. Constructs (A) without, and (B) with shifting of the strands. The control was the cell-seeded PCL-GelMA incubated for 1 day in culture media. Images were pseudocolored. Blue: TO-PRO (nuclei), red: Alexafluor 532 (COL I), and green: Alexafluor 488 (COL II). Dashed line: border between the GelMA-embedded and unembedded PCL. U: unembedded, S: surface, C: center. Scale bars: 250 μm .

Collagen deposition on PCL-(GelMA-Ag) was high (Fig. 3.39). Collagen deposition on the non-shifted (Fig. 3.39A) and shifted (Fig. 3.39B) constructs was similar. Higher COL I deposition was observed on the constructs than COL II, but COL II deposition was also high.

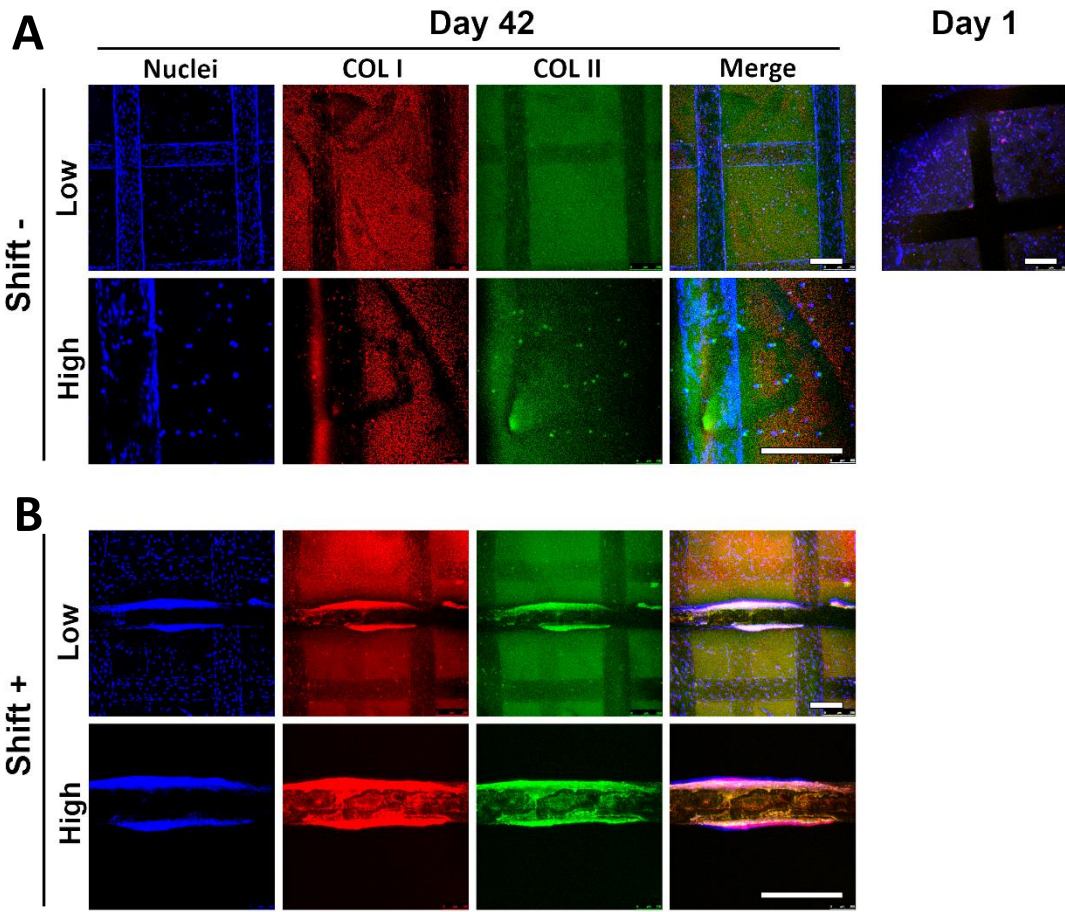


Figure 3.39. Collagen deposition on the human fibrochondrocyte-seeded square prism-shaped PCL-(GelMA-Ag) constructs. Constructs (A) without, and (B) with shifting of the strands. The control was the cell-seeded PCL-(GelMA-Ag) incubated for 1 day in culture media. Images were pseudocolored. Blue: TO-PRO (nuclei), red: Alexafluor 532 (COL I), and green: Alexafluor 488 (COL II). Scale bars: 250 μ m.

In summary, the highest collagen (both COL I and II) production was obtained on PCL-GelMA, and the lowest on PCL. Embedding of PCL in agarose resulted in an increase in collagen production, but to a lesser extent than when embedded in GelMA. Blending of GelMA and agarose resulted in a medium level collagen production. These results are similar to the results obtained in the previous sections, where collagen production was shown to be higher on GelMA-based constructs than agarose- and PCL-based ones (Sections 3.4.1.5, 3.4.2.6, and 3.4.3.5).

The results presented in the current study are similar to the previous reports. On agarose gels, higher COL II was reported than COL I, whereas on GelMA, higher COL I than COL II (Daly *et al.*, 2016). However, unlike the current study, they reported higher COL I deposition on GelMA than agarose, and higher COL II deposition on agarose than GelMA. In another study, low COL I and II deposition was reported on the 3D printed PCL scaffolds, and COL I deposition was enhanced by treatment of the constructs with CTGF, and COL II deposition was enhanced by treatment with TGF- β (Lee *et al.*, 2014). Baek *et al.* reported high deposition of COL I on the electrospun PCL, and showed that GAG deposition increased with the addition of alginate (a non-bioactive gel resembling agarose) (2015). Similarly, high COL I deposition was reported on the fibrochondrocyte-seeded domains of the electrospun PCL, and high COL II deposition on the MSC-seeded domains (Han *et al.*, 2016), which is similar to the GelMA-rich regions in the current study that exhibited high COL I deposition, and Ag-rich region that exhibited high COL II. Zhang *et al.* (2017) reported higher COL II deposition on the 3D printed PCL scaffolds implanted in a rabbit model, which was not in accordance with our results.

In the light of the above results, GelMA-Ag was selected as the embedding material for use in the inner portion of the meniscus-shaped constructs instead of agarose. Presence of agarose in the inner portion of the constructs is expected to enhance GAG production, and presence of GelMA is expected to enhance COL II production.

3.5.2. Meniscus-Shaped PCL/Hydrogel Composite Constructs

The final meniscus-shaped constructs were produced by printing PCL 50 with or without circumferential strands, and with or without strand shifts. The PCL scaffolds were seeded with human fibrochondrocytes and incubated for 2 weeks in culture media. The constructs were then embedded in cell-laden agarose or GelMA-Ag at the inner region, and in cell-laden GelMA at the outer region, incubated for an additional 4 weeks (total of 6 weeks until Day 42), and analyzed for cell viability, cell morphology, and collagen production.

3.5.2.1. Macro- and Microarchitecture of the Scaffolds

The coliseum-shaped scaffolds were produced with circumferential strands to mimic the collagen fiber orientation in the native meniscus (Petersen and Tillmann, 1998). Top view of the scaffolds show that the width of the constructs was slightly larger when scaffolds were produced with the circumferential strands (26 mm) than without them (24 mm) and the shape was more defined (Fig. 3.40A).

Bottom view show the base of the scaffolds and the interior structure (Fig. 3.40B). The scaffolds were produced successfully as designed. A closer examination with SEM revealed that the bottom surface of the strands was rough (Fig. 3.40C), which could enhance cell adhesion on the scaffolds. The strands were straight, but the thickness changed along the strands. Cross sectional view revealed straight and parallel strands with around 150 μm distance between the strands as planned. Top view revealed good alignment of the circumferential strands on the surface of the scaffolds. Therefore, the final 3D constructs were produced with circumferential strands.

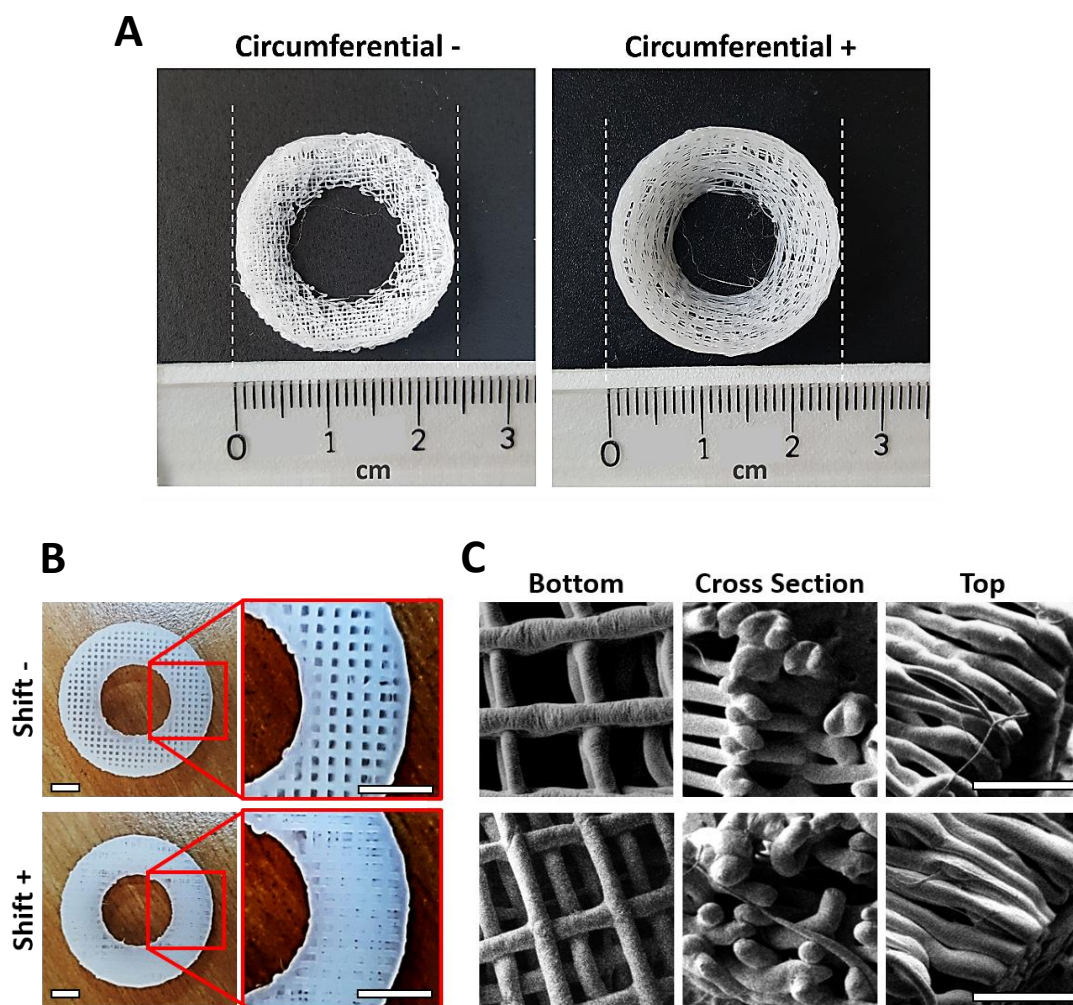


Figure 3.40. Macro- and micro-architecture of the meniscus-shaped PCL scaffolds. (A) Top view of the scaffolds produced without (left) or with (right) circumferential strands. (B) Bottom view of the scaffolds produced without (upper panel) or with (lower panel) shifting. Scale bars: 5 mm. (C) SEM images of the scaffolds. Scale bars: 1 mm.

3.5.2.2. Cell Morphology on PCL Scaffolds

In order to study the effect of circumferential strands on cell behavior, the PCL scaffolds with the circumferential strands were seeded with the human fibrochondrocytes and incubated for 14 days in the culture media. CLSM images revealed that the cells were aligned along the strands on the top of the scaffolds in

parallel direction with the circumferential strands (upper panel), and were perpendicular to the strands at the base of the scaffolds (lower panel) (Fig. 3.41), due to the perpendicular groves on the PCL strands which were resulted from the shear between the PCL strand and the ground during printing (Fig. 3.40C). This shows that the circumferential strands were useful in guiding the cells to align along the strands, and finally produce circumferentially aligned collagen fibers.

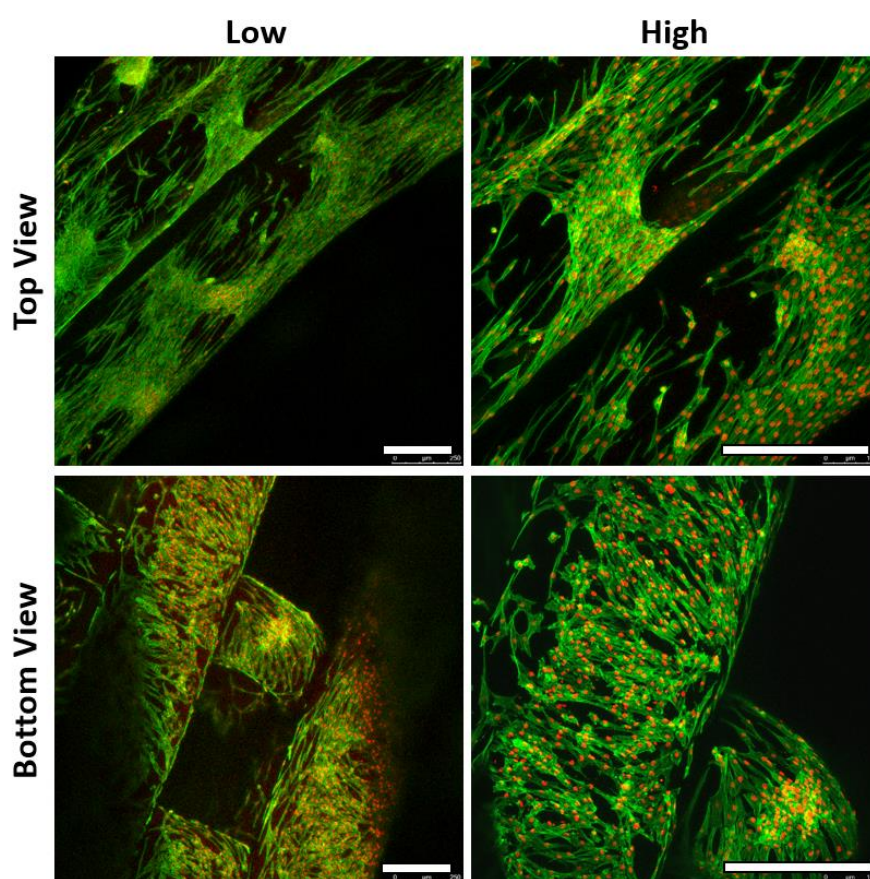


Figure 3.41. CLSM images of the human fibrochondrocyte-seeded PCL scaffolds after incubation for 14 days in culture media. Top (upper panel) and bottom (lower panel) views of the scaffolds at low (left) and high (right) magnifications. Green: Alexafluor 488-labelled phalloidin for the actin, and red: DRAQ5 for the nuclei. Scale bars: 250 μm .

3.5.2.3. Preparation of the Final 3D Composite Constructs

The final 3D PCL scaffolds with or without shifting of the strands at consecutive layers were seeded with human fibrochondrocytes and incubated for 2 weeks. Then, the scaffolds were embedded in GelMA-Ag at the inner regions (green), and in GelMA at the outer regions (pink) (Fig. 3.42A), and incubated for additional 4 weeks in culture media. On Day 42 (left), the constructs looked similar to the native menisci (right) (Fig. 3.42B).

3.5.2.4. Cell Viability on the Final 3D Composite Constructs

Live/dead assay results are shown in Figure 3.43. CLSM images of the constructs revealed high viability on the constructs, especially on the surface (Fig. 3.43). ImageJ analysis of the CLSM images revealed similar cell viability (80%) on the GelMA-embedded outer portion of the constructs and GelMA-Ag embedded inner portions. However, a higher cell viability was observed on the surface of the GelMA-embedded construct (90%) than in the center (around 70%).

Others also reported cell viability in the range of 70-90% on the bioprinted hydrogels (Hölzl *et al.*, 2016; Daly *et al.*, 2016; Rhee *et al.*, 2016), and around 80% on FDM printed (Daly *et al.*, 2016) or melt electrospun (Visser *et al.*, 2015) PCL scaffolds. In another study, cell viability was reported to be similar on PCL-agarose and PCL-GelMA (both 80%), but higher on agarose (90%) than GelMA (80%) (Daly *et al.*, 2016).

3.5.2.5. Immunofluorescence

Immunofluorescence revealed very high COL I and II deposition on the GelMA-embedded portion of the meniscus-shaped constructs and high COL I and II production on the (GelMA-Ag)-embedded portion (Fig 3.44). COL I deposition was more intense than COL II at the GelMA-embedded region, while COL II was more intense than COL I at the (GelMA-Ag)-embeddd region.

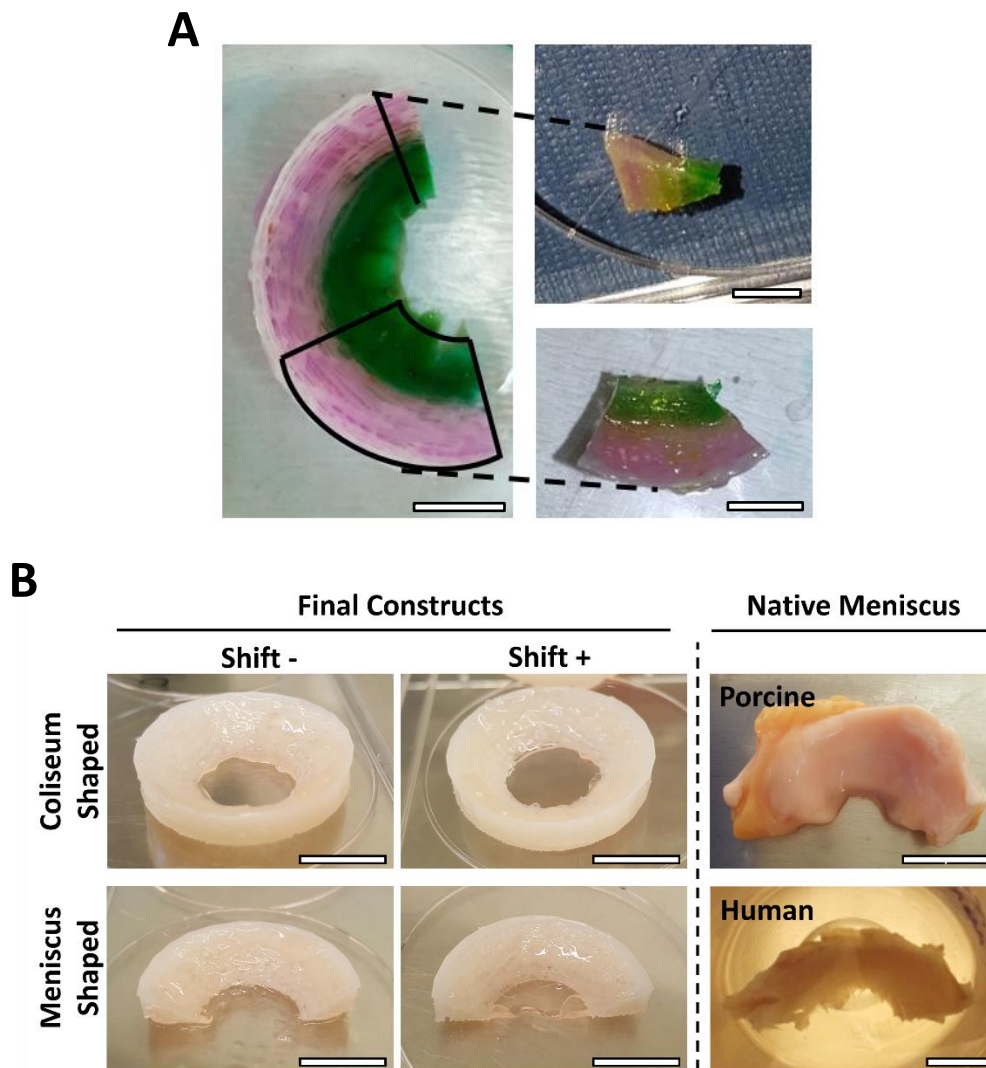


Figure 3.42. Representative photographs of the final constructs and their comparison to the native menisci. (A) Representative images showing the agarose-embedded inner region (green, stained with crescent green), and the GelMA-embedded outer region (purple, phenol red) of the constructs. Scale bars: 500 μ m. (B) The final constructs after incubation for 42 days in culture media (left), and the native menisci (right, porcine (top), and human (bottom)). Scale bars: 1 mm.

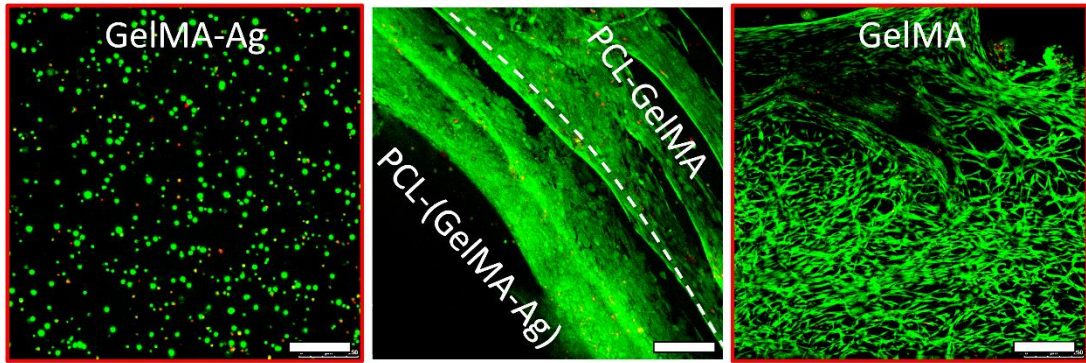


Figure 3.43. Representative images showing cell viability on the final meniscus-shaped constructs as determined with the live/dead assay. Green: calcein-AM (live cells), red: ethidium homodimer-1 (dead cells). Dashed line shows the border between the GelMA-embedded and (GelMA-Ag)-embedded regions. Scale bars: 250 μm .

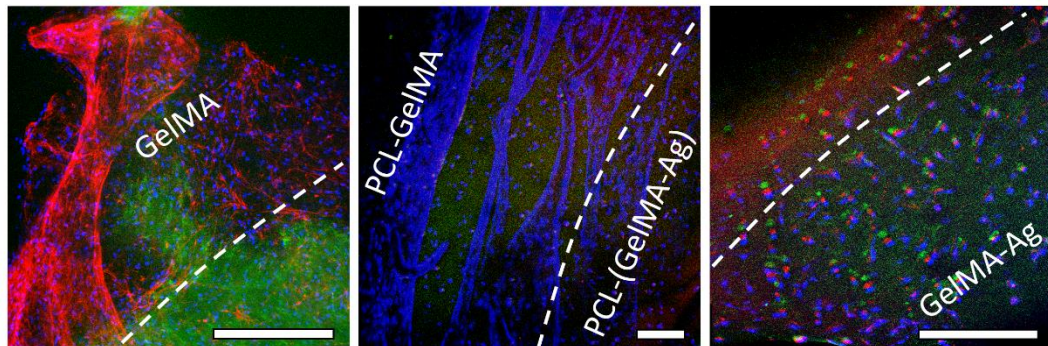


Figure 3.44. Collagen deposition on the human fibrochondrocyte-seeded meniscus-shaped constructs. Constructs were embedded in GelMA at the outer portion, and in GelMA-Ag at the inner portion. Blue: TO-PRO (nuclei), red: Alexafluor 532 (COL I), green: Alexafluor 488 (COL II). Dashed lines point to the border between the GelMA-embedded outer region and the (GelMA-Ag)-embedded inner region. Scale bars: 250 μm .

These results are similar to the biochemical content of the meniscus, in which the outer region consists of high COL I, and the inner portion consists of high COL II (Sanchez-Adams *et al.*, 2013). Region specific collagen deposition was achieved by other researchers who used CTGF-loaded microspheres in the outer region of the meniscus-shaped constructs to induce COL I production, and TGF- β -loaded microspheres in the inner region to induce COL II production (Lee *et al.*, 2014). Similar to the GelMA- and (GelMA-Ag)-embedded regions of the constructs in the current study, electrospun PCL containing two heterodomains (one fibrochondrocyte-seeded and the other MSC-seeded) was reported to exhibit high COL I deposition on the fibrochondrocyte-seeded domains and high COL II deposition on the MSC-seeded domains (Han *et al.*, 2016). Heterodomains were reported to enhance cartilaginous ECM deposition.

In the current study we were able to mimic the different zones of the meniscus by using different hydrogels, which is a quite simple and safe approach.

CHAPTER 4

4. CONCLUSION

Meniscus is a crescent-shaped fibrocartilage with a unique structure; it is avascular and cartilaginous with high contents of type II collagen (COL II) and glycosaminoglycans (GAGs) at the inner region, and vascular and fibrous with circumferential oriented type I collagen (COL I) fibers at the outer region. Meniscal tears are encountered during harsh sports activities and due to degeneration as a result of ageing. Seriously torn menisci are resected and replaced with transplants or prostheses. However, these techniques are not functional and do not prevent osteoarthritis. Tissue engineering has been proposed as an alternative treatment method for more than two decades; however, there is no functional tissue engineered scaffold in the market yet.

This study aims at designing a novel tissue engineering construct that can restore or replace the function of the resected meniscus. The approach involves 3D printing of a poly(ϵ -caprolactone) (PCL) scaffold with circumferential strands that resemble the collagen fibers in the native meniscus, and embedding of this scaffold in different hydrogels at the inner and outer regions to produce cartilaginous and fibrous zones, respectively, resembling those in the native meniscus. The study was divided into two parts: porcine and human fibrochondrocyte-based studies.

In the first part of the study, porcine fibrochondrocytes were used. To start with, different hydrogels including agarose, gelatin methacrylate (GelMA), methacrylated hyaluronic acid (MeHA), and a blend of GelMA and MeHA were tested for mechanical strength, cell viability, and GAG and collagen production under static

(no load) or dynamic compressive load (5-15% strain) conditions. A three dimensional (3D) printed PCL scaffold was used as a control. Porcine fibrochondrocytes exhibited higher cell viability on PCL than on the hydrogels after a 35-day culture. Among hydrogels agarose and GelMA exhibited the highest viability. Hydrogels resulted in higher production of GAGs and collagen than unembedded PCL. Cells exhibited a round morphology and an enhanced GAG production when encapsulated in agarose, and a dendritic morphology and an enhanced collagen production when encapsulated in GelMA. This was attributed to the cell-material interactions; cells adhered strongly on on GelMA than Ag. Dynamic compression further enhanced GAG production in Ag, but did not have any effect on ECM production in GelMA. As a conclusion, agarose is a good candidate to be used in engineering of the inner region of the meniscus, and GelMA is a good candidate for the outer region, but they need to be reinforced before used in the body, because they have low mechanical properties.

Next, 3D printed PCL (Mw: 80 kDa) was embedded in Ag or GelMA to produce mechanically strong PCL-Ag and PCL-GelMA composite constructs. These constructs, and the unembedded PCL, were tested for mechanical properties, cell viability, and GAG and collagen production after incubation for 56 days under static and dynamic culture conditions. Compressive mechanical properties of the constructs were very high (10 MPa) compared to that of the meniscus (0.3-2 MPa). Addition of hydrogels did not change the compressive and tensile properties of PCL. Cell viability was high in all of the constructs. Similar to the previous findings, agarose was shown to enhance GAG production, and GelMA to enhance collagen production on the 3D printed PCL. Dynamic compression at 5 to 15% strain slightly reduced ECM production on the constructs in the first two weeks of application, but it enhanced GAG and collagen production during the last two weeks. It was concluded that agarose and GelMA can be used in regeneration of the inner and outer regions of the meniscus, respectively.

Later, a meniscus-shaped PCL scaffold was printed and embedded in porcine fibrochondrocyte-laden agarose at the inner portion and GelMA at the outer portion. This construct was tested for cell viability and meniscal ECM production after

incubation for 56 days under static and dynamic culture conditions. Similar to the previous findings, Ag enhanced the GAG production in the inner portion of the PCL constructs, and GelMA enhanced collagen production in the outer portion. Dynamic compression was applied using a compression platen fitting on the amphitheater-shaped constructs, thus resulting in gradual increase in compressive strain from the outer (1-3%) to the inner (5-15%) regions of the constructs. Dynamic compression at 5-15% strain was shown to reduce ECM production in the Ag-embedded inner region, while that at 1-3% strain to enhance collagen production in the GelMA-embedded outer region. It was concluded that these constructs should be further optimized to produce a tissue engineered meniscal construct that fully mimics the structural organization and biochemistry of the native meniscus. Further, the constructs can be tested with human fibrochondrocytes. One potential problem with these constructs can be their very high compressive modulus, which can result in the degeneration of the cartilage after implantation in the knee.

In the second part of the study, PCL/hydrogel constructs were tested using human fibrochondrocytes. In this part, a lower molecular weight PCL (Mw: 50 kDa) was used to obtain lower compressive mechanical properties for the final constructs, which would match those of the native meniscus. Moreover, PCL scaffolds with and without shifted strands were produced to optimize the mechanical properties. In addition, scaffolds with and without circumferential strands were produced to mimic the circumferential collagen fibers in the meniscus. Finally, GelMA-Ag blends were produced to embed the inner portions of the constructs in. The square prism and meniscus shaped constructs were tested for cell viability and collagen production. Higher mechanical properties were obtained with the circumferential strand-confined constructs than those lacking these strands, and the highest compressive and tensile modulus were obtained with the scaffolds having the shifted and circumferential strands. High COL I and II deposition was observed on the GelMA-embedded PCL, and high COL II relative to COL I was observed on Ag-embedded constructs. Collagen deposition was higher on the (GelMA-Ag)-embedded constructs than Ag-embedded ones. When the meniscus-shaped constructs were embedded in GelMA-Ag at the inner portion and in GelMA at the outer portion, high COL I was deposited

on the outer region and high COL II on the inner region, which is the same with the collagen content of the native meniscus. It was concluded that these constructs could be implanted and tested in animal models, including rabbits and pigs.

In conclusion, the constructs proposed in the current study highly mimic the structural organization and biochemical content of the native meniscus, and could be used to regenerate or replace the meniscectomized menisci.

REFERENCES

- Abdelgaied A, Stanley M, Galfe M, Berry H, Ingham E, Fisher J. Comparison of the biomechanical tensile and compressive properties of decellularised and natural porcine meniscus. *J Biomech.* 2015; 48: 1389-1396.
- Adams M, Hukins D. The extracellular matrix of the meniscus. In: Mow VC, Arnoczky S, Jackson D, eds. *Knee Meniscus: Basic and Clinical Foundations.* New York, Raven Press; 1992; 15-28.
- Adams ME, Muir H. The glycosaminoglycans of canine menisci. *Biochem J.* 1981; 197: 385-389.
- American Academy of Orthopaedic Surgeons Web page. Retrieved December 22, 2017 from <https://www.aaos.org/>
- Angele P, Johnstone B, Kujat R, Zellner J, Nelrich M, Goldberg V, Yoo J. Stem cell based tissue engineering for meniscus repair. *J Biomed Mater Res.* 2008; 85:445-55.
- Annabi N, Tamayol A, Uquillas JA, Akbari M, Bertassoni LE, Cha C, Camci-Unal G, Dokmeci MR, Peppas NA, Khademhosseini A. 25th anniversary article: Rational design and applications of hydrogels in regenerative medicine. *Adv Mater.* 2014; 26: 85-123.
- Arnoczky S. Gross and vascular anatomy of the meniscus and its role in meniscal healing. In: Mow VC, Arnoczky S, Jackson D, eds. *Knee Meniscus: Basic and Clinical Foundations.* New York, Raven Press; 1992; 1-14.
- Arnoczky SP, Warren RF, Spivak JM: Meniscal repair using an exogenous fibrin clot. An experimental study in dogs. *J Bone Joint Surg Am.* 1988; 70:1209-17.
- Arnoczky SP, Warren RF. The microvasculature of the meniscus and its response to injury. An experimental study in the dog. *Am J Sports Med.* 1983; 11:131-41.
- Atala A. Engineering Organs. *Curr Op Biotechnol.* 2009; 20:575-92.
- Aufderheide AC, Athanasiou KA. A direct compression stimulator for articular cartilage and meniscal explants. *Ann Biomed Eng.* 2006; 34: 1463-1474.
- Aufderheide AC, Athanasiou KA. Comparison of scaffolds and culture conditions for tissue engineering of the knee meniscus. *Tissue Eng.* 2005;11:1095-104.
- Azellon Cell Therapeutics Web Page. Retrieved December 22, 2017 from <https://www.azellonctx.com/>

- Babalola OM, Bonassar LJ. Parametric finite element analysis of physical stimuli resulting from mechanical stimulation of tissue engineered cartilage. *J Biomech Eng.* 2009; 131:061014.
- Baek J, Chen X, Sovani S, Jin S, Grogan SP, D'Lima DD. Meniscus tissue engineering using a novel combination of electrospun scaffolds and human meniscus cells embedded within an extracellular matrix hydrogel. *J Orthop Res.* 2015; 33: 572-83.
- Bahcecioglu G, Buyuksungur A, Kiziltay A, Hasirci N, Hasirci V. Construction and in vitro testing of a multilayered, tissue-engineered meniscus. *J Bioact Compat Polym.* 2014;29: 235-253.
- Bahcecioglu G, Hasirci N, Hasirci V. Effects of microarchitecture and mechanical properties of 3D microporous PLLA-PLGA scaffolds on fibrochondrocyte and L929 fibroblast behavior. *Biomed Mater.* 2018. <https://doi.org/10.1088/1748-605X/aaa77f>.
- Baker BM, Shah RP, Huang AH, Mauck RL. Dynamic tensile loading improves the functional properties of mesenchymal stem cell-laden nanofiber-based fibrocartilage. *Tissue Eng.* 2011; 17:1445-55.
- Ballyns JJ, Bonassar LJ. Dynamic compressive loading of image-guided tissue engineered meniscal constructs. *J Biomech.* 2011;44: 509-516.
- Ballyns JJ, Cohen D, Malone E, Maher SA, Potter HG, Wright TM, Lipson H, Bonassar LJ. An optical method for evaluation of geometric fidelity for anatomically shaped tissue engineered constructs. *Tissue Eng Part C Methods.* 2010; 16: 693-703.
- BD Biosciences Web Page. Human and mouse CD marker handbook. Becton, Dickinson, and Company. 2010.
- Bencherif SA, Srinivasan A, Horkay F, Hollinger JO, Matyjaszewski K, Washburn NR. Influence of the degree of methacrylation on hyaluronic acid hydrogels properties. *Biomaterials.* 2008;29:1739-1749.
- Bhargava MM, Attia ET, Murrell GA, Dolan MM, Warren RF, Hannafin JA. The effect of cytokines on the proliferation and migration of bovine meniscal cells. *Am J Sports Med.* 1999; 27:636-43.
- Bian L, Fong JV, Lima EG, Stoker AM, Ateshian GA, Cook JL, Hung CT. Dynamic mechanical loading enhances functional properties of tissue engineered cartilage using mature canine chondrocytes. *Tissue Eng Part A.* 2010; 16:1781-1790.
- Bilgen B, Chu D, Stefani R, Aaron RK. Design of a biaxial mechanical loading bioreactor for tissue engineering. *J Vis Exp.* 2013; 74: e50387.
- Birk DE, Silver FH, Trelstad RL. Matrix assembly. In: Hay ED, ed. *The Cell Biology of the Extracellular Matrix*. 2nd ed. New York, Academic Press; 1991.

- Boere KW, Visser J, Seyednejad H, Rahimian S, Gawlitta D, van Steenberg MJ, *et al.* Covalent attachment of a three-dimensionally printed thermoplast to a gelatin hydrogel for mechanically enhanced cartilage constructs. *Acta Biomater.* 2014; 10: 2602-2611.
- Bostman OM. Absorbable implants for the fixation of fractures. *J Bone Joint Surg.* 1991; 73:148-53.
- Branco da Cunha C, Klumpers DD, Li WA, Koshy ST, Weaver JC, Chaudhuri O, Granja PL, Mooney DJ. Influence of the stiffness of three-dimensional alginate/collagen-I interpenetrating networks on fibroblast biology *Biomaterials.* 2014; 35: 8927-8936.
- Brophy RH, Cottrell J, Rodeo SA, Wright TM, Warren RF, Maher SA. Implantation of a synthetic meniscal scaffold improves joint contact mechanics in a partial meniscectomy cadaver model. *J Biomed Mater Res A.* 2010;92(3):1154-61.
- Brown TD, Dalton PD, Hutmacher DW. Melt electrospinning today: An opportune time for an emerging polymer process. *Progress Polym Sci.* 2016; 56: 116-166.
- Brunger JM, Huynh NPT, Guenther CM, Perez-Pinera P, Moutos FT, Sanchez-Adams J, Gersbach CA, Guilak F. Scaffold-mediated lentiviral transduction for functional tissue engineering of cartilage. *Proc Natl Acad Sci USA.* 2014; 111: E798-E806.
- Bruns J, Kahrs J, Kampen J, Behrens P, Plitz W. Autologous perichondral tissue for meniscal replacement. *J Bone Jt Surg Br.* 1998; 80:918-23.
- Bruns J, Kampen J, Kahrs J, Plitz W. Autologous meniscus replacement with rib perichondrium. Experimental results. *Orthopade.* 2000; 29:145-50.
- Buckley CT, Thorpe SD, O'Brien FJ, Robinson AJ, Kelly DJ. The effect of concentration, thermal history and cell seeding density on the initial mechanical properties of agarose hydrogels. *J Mech Behav Biomed Mater.* 2009;2: 512-521.
- Buma P, Ramrattan NN, van Tienen TG, Veth RPH. Tissue engineering of the meniscus. *Biomaterials.* 2004; 25:1523-32.
- Buyuksungur S, Endogan Tanir T, Buyuksungur A, Bektas EI, Torun Kose G, Yucel D, Beyzadeoglu T, Cetinkaya E, Yenigun C, Tönük E, Hasirci V, Hasirci N. 3D printed poly(ϵ -caprolactone) scaffolds modified with hydroxyapatite and poly(propylene fumarate) and their effects on the healing of rabbit femur defects. *Biomater Sci.* 2017; 5(10): 2144-2158.
- Cengiz IF, Pitikakis M, Cesario L, Parascandolo P, Vosilla L, Viano G, Oliveira JM, Reis RL. Building the basis for patient-specific meniscal scaffolds: From human knee MRI to fabrication of 3D printed scaffolds. *Bioprinting.* 2016; 1–2: 1-10.

- Chan V, Zorlutuna P, Jeong JH, Kong H, Bashir R. Three-dimensional photopatterning of hydrogels using stereolithography for long-term cell encapsulation. *Lab Chip*. 2010;10(16):2062-70.
- Chang CC, Boland ED, Williams SK, Hoying JB. Direct-write bioprinting three-dimensional biohybrid systems for future regenerative therapies. *J Biomed Mater Res B Appl Biomater*. 2011;98(1):160-70.
- Cheung HS. Distribution of type I, II, III and V in the pepsin solubilized collagens in bovine menisci. *Connect Tissue Res*, 1987; 16:343-56.
- Chia HN, Hull ML. Compressive moduli of the human medial meniscus in the axial and radial directions at equilibrium and at a physiological strain rate. *J Orthop Res*. 2008;26(7):951-6.
- Chiari C, Koller U, Dorotka R, Eder C, Plasenzotti R, Lang S, Ambrosio L, Tognana E, Kon E, Salter D, Nehrer S. A tissue engineering approach to meniscus regeneration in a sheep model. *Osteoarthritis Cartilage*. 2006;14(10):1056-65.
- Chung C, Beecham M, Mauck RL, Burdick JA. The influence of degradation characteristics of hyaluronic acid hydrogels on in vitro neocartilage formation by mesenchymal stem cells. *Biomaterials*. 2009;30:4287-4296.
- Cohen DL, Malone, E, Lipson H, Bonassar LJ. Direct freeform fabrication of seeded hydrogels in arbitrary geometries. *Tissue Eng*. 2006; 12:1325-35.
- Collier S, Ghosh P. Effects of transforming growth factor beta on proteoglycan synthesis by cell and explant cultures derived from the knee joint meniscus. *Osteoarthritis Cartilage*. 1995; 3:127-38.
- Cook JL, Tomlinson JL, Kreeger JM, Cook CR. Induction of meniscal regeneration in dogs using a novel biomaterial. *Am J Sports Med*. 1999; 27:658-65.
- Daly AC, Critchley SE, Rencsok EM, Kelly DJ. A comparison of different bioinks for 3D bioprinting of fibrocartilage and hyaline cartilage. *Biofabrication*. 2016; 8(4):045002.
- de Groot J. Actifit, Polyurethane meniscus implant: basic science. *The Meniscus*. Springer-Verlag. Berlin, Heidelberg. 2010. pp. 383-387.
- de Groot JH, Nijenhuis AJ, Bruin P, Pennings AJ, Veth RPH, Klompmaker J, Jansen HWB. Use of porous biodegradable polymer implants in meniscus reconstruction. 1) Preparation of porous biodegradable polyurethanes for the reconstruction of meniscus lesions. *Colloid and Polymer Science*. 1990; 268: 1073–1081.
- Demange M, Gomoll AH. The use of osteochondral allografts in the management of cartilage defects. *Curr Rev Musculoskelet Med*. 2012; 5:229–35.
- Dienst, M, Greis PE, Ellis BJ, Bachus KN, Burks RT. Effect of lateral meniscal allograft sizing on contact mechanics of the lateral tibial plateau: an

- experimental study in human cadaveric knee joints. *Am J Sports Med.* 2007; 35:34-42.
- Donnelly PE, Chen T, Finch A, Brial C, Maher SA, Torzilli PA. Photocrosslinked tyramine-substituted hyaluronate hydrogels with tunable mechanical properties improve immediate tissue-hydrogel interfacial strength in articular cartilage. *J Biomater Sci Polym Ed.* 2017; 28: 582-600.
- Drengk A, Sturmer KM, Frosch KH. Current concepts in meniscus tissue engineering. *Current Rheumatology Reviews.* 2008; 4:196-201.
- Efe T, Getgood A, Schofer MD, Fuchs-Winkelmann S, Mann D, Paletta JR, Heyse TJ. The safety and short-term efficacy of a novel polyurethane meniscal scaffold for the treatment of segmental medial meniscus deficiency. *Knee Surg Sports Traumatol Arthrosc.* 2012; 20:1822-30.
- Eke G, Mangir N, Hasirci N, MacNeil S, Hasirci V. Development of a UV crosslinked biodegradable hydrogel containing adipose derived stem cells to promote vascularization for skin wounds and tissue engineering. *Biomaterials.* 2017; 129: 188-198.
- Elsner JJ, Portnoy S, Zur G, Guilak F, Shterling A, Linder-Ganz E. Design of a free-floating polycarbonate-urethane meniscal implant using finite element modeling and experimental validation. *J Biomech Eng.* 2010; 132:095001.
- Ermis M, Akkaynak D, Chen P, Demirci U, Hasirci V. A high throughput approach for analysis of cell nuclear deformability at single cell level. *Scientific Reports.* 2016; 6: 36917.
- Eyre DR, Wu JJ. Collagen of fibrocartilage: a distinctive molecular phenotype in bovine meniscus. *FEBS Lett.* 1983; 158:265-70.
- Farr J, Cole B, Dhawan A, Kercher J, Sherman S. Clinical cartilage restoration: evolution and overview. *Clin Orthop Relat Res.* 2011; 469:2696–705.
- Fischenich KM, Boncella K, Lewis JT, Bailey TS, Haut Donahue TL. Dynamic compression of human and ovine meniscal tissue compared with a potential thermoplastic elastomer hydrogel replacement. *J Biomed Mater Res A.* 2017; 105(10): 2722-2728.
- Fithian DC, Kelly MA, Mow VC. Material properties and structurefunction relationship in the menisci. *Clin Orthop.* 1990; 25:19-31.
- Freutel M, Seitz AM, Galbusera F, Bornstedt A, Rasche V, Knothe Tate ML, *et al.* Medial meniscal displacement and strain in three dimensions under compressive loads: MR assessment. *J Magn Reson Imaging.* 2014;40: 1181-1188.
- Furthmayr H, Timpl R. Immunochemistry of collagens and procollagens. *Int Rev Connect Tissue Res.* 1976; 7:61-99.

- Gao J, Wei S, Messner K. Healing of the anterior attachment of the rabbit meniscus to bone. *Clin Orthop*. 1998; 348:246-58.
- Gao S, Guo W, Chen M, Yuan Z, Wang M, Zhang Y, Liu S, Xi T, Guo Q. Fabrication and characterization of electrospun nanofibers composed of decellularized meniscus extracellular matrix and polycaprolactone for meniscus tissue engineering. *J Mater Chem B*, 2017; 5: 2273-2285.
- Gao S, Yuan ZG, Xi TF, Wei XJ, Guo QY. Characterization of decellularized scaffold derived from porcine meniscus for tissue engineering applications. *Front. Mater. Sci.*, 2016: 10:101–112.
- Ghadially FN, Lalonde JM, Wedge JH. Ultrastructure of normal and torn menisci of the human knee joint. *J Anat*. 1983; 136:773-91.
- Ghadially FN, Thomas I, Yong N, Lalonde JM. Ultrastructure of rabbit semilunar cartilages. *J Anat*. 1978; 125: 499–517.
- Ghassemi S, Meacci G, Liu S, Gondarenko AA, Mathur A, Roca-Cusachs P, *et al*. Cells test substrate rigidity by local contractions on submicrometer pillars. *Proc Natl Acad Sci USA*. 2012;109: 5328-5333.
- Glennon-Alty L, Williams R, Dixon S, Murray P. Induction of mesenchymal stem cell chondrogenesis by polyacrylate substrates. *Acta Biomater*. 2013; 9(4): 6041-51.
- Gorgieva S, Kokol V. Collagen- vs. gelatine-based biomaterials and their biocompatibility: Review and perspectives. INTECH Open Access Publisher, 2011.
- Greis PE, Bardana DD, Holmstrom MC, Burks RT. Meniscal injury: I. Basic science and evaluation. *J Am Acad Orthop Surg*. 2002; 10:168-76.
- Grogan SP, Chung PH, Soman P, Chen P, Lotz MK, Chen S, *et al*. Digital micromirror device projection printing system for meniscus tissue engineering. *Acta Biomater*. 2013; 9: 7218-7226.
- Gruber HE, Mauerhan D, Chow Y, Ingram JA, Norton HJ, Hanley Jr EN, Sun Y. Three-dimensional culture of human meniscal cells: extracellular matrix and proteoglycan production. *BMC Biotechnol*. 2008; 8:54-60.
- Gunja NJ, Athanasiou KA. Effects of co-cultures of meniscus cells and articular chondrocytes on PLLA scaffolds. *Biotechnol Bioeng*. 2009; 103:808-16.
- Gunja NJ, Uthamanthil RK, Athanasiou KA. Effects of TGF-beta1 and hydrostatic pressure on meniscus cell-seeded scaffolds. *Biomaterials*. 2009; 30:565-73.
- Guvendiren M, Molde J, Soares RM, Kohn J. Designing biomaterials for 3D printing. *ACS Biomater Sci Eng*. 2016; 2: 1679-1693.

- Hachet E, Van Den Berghe H, Bayma E, Block MR, Auzély-Velty R. Design of biomimetic cell-interactive substrates using hyaluronic acid hydrogels with tunable mechanical properties. *Biomacromolecules*. 2012; 13: 1818-1827.
- Halili AN, Hasirci N, Hasirci V. A multilayer tissue engineered meniscus substitute. *Journal of Materials Science: Materials in Medicine*. 2014;25 (4):1195-1209.
- Han WM, Heo SJ, Driscoll TP, Delucca JF, McLeod CM, Smith LJ, Duncan RL, Mauck RL, Elliott DM. Microstructural heterogeneity directs micromechanics and mechanobiology in native and engineered fibrocartilage. *Nat Mater*. 2016; 15(4): 477-84.
- Harley BA, Leung JH, Silva ECCM, Gibson LJ. Mechanical characterization of collagen-glycosaminoglycan scaffolds. *Acta Biomaterialia*. 2007; 3:463-74.
- Harston A, Nyland J, Brand E, McGinnis M, Caborn DN. Collagen meniscus implantation: a systematic review including rehabilitation and return to sports activity. *Knee Surg Sports Traumatol Arthrosc*. 2012;20(1):135-146.
- Hasirci N, Kilic C, Kömez A, Bahcecioglu G, Hasirci V. Hydrogels in regenerative medicine. In: *GELS HANDBOOK: Fundamentals, Properties and Applications. Volume 2- Applications of Hydrogels in Regenerative Medicine. Volume Eds: Abidin MR, Gurkan UA, Edalat F. Eds: Demirci U, Khademhosseini A. World Scientific Publishing. Singapore. 2016.*
- Hasturk O, Sivas A, Karasozen B, Demirci U, Hasirci N, Hasirci V. Quantification of Type, Timing, and Extent of Cell Body and Nucleus Deformations Caused by the Dimensions and Hydrophilicity of Square Prism Micropillars. *Adv Healthc Mater*. 2016; 5(23): 2972-2982.
- Hayes JC, Curley C, Tierney P, Kennedy JE. Biomechanical analysis of a salt-modified polyvinyl alcohol hydrogel for knee meniscus applications, including comparison with human donor samples. 2016; 56: 156-164.
- Heijkants RG, van Calck RV, de Groot JH, Pennings AJ, Schuuten AJ, van Tienen TG, Ramrattan N, Buma P, Veth RP. Design, synthesis and properties of a degradable polyurethane scaffold for meniscus regeneration. *J Mater Sci Mater Med* 2004; 15: 423-7.
- Hellio Le Graverand MP, Ou Y, Schield-Yee T, Barclay L, Hart D, Natsume T, Rattner JB. The cells of the rabbit meniscus: their arrangement, interrelationship, morphological and cytoarchitecture. *J Anat*. 2001; 198:525-35.
- Heo J, Koh RH, Shim W, Kim HD, Yim HG, Hwang NS. Riboflavin-induced photocrosslinking of collagen hydrogel and its application in meniscus tissue engineering. *Drug Deliv Transl Res*. 2016;6(2):148-158.
- Herwig J, Egner E, Buddecke. Chemical changes of human knee joint menisci in various stages of degeneration. *Ann Rheum Dis* 1984; 43: 635-640.

- Ho ST, Yang Z, Hui HP, Oh KW, Choo BH, Lee EH. A serum free approach towards the conservation of chondrogenic phenotype during in vitro cell expansion. *Growth Factors*. 2009; 27: 321-33.
- Hoch E, Schuh C, Hirth T, Hirth T, Tovar GE, Borchers K. Stiff gelatin hydrogels can be photo-chemically synthesized from low viscous gelatin solutions using molecularly functionalized gelatin with a high degree of methacrylation. *J Mater Sci Mater Med*. 2012; 23: 2607–2617.
- Hollander AP, Heathfield TF, Webber C, Iwata Y, Bourne R, Rorabeck C, *et al*. Increased damage to type II collagen in osteoarthritic articular cartilage detected by a new immunoassay. *J Clin Invest*. 1994; 93: 1722-1732.
- Holloway JL, Lowman AM, Palmese GR. Mechanical evaluation of poly(vinyl alcohol)-based fibrous composites as biomaterials for meniscal tissue replacement. *Acta Biomaterialia*. 2010; 6:4716-24.
- Hölzl K, Lin S, Tytgat L, Van Vlierberghe S, Gu L, Ovsianikov A. Bioink properties before, during and after 3D bioprinting. *Biofabrication*. 2016; 8(3): 032002.
- Huey DJ, Athanasiou KA. Tension-compression loading with chemical stimulation results in additive increases to functional properties of anatomic meniscal constructs. *PLoS ONE*. 2011;6: e27857.
- Hutmacher DW, Dalton PD. Melt electrospinning. *Chem Asian J*. 2011;6(1):44-56.
- Hutmacher DW. Scaffolds in tissue engineering bone and cartilage. *Biomaterials*. 2000; 21:2529-43.
- Imler SM. In vitro modulation of meniscus biosynthesis: a basis for understanding cellular response to physiologically relevant stimuli. PhD thesis. Georgia Institute of Technology. USA. 2005.
- Jang J, Park JY, Gao G, Cho DW. Biomaterials-based 3D cell printing for next-generation therapeutics and diagnostics. *Biomaterials* 2018; 156: 88-106.
- Johnson LL, Feagin JA Jr. Autogenous tendon graft substitution for absent knee joint meniscus: a pilot study. *Arthroscopy*. 2000;16(2):191-6.
- Joshi MD, Suh JK, Marui T, Woo SL. Interspecies variation of compressive biomechanical properties of the meniscus. *J Biomed Mater Res*. 1995; 29: 823-28.
- Joshi MK, Pant HR, Tiwari PA, Kim HJ, Park CH, Kim CS. Multi-layered macroporous three-dimensional nanofibrous scaffold via a novel gas foaming technique. *Chem Eng J*. 2015; 275: 79-88.
- Kalpakci KN, Kim EJ, Athanasiou KA. Assessment of growth factor treatment on fibrochondrocyte and chondrocyte co-cultures for TMJ fibrocartilage engineering. *Acta Biomater*. 2011;7(4):1710-1718.

- Karim A, Hall AC. Chondrocyte morphology in stiff and soft agarose gels and the influence of fetal calf serum. *J Cell Physiol.* 2016;5: 1041-1052. doi: 10.1002/jcp.25507.
- Kelly BT, Robertson W, Potter HG, Deng XH, Turner AS, Lyman S, Warren RF, Rodeo SA. Hydrogel meniscal replacement in the sheep knee: preliminary evaluation of chondroprotective effects. *Am J Sports Med.* 2007; 35(1) :43–52.
- Kilic Bektas C, Hasirci V. Mimicking corneal stroma using keratocyte loaded photopolymerizable methacrylated gelatin hydrogels. *J Tissue Eng Regen Med.* 2017. DOI: 10.1002/term.2621.
- Kim BS, Mooney DJ. Development of biocompatible synthetic extracellular matrices for tissue engineering. *Trends Biotechnol.* 1998; 16:224-30.
- Kisiday JD, Jin M, DiMicco MA, Kurz B, Grodzinsky AJ. Effects of dynamic compressive loading on chondrocyte biosynthesis in self-assembling peptide scaffolds. *J Biomech.* 2004; 37: 595-604.
- Kisiday JD, Lee JH, Siparsky PN, Frisbie DD, Flannery CR, Sandy JD, Grodzinsky AJ. Catabolic responses of chondrocyte-seeded peptide hydrogel to dynamic compression. *Ann Biomed Eng.* 2009; 37: 1368-1375.
- Kobayashi M, Toguchida J, Oka M. Development of an artificial meniscus using polyvinyl alcohol hydrogel for early return to, and continuance of, athletic life in sportspersons with severe meniscus injury, I: mechanical evaluation. *Knee.* 2003; 10:47-51.
- Kobayashi MI, Chang YS, Oka M. A two year in vivo study of polyvinyl alcohol-hydrogel (PVA-H) artificial meniscus. *Biomaterials.* 2005;26(16):3243-8.
- Kohn D, Wirth CJ, Reiss G, Plitz W, Maschek H, Erhardt W, Wulker N. Medial meniscus replacement by a tendon autograft. Experiments in sheep. *J Bone Jt Surg Br.* 1992; 74:910-7.
- Komez A, Baran ET, Erdem U, Hasirci N, Hasirci V. Construction of a patterned hydrogel-fibrous mat bilayer structure to mimic choroid and Bruch's membrane layers of retina. *J Biomed Mater Res Part A.* 2016;104(9): 2166-2177.
- Kon E, Chiari C, Marcacci M, Delcogliano M, Salter DM, Martin I, Ambrosio L, Fini M, Tschon M, Tognana E, Plasenzotti R, Nehrer S. Tissue engineering for total meniscal substitution: animal study in sheep model. *Tissue Eng.* 2008; 14:1067-80.
- Kon E, Filardo G, Tschon M, Fini M, Giavaresi G, Marchesini Reggiani L, Chiari C, Nehrer S, Martin I, Salter DM, Ambrosio L, Marcacci M. Tissue engineering for total meniscal substitution: animal study in sheep model--results at 12 months. *Tissue Eng Part A.* 2012;18(15-16):1573-82.
- Krouwels A, Melchels FPW, van Rijen MHP, Ten Brink CBM, Dhert WJA, Cumhur Öner F, *et al.* Focal adhesion signaling affects regeneration by human nucleus

- pulposus cells in collagen- but not carbohydrate-based hydrogels. *Acta Biomater.* 2017. pii: S1742-7061(17)30713-4. doi:10.1016/j.actbio.2017.11.029. (Epub ahead of print).
- Kuhn JE, Wojtys EM. Allograft meniscus transplantation. *Clin Sports Med.* 1996; 15:537-46.
- Lake SP, Barocas VH. Mechanical and structural contribution of non-fibrillar matrix in uniaxial tension: a collagen-agarose co-gel model. *Ann Biomed Eng.* 2011;39: 1891-1903.
- Langer R, Vacanti JP. Tissue engineering. *Science.* 1993; 260:920-26.
- Lee CH, Rodeo SA, Fortier LA, Lu C, Erisken C, Mao JJ. Protein-releasing polymeric scaffolds induce fibrochondrocytic differentiation of endogenous cells for knee meniscus regeneration in sheep. *Sci Transl Med.* 2014; 6(266):266ra171.
- Lee SB, Kim YH, Chong MS, Hong SH, Lee YM. Study of gelatin-containing artificial skin V: fabrication of gelatin scaffolds using a salt-leaching method. *Biomaterials* 2005; 26:1961-1968.
- Lee YH, Lee JH, An IG, Kim C, Lee DS, Lee YK, Nam JD. Electrospun dual-porosity structure and biodegradation morphology of Montmorillonite reinforced PLLA nanocomposite scaffolds. *Biomaterials.* 2005; 26: 3165-3172.
- Levett PA, Hutmacher DW, Malda J, Klein TJ. Hyaluronic acid enhances the mechanical properties of tissue-engineered cartilage constructs. *PLoS ONE.* 2014; 9: e113216.
- Levett PA, Hutmacher DW, Malda J, Klein TJ. Hyaluronic acid enhances the mechanical properties of tissue-engineered cartilage constructs. *PLoS ONE.* 2014;9: e113216.
- Li J. Biofabrication and characterization of meniscal scaffolds via an electrohydrodynamic jet printing technique. Ph.D. Dissertation. National University of Singapore; Singapore: 2014.
- Li Z, Peng Z, Teng J, Wang Y. Experimental Study of Damage Evolution in Circular Stirrup-Confined Concrete. *Materials (Basel).* 2016; 9(4). pii: E278.
- Linder-Ganz E, Elsner JJ, Danino A, Guilak F, Shterling A. A novel quantitative approach for evaluating contact mechanics of meniscal replacements. *J Biomech Eng.* 2010; 132 :024501.
- Liu Y, Chan-Park MB. A biomimetic hydrogel based on methacrylated dextran-graft-lysine and gelatin for 3D smooth muscle cell culture. *Biomaterials.* 2010;31: 1158-1170.

- Lohmander LS, Englund PM, Dahl LL, Roos EM. The long-term consequence of anterior cruciate ligament and meniscus injuries: osteoarthritis. *Am J Sports Med.* 2007;35: 1756-1769.
- Lynn AK, Yannas LV, Bonfield W. Antigenicity and immunogenicity of collagen. *J Biomed Mater Res B: Appl Biomater* 2004; 71: 343-354.
- Maher SA, Rodeo SA, Doty SB, Brophy R, Potter H, Foo LF, Rosenblatt L, Deng XH, Turner AS, Wright TM, Warren RF. Evaluation of a porous polyurethane scaffold in a partial meniscal defect ovine model. *Arthroscopy.* 2010; 26(11): 1510-9.
- Maier D, Braeun K, Steinhauser E, Ueblacker P, Oberst M, Kreuz PC, Roos N, Martinek V, Imhoff AB. In vitro analysis of an allogenic scaffold for tissue-engineered meniscus replacement. *J Orthop Res.* 2007; 25:1598–1608.
- Makris EA, Hadidi P, Athanasiou KA. The knee meniscus: structure-function, pathophysiology, current repair techniques, and prospects for regeneration. *Biomaterials.* 2011; 32:7411–7431.
- Mandal BB, Park SH, Gil ES, Kaplan DL. Multilayered silk scaffolds for meniscus tissue engineering. *Biomaterials.* 2011a; 32:639-51.
- Mandal BB, Park SH, Gil ES, Kaplan DL. Stem cell-based meniscus tissue engineering. *Tissue Eng.* 2011b.
- Marsano A, Vunjak-Novakovic G, Martin I. Towards tissue engineering of meniscus substitutes: selection of cell source and culture environment. *Conf Proc IEEE Eng Med Biol Soc.* 2006; 1:3656-8.
- Martinek V, Ueblacker P, Braun K, Nitschke S, Mannhardt R, Specht K, Gansbacher B, Imhoff AB. Second generation of meniscus transplantation: in-vivo study with tissue engineered meniscus replacement. *Arch Orthop Trauma Surg.* 2006; 126:228-34.
- Mauck RL, Byers BA, Yuan X, Tuan RS. Regulation of cartilaginous ECM gene transcription by chondrocytes and MSCs in 3D culture in response to dynamic loading. *Biomech Model Mechanobiol.* 2007; 6:113- 125.
- Maurer PH. II. Antigenicity of gelatin in rabbits and other species. *J Exp Med.* 1954; 100: 515-523.
- McCorry MC, Puetzer JL, Bonassar LJ. Characterization of mesenchymal stem cells and fibrochondrocytes in three-dimensional co-culture: analysis of cell shape, matrix production, and mechanical performance. *Stem Cell Res Ther.* 2016;7: 39.
- McDermott, ID, Masouros SD, Amis AA. Biomechanics of the menisci of the knee. *Current Orthopaedics.* 2008; 22:193-201.

- McDevitt CA, Webber RJ. The ultrastructure and biochemistry of meniscal cartilage. *Clin Orthop*. 1990; 8-18.
- Medtech Insight Web Page. Retrieved December 22, 2017 from <https://medtech.pharmaintelligence.informa.com/>
- Messner K, Gillquist J. Prosthetic replacement of the rabbit medial meniscus. *J Biomed Mater Res*. 1993;27(9):1165-73.
- Messner, K. Meniscal substitution with a Teflon-periosteal composite graft: a rabbit experiment. *Biomaterials*. 1994; 15:223-30.
- Meyers E, Zhu W, Mow V. Viscoelastic properties of articular cartilage and meniscus. In: Nimni M, ed. *Collagen: Chemistry, Biology and Biotechnology*. FL, Boca Raton, CRC; 1988.
- Moradi L, Vasei M, Dehghan MM, Majidi M, Farzad Mohajeri S, Bonakdar S. Regeneration of meniscus tissue using adipose mesenchymal stem cells-chondrocytes co-culture on a hybrid scaffold: In vivo study. *Biomaterials*. 2017; 126: 18-30.
- Moroni L, Lambersb FM, Wilsonb W, van Donkelaarb CC, de Wijna JR, Huiskeb R, van Blitterswijk CA. Finite Element Analysis of Meniscal Anatomical 3D Scaffolds: Implications for Tissue Engineering. *Open Biomed Eng J* 2007; 1:23-34.
- Mueller SM, Schneider TO, Shortkroff S, Breinan HA, Spector M. Alpha-smooth muscle actin and contractile behavior of bovine meniscus cells seeded in type I and type II collagen-GAG matrices. *J Biomed Mater Res*. 1999;45(3):157-66.
- Murakami T, Otsuki S, Nakagawa K, Okamoto Y, Inoue T, Sakamoto Y, Sato H, Neo M. Establishment of novel meniscal scaffold structures using polyglycolic and poly-l-lactic acids. *J Biomater Appl*. 2017; 32: 150-161.
- Murphy CM, Haugh MG, O'Brien FJ. The effect of mean pore size on cell attachment, proliferation and migration in collagen-glycosaminoglycan scaffolds for bone tissue engineering. *Biomaterials*. 2010; 31: 461-466.
- Nam YS, Yoon JJ, Park TG. A novel fabrication method of macroporous biodegradable polymer scaffolds using gas foaming salt as a porogen additive. *J Biomed Mater Res*. 2000;53(1):1-7.
- Naqvi T, Duong TT, Hashem G, Shiga M, Zhang Q, Kapila S. Relaxin's induction of metalloproteinases is associated with the loss of collagen and glycosaminoglycans in synovial joint fibrocartilaginous explants. *Arthritis Res Ther*. 2005;7: R1-11.
- Ndreu A. Electrospun nanofibrous scaffolds for tissue engineering. Master's Thesis. Middle East Technical University, Ankara: 2007.

- Necas J, Bartosikova L, Brauner P, Kolar J. Hyaluronic acid (hyaluronan): a review. *Vet Med-Czech*. 2008;53: 397-411.
- Nerurkar NL, Han W, Mauck RL, Elliot DL. Homologous structure-function relationships between native fibrocartilage and tissue engineered from MSC-seeded nanofibrous scaffold. *Biomaterials*. 2011; 32:461-8.
- Newman AP, Anderson DR, Daniels AU, Dales MC. Mechanics of the healed meniscus in a canine model. *Am J Sports Med*. 1989; 17:164-75.
- Nichol JW, Koshy ST, Bae H, Hwang CM, Yamanlar S, Khademhosseini A. Cell-laden microengineered gelatin methacrylate hydrogels. *Biomaterials*. 2010; 31: 5536-5544.
- Noyes FR, Barber-Westin SD. Arthroscopic repair of meniscal tears extending into the avascular zone in patients younger than twenty years of age. *Am J Sports Med*. 2002;30: 589-600.
- Park SA, Lee SH, Kim WD. Fabrication of porous polycaprolactone/hydroxyapatite (PCL/HA) blend scaffolds using a 3D plotting system for bone tissue engineering. *Bioprocess Biosyst Eng*. 2011; 34: 505–513.
- Patel JM, Merriam AR, Culp BM, Gatt CJ Jr, Dunn MG. One-Year Outcomes of Total Meniscus Reconstruction Using a Novel Fiber-Reinforced Scaffold in an Ovine Model. *Am J Sports Med*. 2016; 44(4):898-907.
- Paul JP. Force actions transmitted by joints in the human body. *Proc R Soc Lond B Biol Sci*. 1976; 192:163-72.
- Petersen W, Tillmann B. Collagenous fibril texture of the human knee joint menisci. *Anal Embryol*. 1998; 197:317-24.
- Petri M, Ufer K, Toma I, Becher C, Lioudakis E, Brand S, *et al*. Effects of perfusion and cyclic compression on in vitro tissue engineered meniscus implants. *Knee Surg Sports Traumatol Arthrosc*. 2012;20: 223-231.
- Pfeifer CG, Berner A, Koch M, Krutsch W, Kujat R, Angele P, Nerlich M, Zellner J. Higher ratios of hyaluronic acid enhance chondrogenic differentiation of human MSCs in a hyaluronic acid-gelatin composite scaffold. *Materials*. 2016;9(5):381; doi:10.3390/ma9050381.
- Puetzer JL, Ballyns JJ, Bonassar LJ. The effect of the duration of mechanical stimulation and post-stimulation culture on the structure and properties of dynamically compressed tissue-engineered menisci. *Tissue Eng Part A*. 2012;18: 1365-1375.
- Puetzer JL, Koo E, Bonassar LJ. Induction of fiber alignment and mechanical anisotropy in tissue engineered menisci with mechanical anchoring. *J Biomech*. 2015; 48: 1436-1443.

- Rath E, Richmond JC, Yassir W, Albright JD, Gundogan F. Meniscal allograft transplantation. Two- to eight-year results. *Am J Sports Med.* 2001; 29:410-4.
- Rhee S, Puetzer JL, Mason BN, Reinhart-King CA, Bonassar LJ. 3D bioprinting of spatially heterogeneous collagen constructs for cartilage tissue engineering. *ACS Biomater Sci Eng.* 2016; 2: 1800–1805.
- Rodkey WG, DeHaven KE, Montgomery WH 3rd, Baker CL Jr, Beck CL Jr, Hormel SE, Steadman JR, Cole BJ, Briggs KK. Comparison of the collagen meniscus implant to partial meniscectomy: a prospective randomized trial. *J Bone Joint Surg Am.* 2008; 90:1413-26.
- Rodkey WG, DeHaven KE, Montgomery WH, III, Baker CL, Jr, Beck CL, Jr, Hormel SE, Steadman JR, Cole BJ, Briggs KK. Comparison of the collagen meniscus implant with partial meniscectomy. A prospective randomized trial. *J Bone Joint Surg Am.* 2008; 90:1413–26.
- Sanchez-Adams J, Willard VP, Athanasiou KA. Regional variation in the mechanical role of knee meniscus glycosaminoglycans. *J Appl Physiol.* 2011; 111(6): 1590-1596.
- Sanchez-Adams JI, Wilusz RE, Guilak F. Atomic force microscopy reveals regional variations in the micromechanical properties of the pericellular and extracellular matrices of the meniscus. *J Orthop Res.* 2013;31(8):1218-25.
- Sarem M, Moztafzadeh F, Mozafari M, Shastri VP. Optimization strategies on the structural modeling of gelatin/chitosan scaffolds to mimic human meniscus tissue. *Mater Sci Eng C: Mater Biol Appl.* 2013; 33:4777–4785.
- Schuh E, Hofmann S, Stok KS, Notbohm H, Müller R, Rotter N. The influence of matrix elasticity on chondrocyte behavior in 3D. *J Tissue Eng Regen Med.* 2012;6: e31-42.
- Sears NA, Seshadri DR, Dhavalikar PS, Cosgriff-Hernandez E. A Review of Three-Dimensional Printing in Tissue Engineering. *Tissue Eng Part B Rev.* 2016; 22: 298-310.
- Selimović S, Oh J, Bae H, Dokmeci M, Khademhosseini A. microscale strategies for generating cell-encapsulating hydrogels. *Polymers (Basel).* 2012;4(3):1554.
- Setton LA, Guilak F, Hsu EW, Vail TP. Biomechanical factors in tissue engineered meniscal repair. *Clin Orthop Relat Res.* 1999; 367Suppl:S254-72.
- Shin H, Olsen BD, Khademhosseini A. The mechanical properties and cytotoxicity of cell-laden double-network hydrogels based on photocrosslinkable gelatin and gellan gum biomacromolecules. *Biomaterials.* 2012;33(11):3143-52.
- Shrive NG, O'Connor JJ, Goodfellow JW. Load-bearing in the knee joint. *Clin Orthop Relat Res.* 1978; 131:279-87.

- Sommerlath K, Gillquist J. The effects of an artificial meniscus substitute in a knee joint with a resected anterior cruciate ligament. An experimental study in rabbits. *Clin Orthop*. 1993; 289:276-84.
- Spaans CJ, Belgraver VW, Rienstra O, de Groot JH, Veth RP, Pennings AJ. Solvent-free fabrication of micro-porous polyurethane amide and polyurethane-urea scaffolds for repair and replacement of the knee-joint meniscus. *Biomaterials*, 2000; 21: 2453-2460.
- Stabile KJ, Odom D, Smith TL, Northam C, Whitlock PW, Smith BP, Van Dyke ME, Ferguson CM. An acellular, allograft-derived meniscus scaffold in an ovine model. *Arthroscopy*. 2010; 26:936–948.
- Stapleton TW, Ingram J, Fisher J, Ingham E. Investigation of the regenerative capacity of an acellular porcine medial meniscus for tissue engineering applications. *Tissue Eng Part A*. 2011; 17:231–242.
- Stapleton TW, Ingram J, Katta J, Knight R, Korossis S, Fisher J, Ingham E. Development and characterization of an acellular porcine medial meniscus for use in tissue engineering. *Tissue Eng Part A*. 2008; 14:505–518.
- Steadman JR, Rodkey WG. Tissue-engineered collagen meniscus implants: 5 to 6-year feasibility study results. *Arthroscopy*. 2005; 21:515-25.
- Steward AJ, Wagner DR, Kelly DJ. The pericellular environment regulates cytoskeletal development and the differentiation of mesenchymal stem cells and determines their response to hydrostatic pressure. *Eur Cell Mater*. 2013; 25:167-178.
- Stocco TD, Rodrigues BVM, Marciano FR, Lobo AO. Design of a novel electrospinning setup for the fabrication of biomimetic scaffolds for meniscus tissue engineering applications. 2017; 196: 221-224.
- Stone KR, Ayala G, Goldstein J, Hurst R, Walgenbach A, Galili U. Porcine cartilage transplants in the cynomolgus monkey. III. Transplantation of alpha-galactosidase-treated porcine cartilage. *Transplantation*. 1998; 65:1577–1583.
- Stone KR, Rodkey WG, Webber R, McKinney L, Steadman JR. Future directions: collagen-based prosthesis for meniscal regeneration. *Clin Orthop Relat Res*. 1990; 252:129-35.
- Stone KR, Rodkey WG, Webber R, McKinney L, Steadman JR. Meniscal regeneration with copolymeric collagen scaffolds: in vitro and in vivo studies evaluated clinically, histologically, biochemically. *Am J Sports Med*. 1992; 20:104-11.
- Stone KR, Steadman JR, Rodkey WG, Li ST. Regeneration of meniscal cartilage with use of a collagen scaffold. Analysis of preliminary data. *J Bone Joint Surg Am*. 1997; 79:1770-7.

- Sweigart MA, Zhu CF, Burt DM, *et al.* Intraspecies and interspecies comparison of the compressive properties of the medial meniscus. *Ann Biomed Eng* 2004; 32: 1569–1579.
- Szójka A, Lahl K, Andrews SHJ, Jomha NM, Osswald M, Adesida A. Biomimetic 3D printed scaffolds for meniscus tissue engineering. 2017;8:1-7.
- Szomor ZL, Murrell GAC, Appleyard RC, Tyler MJ. Meniscal repair with a new biological glue: an ex vivo study. *Tech Knee Surg*. 2008;7(4):261–265.
- Tanaka T, Fujii K, Kumagai Y. Comparison of biochemical characteristics of cultured fibrochondrocytes isolated from the inner and outer regions of human meniscus. *Knee Surg Sports Traumatol Arthrosc*. 1999; 7:75-80.
- Tasoglu S, Demirci U. Bioprinting for stem cell research. *Trends Biotechnol*. 2013; 31: 10-9.
- Thermo Fisher Scientific Inc. web page; 2017 [Cited Sep 19, 2017]. Available from <https://www.thermofisher.com/>.
- Tienen TG, Heijkants RGJC, de Groot JH, Pennings AJ, Schouten AJ, Veth RPH, Buma P. Replacement of the knee meniscus by a porous polymer implant. A study in dogs. *Am J Sports Med*. 2006; 34:64-71.
- Tissakht M and Ahmed AM. Tensile stress-strain characteristics of the human meniscal material. *J Biomech* 1995; 28: 411–422.
- Turner BN, Strong R, Gold SA. A review of melt extrusion additive manufacturing processes: I. Process design and modeling. *Rapid Prototyping Journal* 2014, 20 (3), 192–204.
- Ucar S, Yilgor P, Hasirci V, Hasirci N. Chitosan Based Wet Spun Scaffolds for Bioactive Agent Delivery in Bone Tissue Engineering. *J Appl Polym Sci*, 2013; 130: 3759–3769.
- Uchio Y, Ochi M, Adachi N, Kawasaki K, Iwasa J. Results of rasping of meniscal tears with and without anterior cruciate ligament injury as evaluated by second-look arthroscopy. *Arthroscopy*. 2003;19: 463-469.
- Ulrich TA, Jain A, Tanner K, MacKay JL, Kumar S. Probing cellular mechanobiology in three-dimensional culture with collagen-agarose matrices. *Biomaterials*. 2010;31: 1875-1884.
- Van Bochove B, Hannink G, Buma P, Grijpma DW. Preparation of Designed Poly(trimethylene carbonate) Meniscus Implants by Stereolithography: Challenges in Stereolithography. *Macromol Biosci*. 2016;16(12):1853-1863.
- Van Den Bulcke AI, Bogdanov B, De Rooze N, Schacht EH, Cornelissen M, Berghmans H. Structural and rheological properties of methacrylamide modified gelatin hydrogels. *Biomacromolecules*. 2000;1:31-38.

- Van den Steen PE, Dubois B, Nelissen I, Rudd PM, Dwek RA, Opdenakker G. Biochemistry and molecular biology of gelatinase B or matrix metalloproteinase-9 (MMP-9). *Crit Rev Biochem Mol Biol.* 2002;37: 375-536.
- van der Bracht H, Verdonk R, Verbruggen G, Elewaut D, Verdonk P. Cell-based meniscus tissue engineering. In: Ashammakhi N, Reis R, Chiellini E, eds. *Topics in tissue engineering.* 2007.
- Van Der Straeten C, Bytтеbier P, Eeckhoudt A, Victor J. Meniscal allograft transplantation does not prevent or delay progression of knee osteoarthritis. *PLoS ONE.* 2016;11(5): e0156183.
- Vanderploeg EJ, Imler SM, Brodtkin KR, Garcia AJ, Levenston ME. Oscillatory tension differentially modulates matrix metabolism and cytoskeletal organization in chondrocytes and fibrochondrocytes. *J Biomech.* 2004; 37:1941-52.
- Verdonk P, Beaufils P, Bellemans J, Djian P, Heinrichs EL, Huysse W, Laprell H, Siebold R, Verdonk R. Successful treatment of painful irreparable partial meniscal defects with a polyurethane scaffold: two-year safety and clinical outcomes. *Am J Sports Med.* 2012;40(4):844-53.
- Verdonk PC, Forsyth RG, Wang J, Almqvist KF, Verdonk R, Veys EM, Verbruggen G. Characterisation of human knee meniscus cell phenotype. *Osteoarthritis Cartilage.* 2005;13(7):548-60.
- Veth RPH, Jansen HW, Leenslag JW, Pennings AJ, Hartel RM, Nielsen HK. Experimental meniscal lesions reconstructed with a carbon fiber-lolyurethane-poly(L-lactide) graft. *Clin Orthop.* 1986; 202:286-93.
- Visser J, Melchels FP, Jeon JE, van Bussel EM, Kimpton LS, Byrne HM, Dhert WJ, Dalton PD, Hutmacher DW, Malda J. Reinforcement of hydrogels using three-dimensionally printed microfibres. *Nat Commun.* 2015;6:6933.
- Viswanathan G, Murugesan S, Pushparaj V, Nalamasu O, Ajayan PM, Linhardt RJ. Preparation of biopolymer fibers by electrospinning from room temperature ionic liquids. *Biomacromolecules.* 2006;7(2):415-8.
- Vrancken ACT, Madej W, Hannink G, Verdonschot N, van Tienen TG, Buma P. Short term evaluation of an anatomically shaped polycarbonate urethane total meniscus replacement in a goat model. *PLoS ONE.* 2015; 10(7): e0133138.
- Waldman SD, Couto DC, Grynпас MD, Pilliar RM, Kandel RA. Multi-axial mechanical stimulation of tissue engineered cartilage: review. *Eur Cell Mater.* 2007; 13: 66-73; discussion 73-64.
- Walsh CJ, Goodman D, Caplan AI, Goldberg VM. Meniscus regeneration in a rabbit partial meniscectomy model. *Tissue Eng.* 1999; 5:327-37.

- Wataya CH, Jardini ALM, Paschoal G, Bavaresco VP, Zavaglia CAC. Rapid prototype used to personalize PVA meniscus. 15th International Conference on Experimental Mechanics. 2012.
- Webber RJ, Harris MG, Hough Jr AJ. Cell culture of rabbit meniscal fibrochondrocytes: proliferative and synthetic response to growth factors and ascorbate. *J Orthop Res.* 1985; 3:36-42.
- Welsing RT, van Tienen TG, Ramrattan N, Heijkants R, Schouten AJ, Veth RP, Buma P. Effect on tissue differentiation and articular cartilage degradation of a polymer meniscus implant: a 2-year follow-up study in dogs. *Am J Sports Med.* 2008; 36:1978-89.
- Wilson CG, Nishimuta JF, Levenston ME. Chondrocytes and meniscal fibrochondrocytes differentially process aggrecan during de novo extracellular matrix assembly. *Tissue Eng Part A.* 2009;15: 1513-1522.
- Witsch E, Sela M, Yarden Y. Roles for growth factors in cancer progression. *Physiology (Bethesda).* 2010; 25: 85-101.
- Xu T, Binder KW, Albanna MZ, Dice D, Zhao W, Yoo JJ, Atala A. Hybrid printing of mechanically and biologically improved constructs for cartilage tissue engineering applications. *Biofabrication.* 2013; 5: 015001.
- Yan LP, Oliveira JM, Oliveira AL, Caridade SG, Mano JF, Reis RL. Macro/microporous silk fibroin scaffolds with potential for articular cartilage and meniscus tissue engineering applications. *Acta Biomater.* 2012; 8: 289-301.
- Yang F, Tadepalli V, Wiley BJ. 3D Printing of a double network hydrogel with a compression strength and elastic modulus greater than those of cartilage. *ACS Biomater. Sci. Eng.* 2017; 3: 863–869.
- Yang J, Shi G, Bei J, Wang S, Cao Y, Shang Q, Yang G and Wang W Fabrication and surface 482 modification of macroporous poly(L-lactic acid) and poly(L-lactic co-glycolic acid) (70/30) cell 483 scaffolds for human skin fibroblasts cell culture *J. Biomed. Mater. Res.* 2002; 62: 438-446.
- Yasura K, Mizuno Y, Nakagawa Y, Mori K, Takenaka M, Ohashi T, Yamada K, Kobayashi M, Ando K, Kuroki H, Suzuki T, Ikeuchi K, Tsutsumi S, Nakamura T. Estimation of the mechanical property of meniscus using ultrasound: examinations of native meniscus and effects of enzymatic digestion. *J Orthop Res.* 2007;25:884-93.
- Yue K, Trujillo-de Santiago G, Alvarez MM, Tamayol A, Annabi N, Khademhosseini A. Synthesis, properties, and biomedical applications of gelatin methacryloyl (GelMA) hydrogels. *Biomaterials.* 2015;73:254-71.
- Zaffagnini S, Marcheggiani Muccioli GM, Lopomo N, Bruni D, Giordano G, Ravazzolo G, Molinari M, Marcacci M. Prospective long-term outcomes of the medial collagen meniscus implant versus partial medial meniscectomy: a

minimum 10-year follow-up study. *Am J Sports Med.* 2011 May; 39(5):977-85.

Zhang ZZ, Wang SJ, Zhang JY, Jiang WB, Huang AB, Qi YS, Ding JX, Chen XS, Jiang D, Yu JK. 3D-Printed Poly(ϵ -caprolactone) Scaffold Augmented With Mesenchymal Stem Cells for Total Meniscal Substitution: A 12- and 24-Week Animal Study in a Rabbit Model. *Am J Sports Med.* 2017; 45:1497-1511.

Zheng CH, Levenston ME. Fact versus artifact: avoiding erroneous estimates of sulfated glycosaminoglycan content using the dimethylmethylene blue colorimetric assay for tissue-engineered constructs. *Eur Cell Mater.* 2015; 29: 224-36; discussion 236.

Zielinska B, Killian M, Kadmiel M, Nelsen M, Haut Donahue TL. Meniscal tissue explants response depends on level of dynamic compressive strain. *Osteoarthr Cartil.* 2009;17: 754-760.

Zorlutuna P, Elsheikh A, Hasirci V. Nanopatterning of Collagen Scaffolds Improve the Mechanical Properties of Tissue Engineered Vascular Grafts. *Biomacromolecules.* 2009;10(4):814-821.

Zur G, Linder-Ganz E, Elsner JJ, Shani J, Brenner O, Agar G, Hershman EB, Arnoczky SP, Guilak F, Shterling A. Chondroprotective effects of a polycarbonate-urethane meniscal implant: histopathological results in a sheep model. *Knee Surg Sports Traumatol Arthrosc.* 2011; 19: 255–263.

APPENDIX A

ALAMAR BLUE ASSAY

$$\text{Reduction (\%)} = \frac{((\epsilon_{\text{ox}})_{\lambda_2} \times A_{\lambda_1}) - ((\epsilon_{\text{ox}})_{\lambda_1} \times A_{\lambda_2})}{((\epsilon_{\text{red}})_{\lambda_1} \times A'_{\lambda_2}) - ((\epsilon_{\text{red}})_{\lambda_2} \times A'_{\lambda_1})} \times 100$$

where,

$$\lambda_1 = 570 \text{ nm}$$

$$\lambda_2 = 595 \text{ nm}$$

A_{λ_1} and A_{λ_2} = Absorbance of cell seeded films,

A'_{λ_1} and A'_{λ_2} = Absorbance of the negative control (unseeded unpatterned film)

Molar Extinction Coefficients were:

$$(\epsilon_{\text{ox}})_{\lambda_1} = 80.586 \quad (\epsilon_{\text{red}})_{\lambda_1} = 155.677$$

$$(\epsilon_{\text{ox}})_{\lambda_2} = 117.216 \quad (\epsilon_{\text{red}})_{\lambda_2} = 14.652$$

APPENDIX B

STANDARD CURVE FOR DNA QUANTIFICATION

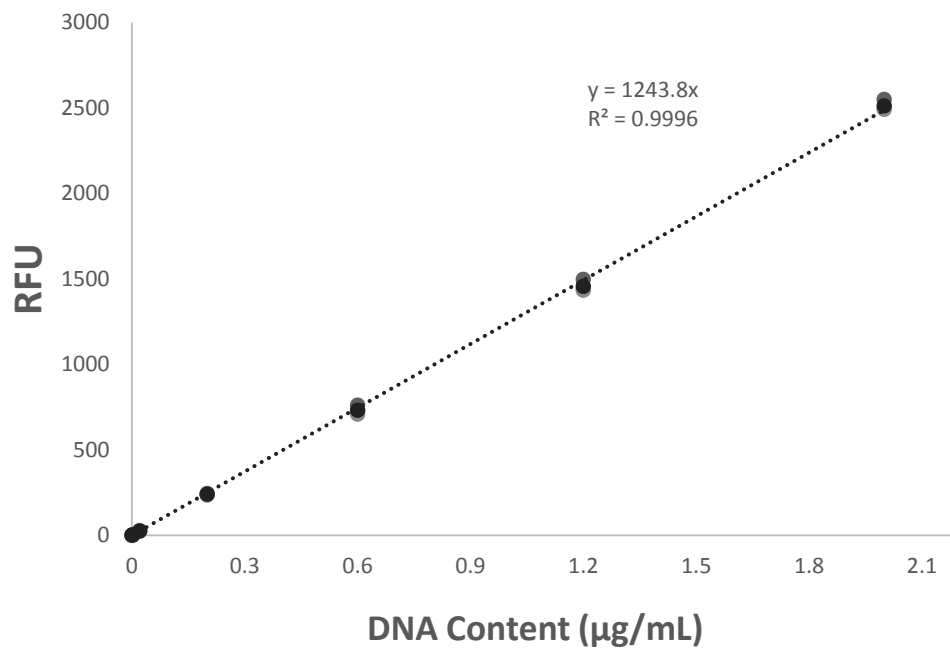


Figure B.1. A representative standard curve for the PicoGreen dsDNA quantification assay. DNA content ($\mu\text{g/mL}$) was plotted against fluorescence intensity (relative fluorescence units (RFU)).

APPENDIX C

STANDARD CURVE FOR sGAG QUANTIFICATION

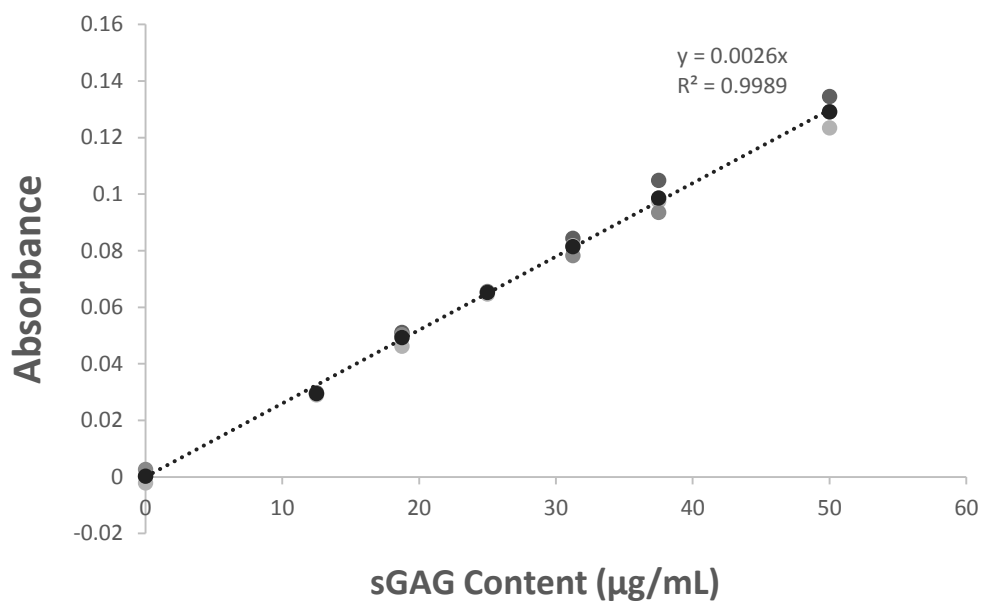


Figure C.1. A representative standard curve for the DMMB assay. Sulfated GAG content (µg/mL) was plotted against absorbance value.

APPENDIX D

STANDARD CURVE FOR COLLAGEN QUANTIFICATION

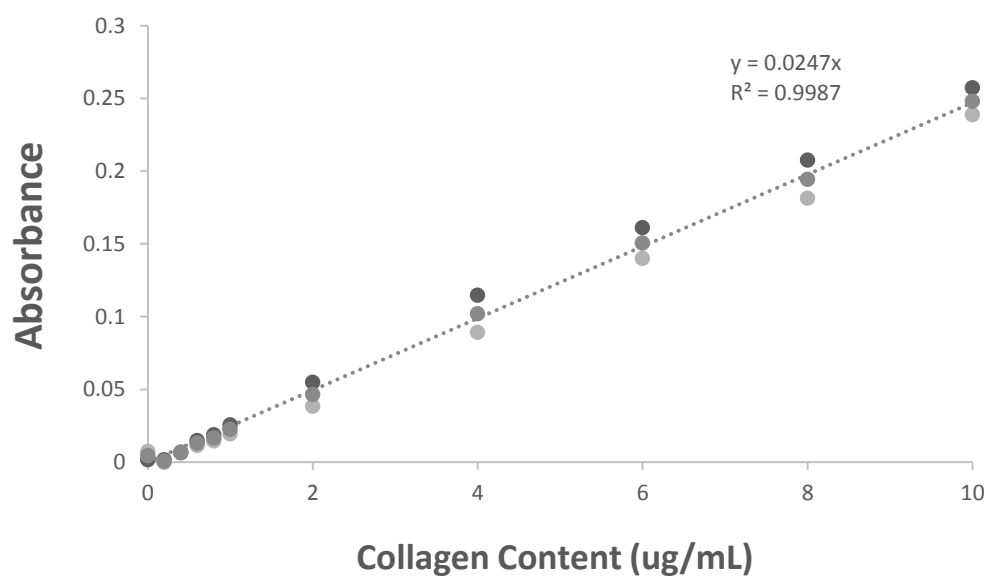


Figure D.1. A representative standard curve for the orthohydroxyproline assay. Collagen content ($\mu\text{g/mL}$) was plotted against absorbance value.

CURRICULUM VITAE

PERSONAL INFORMATION

Surname, Name: Bahçecioğlu, Gökhan
Nationality: Turkish (T.C.)
Marital Status: Married
Phone: +90 539 731 1530
Email: gokhanbace@gmail.com, gbahceci@metu.edu.tr

EDUCATION

Degree	Institution	Year of Graduation
MS	METU Biotechnology	2012
BS	METU Molecular Biology and Genetics	2008
High School	Osman Ötken Anatolian High School	2001

WORK EXPERIENCE

Year	Place	Position
2009-Current	METU Biological Science Dept.	Teaching Assistant
2015-2016	Brown University Dept. of Orthopaedics	Visiting Scholar

FOREIGN LANGUAGES

Arabic (intermediate), Spanish (beginner).

PUBLICATIONS

1. **Bahcecioglu G**, Hasirci N, Bilgen B, Hasirci V. A novel 3D printed PCL/hydrogel scaffold mimicking the zonal differences in the meniscus. *Acta Biomaterialia* (in preparation).
2. **Bahcecioglu G**, Hasirci N, Bilgen B, Hasirci V. Agarose and GelMA hydrogels induce meniscal regeneration on 3D printed PCL scaffolds. *Biomaterials* (in preparation).
3. **Bahcecioglu G**, Hasirci N, Bilgen B, Hasirci V. Hydrogels as supporting materials to induce in vitro meniscus regeneration of 3D printed PCL scaffolds. *PLOS ONE* (submitted).
4. **Bahcecioglu G**, Hasirci N, Hasirci V. Effects of microarchitecture and mechanical properties of 3D microporous PLLA-PLGA scaffolds on fibrochondrocyte and L929 fibroblast behavior. *Biomed Mater.* (In press). <https://doi.org/10.1088/1748-605X/aaa77f>.

5. Hasirci N, Kilic C, Komez A, **Bahcecioglu G**, Hasirci V. Hydrogels in regenerative medicine. GELS HANDBOOK: Fundamentals, Properties and Applications Volume 2. World Scientific Publishing. 2016.
6. **Bahcecioglu G**, Buyuksungur A, Kiziltay A, Hasirci N, Hasirci V. Construction and in vitro testing of a multilayered, tissue-engineered meniscus. J Bioact Compat Polym: Biomed Appl. 2014;29(3):235-253.
7. Ermis M*, **Bahcecioglu G***, Kandemir B*, Hasirci V. Kök hücreler, rejeneratif tıp ve doku mühendisliği [Stem cells, regenerative medicine, and tissue engineering]. In: Türkeri L, Özer A, Narter F, eds. Moleküler Üroloji: Ürolojik Hastalıkların Moleküler Temeli [Molecular Urology: Molecular Basis of Urological Diseases]. 2012. ***Authors contributed equally to the study.**

HOBBIES

Football, Drawing, Karate, Boxing, Guitar, Swimming, Tennis, Sightseeing.